VOLUME 39 APRIL 1961 NUMBER 4

Canadian Journal of Physics

Published by THE NATIONAL RESEARCH COUNCIL

OTTAWA CANADA

CANADIAN JOURNAL OF PHYSICS

Under the authority of the Chairman of the Committee of the Privy Council on Scientific and Industrial Research, the National Research Council issues THE CANADIAN JOURNAL OF PHYSICS and five other journals devoted to the publication, in English or French, of the results of original scientific research. Matters of general policy concerning these journals are the responsibility of a joint Editorial Board consisting of: members representing the National Research Council of Canada; the Editors of the Journals; and members representing the Royal Society of Canada and four other scientific societies.

Manuscripts for publication should be submitted to Dr. H. E. Duckworth, Editor, Canadian Journal of Physics, Hamilton College, McMaster University, Hamilton, Ontario.
For instructions on preparation of copy, see **NOTES TO CONTRIBUTORS** (back cover).

Proof, correspondence concerning proof, and orders for reprints should be sent to the Manager, Editorial Office (Research Journals), Division of Administration and Awards, National Research Council, Ottawa 2, Canada.

Subscriptions, renewals, requests for single or back numbers, and all remittances should be sent to Division of Administration and Awards, National Research Council, Ottawa 2, Canada. Remittances should be made payable to the Receiver General of Canada, credit National Research Council.

The journals published, frequency of publication, and subscription prices are:

Canadian Journal of Biochemistry and Physiology	Monthly	$9.00 a year
Canadian Journal of Botany	Bimonthly	$6.00 a year
Canadian Journal of Chemistry	Monthly	$12.00 a year
Canadian Journal of Microbiology	Bimonthly	$6.00 a year
Canadian Journal of Physics	Monthly	$9.00 a year
Canadian Journal of Zoology	Bimonthly	$5.00 a year

The price of regular single numbers of all journals is $2.00.

Canadian Journal of Physics

Issued by THE NATIONAL RESEARCH COUNCIL OF CANADA

VOLUME 39 APRIL 1961 NUMBER 4

THE 1600 Å BAND SYSTEM OF AMMONIA[1]

A. E. DOUGLAS AND J. M. HOLLAS[2]

ABSTRACT

The progression of ammonia bands which extends from 1689 to 1400 Å has been photographed in absorption at high resolution. Six bands have been analyzed and found to be of the perpendicular type. The analysis shows that the molecule is planar in the excited state and that vibrational levels observed in the progression are those of the out-of-plane vibration. The excited electronic state is of the E'' type. In addition to the normal Coriolis interaction of the degenerate levels, a second effect has been observed which behaves like the Coriolis interaction recently described as 'giant l-type doubling' by Garing, Nielsen, and Rao. No clear evidence has been found for any distortion of the degenerate state from D_{2h} symmetry.

I. INTRODUCTION

The ultraviolet absorption spectrum of ammonia has been the subject of numerous investigations, the most extensive of which have been those of Duncan (1935), Duncan and Harrison (1936), and Walsh and Warsop (1960). Duncan (1935) has reported that there are four band systems between 2200 and 1150 Å. The first of these, which has its origin near 2168 Å, is diffuse and its rotational structure can not be resolved (the corresponding bands of ND_3 do show some structure (Benedict 1935)). The second system, which lies between 1637 and 1400 Å, is much sharper and the rotational structure can be resolved. The band systems at shorter wavelengths have been discussed by Walsh and Warsop (1960) but rather little is known about their structures.

The 1600 Å band system consists of a single progression of bands with an upper state frequency of about 900 cm^{-1}. The first known member of the progression, at 1663 Å, is weak but the intensity increases rapidly along the progression and reaches its maximum at the seventh or eighth member. The rotational structures of a few of the bands have been resolved by Duncan and Harrison and they have given a partial rotational analysis of these bands. Unfortunately, their spectrograph lacked the resolving power necessary to show much of the detail of the bands and it will be shown later that their analysis is not correct.

[1]Manuscript received December 19, 1960.
Contribution from the Division of Pure Physics, National Research Council, Ottawa, Canada.
Issued as N.R.C. No. 6203.
[2]National Research Council Postdoctorate Fellow.

Some of the characteristics of the upper state of the 1600 Å band system can be deduced from its vibrational structure. The fact that a long progression of bands is observed indicates that there is a large change in the dimensions of the molecule during the transition. Though there is no proof, it seems most reasonable to assign the 900 cm^{-1} frequency of the upper state to a vibration which corresponds to the ν_2 ($\sim$950 cm^{-1}) vibration of the ground state. Since the ν_2 vibration corresponds to a normal mode in which the height of the ammonia pyramid changes, it has been argued that the transition is one in which the height of the pyramid undergoes a large change and probably one in which the upper state is planar.

The present work consists of a rotational analysis of a number of the bands of the 1600 Å system. Such an analysis is of interest for a number of reasons. Up till now, no band arising from an electronic transition of a symmetric top has been analyzed in detail. The analysis should give the geometry of the molecule and the symmetry of the electronic wave function of the upper state. Also there exists the possibility that unusual types of interaction between electronic and vibrational motion, such as the Jahn–Teller effect, may be discovered. For these reasons we have undertaken a rotational analysis of the bands and have succeeded in analyzing a sufficient number to show the essential characteristics of the band system.

II. EXPERIMENTAL

The absorption spectrum of ammonia from 1670 to 1400 Å was photographed using a 10-meter concave grating spectrograph. The spectrograph is of the normal incidence type and the seventh and eighth order spectra which were used in this work had dispersions of 0.21 Å/mm and 0.18 Å/mm respectively. Third and fourth order iron lines from a hollow cathode source were used as wavelength standards. Using a Lyman discharge to provide the continuum, spectra could be obtained on Ilford Q2 plates with exposure times which varied between 30 minutes and 2 hours.

The absorption cells used in this work varied in length from 20 to 50 cm. The ammonia gas pressure was varied from about 1 micron up to 2 mm to cover the wide range of intensities of lines within the bands and the large difference in the intensities of the various bands. It would have been desirable to use even higher pressures to obtain the weak bands near 1650 Å but it was found that a continuous absorption blocked all transmission if the pressure was increased beyond about 2 mm. Spectra of the gas were also taken at various temperatures ranging from $-110°$ C to $+300°$ C. Finally, spectra of the isotopically substituted molecule ND_3 were obtained but, as these spectra have not been analyzed, they will not be discussed further.

All the lines in the bands are broad and it is this line width and not the spectrograph that limits the resolution. The diffuseness of the lines increases slowly towards shorter wavelengths. This diffuseness is presumably caused by predissociation and, as with many other examples of predissociation, it is much less noticeable in the deuterium substituted compound.

III. THEORETICAL CONSIDERATIONS

Before giving the details of the analysis the most important results will be given here and the evidence to support them is presented later. The most significant results are as follows:

(1) The bands are of the perpendicular type, the upper state being a degenerate electronic state of species E''.

(2) The molecule is planar in the excited state.

(3) The bands involve a progression of vibrational levels of the out-of-plane vibration.

(4) The upper state rotational levels show a strong Coriolis-type perturbation similar to that recently called giant l-type doubling by Garing, Nielsen, and Rao (1959).

Now we shall consider the characteristics of a band system arising from states having the properties listed above. In its ground electronic state ammonia has a pyramidal structure and C_{3v} symmetry. The symmetry of the ground state electronic wave function is A_1. We wish therefore to consider a transition between this lower state and an upper state in which the molecule is planar (D_{3h} symmetry) and the electronic wave function has E'' symmetry.

Figure 1 shows the vibrational energy levels of the two states and the transitions allowed between them. In the ground electronic state only the

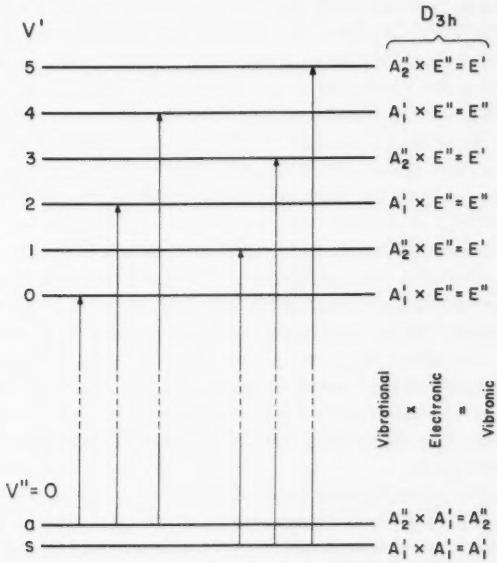

FIG. 1. The vibrational energy levels of ammonia which give rise to the 1600 Å bands. The lower state levels are those caused by the inversion of NH_3 and the upper state levels are the out-of-plane vibrational levels of a planar ammonia molecule. The vibrational, electronic, and vibronic symmetries of the levels are given on the right-hand side.

two lowest levels, which are separated by about .7 cm^{-1}, are shown. This small separation results from the fact that the potential barrier preventing the nitrogen atom from passing through the H_3 plane is low (Herzberg 1945, p. 220). Of the two energy levels, one has a wave function which is symmetric with respect to reflection in a plane that is perpendicular to the axis and passes through the center of mass of the molecule and the other has a wave function antisymmetric with respect to this plane. These levels are therefore usually referred to as the symmetric and the antisymmetric levels of ammonia. If the height of the ammonia pyramid were reduced, thereby reducing the barrier to the reflection, the symmetric and antisymmetric levels would move apart until in the limit, where the ammonia molecule became planar, these two levels would become A_1' and A_2'' vibrational levels of the molecule, which now would possess D_{3h} symmetry. For all barrier heights, however, the symmetric and antisymmetric levels have the characteristics of the A_1' and A_2'' levels and are therefore labelled as such even in the ground state of ammonia in Fig. 1.

In Fig. 1 the only vibrational levels shown in the upper electronic state are those associated with the out-of-plane vibration. We shall refer to this vibration as the ν_2 vibration. Since the transition involves a large change in the height of the ammonia pyramid, from the Franck–Condon principle it follows that we should expect to find a long progression in the ν_2 vibration in the absorption spectrum. Other vibrational levels of the upper state are of no interest at present and are not shown in Fig. 1. The ν_2 vibration has A_2'' symmetry and the higher vibrational levels alternate with A_1' and A_2' symmetry as shown on the right-hand side of Fig. 1. It is important for subsequent discussion to bear in mind that the ν_2 progression is the only progression of vibrational levels of the planar ammonia molecule which alternates in the sense that the wave functions are alternately symmetric and antisymmetric with respect to the plane of the molecule. The vibronic states (electronic $\times$vibrational) are therefore alternately $E''\times A_2'' = E'$ and $E''\times A_1' = E''$ as shown in Fig. 1.

The selection rules for the states shown in Fig. 1 are $E' \leftarrow A_1'$ and $E'' \leftarrow A_2''$. The allowed transitions are shown in the figure. One of the most significant facts is that the symmetric level of the lower state combines only with every other excited state vibrational level and the antisymmetric level combines with those in between. Since the separation between the symmetric and antisymmetric levels in the lower state is only 0.66 cm^{-1}, this effect will not be noticeable in the positions of the bands unless they are measured very precisely. This alternation does, however, have a marked effect on the rotational structures of the bands.

A few of the rotational levels of an E'' state and the antisymmetric (A_2'') state of the lower electronic state are shown in Fig. 2. The selection rules for the transition between these are $\Delta K = \pm 1, \Delta J = 0, \pm 1$. Figure 2 is essentially the same as that given by Herzberg (1945, p. 408) where a full description of a perpendicular-type transition is given. The figure has been modified, however, so that the levels are those of an oblate rather than a prolate top. The

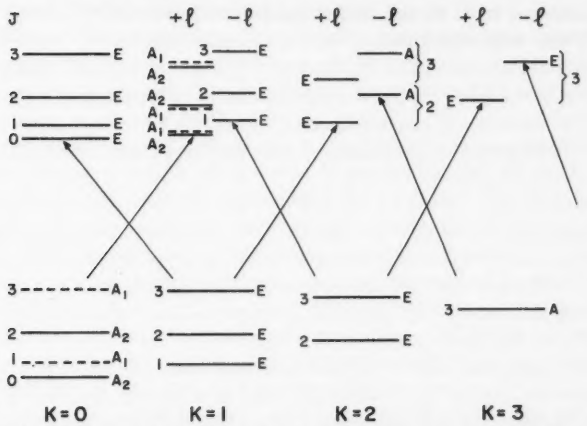

FIG. 2. A few of the rotational energy levels of a degenerate and a non-degenerate state of NH_3. The lower set of levels are those of the antisymmetric ground state of ammonia and the upper set are those of an E'' vibronic state. The A_1 and A_2 rotational species have been separated for $K' = 1$ but not for other K values where they are degenerate and are marked A. The allowed transitions ($\Delta K = \pm 1$) are shown by the arrows.

A_1 rotational levels have been drawn in dotted lines to indicate that in NH_3 where the nuclear spin of the three identical nuclei is $\frac{1}{2}$, these levels do not occur. This is particularly important for the $K'' = 0$ levels since here all odd J levels of the antisymmetric state are A_1 levels and therefore are missing. Furthermore, in the E'' state the A_1 and A_2 rotational levels with $K = 1$ have been separated by an appreciable amount; an effect which we shall show later does indeed occur. Figure 2 refers to an E''–A_2' transition. The alternate bands given in Fig. 1, which are E'–A_1' transitions, have very nearly the same structure, the one important difference being the fact that the A_1 and A_2 rotational levels are interchanged. As a result in the $K = 1 \leftarrow K = 0$ subband, the E''–A_2' bands have lines with even J'' values only while the $E' \leftarrow A_1'$ bands have lines with odd J'' values.

In order to show that the observed band system does indeed result from the transition described above we shall have to show that it has the following characteristics.

(1) The bands are of the perpendicular type. This will at once establish the fact that the upper state vibronic levels are degenerate but a somewhat more detailed argument will be necessary to show that the upper electronic state is degenerate.

(2) The bands in the progression have for their lower states alternately the symmetric and the antisymmetric (A_1' and A_2'') vibrational levels of the lower electronic state. This alternation will show that the upper state vibration is the ν_2 vibration. Proof that this alternation exists can be provided by the $K' = 1 \leftarrow K'' = 0$ subbands which will have alternately only even or only odd lines present.

(3) The $v_2 = 0$ level of the upper state combines with the lower state A_2'' level. This will establish the fact that the upper state is E'' rather than E'.

In the following discussion of the band system it will be shown that the three points listed above can be established. In addition the rotational constants of the molecule in its upper electronic state have been determined and a number of unusual characteristics of the spectrum have been noted.

IV. RESULTS

Absorption spectra of the 3–0 band taken at three different pressures are shown in Fig. 4. It was found that this large range of pressures was necessary in order to bring out the essential features of the band. As Fig. 4 shows, most of the strong lines are near the center of the band and in this region almost all the "lines" are blends of two or more lines.

The wave numbers of the lines in the bands are given in Table I. The accuracy of measurement varies (a good deal) from line to line depending upon the sharpness of the line and degree of overlapping. It is probable that the average error is about 0.07 cm^{-1} but for some lines the error may be as great as 0.2 cm^{-1}.

The analysis of the bands proved to be a difficult task. Unlike the usual progressions of bands, it was found here that every band appeared quite different from all other bands. There did exist a series of about six strong lines in each band which appeared to be similar in all the bands but when these strong lines were correlated no obvious correlations appeared to exist between the other lines.

Though the lines near the center of the band show no regularity, weak lines which occur at the high-frequency end of the bands form regular series and proved to be a suitable point from which to start the analysis. These regular series can be seen in Fig. 4. Starting from these series, with the aid of the excellent lower state combination differences of Benedict, Plyler, and Tidwell (1958), it was possible to obtain an analysis. The regular series proved to be R branches of subbands and the corresponding P and Q branches could be found. When all the lines in the high-frequency series had been assigned to subbands, together with their corresponding Q and P lines there still remained many strong lines unassigned. At this stage it was apparent, both from the relative intensities of the P and R branches in the subbands and from the number of subbands, that the band was of the perpendicular type with two subbands for every value of K''. The subbands giving rise to the regular structure described above were those with $\Delta K = -1$. By extrapolating from these $\Delta K = -1$ series it was possible to find the $\Delta K = +1$ subbands and complete the analysis.

The analysis shows that the major features of the bands are just those expected for perpendicular bands of a symmetric top and are in fact very similar to the infrared bands of NH_3 which have been analyzed by Benedict, Plyler, and Tidwell. It is primarily the poor resolution, caused by the large line width, together with the difficulty in registering lines with wide differences in intensities on vacuum ultraviolet plates, which caused the difficulty in the

analysis. As will be discussed later, the principal reason for every band appearing to be different from all others, lies in the rapid decrease in the upper state B value with increasing v_2. The few strong lines which do appear to be similar from band to band are the $J = K$ lines of the P branches of the $\Delta K = -1$ subbands.

In order to specify a band in an electronic transition of ammonia such as the one we have photographed here it is necessary to give all the vibrational quantum numbers of both the upper and lower states together with some symbol to denote the symmetry of the lower state with respect to reflection (inversion). In the band system under investigation, however, only the ν_2 vibration is excited in both the upper and lower states and we shall designate bands by the symbols ($v_2'-v_2''$ (s or a)) where it shall be understood that all other vibrational quantum numbers are zero. Very often the symbol s or a, which differentiates between the lower state symmetric and antisymmetric levels, is of no importance and will be omitted.

From the analysis of the bands, two unexpected facts emerged at once. Firstly, on the long wavelength side of the 1663 Å band which Duncan (1936), on the basis of the isotope effect, had assigned as the 0–0 band, a very weak band was found. As discussed previously a continuous absorption prevented this band from being investigated with long absorption paths. It was at first thought that this was the 0–1 band. The position of the 0–1 band with respect to the 0–0 band can be calculated exactly from the infrared ν_2 band which has been measured by Garing, Nielsen, and Rao (1959). The positions of the strongest lines of the 0–1s and the 0–1a bands were calculated and it was found that these did not correspond to the positions of the few lines which could be measured in the weak band. The weak band did, however, fall in a position such that it could be considered an additional band of the main progression. Thus it was concluded that the weak band was the 0–0 band and that the vibrational numbering given by Duncan must be increased by one unit.

A definite proof that the weak band is not the 0–1 band was found when the spectrum of ammonia at 300° C was examined. The spectrum showed a number of new lines at the edge of the weak band and their displacement from the 1663 Å band was such that there was no doubt that they arose from the $v_2 = 1(s)$ level of the lower state. Thus there appears no doubt that Duncan's vibrational numbering must be increased by at least one unit. The question of whether or not it can be advanced by more than one unit will be dealt with later. In the remainder of this paper, the new numbering, in which the 1663 Å band is the 1–0 band, will be used.

The second unexpected result arising from the analysis was the displacement of all the Q branches of the $K' = 1 \leftarrow K'' = 0$ subbands. After the P and R branches of these subbands had been found the expected positions of the Q branch lines could be determined. Since these Q branch lines should be some of the strongest lines in the bands, they should have been found without difficulty but none of the lines could be found in the expected positions. After the analysis of all other subbands was completed, several strong lines were

TABLE I

Vacuum wave numbers and assignments for the lines of the NH_3 bands

1 ← 1 band

	$K'=7$–$K''=6$	$K'=6$–$K''=5$	$K'=5$–$K''=4$	$K'=4$–$K''=3$		$K'=1$–$K''=0$	
J''	$R(J)$	$R(J)$	$R(J)$	$R(J)$	$Q(J)$	$R(J)$	$Q(J)$
1						59215.00	
2							
3				59194.42		248.60	59180.97
4			59190.11	213.06	59114.09		
5		59183.77				278.43	186.31
6	59175.96						
7						305.04	

	$K'=2$–$K''=3$		$K'=5$–$K''=6$
J''	$Q(J)$	$P(J)$	$P(J)$
3		59164.41	
4	59122.80		
5			
6			59135.46

0 ← 0 band

	$K'=7$–$K''=6$	$K'=4$–$K''=3$	$K'=1$–$K''=2$	$K'=2$–$K''=3$	$K'=3$–$K''=4$
J''	$R(J)$	$R(J)$	$P(J)$	$P(J)$	$P(J)$
2			59205.18		
3		59229.66		59198.49	
4		254.14		181.4	59190.24
5		280.04			
6	59207.42				

	$K'=4$–$K''=5$	$K'=5$–$K''=6$
J''	$P(J)$	$P(J)$
5	59178.62	
6		59164.49

1 ← 0 band

	$K'=7$–$K''=6$		$K'=6$–$K''=5$		$K'=5$–$K''=4$		$K'=4$–$K''=3$		
J''	$R(J)$	$Q(J)$	$R(J)$	$Q(J)$	$R(J)$	$Q(J)$	$R(J)$	$Q(J)$	$P(J)$
3							60126.08		
4					60120.75		145.73	60046.46	59947.34
5			60113.40		140.33	60021.39	165.00	046.46	
6	60104.18		133.05	59994.26	159.62	021.39	183.82		
7	123.62	59965.24	152.34	994.26	178.61	021.39	202.12		
8	142.91	965.24	171.13	994.26	197.16		219.87		
9	161.91	965.24							

TABLE I (*Continued*)

Vacuum wave numbers and assignments for the lines of the NH_2 bands

	$K'=3$–$K''=2$		$K'=2$–$K''=1$			$K'=1$–$K''=0$		
J''	$R(J)$	$Q(J)$	$R(J)$	$Q(J)$	$P(J)$	$R(J)$	$Q(J)$	$P(J)$
1			60130.80			60147.69	60110.92	
2	60129.22		150.28	60090.75				
3	149.05	60069.56	169.33	090.75		182.40	114.91	60048.51
4	168.27	069.56	187.73		60011.25			
5	187.18		205.23		59991.02	214.28	122.36	004.00
6	205.23		221.87		970.16			
7					948.50	243.62	133.63	59957.86
8								
9						266.59		

	$K'=0$–$K''=1$		$K'=1$–$K''=2$		$K'=2$–$K''=3$		
J''	$Q(J)$	$P(J)$	$Q(J)$	$P(J)$	$R(J)$	$Q(J)$	$P(J)$
1	60127.46	60110.92					
2		087.22	60142.91	60104.18			
3				082.90			60095.90
4				059.79		60155.70	076.20
5					60255.45	155.70	056.59
6						156.17	037.46
7							018.58
8							000.56

	$K'=3$–$K''=4$			$K'=4$–$K''=5$		$K'=5$–$K''=6$		$K'=6$–$K''=7$	$K'=7$–$K''=8$
J''	$R(J)$	$Q(J)$	$P(J)$	$Q(J)$	$P(J)$	$Q(J)$	$P(J)$	$P(J)$	$P(J)$
4	60266.59	60166.86	60087.22						
5			067.42	60175.77	60076.20				
6			048.51	175.77	056.59	60182.40	60063.59		
7			028.87		037.46		043.81	60048.51	
8			009.60		019.24		024.42	028.95	60032.10
9					001.85		005.90		012.00

	$K'=8$–$K''=9$	$K'=9$–$K''=10$
J''	$P(J)$	$P(J)$
9	60013.42	
10	59992.91	59992.91
11	972.23	973.86

2 ← 0 band

	$K'=8$–$K''=7$	$K'=7$–$K''=6$	$K'=6$–$K''=5$	$K'=5$–$K''=4$		$K'=4$–$K''=3$		
J''	$R(J)$	$R(J)$	$R(J)$	$P(J)$	$R(J)$	$R(J)$	$Q(J)$	$P(J)$
3						61055.92		
4					61050.46	070.67	60976.53	
5			61040.99		064.37	084.50	971.54	60877.39
6		61023.04	053.23	60832.23	077.52	097.21	965.87	852.89
7	60995.40	036.71	064.37	806.99	089.50	108.74	958.89	827.46
8	61011.79	047.00	077.52		100.22	119.52	951.19	801.23
9	021.31	056.02	089.50		111.10			774.29
10		064.47						746.48

TABLE I (*Continued*)

Vacuum wave numbers and assignments for the lines of the NH_3 bands

	$K'=3$–$K''=2$			$K'=2$–$K''=1$			$K'=1$–$K''=0$		
J''	$R(J)$	$Q(J)$	$P(J)$	$R(J)$	$Q(J)$	$P(J)$	$R(J)$	$Q(J)$	$P(J)$
0							61061.08		
1				61061.08					
2	61061.08			077.52	61019.68		092.05	61038.95	61000.33
3	075.23	61089.50		093.11	017.86				
4	089.50	60995.40		107.18	013.80		117.63	034.10	60952.85
5	103.28	990.63	60896.65	119.52	008.80				
6	115.41	984.58	871.85	130.56	000.33		137.67	026.65	899.93
7	126.29		846.46	140.05	60990.63				
8	135.85		819.74	148.10	982.11		153.10	017.86	841.99
9	144.35		792.09		971.54				
10			763.06				164.53		780.89

	$K'=0$–$K''=1$			$K'=1$–$K''=2$			$K'=2$–$K''=3$		
J''	$R(J)$	$Q(J)$	$P(J)$	$R(J)$	$Q(J)$	$P(J)$	$R(J)$	$Q(J)$	$P(J)$
1	61095.35	61055.92	61038.95						
2	112.85	055.92	017.86	61128.39	61070.67	61034.10			
3	129.53	053.23	60995.40	144.27	—	011.79	61158.80	61083.33	61026.65
4	146.03	050.46	973.71	160.19	064.37	60989.25	174.24	079.43	003.81
5	162.80	047.00	951.19	175.78	061.08	965.87	189.05	075.23	60980.25
6	179.93	043.30	928.44	191.44	055.92	942.09	203.99	070.67	956.42
7	197.56		906.35	207.51	053.23	919.01	218.81	064.37	932.08
8			884.46			896.62	234.47	061.08	908.21
9									884.46

	$K'=3$–$K''=4$			$K'=4$–$K''=5$			$K'=5$–$K''=6$		
J''	$R(J)$	$Q(J)$	$P(J)$	$R(J)$	$Q(J)$	$P(J)$	$R(J)$	$Q(J)$	$P(J)$
4	61187.49	61093.11	61017.86						
5	202.00	089.50	60994.21	61214.20	61101.11	61006.70			
6	216.04	083.33	969.30	227.84	095.35	60982.11	61238.93	61107.18	60994.21
7	230.22	077.52	944.87	241.08	089.50	956.42	251.45	100.22	968.25
8			920.07			931.34	264.09	092.05	942.09
9			896.62			906.35	276.69	084.50	915.17
10						880.82			887.61
11									864.46

	$K'=6$–$K''=7$	$K'=7$–$K''=8$	$K'=8$–$K''=9$	$K'=9$–$K''=10$	$K'=10$–$K''=11$
J''	$P(J)$	$P(J)$	$P(J)$	$P(J)$	$P(J)$
7	60980.25				
8	952.85	60963.19			
9	924.59	934.81	60944.87		
10	899.93	909.97	917.38	60924.59	
11					60902.62

	$K'=11$–$K''=12$	$K'=12$–$K''=13$
J''	$P(J)$	$P(J)$
12	60878.98	
13		60852.89

TABLE I (*Continued*)

Vacuum wave numbers and assignments for the lines of the NH_3 bands

$3 \leftarrow 0$ band

	$K'=8$–$K''=7$	$K'=7$–$K''=6$			$K'=6$–$K''=5$		
J''	$R(J)$	$R(J)$	$Q(J)$	$P(J)$	$R(J)$	$Q(J)$	$P(J)$
5					62002.19		
6		61993.42			008.30		
7	61984.51	997.37			015.99		
8		62000.58	61838.86	61695.98	015.99	61869.76	61711.67
9		001.44	822.57	661.45	013.01	854.63	677.50
10			804.76	625.72		838.86	642.46
11				588.99			603.99

	$K'=5$–$K''=4$			$K'=4$–$K''=3$			$K'=3$–$K''=2$		
J''	$R(J)$	$Q(J)$	$P(J)$	$R(J)$	$Q(J)$	$P(J)$	$R(J)$	$Q(J)$	$P(J)$
2							62018.73		
3				62015.14			030.74	61959.23	
4	62009.59			025.03	61935.75		040.30	951.22	
5	017.51	61910.32		033.09	925.85	61836.53	048.63	941.46	61852.22
6	023.85	898.65	61791.66	039.73	914.38	806.77	054.83	929.92	822.57
7	028.58	885.59	760.18	044.19	901.31	776.08	058.76		791.66
8		870.19	727.67	047.14	886.69	743.42	060.90		758.95
9			693.89	048.63	870.19	709.70			724.76
10			658.70			674.43			688.82
11			622.52			637.97			651.64
12						600.40			

	$K'=2$–$K''=1$			$K'=1$–$K''=0$			$K'=0$–$K''=1$		
J''	$R(J)$	$Q(J)$	$P(J)$	$R(J)$	$Q(J)$	$P(J)$	$R(J)$	$Q(J)$	$P(J)$
1	62020.62			62035.01	62001.44		62053.16	62015.99	62000.58
2	034.63	61980.86					067.39	013.01	61977.45
3	046.18	974.85		057.73	61994.21	61935.75	079.79	007.61	953.90
4	055.79	966.78	61895.47				091.40	000.58	928.27
5	062.99	956.52	867.67	071.25	982.64	879.28	102.06	61993.42	901.31
6	068.14	944.37	838.11				111.89	982.64	873.36
7	071.25	929.93	806.41	076.88	955.74	814.52			845.06
8	071.25		772.48						816.36
9			737.04	076.88		742.90			785.98
10			700.05						
11			661.45						

	$K'=1$–$K''=2$			$K'=2$–$K''=3$			$K'=3$–$K''=4$		
J''	$R(J)$	$Q(J)$	$P(J)$	$R(J)$	$Q(J)$	$P(J)$	$R(J)$	$Q(J)$	$P(J)$
2	62083.39	62029.62	61994.21						
3	095.64	023.85	969.97	62111.89	62040.30	61986.57			
4	106.48	015.99	944.37	122.19	032.52	960.69	62138.89	62048.63	61977.45
5	116.14	007.61	917.12	131.42	023.18	933.17	146.95	039.73	949.61
6	125.06	61997.37	888.75	138.89	013.01	904.34	154.25	028.58	920.23
7	133.45	986.57	859.21		000.58	874.22	161.12		889.50
8	141.85	976.13	829.34		61989.36	843.43	166.91		858.23
9		965.12	799.07			812.45	172.99		826.28
10			769.13			781.09			794.17
11						750.31			761.83
12						719.87			

TABLE I (*Continued*)

Vacuum wave numbers and assignments for the lines of the NH_3 bands

	$K'=4$–$K''=5$			$K'=5$–$K''=6$			$K'=6$–$K''=7$		$K'=7$–$K''=8$
J''	$R(J)$	$Q(J)$	$P(J)$	$R(J)$	$Q(J)$	$P(J)$	$R(J)$	$P(J)$	$P(J)$
5	62163.10		61967.34						
6	169.81	62044.19	936.57	62185.83	62060.90	61953.90			
7	175.61		905.35	190.65	047.14	921.93	62206.63	61939.62	
8	180.74		873.36	194.83	032.52	888.75	209.48	905.35	61923.28
9			840.43	198.16	017.51	854.63	211.83	870.19	886.69
10			806.77	201.52	001.44	820.40		834.65	849.76
11						785.98		799.07	
12						752.03			

	$K'=8$–$K''=9$	$K'=9$–$K''=10$		
J''	$P(J)$	$P(J)$		
9	61904.34			
10	866.43	61883.21		

$4 \leftarrow 0$ band

	$K'=11$–$K''=10$	$K'=10$–$K''=9$	$K'=9$–$K''=8$	$K'=8$–$K''=7$	$K'=7$–$K''=6$
J''	$R(J)$	$R(J)$	$R(J)$	$R(J)$	$R(J)$
6					62973.21
7				62962.77	969.54
8			62950.22	956.25	964.31
9		62936.29	941.32		
10	62920.37	923.83			

	$K'=6$–$K''=5$		$K'=5$–$K''=4$		$K'=4$–$K''=3$		
J''	$R(J)$	$Q(J)$	$R(J)$	$Q(J)$	$R(J)$	$Q(J)$	$P(J)$
3					62994.94		
4			62989.33		63000.32	62915.47	
5	62981.96		992.18	62889.58	003.18	901.19	62816.31
6	981.96		992.18	873.17	003.18	884.37	782.43
7	980.43		989.33	853.66	000.32	865.06	745.98
8		62822.74		831.50			707.58

	$K'=3$–$K''=2$			$K'=2$–$K''=1$			$K'=1$–$K''=0$		
J''	$R(J)$	$Q(J)$	$P(J)$	$R(J)$	$Q(J)$	$P(J)$	$R(J)$	$Q(J)$	$P(J)$
0							63000.92		
1				63001.02					
2	62998.80			012.18	62961.06		024.20	62977.02	62941.32
3	63006.93	62939.20		020.12	952.44	62901.19			
4	012.18	927.62	62859.05	025.36	940.83	873.17	034.80	960.29	885.29
5	015.31	913.35	828.53	027.52	926.23	841.71			
6	012.18	896.57	794.66	027.52	909.00	807.77	034.80	935.72	817.19
7			758.52		889.58	771.07			
8			719.88			731.86		905.53	738.72

TABLE I (*Continued*)

Vacuum wave numbers and assignments for the lines of the NH_3 bands

	$K'=0$–$K''=1$			$K'=1$–$K''=2$			$K'=2$–$K''=3$		
J''	$R(J)$	$Q(J)$	$P(J)$	$R(J)$	$Q(J)$	$P(J)$	$R(J)$	$Q(J)$	$P(J)$
1	63031.28	62997.26	62980.43						
2	042.66	991.64	957.77	63059.35	63008.36	62974.60			
3	051.49	982.90	931.98	067.90	62999.80	948.84	63085.65	63017.74	62967.08
4	058.25	972.26	903.88	074.09	988.62	920.07	091.52	006.31	938.35
5	063.17	959.28	973.17	078.26	975.19	889.58	095.22	62992.18	907.23
6		944.55	840.73		959.28	856.21			873.54
7			806.56						837.75
8									798.75

	$K'=3$–$K''=4$			$K'=4$–$K''=5$			$K'=5$–$K''=6$		
J''	$R(J)$	$Q(J)$	$P(J)$	$R(J)$	$Q(J)$	$P(J)$	$R(J)$	$Q(J)$	$P(J)$
4	63110.31	63025.36	62957.77						
5	113.36	011.08	926.23	63133.11	63031.28	62946.85			
6		62994.83	892.17		014.16	912.23		63034.80	62934.28
7		974.45	856.21			875.50	63151.19		896.57
8		960.29	817.19					62991.64	856.21
9			772.98						814.16

	$K'=6$–$K''=7$	$K'=7$–$K''=8$	$K'=8$–$K''=9$
J''	$P(J)$	$P(J)$	$P(J)$
7	62920.07		
8		62903.90	
9			62886.39

$5 \leftarrow 0$ band

	$K'=10$–$K''=9$	$K'=9$–$K''=8$	$K'=8$–$K''=7$	$K'=7$–$K''=6$
J''	$R(J)$	$R(J)$	$R(J)$	$R(J)$
6				63973.28
7			63962.85	965.18
8		63950.90		950.90
9	63937.07			

	$K'=6$–$K''=5$			$K'=5$–$K''=4$		$K'=4$–$K''=3$		
J''	$R(J)$	$Q(J)$	$P(J)$	$R(J)$	$Q(J)$	$R(J)$	$Q(J)$	$P(J)$
3						63994.75		
4				63989.26		995.98	63915.20	
5	63981.98			987.21	63889.93	993.56	896.44	63816.22
6	975.38	63863.15		980.14	868.23	986.35	874.67	777.81
7	962.85	836.64	63724.43		841.61	973.28	847.93	736.54
8			678.68			952.93		

TABLE I (*Continued*)

Vacuum wave numbers and assignments for the lines of the NH_2 bands

	$K'=3$–$K''=2$			$K'=2$–$K''=1$			$K'=1$–$K''=0$		
J''	$R(J)$	$Q(J)$	$P(J)$	$R(J)$	$Q(J)$	$P(J)$	$R(J)$	$Q(J)$	$P(J)$
1				64001.30			64014.07	63982.64	
2	63998.76			009.35	63961.47				
3	64003.45	63939.26		014.84	949.32		026.22	965.18	63914.69
4	004.45	923.79	63859.80	014.07	934.73	63870.54			
5	002.02	905.31	824.89	012.55	915.20	835.31	019.74	936.51	846.81
6	63997.64	883.28	786.66		893.61	796.23			
7			745.22			755.67	002.02	895.72	762.98
8									
9									668.14

	$K'=0$–$K''=1$			$K'=1$–$K''=2$			$K'=2$–$K''=3$		
J''	$R(J)$	$Q(J)$	$P(J)$	$R(J)$	$Q(J)$	$P(J)$	$R(J)$	$Q(J)$	$P(J)$
1	64030.07	63997.64	63981.26						
2	038.45	989.94	958.18	64055.66	64007.11	63975.38			
3	043.65	978.72	930.44	060.63	63995.98	947.56	64079.35	64014.84	63967.59
4	045.75	964.25	899.45	062.15	981.26	916.51	081.29	000.16	935.64
5	045.75	947.22	865.29	060.63	962.85	882.00	079.35	63981.98	900.88
6	041.71	926.36	828.01	056.90	942.20	844.41	074.61	961.47	863.15
7		903.70	788.27	050.73	918.84	804.13	067.91	936.51	822.17
8						761.23	058.65	910.16	778.67
9								882.00	733.35
10									685.81

	$K'=3$–$K''=4$			$K'=4$–$K''=5$			$K'=5$–$K''=6$	
J''	$R(J)$	$Q(J)$	$P(J)$	$R(J)$	$Q(J)$	$P(J)$	$Q(J)$	$P(J)$
4		64022.61	63958.18					
5	64100.06	002.02	923.79	64124.38	64026.22	63947.73		
6	094.57	63981.26	883.28	117.18		908.39	64030.63	63934.73
7	087.03	956.08	842.64			867.00	006.46	891.78
8	077.40	929.18	798.23			820.68	63981.98	847.93
9			752.02					804.13

	$K'=6$–$K''=7$	$K'=7$–$K''=8$	$K'=8$–$K''=9$	$K'=9$–$K''=10$
J''	$P(J)$	$P(J)$	$P(J)$	$P(J)$
7	63920.43			
8	874.67	63904.63		
9			63887.25	
10			831.86	63867.00

$8 \leftarrow 0$ band

	$K'=9$–$K''=8$	$K'=8$–$K''=7$	$K'=7$–$K''=6$	$K'=6$–$K''=5$
J''	$R(J)$	$R(J)$	$R(J)$	$R(J)$
5		67015.99		67058.73
6			67040.32	035.66
7			015.99	010.48
8	66977.93	66984.78	66988.17	

TABLE I (*Concluded*)

Vacuum wave numbers and assignments for the lines of the NH_3 bands

	$K'=5$–$K''=4$		$K'=4$–$K''=3$			$K'=3$–$K''=2$		
J''	$R(J)$	$Q(J)$	$R(J)$	$Q(J)$	$P(J)$	$R(J)$	$Q(J)$	$P(J)$
2						67080.93		
3			67076.84			076.84	67021.67	
4	67069.87		065.82	66997.39		065.82	66997.39	
5	053.32	66970.91	048.86	967.14	66898.13	048.86	967.14	66898.13
6	030.91		026.38	930.03	847.88		930.03	847.88
7	002.59		66999.01	888.34	791.65			791.65
8			965.53	840.77	730.77			
9				788.48				

	$K'=2$–$K''=1$			$K'=1$–$K''=0$			$K'=0$–$K''=1$		
J''	$R(J)$	$Q(J)$	$P(J)$	$R(J)$	$Q(J)$	$P(J)$	$R(J)$	$Q(J)$	$P(J)$
0				67085.48					
1	67084.05						67107.16	67079.75	67065.82
2	085.48	67044.31		093.49	67054.28	67025.84	108.48	067.09	039.96
3	080.93	025.84	66984.78				103.91	048.86	007.82
4	069.87	001.76	946.56	076.84	012.39	66954.72	093.49	024.76	66969.46
5	053.32	66970.91	902.21				076.84	66994.52	925.59
6	030.91	934.82	852.39	035.66	66948.83	859.16		958.72	875.91
7	002.59	892.62	796.35					918.20	820.99
8		845.02	735.08		864.80	740.16			760.79

	$K'=1$–$K''=2$			$K'=2$–$K''=3$			$K'=3$–$K''=4$		
J''	$R(J)$	$Q(J)$	$P(J)$	$R(J)$	$Q(J)$	$P(J)$	$R(J)$	$Q(J)$	$P(J)$
2	67127.11	67085.48	67058.73						
3	122.46	067.09	025.84	67145.67	67090.88	67050.12			
4	111.82	043.02	66988.17	134.96	065.82	011.69	67162.38	67093.49	67040.32
5	095.39	012.39	944.11	118.02	035.66	66967.14	145.67	063.51	66994.52
6		66977.10	894.10	096.86	66999.01	917.00	123.17	026.38	944.11
7		935.72	838.74		958.72	860.97		66984.78	888.34
8			778.39		910.73	800.77			827.04
9						733.99			

	$K'=4$–$K''=5$	$K'=5$–$K''=6$		$K'=6$–$K''=7$		$K'=7$–$K''=8$	$K'=8$–$K''=9$
J''	$P(J)$	$Q(J)$	$P(J)$	$Q(J)$	$P(J)$	$P(J)$	$P(J)$
5	67028.72						
6	66977.10	67097.35	67015.99				
7	922.07		66958.72	67096.86	67001.76		
8	864.80		896.15		66938.07	66986.34	
9			827.04		869.11	916.27	66969.46
10					795.48	840.77	892.47
11							810.59

	$K'=9$–$K''=10$	$K'=10$–$K''=11$	$K'=11$–$K''=12$
J''	$P(J)$	$P(J)$	$P(J)$
10	66951.14		
11		66931.45	
12			66910.73

found in every band, which could only be accounted for by assuming they were lines of the missing Q branch, displaced from the expected positions. The displacement of the lines of the Q branches varies with the J value and must be the result of a splitting between the A_1 and A_2 rotational levels in the $K' = 1$ levels as is shown in Fig. 1. The explanation of this observation will be discussed later.

In order to determine the rotational constants of the excited electronic state, the energy levels of the excited state were determined. This was done by first calculating the energy levels of the lower state from the data of Benedict, Plyler, and Tidwell (1958) and then adding to these lower state energies the frequencies of appropriate observed lines. The constants in the equations describing the rotational levels were then adjusted to give a best fit to these upper state energy levels. This method of evaluating molecular constants is more suitable than one using combination differences if the spectrum has many overlapped lines.

An attempt was made to fit the rotational energy levels of the upper state to the equations usually applicable to the degenerate state of a symmetric top, that is

$$F(JK) = B_v J(J+1)+(C_v-B_v)K^2 \pm 2C_v\zeta_v K - D_{J,v}J^2(J+1)^2 - D_{JK,v}J(J+1)K^2 - D_{K,v}K^4. \tag{1}$$

Two major difficulties were encountered. Firstly, as mentioned above, in the $K' = 1$ level the observed A_2 levels which give rise to Q branch lines are not in the positions calculated from the levels giving rise to P and R branch lines. The displacements from the expected positions were as great as 50 cm^{-1}. This effect can best be thought of as a splitting between the A_1 and A_2 levels for $K = 1$ although in fact all A_1 levels are missing in ammonia. The second major difficulty in trying to fit equation (1) to the observed levels was that the energy difference between the $+l$ and $-l$ levels for a given K, which by the equation should be $4C\zeta K$ and independent of J, was found to be very dependent on J. For example, this difference for $K = 2$ in the $v_2 = 2$ level varies between 36 and 57 cm^{-1} as J varies from 2 to 9.

Both of the above difficulties can be resolved if it is assumed that the rotational levels are perturbed by a Coriolis interaction of the type described as giant l-type doubling by Garing, Nielsen, and Rao (1959). They have shown that an interaction between an A and an E type vibrational state can modify the rotational energies of the latter such that for the A_1 and A_2 levels with $K = 1$

$$F(J,1) = \left(B_v+\frac{q_v}{2}\right)J(J+1)+\left(C_v-B_v-\frac{q_v}{2}\right)-2\zeta_v C_v\left(1-\frac{q_v}{4C}\right) \pm \frac{q_v}{2}J(J+1) \tag{2}$$

and for all other levels

$$(3)\quad F(J,K) = \left(B_v+\frac{q_v}{2}\right)J(J+1)+\left(C_v-B_v-\frac{q_v}{2}\right)K^2\mp 2K\zeta_v C_v\left(1-\frac{q_v}{4C}\right) \pm\frac{q_v^2[J(J+1)-K(K\mp1)][J(J+1)-(K\mp1)(K\mp2)]}{16(K\pm1)[(1-\zeta_v)C_v-B_v]}.$$

Here the equations of Garing, Nielsen, and Rao have been modified by letting $\alpha'^2/\delta = q_v$ and dropping a small term β'. The centrifugal stretching terms have been omitted but it is assumed that these will have the same form as in equation (1).

Equations (2) and (3) introduce only one new constant beyond those given in equation (1). This constant q_v can be determined by the A_1A_2 splitting of the $K = 1$ levels which according to equation (2) is equal to $q_vJ(J+1)$. Thus a test of whether or not equations (2) and (3) are applicable to the observed rotational levels is to determine q from equation (2) and to insert this value into equation (3) and see if the last term will give the observed J dependence of the splitting between the $+l$ and $-l$ levels. This calculation was carried out and it was indeed found that most of this J dependence could be accounted for by equation (3). This result is shown in Fig. 3 where the splitting between the

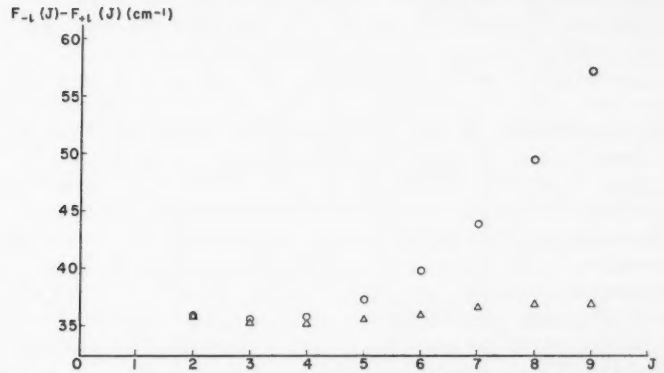

FIG. 3. The open circles show the separation of the $+l$ and $-l$ levels of the same J value for $K = 2$ in the $v' = 2$ state. The triangles show the same separation after adding the last term of equation (3) to the value of each energy level.

$+l$ and $-l$ levels for $K = 2$ and $v_2' = 2$ is shown as it exists before and after the correction has been applied. That there still should remain a small dependence of this splitting on J is not unexpected (see Benedict, Plyler, and Tidwell 1958, equation 3*a*) and we must conclude that the equations (2) and (3) do account for the positions of the observed levels.

In the final determination of the rotational constants, the value of q for each vibrational level was determined from the $K = 1$ level. With this value

of q_v and approximate values of B, C, and ζ the last term of equation (3) was calculated and added to the observed energies of the rotational levels. With these corrections added, the rotational levels were represented by the equation

$$(4) \qquad F(J,K) = B_v^* J(J+1) + (C_v - B_v^*)K^2 \mp 2KC_v\zeta_v^* - D_{J,v}J^2(J+1)^2 - D_{K,v}K^4 - D_{JK,v}K^2J(J+1)$$

where $B_v^* = B_v + (q_v/2)$ and $\zeta_v^* = [1-(q/4C_v)]$. The constants B^*, C, ζ^*, D_K, and D_{JK} were adjusted to give the best fit to the observed levels. The final constants B, C, ζ, q, ν_0, D_{JK}, and D_K are given in Table II. The accuracy of the centrifugal distortion constants given in this table is quite low and force constants determined from them might be far from correct.

TABLE II

Constants for the upper state of NH_2

v'	B_v	C_v	ζ_v	ν_0	q	$D_{JK}\times10^{-4}$	$D_K\times10^{-4}$
0	(10.29)*	(5.17)*		59224.7			
1	9.73	5.21	0.873	60123.8	0.758	−58	+91
2	9.21	5.33	0.859	61054.7	0.550	−28	+49
3	8.73	5.37	0.842	62014.9	0.529	−57	+58
4	8.27	5.35	0.839	62996.9	0.428	−44	+42
5	7.87	5.46	0.832	63997.7	0.258	−83	+67
8	6.83	5.55	0.804	67082.3	0.170	−95	+55

*Values obtained by extrapolation:
$B_v = 10.29 - .577v + .018v^2$
$C_v = 5.21 + .043v$

The agreement between the values of the rotational energy levels calculated from equations (2) and (3) with the constants given in Table II and the observed values is not good. Differences of 1 cm^{-1} between the observed and calculated values are common and a few differences as great as 10 cm^{-1} are found. The largest difference seems to occur in terms with low K and high J but in equations (2) and (3) there are eight constants which can be adjusted to fit the rotational levels in any one vibrational state and it is difficult to determine which levels actually fail to fit the equations and which merely appear to fail because of the particular choice of constants. The constant D_J is particularly troublesome since it seems to vary greatly with K and no single meaningful value could be obtained. Though a better fit of the observed levels could be obtained by introducing additional terms, the relatively low accuracy of the observations would make the new constants of doubtful value.

The vibrational energy levels of the upper state can be represented by the equation

$$\nu_{(vib)} = 59225.51 + 880.60v_2 + 18.437v_2^2 - 0.71863v_2^3.$$

The positions of the band origins differ from the values measured by Duncan on low dispersion plates by as much as 20 cm^{-1}.

One of the unusual features of the upper state is the large value of the vibration–rotation interaction constant α_2^B. The value of 0.58 cm^{-1} found for

this constant can be compared with a value of 0.015 cm^{-1} for α_2^B in the lower state. Though it is true that these α values are not exactly comparable it is difficult to believe that the change in the geometry and the force constants could change α_2 by a factor of about 40.

The B_0 value corresponds to an N—H bond distance of 1.027 Å. If instead of B_0 we use $B_0+\frac{1}{2}\alpha_2^B$ then we find an N—H distance of 1.040 Å. In either case, it is apparent that the NH bond distance is little different from the ground state value $r_e = 1.011$ Å (Benedict and Plyler 1957).

In Section III the structure of a band system resulting from a particular transition was discussed and three essential characteristics were given. We shall now consider whether or not these characteristics have been found to exist in the observed system.

(1) There is no doubt that the bands are perpendicular bands. Both the number of subbands and the intensity of the branches in the subbands can be explained only by assuming that the bands are of the perpendicular type. Thus the upper state levels must be degenerate (E) states.

The question of whether this degeneracy in the upper state arises from a degeneracy in the electronic wave function or in the vibrational wave function requires some consideration. Since the upper state is planar and of D_{3h} symmetry (see the following section) the possible symmetry types of the electronic wave function are A_1', A_2'', A_1'', A_2', E', and E''. Since the electronic selection rules are determined by the C_{3v} symmetry of the lower state an A_1' or A_2'' state would give an allowed transition but the bands would be of the parallel type. The fact that perpendicular bands are observed therefore rules out this possibility. An A_1'' or A_2' state can not combine with the ground state. A forbidden transition to an A_1'' or A_2' state can be made allowed and can give rise to perpendicular bands if one quantum of an E type vibration is excited. Such a band system would be a weak one whereas the 1600 Å system is strong and according to Walsh and Warsop (1960) is the first member of a Rydberg series. It therefore appears most probable that the band system is allowed and has an electronically degenerate excited state.

(2) As shown in Table II the $K'' = 0$ subbands have every other line missing in all their branches. Since these subbands are strong there is no doubt about this conclusion. Furthermore it was found that in the 0–0, 2–0, 4–0, and 8–0 bands the even lines are present while in the 1–0, 3–0, and 5–0 levels the odd lines are present. This alternation, according to the argument given previously, arises from the fact that the upper state levels combine alternately with the symmetric and antisymmetric lower states and provides us with a proof that the upper state progression is in the ν_2 vibration.

Having established that the upper state progression is in the out-of-plane vibration ν_2 we can decide the question of the planarity of the molecule in this state. Here the vibrational spectrum gives the best evidence. In a molecule such as ammonia, if the structure could be changed progressively from a planar to a pyramidal type, the energy of the lowest level out-of-plane vibration ν_2 would drop very rapidly and finally become the antisymmetric component of the ground state. In the ground electronic state of ammonia, for

example, this vibrational level has dropped until it is only 0.66 cm^{-1} above the ground state. If in the upper state of the 1600 Å band system the molecule were far from planar then successive pairs of the A_1' and A_2'' levels would coalesce and the observed alternation in band structure could not occur. Therefore there remains only the question of whether or not the molecule is slightly non-planar. If the molecule were slightly non-planar we would not expect successive vibrational quanta to form a regular series and, in particular, we would expect the second vibrational quantum to be larger than the first or third. The fact that the first few vibrational levels do form a regular progression must be taken as proof that the NH_3 molecule is planar in the excited state.

(3) In order to show that the upper electronic state is of E'' rather than E' symmetry, it is necessary to show that the $v_2' = 0$ level combines with the antisymmetric A_1'' level of the lower state. Though there is no doubt that the level we have numbered $v_2' = 0$ does combine with the A_2'' level, as mentioned previously, there can be some question as to the correct numbering of the vibrational levels. From the vibrational spectrum alone there is no proof that the level we have called $v_2' = 0$ is not $v_2 = 1, 2, 3 \ldots$. The best evidence that the numbering we have used is the correct numbering, comes from the rotational constants. For a planar symmetric top molecule $B_e = 2C_e$ and we expect B_0 to be very nearly equal to $2C_0$. With the vibrational numbering we have used, $B_0 = 10.29$ and $2C_0 = 10.34$. If this numbering is increased by one then, by extrapolating, we find that $B_0 = 10.89$ and $2C_0 = 10.26$. Thus it appears that the rotational constants give strong evidence in support of the vibrational numbering which we have used. It must be admitted, however, that we have observed a very large α_2^B and it is possible that the other α^B values are equally large. If this is so, then it is possible that the agreement between B_0 and $2C_0$ which we have observed is fortuitous.

From the above discussion it appears that, though some of the characteristics of the band system have not been established with certainty, most of the major characteristics can be deduced with confidence and that these are in agreement with the transition discussed in Section II.

In addition to the ν_2 progression described above, a weaker progression with about the same spacing has been observed. One of these bands is shown in Fig. 5. Bands have been observed at 64687, 65639, 66607, 67602, and 68598 cm^{-1}. The first observed member of this progression is on the low-frequency side of the 6–0 band and further members occur between succeeding bands of the main progression. Each band is characterized by a very diffuse absorption maximum at the high-frequency side and about 10 strong diffuse lines at lower frequencies. At still lower frequencies there are a number of somewhat sharper lines which show no regularity except in the first band of the progression where perhaps by accidental coincidences a series of strong broad lines appears. One particularly strong line which occurs near the center of each band and which appears to be similar in all the bands was measured and is given above as the position of the band.

PLATE I

FIG. 4. The 3-0 band of the 1600 Å system of NH_2. The lines of the two subbands with $K'' = 3$ are shown. These subbands are strong since levels in which K'' is an even multiple of 3 have statistical weights twice that of the others.

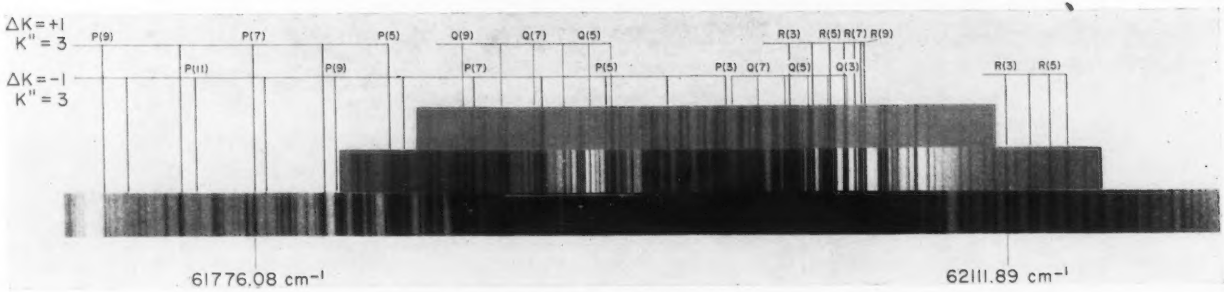

FIG. 5. The 66607 cm^{-1} band of the weaker progression.

An attempt was made to analyze the bands but without success.* The diffuseness of the lines prevented accurate measurements and the number of lines observed is considerably less than expected for either a parallel or perpendicular band. It is possible that the extent of the predissociation depends on the J and K value of the levels and that certain of the levels are so diffuse that they do not give rise to recognizable lines.

In the weaker progression as in the main progression the bands fade out at longer wavelengths. Hence it is not possible to determine whether or not the first observed band is the first member of the progression. Thus, without an analysis of the bands and without even a true vibrational numbering of the bands it is impossible to determine whether they arise from an excited electronic state different from that of the main progression or from a $\nu_1+n\nu_2$ progression of the same electronic state. If we consider electronic–vibrational interaction discussed below, it is also possible that the bands arise from a $\nu_3+n\nu_2$ progression where ν_3 is the degenerate N—H stretching vibration.

V. DISCUSSION

Walsh and Warsop have considered the various electronic states of ammonia and have assigned the 1600 Å system to a transition in which an electron is excited from a non-bonding orbital to a Rydberg orbital. They have also pointed out that the latter orbital probably correlates with a p-type atomic orbital and that in the excited state the molecule should become planar (or nearly so) and that the N—H bond distance should change very little. The results of the analysis of the bands are largely in agreement with this assignment and only in the assignment of the upper state to the E'' rather than the A_1' state resulting from the (a_2'') (np) configuration must this interpretation be altered.

Jahn and Teller have pointed out that if a molecule such as NH_3 is excited to a degenerate electronic state the molecule may be unstable with respect to motions of the nuclei which correspond to the degenerate modes of vibration of the molecule. Under these conditions the molecule assumes some symmetry lower than C_{3v} and the degeneracy of the electronic state will be split. No detailed analysis of the spectrum of any molecule showing a Jahn–Teller effect has yet been carried out and the 1600 Å bands of ammonia, which have a degenerate upper state, were examined to see if they showed evidence of this effect. As has been discussed earlier, the rotational analysis showed that the energy levels of the upper state are those of a symmetric top modified only by a Coriolis perturbation of the type described by Garing, Nielsen, and Rao. It is true that the rotational energy levels can not be reproduced very precisely by the equations but, nevertheless, they give no clear evidence of molecular distortion. It has been pointed out by Longuet-Higgins, Öpik, Pryce, and Sack (1958) and by Moffitt and Liehr (1957) that one of the major effects of a Jahn–Teller interaction is the appearance of one or more of the degenerate

*These bands have now been shown to be parallel bands. A report on the analysis of this band system will be published in the near future.

modes of vibration in the absorption spectrum. As we have seen there is no clear-cut evidence for this, though it is just possible that the weak progression described previously does involve the degenerate ν_3 vibration. Thus we must conclude that the 1600 Å bands yield no information regarding the Jahn–Teller effect.

The separation between the A_1 and A_2 levels with $K = 1$ and the J dependence of the separation between the $+l$ and $-l$ levels of a given K have been interpreted above as 'giant l-type doubling' of the type described by Garing, Nielsen, and Rao. This effect is the result of an interaction between an E and an A type vibrational level which are separated by only a small energy difference. In the excited state of ammonia, we have no knowledge of the A levels but the only ones likely to be close to the observed $v_2 = 1$ state are those resulting from the E type in-plane bending vibration. It is possible that this in-plane vibration may have a much lower frequency than the corresponding one in the ground state where it lies at 1626 cm^{-1}. It also appears possible that the observed effect is electronic rather than vibrational in origin and that the interaction is between the observed E'' state and an unknown non-degenerate electronic state. The question of whether the interaction is electronic or vibrational in origin could be settled by an examination of the $v' = 0$ vibrational level, which should show the effects of an electronic but not a vibrational interaction. Unfortunately the few lines of the 0–0 band which can be measured and assigned with certainty have, as their upper states, rotational levels which are not particularly sensitive to the value of q. Finally we can not rule out the possibility that it is a slight 'Jahn–Teller distortion' of the molecule rather than a 'giant l-type doubling' which is responsible for the observed effect.

There remain several aspects of the upper state, discussed here, which could be investigated further. It may be possible theoretically to obtain some understanding of the large value of α_2^B and of the particular value of ζ which has been found. The spectrum of ND_3 has in part been photographed and this remains to be analyzed. Also the spectra of the mixed species NH_2D and ND_2H have not been analyzed. These two molecules are particularly interesting since they are of C_{3v} symmetry in the sense that the electronic wave function will have a threefold symmetry but are very asymmetric tops in that the three moments of inertia are widely different from each other. A study of the interaction between electronic vibrational and rotational motion in these molecules would be of considerable interest.

The authors are indebted to Dr. G. Herzberg, who read the manuscript and made numerous suggestions, and to Mr. F. Alberti for taking the plates.

REFERENCES

BENEDICT, W. S. 1935. Phys. Rev. **47**, 641.
BENEDICT, W. S. and PLYLER, E. K. 1957. Can. J. Phys. **35**, 1235.
BENEDICT, W. S., PLYLER, E. K., and TIDWELL, E. D. 1958. J. Research Natl. Bur. Standards, **61**, 123.
DUNCAN, A. B. F. 1935. Phys. Rev. **47**, 822.
——— 1936. Phys. Rev. **50**, 700.

DUNCAN, A. B. F. and HARRISON, G. R. 1936. Phys. Rev. **49**, 211.
GARING, J. S., NIELSEN, H. H., and RAO, K. N. 1959. J. Mol. Spectroscopy, **3**, 496.
HERZBERG, G. 1945. Infrared and Raman spectra of polyatomic molecules (D. Van Nostrand Company, Inc., New York).
LONGUET-HIGGINS, H. C., ÖPIK, U., PRYCE, M. H. L., and SACK, R. A. 1958. Proc. Roy. Soc. A, **244**, 1.
MOFFITT, W. and LIEHR, A. D. 1957. Phys. Rev. **106**, 1195.
WALSH, A. D. and WARSOP, P. A. 1960. In press.

RADIO-STAR SCINTILLATIONS AND THE AURORAL ZONE[1]

P. A. Forsyth and K. V. Paulson

ABSTRACT

A continuous series of observations of scintillations of the radio star, Cassiopeia A, carried out at Saskatoon at a frequency near 53 Mc/s over a period of nearly 4 years has been analyzed. The altitude-angle dependence of the scintillations was very strong in 1955 but weak in 1958. This behavior suggests that the scintillations are not produced in a uniform layer of the atmosphere. It seems more likely that the scintillations arise most strongly in regions of the atmosphere closely associated with the auroral zone and that these regions migrate southward during years of intense sunspot activity.

INTRODUCTION

When a radio star is observed at frequencies in the very high frequency range the signal strength fluctuates in a random manner. These scintillations have been shown to arise in the ionosphere (Little 1951; Hewish 1952*a*), but the nature and precise location of the ionic inhomogeneities that cause the scintillations are uncertain. The earlier investigations (see, for example, Hewish 1952*b*) found that the scintillations showed a strong solar-diurnal variation, with a maximum of occurrence during the night hours. Later, when regular observations were begun in Canada in 1953 (Hartz 1955) it was noticed immediately that the solar-diurnal variation was not particularly strong. This fact was attributed to the proximity of the auroral zone. One possibility is that a new mechanism becomes dominant in the production of scintillations near the auroral zone, but convincing evidence of this new mechanism has still to be presented. The usual assumption has been that the scintillations are generated in the ionosphere at heights of 300 to 400 km and that this height range applies equally well to the scintillations observed near the auroral zone and to those observed at lower latitudes.

The principal radio source for scintillation studies in Canada has been the very intense radio star, Cassiopeia A, which is circumpolar for all Canadian stations (Dec. +58.5°). With very simple equipment it is possible to observe this source continuously, even though it greatly changes its position in the observer's sky during the course of a day. For example, at Saskatoon (latitude 52.1° N.) the source is about 6.4° north of the zenith at upper transit and about 20.6° above the northern horizon at lower transit. The necessary equipment has been described by Hartz (1955) and by Reid (1957).

The variation of occurrence of scintillations with altitude angle (or with sidereal time) has been studied by Hartz (1955) for Ottawa and by Reid (1957) for Ottawa and Saskatoon. Hartz observed that scintillations occurred much more often when the source was at low altitude angles. He interpreted this effect as being due to the longer transmission path through the ionosphere

[1]Manuscript received January 12, 1961.
Contribution from the Institute of Upper Atmospheric Physics, University of Saskatchewan, Saskatoon, Sask.

for the smaller altitude angles. Using this interpretation, it should be possible, at least in principle, to determine the height of the active region by studying in detail the dependence of the scintillations upon altitude angle. Hartz attempted this determination but his results were not conclusive. Reid noticed an asymmetry about the time of lower transit in the scintillation rates observed at Saskatoon, and subsequently detected a similar asymmetry (in the opposite sense) in some records obtained at Ottawa. He deduced that the irregularities responsible for the scintillations were greatly elongated along the magnetic field direction and tended to drift along circular paths centered on the magnetic dip pole.

Still more recently, Hartz (1959) has pointed out that many features of the observed sidereal-time variations might be explained equally well by postulating that the ionosphere becomes progressively more disturbed as the auroral zone is approached, and that the occurrence of scintillations depends only on the degree of disturbance that exists in that part of the ionosphere traversed by the radio path from the radio star to the receiver. Since this path typically traverses the ionosphere at points separated by several hundreds of kilometers for upper and lower transits, a quite reasonable gradient of ionospheric disturbance with distance from the center of the auroral zone would be required to explain the observations. In support of this suggestion Hartz refers to unpublished results obtained by Ryan and Harrower (at Kingston, Ontario) which apparently showed that the scintillation behavior of radio sources in the southern sky was quite different from that of sources in the northern sky. Hvatum and Orhaug (1957) advanced a somewhat similar suggestion to explain a "scintillation rate step" that they observed at Gothenburg, Sweden. In their case, the change appeared suddenly as the transmission path entered or left a region of the ionosphere which the authors associated with the auroral zone. Also, the observations of Tuominen, Kataja, and Riihimaa (1960), made in Finland, indicate a relatively small variation of scintillation rate with altitude angle of the source. Although they suggest that this effect is due to systematic motions it can also be ascribed to the presence of disturbed (auroral) regions at high altitude angles. The purpose of the present paper is to draw attention to the fact that the nature of the sidereal-time variation of scintillations, observed at Saskatoon, changed very considerably over a period of 4 years. This change is such as to rule out the variation of ionospheric path-length as the dominant factor in the sidereal-time variation. It seems more likely that a disturbed region of the ionosphere in the neighborhood of the auroral zone gives rise to the more intense scintillations. According to this interpretation the Saskatoon data indicate a movement of the auroral zone toward lower latitudes during years of high sunspot number, as has been deduced previously by Davies (1948) from optical evidence.

ANALYSIS AND RESULTS

For studies of radio-star scintillations it is customary to record the received signal strength by means of a moving chart recorder. In the analysis of the

charts a scintillation amplitude index and a scintillation rate index are assigned to each hour. Ideally, the amplitude index is proportional to the fractional fluctuation of the signal amplitude, and the rate index to the number of fluctuation peaks that occur in a given time interval. In practice, because of the limited resolution of the record, the two indices are assigned to each hour on the basis of the visual appearance of the record. A relatively small number of classes is used for each index. Two analysts may differ in the class assignment of a particular record, but there is no reason to suspect that the use of an absolute scale would greatly improve the quality of the data. Typical examples of chart records corresponding to different amplitude indices have been given by Hartz (1959) and to different rate indices by Reid (1957).

At Saskatoon, the scintillation recorder was put into operation on a frequency of about 53 Mc/s, in 1954 and a consistent set of records is available covering the period from January 1955 through to the autumn of 1958. These records were scaled on a routine basis as they were produced. Recently, in the course of a study of some of the later data it was noticed that the sidereal-time behavior was quite different from that found earlier by Costain (1955) and that reported by Reid (1957). Since several different analysts had carried out the scaling of the records for various parts of the 4-year period it was first necessary to verify the consistency of the chart analysis. This was done by having a single analyst go back to the original records and scale sample periods overlapping each of the original changes in analyst. Also, randomly picked samples of record were scaled and the indices compared with those derived earlier. While occasional differences (of one unit) occurred between the new and old indices there were no systematic differences that could affect the averaged results. Also, it was apparent from the records that while changes of equipment sensitivity had occurred, the reliability of the derived indices had not been affected thereby.

The mean monthly index for each hour of sidereal time after upper transit of the radio source was derived. These indices were used to compute 6-month running means. This computation resulted in a group of 40 monthly sets, each set consisting of 24 individual numbers, and each number representing the index for a single hour of sidereal time averaged over a 6-month period. Each set was then subjected to an harmonic analysis to determine the phase and amplitude of the harmonic component representing the 24-hour (sidereal) component of the variation. The results are shown in Figs. 1 and 2 on harmonic dials of the type described by Chapman and Bartels (1940). These dials show the time of maximum by angular position measured clockwise from the vertical, and amplitude by distance from the origin, of the 24-hour harmonic component of the time variation. Figure 1 shows the 40 values for the rate index variation plotted on the harmonic dial with the successive values joined by a straight line. Figure 2 gives the same information for the amplitude index variation.

Figures 1 and 2 give no information concerning the fractional variation of the index values within each monthly set. In order to indicate the long term trend of the mean monthly indices in relation to the harmonic variations shown

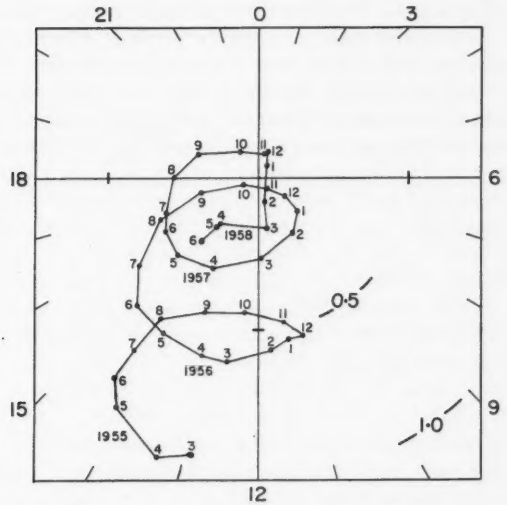

FIG. 1. Harmonic dial showing the phase and amplitude of the 24-hour sidereal component of the variation in scintillation rate index. Time is measured from upper transit of the source.

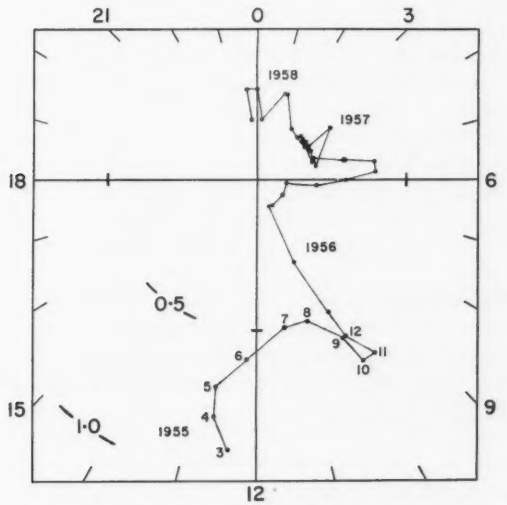

FIG. 2. Harmonic dial for the 24-hour variation in amplitude index covering the same period as that of Fig. 1.

in Figs. 1 and 2 the data were treated in the manner indicated in Figs. 3 and 4. In each monthly set the 12 values corresponding to the 6 hours before and 6 hours after upper transit were averaged to produce a mean "upper transit index". The remaining 12 values were averaged to produce a mean "lower transit index". These two values are plotted against time (in months) in Fig. 3 for the rate indices and in Fig. 4 for the amplitude indices. The smoothed sunspot numbers for the same period are plotted also in each of these figures.

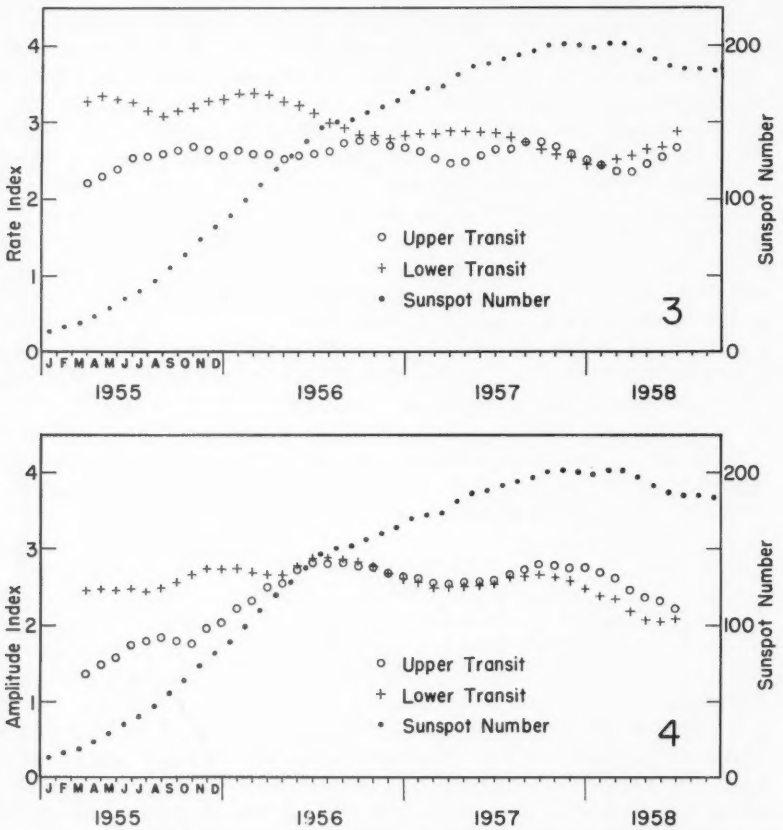

FIG. 3. Graph of the 6-month running means of the scintillation rate index for the 12 hours near upper transit, and for the 12 hours near lower transit, together with the smoothed observed sunspot numbers.

FIG. 4. Graph showing the same information as that of Fig. 3, for the amplitude indices.

DISCUSSION

An examination of Fig. 1 shows an interesting trend in the sidereal-time variation of the rate indices over the 46-month period of observation. The amplitude of the variation decreases from one index unit at the beginning of

the period to a small value at the end. The annual loops formed on the harmonic dial are obviously due to a solar-diurnal variation. The phase of this variation indicates that the maximum occurs near midnight (in general agreement with the British observations) but the amplitude is very much less than the sidereal-time variation.

The phase of the main (sidereal) variation, as shown in Fig. 1, indicates that the maximum occurs about 13 hours after upper transit or about 1 hour after lower transit. This displacement of the maximum from the time of lower transit is just the asymmetry found by Reid by a different method, using some of these same data. It is interesting to note that the 1-year period chosen by Reid (starting in April 1955) happened to be the year when the sidereal variation was strongest in the Saskatoon observations. By 1958 there was little variation of the scintillation rate with position in the sky. Figure 3 shows that the effect can not be ascribed to a general decrease in scintillation activity. The mean level of activity changed very little over the 4-year period, but the "lower transit index" decreased to the value of the "upper transit index".

The behavior of the amplitude index, as indicated in Figs. 2 and 4, is only slightly different from that of the rate index. From Fig. 2 it may be seen that the sidereal-time variation disappeared more rapidly for the amplitude index than for the rate index, being virtually complete about midway through 1956. From Fig. 4, the predominant effect in this change seems to have been an increase in the "upper transit index".

It seems most likely that the observed behavior of the scintillation indices is linked in some way to solar activity. It may be noted that the sidereal (altitude angle) variation was very prominent for periods when the sunspot number was appreciably less than 100, and very small for periods when the sunspot number was much above 100. Unfortunately there seems to be no way in which this link can be established firmly from the present data. A much longer series of observations, extending over about 10 years, would be required.

On the other hand, the present data do seem to rule out the possibility that the sidereal variation is due to the variation of path-length in a relatively uniform layer. This mechanism, considered in some detail by Hartz (1955) and Reid (1957), would lead to a decrease in sidereal variation only for periods when the mean scintillation activity was low.

The recurring suggestion that the scintillation activity at Saskatoon is directly connected with the auroral zone gains some support from the present measurements. The observations could be explained by a southward migration of the auroral zone during periods of intense auroral (and solar) activity. Such a migration was reported by Davies (1948) based on a large number of visual observations of aurora obtained at various times in the period 1932 to 1947. He deduced that the southern limit of the auroral zone is nearly overhead at Saskatoon during sunspot minima and well to the south of Saskatoon during sunspot maxima. Although not as clearly established, the northern edge of the auroral zone seems to be subject to a similar migration. The variation of auroral activity with geomagnetic latitude is reasonably well known, and

there is some evidence that the variation of radio-auroral activity is similar (Forsyth, Green, and Mah 1960). The radio-aurora (detected by radar or radio-scatter measurements) is generally located at heights near the 100-kilometer level and it is usually assumed that the scintillations are produced at heights near or above the 300-kilometer level, although the evidence supporting this assumption, at least for the Canadian observations, is so scanty as to be suspect. It can be argued that, whatever the nature of other sources involved, radio-aurora should contribute to the production of scintillations.

In any case, the assumption of a geographic distribution of scintillation-producing regions, similar to that of aurora, leads to an acceptable explanation of the trends shown in Figs. 1–4. In principle, it is possible to use the details of Davies' description of the auroral zone migration and the data of Figs. 3 and 4 to deduce the height of the active region. However, the details of the migration and the causative link between aurora and scintillations, do not seem to be well enough established to justify such an analysis at this time.

Scintillation data for a frequency of 79 Mc/s obtained at Jodrell Bank in England (latitude 53° N.) and covering the same period as that of the present study have recently appeared in the literature. The detailed analysis of these data, reported by Chivers (1960), shows many interesting contrasts between the Jodrell Bank and the Saskatoon scintillations. In particular, the solar-diurnal variation of both scintillation rate and scintillation amplitude at Jodrell Bank was more pronounced than the sidereal-time variation, for the whole period of observation. The sidereal-time variation, which was weak in 1955, became stronger in 1958. This change occurred earlier in the period and more abruptly for the scintillation amplitudes than for the scintillation rates. It appears that similar changes were taking place simultaneously at Jodrell Bank and Saskatoon, but in opposite senses. The Jodrell Bank results are consistent with the suggested migration of a scintillation-producing auroral zone, if it is assumed that the zone is too far north to be observed from Jodrell Bank during years of low sunspot activity and comes into view at low elevation angles during years of high sunspot activity. Further support for this picture is provided by the fact that, in contrast to the Saskatoon results, the scintillation activity at Jodrell Bank increased markedly with increasing sunspot number.

ACKNOWLEDGMENTS

The authors are indebted to the several people who, at various times, operated the scintillation recorder or analyzed the records. Special mention should be made of C. H. Costain, H. Grigg, and D. G. Glass. The careful intercomparisons of the data to establish the consistency of scaling were carried out by Mr. C. A. Townsend.

REFERENCES

CHAPMAN, S. and BARTELS, J. 1940. Geomagnetism (The Clarendon Press, Oxford).
CHIVERS, H. J. A. 1960. J. Atmospheric and Terrest. Phys. **19**, 54.
COSTAIN, C. H. 1955. M.A. Thesis, University of Saskatchewan.
DAVIES, F. T. 1948. Paper presented to VIIIth General Assembly I.U.G.G.
FORSYTH, P. A., GREEN, F. D., and MAH, W. 1960. Can. J. Phys. **38**, 770.

HARTZ, T. R. 1955. Can. J. Phys. **33**, 476.
——— 1959. Can. J. Phys. **37**, 1137.
HEWISH, A. 1952*a*. Proc. Roy. Soc. A, **209**, 81.
——— 1952*b*. Proc. Roy. Soc. A, **214**, 494.
HVATUM, H. and ORHAUG, T. 1956. Paper presented to XIIth General Assembly, U.R.S.I.
LITTLE, C. G. 1951. Monthly Notices Roy. Astron. Soc. **111**, 289.
REID, G. C. 1957. Can. J. Phys. **35**, 1004.
TUOMINEN, J., KATAJA, E., and RIIHIMAA, J. 1960. Ann. Acad. Sci. Fennicae, A, **VI**, 62.

REPRESENTATIONS OF THE UNITARY GROUP AND WAVE FUNCTIONS[1]

H. A. VENABLES

ABSTRACT

A number of wave functions besides the spherical harmonics are obtainable from the irreducible representations of the two-dimensional unitary group.

INTRODUCTION

The irreducible representations of the rotational group as obtained from the two-dimensional unitary group $D^j_{mm'}$ are well known. Their use in the quantum theory of angular momentum has been extensively treated (Rose 1957; Sharp 1957; Wigner 1959). Where (ϕ, θ, ψ) are Euler angles

$$D^j_{mm'}(\phi, \theta, \psi) = e^{-im\phi} d^j_{mm'}(\theta) e^{-im'\psi}.$$

Here

$$d^j_{mm'}(\theta) = [(j+m)!(j-m)!(j+m')!(j-m')!]^{1/2} \cdot \frac{\sum (-1)^q \cos^{2j+m-m'-2q}\frac{\theta}{2} \sin^{2q-m+m'}\frac{\theta}{2}}{(j+m-q)!(j-m'-q)!q!(q-m+m')!}.$$

Now in the case $m' = 0$ and $\psi = 0$ the function $D^j_{m0}(\phi, \theta, 0)$ is simply related to spherical harmonics. The relation involves constants and perhaps taking the conjugate function, depending on the convention in use by the particular author (Rose 1957; Sharp 1957; Wigner 1959).

Besides the spherical harmonics it seems worth while to point out that there are wave functions, which can be obtained from the unitary representation. These functions are among the simplest and most successful in quantum mechanics. They are, where constants are omitted (Bethe and Salpeter 1957; Schiff 1949),

(i) hydrogen radial wave function

$$e^{-R/2} R^l L^{2l+1}_{n+l}(R),$$

(ii) hydrogen parabolic wave function

$$e^{-\frac{1}{2}(\xi+\eta)} (\xi\eta)^{m/2} L^m_{n_1+m}(\xi) L^m_{n_2+m}(\eta),$$

(iii) harmonic oscillator wave function

$$e^{-x^2/2} H_n(x).$$

Each function can be derived from $D^j_{mm'}$ in entirety, except for a minor adjustment required in the radial case.

[1]Manuscript received December 14, 1960.
Contribution from the University of Alberta, Edmonton, Alberta.

Attention will be fixed on $D^j_{mm'}(0, \theta, 0)$ or $d^j_{mm'}(\theta)$. This is known to be expressible in terms of Jacobi polynomials (Rose 1957; Sharp 1957)

$$d^j_{mm'}(\theta) =$$

$$(-1)^{m'-m}\left[\frac{(j-m)!(j+m)!}{(j-m')!(j+m')!}\right]^{\frac{1}{2}} \sin^{m-m'}\frac{\theta}{2}\cos^{m+m'}\frac{\theta}{2}P_{j-m}^{(m-m',\, m+m')}(\cos\theta),$$

or for $x = \cos\theta$

$$(1)\quad d^j_{mm'}(x) =$$

$$\frac{(-1)^{m'-m}}{2^m}\left[\frac{(j-m)!(j+m)!}{(j-m')!(j+m')!}\right]^{\frac{1}{2}}(1-x)^{(m-m')/2}(1+x)^{(m+m')/2}P_{j-m}^{(m-m',\, m+m')}(x).$$

LIMITING FORMS OF $d^j_{mm'}$

The Jacobi polynomials yield the Laguerre and Hermite polynomials under special conditions. Szegö (1959) and Tricomi (1955) give the relation between the Jacobi and Laguerre polynomials

$$(2)\qquad \lim_{\beta\to\infty} P_n^{(\alpha,\beta)}\left(1-\frac{2y}{\beta}\right) = L_n^{\alpha}(y),$$

and a similar relation holds for the Hermite polynomials

$$(3)\qquad \lim_{\beta\to\infty} P_n^{(\beta,\beta)}\left(\frac{y}{\sqrt{\beta}}\right) \to H_n(y).$$

These may be obtained in a number of ways. One method is to employ the differential equation (Poole 1960) to $P_n^{(\alpha,\beta)}(x)$,

$$(4)\qquad (1-x^2)\frac{d^2P}{dx^2}+\{(\beta-\alpha)-(\alpha+\beta+2)x\}\frac{dP}{dx}+n(n+\alpha+\beta+1)P = 0.$$

For the Laguerre equation change the variable x to $[1-(2y/\sqrt{\beta})]$ and let $\beta \to \infty$

$$y\frac{d^2L}{dy^2}+(\alpha+1-y)\frac{dL}{dy}+nL = 0.$$

For the Hermite equation change the variable x to $y/\sqrt{\beta}$ and let $\alpha = \beta$ followed by $\beta \to \infty$

$$\frac{d^2H}{dy^2}-2y\frac{dH}{dy}+2nH = 0.$$

The three wave functions will now be considered in turn. For the first case choose for the indices

$$j = \tfrac{1}{2}(k+4l+2n+1),$$
$$m = \tfrac{1}{2}(k+2l+1),$$
$$m' = \tfrac{1}{2}(k-2l-1),$$

and let

$$x = [1-(2R/k)].$$

This gives in (1)

$$R^{(2l+1)/2}\left(1-\frac{R}{k}\right)^{k/2} P_{n+1}^{2l+1,k}\left(1-\frac{2R}{k}\right),$$

which in the limit (2) becomes

$$R^{\frac{1}{2}}\{R^l e^{-R/2} L_{n+l}^{2l+1}(R)\}.$$

The function in the brackets constitutes the radial function. It is only the presence of the factor $R^{\frac{1}{2}}$ which prevents precise agreement between $d^j_{mm'}$ and (i).

In order to deal with the parabolic case the following indices are chosen

$$j = \tfrac{1}{2}(k+3m_1+2n_1),$$
$$m = \tfrac{1}{2}(k+m_1),$$
$$m' = \tfrac{1}{2}(k-m_1),$$

and

$$x = [1-(2\xi/k)].$$

Taking the limit as before gives

$$\xi^{m_1/2} e^{-\xi/2} L_{n_1+m_1}^{m_1}(\xi).$$

A similar function to this can be found with η as the variable, and so the product of the two functions will give (ii).

For the harmonic oscillator (iii) it is only necessary to take the limit (3) of

$$\left(1-\frac{x}{\sqrt{m}}\right)^{m/2}\left(1+\frac{x}{\sqrt{m}}\right)^{m/2} P_n^{(m,m)}\left(\frac{x}{\sqrt{m}}\right)$$

to give

$$e^{-x^2/2} H_n(x).$$

Here we have used in (1)

$$m' = 0,$$
$$j-m = n,$$

and changed the variable to $x/\sqrt{m}$.

DISCUSSION

Instead of the Jacobi equation (4) the Riemann–Papperitz equation (Whittaker and Watson 1927) to $d^j_{mm'}$ may be found and used. By procedures similar to those already employed the wave equations to the hydrogen atom and the harmonic oscillator can be readily obtained. It is interesting to observe that the Coulomb potential and the quantum differential operator are derived together simultaneously in a unified way. This seems to suggest that further examination may be of interest.

REFERENCES

BETHE, H. A. and SALPETER, E. E. 1957. Quantum mechanics of one- and two-electron atoms (Springer-Verlag, Berlin).
POOLE, E. G. C. 1960. Introduction to the theory of ordinary differential equations (Dover Publications, New York).
ROSE, M. E. 1957. Elementary theory of angular momentum (John Wiley & Sons, Inc., New York).
SCHIFF, L. I. 1949. Quantum mechanics (McGraw-Hill Book Co., Inc., New York).
SHARP, W. T. 1957. The quantum theory of angular momentum, CRL-43 (Chalk River).
SZEGÖ, G. 1959. Orthogonal polynomials (American Mathematical Society, New York), p. 59.
TRICOMI, F. G. 1955. Vorlesungen über Orthogonalreihen (Springer-Verlag, Berlin), p. 215.
WHITTAKER, E. T. and WATSON, G. N. 1927. A course in modern analysis (Cambridge University Press, London), p. 207.
WIGNER, E. P. 1959. Group theory (Academic Press, Inc., New York).

ROOM TEMPERATURE STABILIZATION OF RADIATION-PRODUCED FREE RADICALS IN BARBITURIC ACIDS[1]

J. A. R. Cloutier

ABSTRACT

Experimental evidence has shown that a boric acid glass may be used to stabilize at room temperature organic free radicals produced by radiation in a number of barbituric acid derivatives. The method and the experimental results are discussed.

INTRODUCTION

The immediate effect of radiation in most organic compounds is generally believed to be the production of free radicals which initiate several unexpected reactions. Due to the tremendous energy outbalance, it is difficult to predict where and how bond ruptures will be effected. Fortunately, experimental evidence indicates that radiation damage in many organic compounds (Smaller and Matheson 1958; Gordy, Ard, and Shields 1955*a*; O'Meara and Shaw 1957) and even in complex biological systems (Conger and Randolph 1959) follow a general pattern where most important processes may be observed, modified, and partially controlled (Patt 1953; Gordy and Miyagawa 1960). The understanding of a radiation damage mechanism presupposes the knowledge of the types of free radicals being formed and a study of their properties. The method of paramagnetic resonance has great potentialities for the identification of radicals and has been used successfully by a number of workers (Ingram 1955; Shoolery and Weaver 1955; Whiffen 1958). One of the main difficulties is that some of the free radicals are very reactive in character and must be stabilized in order to obtain concentrations which are detectable with current instrumental sensitivities. Low temperature offers an immediate solution to this problem. Free radicals are formed in a rigid medium which interferes with their recombination and allows their detection. However, when biological applications are considered, low temperature results may be misleading. It is far from being proved that reactions which occur at boiling helium or nitrogen temperature, where molecular vibrational and rotational energies are much reduced and molecular resonance conditions altered, have some significance at room temperature. Radiation damage mechanism may be totally different as more or less exemplified by Gordy, Ard, and Shields (1955*b*) with irradiated acetic acid studied at various temperatures. Room temperature irradiation and measurement under a nitrogen or helium atmosphere has also been used extensively by various research groups. However, oxidation of the unpaired electron is so pronounced with some free radical species that weak para-

[1]Manuscript received December 29, 1960.
Contribution from the Food and Drug Directorate, Department of National Health and Welfare, Ottawa, Canada.

magnetic resonances are detected only for a short time. Further, when gaseous by-products are produced during irradiation, recombination of the free radicals occurs independently of the nature of the atmosphere above the sample.

Some two years ago, initial experiments were made to study radiation effect on a series of 5,5-disubstituted barbituric acids. No resonance signals were observed when the samples were irradiated in air; only two cases yielded some information when kept under a nitrogen atmosphere. Since it was intended to carry out this research at room temperature, a search was made on how to stabilize the free radicals produced by radiation in these acids. The experimental material was dispersed in a number of substances solid at room temperature, irradiated, and tested for paramagnetic resonance absorption. Interesting results were obtained with a boric acid glass. It is the purpose of this paper to present the experimental method and data obtained over a 15-month period.

APPARATUS

Figure 1 shows a block diagram of the electron paramagnetic resonance spectrometer used in this investigation. It is of a conventional design except that it has been assembled using standard commercial units as building

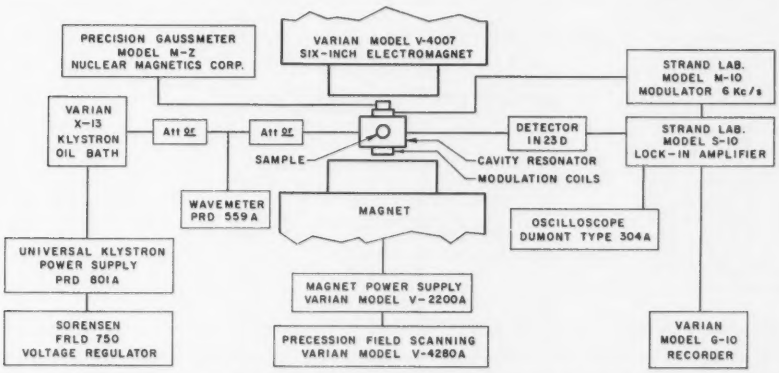

FIG. 1. Block diagram of the electron paramagnetic resonance spectrometer. Nominal operating frequency 9500 megacycles per second. Modulation frequency 6 kilocycles per second.

blocks. It operates at a nominal frequency of 9500 megacycles per second. The transmission type microwave cavity resonator is an H_{012} rectangular cell, silver-plated on the inside, fitted with two coupling irises, 0.25 in. in diameter. The Zeeman modulation coils are connected in series. Each coil was made of 500 turns #32 H.F. wire mounted on a 0.50-in. spool, has resistance of 7 ohms, and can carry a maximum current of 0.32 amp. The modulation frequency is 6 kilocycles per second. The air gap between the two cylindrical pole pieces is $1\frac{3}{4}$ inch. The homogeneity of the magnetic field at the sample position is of the order of 0.2%, as determined with a proton resonance meter. The klystron

is in a constant temperature oil bath. To date, no microwave frequency stabilization has been required, the frequency being stable enough for the type of measurement being made. The spectrometer is similar to the one used by O'Meara and Shaw (1957) and its sensitivity is of the same order of magnitude, 2×10^{14} unpaired electrons in a 100-mg sample. The information is obtained as the first derivative of the microwave energy absorption by the sample. Figure 2 shows the signal observed from diphenyl picryl hydrazyl (D.P.P.H.) in the dry state. The distance between points of maximum slope is slightly under 2 oersteds, a line width which compares quite well with published information (Gordy, Smith, and Trambarulo 1953).

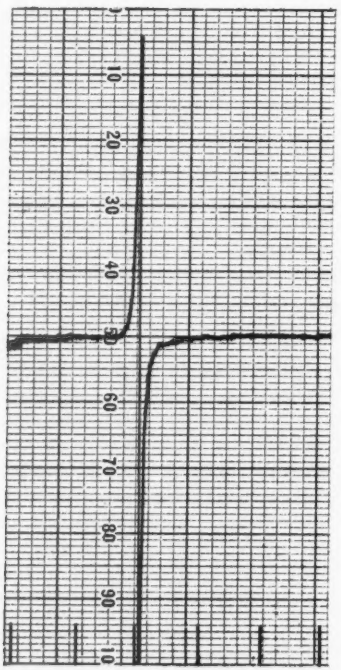

FIG. 2. Paramagnetic resonance absorption signal from diphenyl picryl hydrazyl in dry powder form. First derivative curve. $g = 2.0036$. Markers are 50 oersteds apart. Distance between points of maximum slope is slightly under 2 oersteds.

Some of the results reported here were obtained using an earlier design of the electron paramagnetic resonance spectrometer. The Zeeman modulation frequency was generated by a Krohn-Hite ultra-low frequency oscillator operating at 700 cycles per second. The output of the oscillator was amplified by a 20-watt MacIntosh power amplifier and connected to the modulation coils. The crystal detector current was fed to a Browning standing wave ratio amplifier, model TAA-16B, whose output rectifier system had been by-passed. This was followed by a Krohn-Hite model 310-AB variable band-pass filter

and a synchronous demodulator driven by the Zeeman modulation frequency oscillator. This earlier design was more flexible than the later one in the sense that either the actual signal or its first or second derivative could be selected. However, the noise level of the detecting system was much higher and made necessary the reported modifications.

MATERIAL

The barbituric acids used in this investigation are commercial products of high purity. Samples from the same lot numbers have already been characterized by members of this laboratory (Levi and Hubley 1956; Chatten and Levi 1957). Pertinent published information (Chatten and Levi 1957) is summarized in Table I for discussion purposes. Levi (1957) has reviewed the

TABLE I

Melting points of disubstituted barbituric acids

Trade name	Chemical name	Melting point, °C
Alphenal	5-Allyl-5-phenylbarbituric acid	156.0–156.7
Alurate	5-Allyl-5-isopropylbarbituric acid	140.0–143.0
Amytal	5-Ethyl-5-isoamylbarbituric acid	156.3–156.9
Cyclopal	5-Allyl-5-(1-cyclopenten-2-yl) barbituric acid	139.8–140.3
Delvinal	5-Ethyl-5-(1-methyl-1-butenyl) barbituric acid	166.0–166.9
Dial	5,5-Diallylbarbituric acid	172.5–173.0
Evipal	5-(1-Cyclohexen-1-yl)-3,5-dimethylbarbituric acid	144.8–145.2
Ipral	5-Ethyl-5-isopropylbarbituric acid	201.2–201.7
Luminal	5-Ethyl-5-phenylbarbituric acid	174.1–174.9
Mebaral	N-Methyl-5-ethyl-5-phenylbarbituric acid	115.0–116.0
Medomin	5-Ethyl-5-(1-cyclohepten-1-yl) barbituric acid	171.0–172.2
Nembutal	5-Ethyl-5-(1-methylbutyl) barbituric acid	128.8–129.4
Neonal	5-Ethyl-5-n-butylbarbituric acid	127.4–128.5
Nostal	5-(2-Bromoallyl)-5-isopropylbarbituric acid	180.3–181.2
Pernoston	5-(2-Bromoallyl)-5-(1-methylpropyl) barbituric acid	131.5–132.2
Phandorn	5-Ethyl-5-(1-cyclohexen-1-yl) barbituric acid	171.8–172.2
Rutonal	5-Methyl-5-phenylbarbituric acid	225.5–226.2
Seconal	5-Allyl-5-(1-methylbutyl) barbituric acid	96.1– 96.9
Sigmodal	5-(2-Bromoallyl)-5-(1-methylbutyl) barbituric acid	167.3–168.2
Veronal	5,5-Diethylbarbituric acid	189.6–190.4

chemical structure, synthesis, and nomenclature of the barbituric acids. The compounds studied have all the same basic structure shown in Fig. 3, the malonylurea ring to which are attached in position 5 two groups of varying

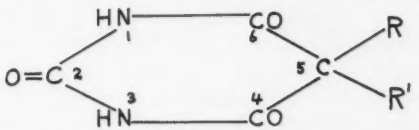

FIG. 3. Structural formula of 5,5-disubstituted barbituric acids.

complexity. (In addition, evipal and mebaral have a methyl group in position 3.) Barbituric acid itself (R = R′ = H) is non-toxic and has no hypnotic properties. It is only when both R and R′ are replaced by an alkyl, aryl, or alicyclic group that the molecule possesses hypnotic, sedative, or anaesthetic properties (Levi 1957). The heterocyclic system is a resonating structure; therefore, the

substituted barbituric acids are relatively stable molecules except when submitted to an alkaline hydrolysis. Normal physiological processes destroy only the side chains R and R′ through direct oxidative attack (Maynert and van Dyke 1949). It is thus of interest to determine the effect of radiation on this type of molecule since corresponding changes in physiological properties will likely ensue.

IRRADIATION OF THE SAMPLES

The samples were irradiated using the facilities kindly offered to this laboratory by the Commercial Products Division of Atomic Energy of Canada Limited. These were a 4000-curie Co-60 gamma cell 220, average dose rate of 350,000 rads/hour, and a 500-curie Co-60 transfer case irradiator, average dose rate of 220,000 rads/hour. Some of the samples were also irradiated with an X-ray therapy unit operated at 34 kv (peak) and 15 ma. No filter was used and the samples were simply taped to the exit window frame of the X-ray tube. In this instance, the dose rate has not been measured; however, due to the large proportion of soft radiation, it must be of the order of a few thousand rads per minute. Samples were irradiated either with the Co-60 sources or the X-ray therapy unit; no differences were observed as far as the experimental data presented in this paper are concerned.

RIGID DISPERSIVE MEDIUM

A number of substances were irradiated and studied for electron paramagnetic resonance (E.P.R.) absorption. The irradiation and the measurements were performed at room temperature and in air. The samples received a dose which varied from 5 megarads to 50 megarads. The E.P.R. determinations were done within one half of an hour after removal from the radiation source. Figure 4 presents the results observed for commercial grade beeswax, sulphur, gelatine, paraffin, m.p. 55°–56° C, and boric acid. It is evident that, for this experiment, the spectrometer had to be operated at maximum sensitivity and high amplification to detect any possible resonance.

Beeswax, Fig. 4A, gave a signal which disappeared in about two hours after irradiation. It is an odd line spectrum of width 100 oersteds, centered on a g-value equal to that of D.P.P.H. No other attempts were made to study this signal as this observation eliminated beeswax as a possible dispersive medium to use in this experiment. Sulphur powder, Fig. 4B, was melted, allowed to solidify in rod form, and irradiated. Gelatine, Fig. 4C, was dissolved in a little water, the solution was allowed to set overnight in a mold and irradiated the following day. Paraffin, m.p. 55°–56° C, Fig. 4D, was simply heated, shaped into small cylinders, and irradiated. Boric acid, Fig. 4E, was heated slowly until a viscous liquid formed; some of this liquid was drawn out at the end of a pyrex rod and rapidly shaped into a cylindrical rod by rolling it between two microscope slides. No E.P.R. signals could be observed from these last four cases, even at the highest radiation dose. It is understood that, possibly, with a more sensitive spectrometer, resonances might have been observed at room temperature from these irradiated substances. However, several experiments showed without doubt that the apparatus

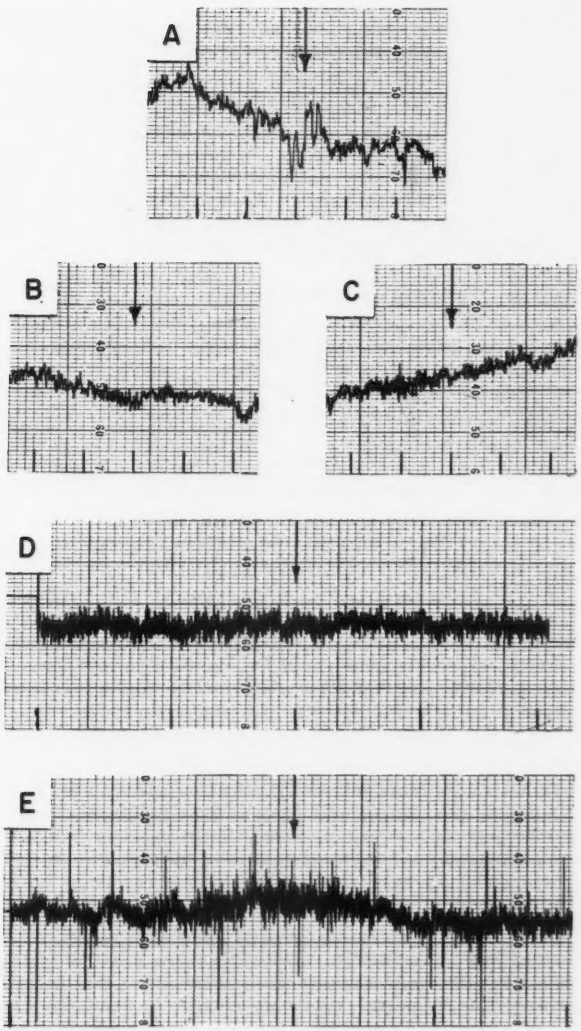

FIG. 4. Substances investigated for use as rigid dispersive medium. A, beeswax; B, sulphur; C, gelatine; D, paraffin 55°–56° C; E, boric acid glass. First derivative curves. Markers are 100 oersteds apart for A, B, and C and 25 oersteds for D and E. Vertical arrows indicate the position of D.P.P.H. resonance.

used in this research was unable to detect any absorption signal from these blanks. For practical reasons, only the paraffin and the boric acid methods were applied to this study.

Paraffin is known to easily form hydrogen bonding; therefore, it has always been used with circumspection and mainly as a check on the results obtained with boric acid. On the other hand, boron forms a variety of complexes with many organic compounds (Lappert 1956). However, boron has two isotopes of non-zero ground spin: B-10, 18.83% abundance, spin 3, and B-11, 81.17% abundance, spin 3/2 (Hollander, Perlman, and Seaborg 1953). The presence of boron near a resonating electron will then be indicated by a further hyperfine splitting of the signal into equal intensity septets or quartets. These types of hyperfine splittings have not been observed in this study.

PREPARATION OF SAMPLES

The microwave cavity resonator is designed to accept standard pyrex tubes of 2 mm i.d. The samples irradiated in air were simply transferred to one such tube after irradiation and studied. For irradiation and measurement under a nitrogen atmosphere, the sample was introduced into a long tube and flushed slowly for a few minutes with nitrogen; the tube was then sealed during the flushing. Only the small portion of the tube containing the sample was irradiated, the rest being carefully shielded from the main X-ray or gamma-ray beam. After irradiation, the sample was shifted by tapping to the non-irradiated end of the tube and the E.P.R. measurements were made. This technique was used by O'Meara and Shaw (1957) and many others. For preparation in paraffin, a 30% mixture by volume of the dry sample powder was made with paraffin held at 60° C; the mixture was molded into small cylinders $\frac{1}{2}$ in. long and 3.5 mm in diameter. The cylinders were irradiated and then gently pressed into position at the end of an empty pyrex tube for their introduction into the spectrometer cavity. To prepare the samples in a boric acid glass, the boric acid was rapidly heated on a hot plate to 155°±5° C in a 5-ml beaker. Small amounts were used to make sure that a transparent liquid would be obtained without the formation of a white crust. The powder sample was added and swiftly mixed with the viscous liquid. Twenty to thirty per cent concentration was normally used. The small cylinders were shaped as already outlined above. They were irradiated and mounted for study at the end of a pyrex tube with a drop of household cement.

Referring to Table I, it is seen that almost half of the barbituric acids studied were melted during the preparation of the boric acid glass. Boric acid and the barbituric acids being polar compounds, a molecular dispersion of one into the other does take place. This represents ideal cases where individual barbituric acid molecules are trapped within spherical holes in the rigid matrix. No free radical is likely to diffuse from one site to the other and yet it may be assumed that the energy levels of the solute molecules are not markedly altered by the presence of the rigid surroundings. For those acids which remained a solid during the preparation of the glass, it is known that

barbituric acids are moderately soluble in hot water. Therefore, the water resulting from the decomposition of boric acid dissolves some of the powder sample or helps breaking the larger crystals into much smaller fragments. In any case, a molecular dispersion of this second group of compounds of melting points higher than 160° C in the boric acid glass is also achieved but to a smaller extent. Incidentally, it is interesting to note at this time that E.P.R. signals recorded from glasses containing samples of lower melting points than 160° C were noticeably stronger than those of higher melting points.

Glassy solvents were introduced in spectroscopy as early as 1896 by Schmidt for the study of the phosphorescence of ultraviolet irradiated molecules. This technique was then used extensively by many others (Reid 1958) in a similar application. Lewis, Lipkin, and Magel (1941) showed, for instance, using fluorescein dissolved in boric acid, that the phosphorescent state could be characterized by its absorption spectrum. Phosphorescence is explained by the presence of a metastable excited state, the triplet state, which delays the return of an excited molecule to its normal ground state. The study of the triplet state is not too distant from the research reported in this paper since both investigations are concerned with the study of the behavior of unpaired electrons: the former makes use of the delayed light emission by the excited molecule; the latter, the paramagnetic property of the radicals which are formed.

EXPERIMENTAL RESULTS AND DISCUSSION OF INDIVIDUAL CASES

1. Alurate

It has already been shown that when a boric acid glass or a paraffin rod was irradiated alone, no paramagnetic resonance absorption signal could be detected at room temperature and at the operating sensitivity of the spectrometer used for this research. It is now pertinent to show that with the class of compounds studied, the effect of the solid matrix on the shape of the recorded signals was but negligible. Figure 5 illustrates a comparative study which could be made with alurate. Photographs A to E were obtained from irradiated alurate in a boric acid glass, photographs F and G from irradiated alurate in paraffin, and photograph H from irradiated alurate dry powder kept under a nitrogen atmosphere. Concentrating on the main structure of the signal, which evidently is an odd line spectrum of five resolved components, it is seen that the same type of signals was obtained from the same compound irradiated under three completely different experimental conditions. The slight discrepancies may easily be accounted for by the following consideration of the individual signals.

Figure 5A was recorded 15 minutes after irradiation. The symmetrical pattern has a non-uniform spacing. Numbering the peaks from left to right, 1, 2, 3, 4, 5, 6, 7, the two satellites 1 and 7 stand out from the main pattern at a greater distance than the uniform spacing between the central lines. These two satellites may be thought to be the normal H doublet; however, their separation of only 115 oersteds precludes this assignment. It is rather believed that Fig. 5A is a complex pattern resulting from the superposition of two

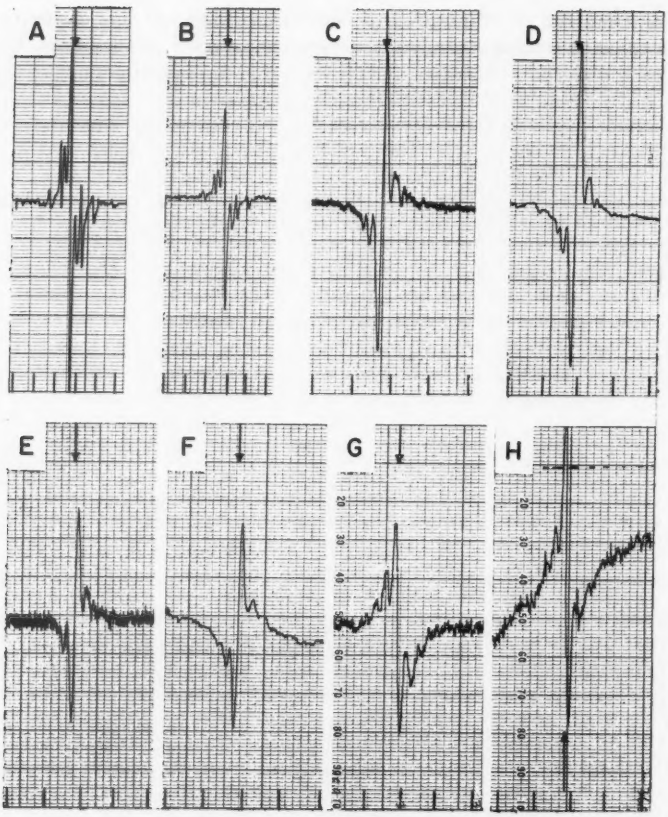

FIG. 5. Paramagnetic resonance absorption signals from irradiated alurate. First derivative curves. Photographs A, B, C, D, and E are from a boric acid glass; F and G from paraffin; and H from the dry salt under a nitrogen atmosphere. Times after irradiation: A, 15 min; B, 130 hours; C, 3 months; D, 4 months; E, 15 months; F, 1 hour; G, 1½ months; H, 30 min. Markers are 50 oersteds apart. Vertical arrows indicate the position of D.P.P.H. resonance.

equally spaced quintets: quintet I (1, 2, 4, 6, 7), average spacing 26 oersteds, and quintet II (2, 3, 4, 5, 6), average spacing 12 oersteds. The time effect study on this signal indicates such a possibility. Figure 5B was obtained 130 hours after irradiation. It is noticed that the relative heights of peaks 1, 2, 6, and 7 have decreased with respect to those of peaks 3 and 5. Further, this decrease is more and more pronounced in Figs. 5C and 5D which were obtained 3 and 4 months after irradiation. At the end of 15 months after irradiation, Fig. 5E, the two satellites are not resolvable from noise. The intensity of the signal as such is evidently reduced; however, the contour of the first derivative plot does not significantly differ from that at 4 months after irradiation. It would therefore seem that during the first 4 months after

irradiation, quintet I corresponding to some reactive free radical disappear even when the sample is dispersed in a boric acid glass. Quintet II, associated with the more stable free radical which remains after 15 months in a boric acid glass, is also obtained from alurate irradiated in paraffin, Figs. 5F and 5G, and the dry powder kept under a nitrogen atmosphere, Fig. 5H. The signal width is 5 to 10 oersteds larger with the later two methods of preparation. However, an effective reduction in the spin–spin interaction may readily explain the narrowing of the signal when alurate was dispersed through the boric acid glass.

The presence of quintets in the resonance absorption pattern from irradiated alurate eliminates the possibility that the odd electron was located anywhere along the ring structure of the molecule. Assuming the hyperfine splitting of the observed signal was due to proton interaction exclusively, the required free radicals with four nearly equivalent protons may be obtained by modification of either one of the alkyl groups in position 5 of the malonylurea ring: such as the removal of one CH_3 of the isopropyl group or the removal of the hydrogen atom on carbon 2 of the allyl group. More complex mechanisms could be formulated. Specific assignment of the two observed quintets to given free radical species would require more experimental work. It is nevertheless useful to note that the main effect of radiation on alurate was centered about the two side chains in position 5. Further, the boric acid glass preparation yielded the same information as that obtained from the other two methods of preparation. The boric acid glass, however, seemed to stabilize an additional free radical species which apparently was too reactive to be detected with the other two methods of preparation. Other cases of good agreement between the results obtained with the boric acid glass and the paraffin methods of preparation were observed during this study. These will be reported in their appropriate sections. Alurate presented the definite advantage over the other cases studied that the results from the above two methods of preparation could also be compared to those obtained from the dry powder itself kept under a nitrogen atmosphere.

2. Neonal, Amytal, and Dial

Neonal, amytal, and dial, when prepared in a boric acid glass, all gave the same E.P.R. signal 1 hour after irradiation. It was, as presented in Figs. 6A, 6E, and 6H for these compounds in the above order, a well resolved triplet of approximately equal intensity. The field separation between adjacent lines was 12 oersteds. Three months after irradiation, the shape of the signals from neonal and amytal, Figs. 6B and 6F, was unaltered, while that from dial, Fig. 6I, was somewhat less resolved. The three signals were all narrower, the line separation being 10 oersteds. This line separation remained constant over the next 12-month period as shown in Figs. 6C, 6G, and 6J for neonal, amytal, and dial, respectively. The resolution of the lines was preserved and their intensities were only slightly reduced.

The appearance of an equal intensity triplet leaves no doubt as to the location of the odd electron. Nitrogen is the only atom with spin 1 in these three molecules. Further, since nitrogen is absent from the side structures of

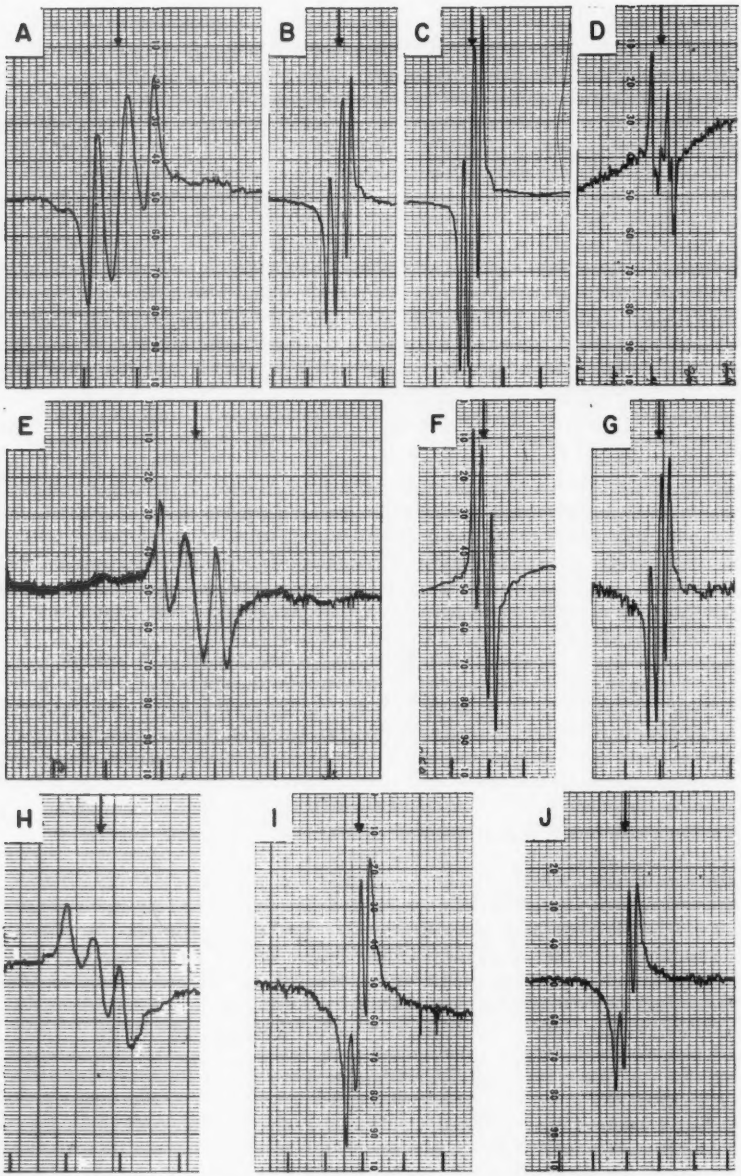

FIG. 6. Paramagnetic resonance absorption signals from irradiated neonal, A, B, C; from irradiated amytal, D, E, F, G; and irradiated dial, H, I, J. First derivative curves. The above curves were obtained from a boric acid glass except photograph D which was from paraffin. Times after irradiation: A, D, E, H, 1 hour; B, F, I, 3 months; and C, G, J, 15 months. Markers are 25 oersteds apart for A, E, H and 50 oersteds for the others. Vertical arrows indicate the position of D.P.P.H. resonance.

the molecules, it follows that the odd electron is located about one of the two nitrogen atoms in positions 1 and 3 of the malonylurea ring. Referring to Fig. 3, it seems obvious that once an H atom has been removed by radiation, for example from position 1, the odd electron would circulate around the ring structure and interact with not only the N atom in position 1 but also that in position 3 along with its associated H atom. In other words, if this were so, one would expect not a single triplet but a triplet of triplets of doublets, since these are non-equivalent atoms. However, it has already been shown (Newman 1956) that the barbituric ring is not planar. Position 5 acts as a potential barrier which prohibits motion of the π-electron around the ring. Therefore, it is quite possible that the odd electron is compelled to spend all of its time close to a given N atom, either in position 1 or position 3.

When neonal was prepared in paraffin and irradiated, a complex signal was obtained, Fig. 6D. It is believed that this signal is an unresolved triplet of doublets. The total width of the signal and the separation of each doublet are about the same as those already reported for the boric acid glass preparation. Therefore with the paraffin preparation, it is assumed that the same free radical is produced; however, coupling to a hydrogen atom from the surrounding matrix promptly takes place.

The resonance signals presented in Fig. 6 match perfectly well those given by Cole *et al.* (1957, 1958) and Foner *et al.* (1958), who studied the paramagnetic resonance of nitrogen atoms trapped in a molecular nitrogen matrix at 4.2° K. Figure 6E even shows evidence of a side structure to the main triplet, which was discussed by Cole *et al.* in their second article (1958) in terms of zero field splittings in atomic nitrogen. The only discrepancy is in the splitting constant which apparently is a factor 2 larger when nitrogen is bound as it is in the barbituric acid ring as compared to when a free nitrogen atom is simply trapped in a solid matrix.

3. Cyclopal

Irradiated cyclopal in paraffin, Fig. 7A, under a nitrogen atmosphere, Fig. 7B, and prepared in a boric acid glass, Fig. 7C, yielded essentially the same E.P.R. signal right after irradiation. It was a complex pattern of about 130 oersteds, total spread. Four months after irradiation, the signal from the boric acid glass preparation, Fig. 7D, showed some changes in the relative heights of the first derivative peaks and a definite narrowing. When preparing the boric acid glass, it was noticed that, in a few instances, a strong reaction would take place as soon as the cyclopal powder was added to the molten boric acid. Some gas would be liberated and the mixture would turn black. This would happen when the mixture was at a temperature slightly over 165° C. These black glasses were irradiated. An equal intensity triplet of averaged spacing 12 oersteds, Fig. 7E, was obtained shortly after irradiation and was still showing with minor contour changes 4 months after irradiation, Fig. 7F.

The signal from the black glasses is undoubtedly due to nitrogen nuclear coupling with the electron spin. A similar free radical assignment to that of the previous group of compounds just studied is then suggested. It is believed

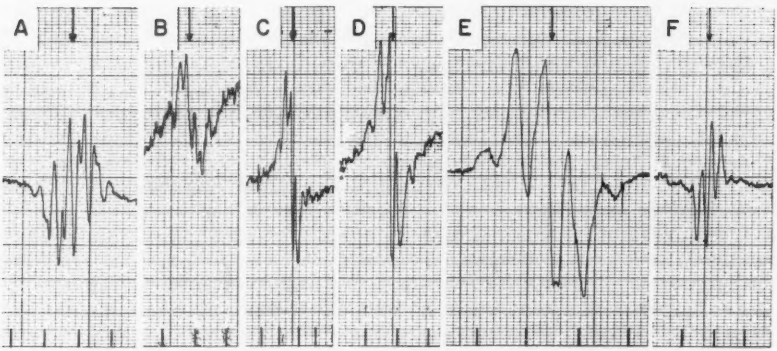

FIG. 7. Paramagnetic resonance absorption signals from irradiated cyclopal. First derivative curves. Photograph A was obtained from paraffin, B from the salt under a nitrogen atmosphere, and the others from a boric acid glass. Times after irradiation: A, B, C, E, 1 hour; D, F, 4 months. Markers are 25 oersteds apart for E and 50 oersteds for the others. Vertical arrows indicate the position of D.P.P.H. resonance.

that the reaction at temperature above 165° C is accompanied by destruction of the ring structure, 2-cyclopenten, in position 5 of the cyclopal molecule. The mixed signal observed from the unaltered cyclopal molecule, Figs. 6A, B, C, would then be taken to include a contribution coming from one of the side chains of position 5, possibly the 2-cyclopenten group. Such a contribution is assumed to be removed by preparation above 165° C, leaving a strong equal intensity triplet due to nitrogen interaction. The time effect observed in the signal from the boric acid glass preparation seems to favor such an explanation. At 4 months after irradiation, Figs. 6D and 6F are almost alike, indicating that the whatever additional component responsible for the initial discrepancies is slowly disappearing with time.

4. Barbital and Medomin

A triplet of total width 50 oersteds was obtained from barbital, Fig. 8A, and medomin, Fig. 8B, both prepared in a boric acid glass. The line spacing was uniform at about 11 oersteds. No appreciable time effect was observed in the signal from barbital, as shown in Fig. 8C, 3 months after irradiation, and Fig. 8D, 15 months after irradiation.

Both molecules have in common an ethyl group as one of the substituents in position 5 of the barbituric acid ring. It would therefore appear that radiation removes a CH_3 from this ethyl group leaving a radical which has the required two equivalent protons.

5. Ipral, Sigmodal, Nembutal, and Seconal

Ipral in a boric acid glass gave immediately after irradiation, Fig. 9A, a quintet with a uniform line spacing of 12 oersteds. Fifteen months after irradiation, Fig. 9B, the signal had decreased in intensity; however, the original quintet with the same line spacing was still resolvable from noise. Ipral prepared in paraffin, Fig. 9C, yielded a complex signal which is most

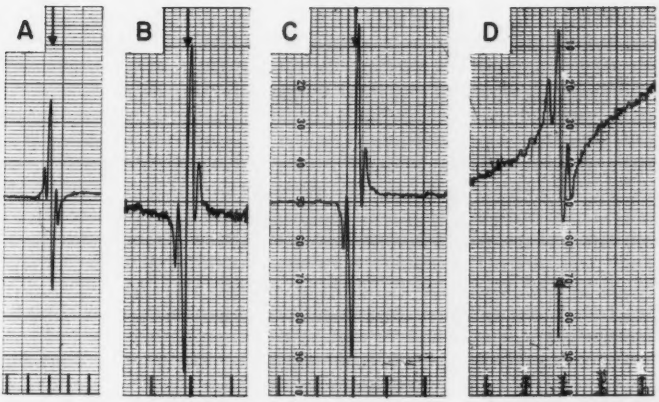

FIG. 8. Paramagnetic resonance absorption signals from irradiated barbital, A, B, C; and irradiated medomin, D. First derivative curves. The above curves were obtained from a boric acid glass. Times after irradiation: A, 76 hours; B, 3 months; C, 15 months; D, 3 months. Markers are 50 oersteds apart. Vertical arrows indicate the position of D.P.P.H. resonance.

likely due to coupling with the surrounding matrix. It is interesting to note that the molecule of ipral has in position 5 two groups, an ethyl and isopropyl group, which, by removal of a single CH_3 by radiation, could contribute to the observed signal. The isopropyl group with the loss of a CH_3 would give rise to a quintet, average spacing 12 oersteds, as already seen for alurate; the ethyl group without the end CH_3 would produce a triplet, average spacing 11 oersteds, as in the case of barbital and medomin. These two signals being centered about the same g-value may be added together to form the observed regular and symmetrical quintet.

Sigmodal, Fig. 9D, nembutal, Fig. 9G, and seconal, Fig. 9I, gave also a quintet of average spacing 12 oersteds immediately after irradiation in a boric acid glass. The shape of the signal was not significantly changed after 3 and 15 months for sigmodal, Figs. 9E and 9F, and after 15 months for nembutal and seconal, Figs. 9H and 9J. Sigmodal, nembutal, and seconal have a 1-methyl butyl group common in position 5. Breakage by radiation of the C—C bond between carbon 1 and 2 would leave the required 4 nearly equivalent H atoms to explain the observed quintets. For nembutal, a contribution from the other substituent in position 5, an ethyl group, should also be considered as already discussed for ipral. A major contribution from such a triplet would actually explain the relative weakness of the two outer components of the quintet reported for nembutal, Fig. 9G.

6. Rutonal, Luminal, Mebaral, and Alphenal

A well-defined triplet of triplets of varying intensity was observed from rutonal, luminal, and mebaral, Figs. 10A, 10D, and 10K respectively, immediately after irradiation in a boric acid glass. The total width of the signal was on the average 140 oersteds. The distance between the components of the

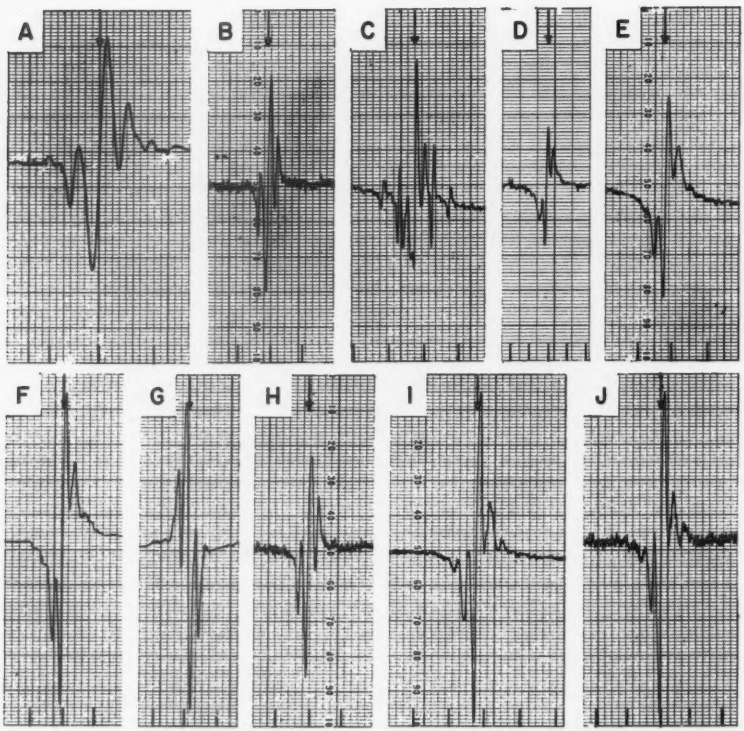

FIG. 9. Paramagnetic resonance absorption signals from irradiated ipral, A, B, C; from irradiated sigmodal, D, E, F; from irradiated nembutal, G, H; and from irradiated seconal, I, J. First derivative curves. The above curves were obtained from a boric acid glass except photograph C which was from paraffin. Times after irradiation: A, C, D, G, I, 1 hour; E, 3 months; B, F, H, J, 15 months. Markers are 25 oersteds apart for A and 50 oersteds for the others. Vertical arrows indicate the position of D.P.P.H. resonance.

large triplet was 40 oersteds. The lines of the small triplets were uniformly spaced at 10 oersteds. The signals were effectively unaltered after 3 months, Figs. 10B, 10E, and 10L, and not significantly reduced after 15 months, Figs. 10C, 10F, and 10M for rutonal, luminal, and mebaral respectively. Irradiation of luminal sodium in a boric acid glass gave the same type of signals right after irradiation, Fig. 10H; this signal did not change after 3 months, Fig. 10I, and 15 months, Fig. 10J. Luminal and mebaral were also prepared in paraffin and irradiated, Figs. 10G and 10N. The same signal as above with effectively the same component spacings was obtained.

Assuming that the observed signals are not complex and result from a given free radical species, the assignment of a triplet of triplets of varying intensity to any given modified area of the molecules of rutonal, luminal, and mebaral is not at all evident. However, it will be observed that of all the compounds reported in this study, only rutonal, luminal, mebaral, and alphenal have a phenyl group as one of the substituents in position 5. Alphenal prepared in a

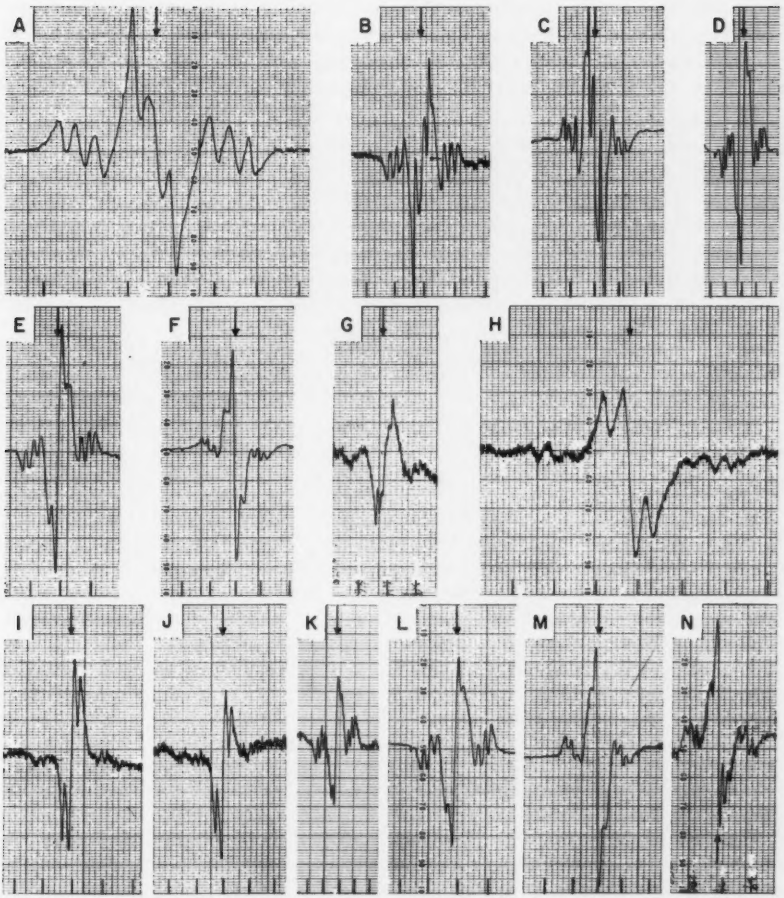

FIG. 10 Paramagnetic resonance absorption signals from irradiated rutonal, A, B, C; from irradiated luminal, D, E, F, G; from irradiated luminal sodium, H, I, J; and from irradiated mebaral, K, L, M, N. First derivative curves. The above curves were obtained from a boric acid glass except photographs G and N which were from paraffin. Times after irradiation: A, D, G, H, K, N, 1 hour; B, E, I, L, 3 months; C, F, J, M, 15 months. Markers are 25 oersteds apart for A, H and 50 oersteds for the others. Vertical arrows indicate the position of D.P.P.H. resonance.

boric acid glass yielded also right after irradiation, Fig. 11N, a signal which may be taken as a partially resolved triplet of triplets. The total width of the signal is the same as that for the other three, 140 oersteds. The signal was not changed after 15 months, Fig. 11O. It is therefore very tempting to relate the common signal observed from these four irradiated molecules to their common structural feature, a phenyl group in position 5. The proposed explanation would be that radiation removes an H atom from the para position on the phenyl ring. The "resonance condition of the ring" is assumed

to be modified to the point that the remaining four H atoms effectively interact with the free electron in two groups of two.

If, on the other hand, the observed signals are assumed to be complex, they may be taken to result from the superposition of a 40 to 50 oersted wide odd line spectrum at the center of an equal intensity, evenly spaced triplet of triplets of 140 oersteds, total width. The odd line spectrum would originate from side chain alterations, as seen before; while the equal intensity triplet of triplets would be due to the two N atoms in the malonylurea ring. It has already been mentioned that the malonylurea ring is not planar. Therefore, the odd electron is not free to move around the ring, position 5 acting as a potential barrier. However, this odd electron may quite well encompass the remaining five positions of the ring. A hyperfine structure would then be expected from the N atoms in position 1 and 3.

It is evident that more experimental work is required to test the above two possibilities.

7. Evipal, Delvinal, Phandorn, Nostal, Pernoston, and Barbituric Acid

Signals of varying complexities were obtained from this last group of compounds. Interpretation of most of these signals will not be possible. However, it is believed that a survey of clinically important barbiturates would not be complete without including the above compounds.

The signal recorded from evipal right after irradiation in a boric acid glass, Fig. 11A, differed from that observed when prepared in paraffin, Fig. 11B. Both were complex signals of about the same total width, 130 oersteds. After 3 months in a boric acid glass, the signal became asymmetric, Fig. 11C, and remained unchanged for the following year, Fig. 11D. However, its intensity was much reduced.

Delvinal was prepared in a boric acid glass only. The signal, right after irradiation, Fig. 11E, was asymmetric and had a total spread of 100 oersteds. No significant change in shape or intensity was observed after 15 months, Fig. 11F.

Phandorn, irradiated in a boric acid glass, gave a symmetrical signal of total width 120 oersteds, right after irradiation, Fig. 11G. After 15 months, Fig. 11H, the signal was just as intense and practically unchanged.

The same complex signal, 100 oersteds wide, was obtained right after irradiation from nostal prepared in a boric acid glass, Fig. 11I, and in paraffin, Fig. 11J. This complex signal was reduced to an evenly spaced quintet after 15 months in a boric acid glass, Fig. 11K. This quintet had a line separation of about 12 oersteds. It is believed that the isopropyl substituent in position 5 is at the origin of the quintet. The mechanism would be similar to that seen for ipral and alurate, that is to say, radiation would remove a CH_3 from the isopropyl group leaving a set of four nearly equivalent protons. The component of the signal which had disappeared after 15 months in a boric acid glass, is probably due to the other substituent in position 5 of the molecule of nostal, a 2-bromoallyl group. However, the two stable isotopes of bromine, Br-79 and Br-81, have a spin of 3/2. It is therefore difficult to speculate on the possible contribution from this group.

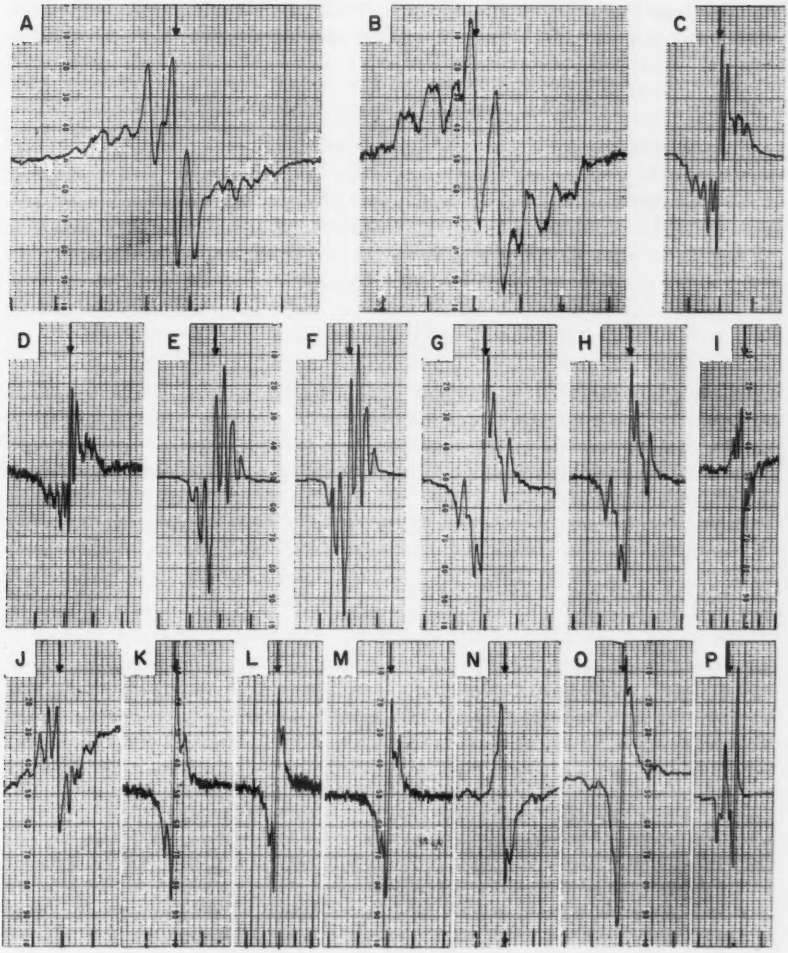

FIG. 11. Paramagnetic resonance absorption signals from irradiated evipal, A, B, C, D; from irradiated delvinal, E, F; from irradiated phandorn, G, H; from irradiated nostal, I, J, K; from irradiated pernoston, L, M; from irradiated alphenal, N, O; and from irradiated barbituric acid, P. First derivative curves. The above curves were obtained from a boric acid glass except photographs B, J, which were from paraffin. Times after irradiation: A, B, E, G, I, J, L, N, 1 to 2 hours; C, P, 3 months; D, F, H, K, M, O, 15 months. Markers are 25 oersteds apart for A, B and 50 oersteds for the others. Vertical arrows indicate the position of D.P.P.H. resonance.

The signal obtained from pernoston irradiated in a boric acid glass was comparatively weak right after irradiation, Fig. 11L, and remained unchanged after 15 months, Fig. 11M. The total width of the signal was about 100 oersteds.

Barbituric acid was expected to yield a simple E.P.R. signal which could

have been used to interpret those from some of its derivatives. However, when prepared in a boric acid glass, an asymmetric signal, Fig. 11P, 50 oersteds wide, was obtained.

GENERAL DISCUSSION

The numerous experimental results presented in this paper have undoubtedly shown that the boric acid glass method of preparation may be used to stabilize at room temperature the free radicals produced by radiation in barbituric acid derivatives. In two cases, with alurate and cyclopal, it was possible to compare the results to those obtained directly from the dry salt irradiated and analyzed under a nitrogen atmosphere. No major discrepancies in the size and shape of the signals were reported. Further, many of the results were also compared to those obtained when the compounds were dispersed in paraffin and irradiated. Neglecting the instances where hydrogen interaction with the surrounding matrix was more or less evident, the similarity of the results was easily established. The boric acid glass method of preparation will eventually be applied to other groups of chemical compounds. It is hoped it will be useful in certain cases to study at room temperature the effect of radiation on chemical and biochemical material.

The barbituric acid derivatives studied are all of the same basic formula. The main differences reside in the types of substituents in position 5 of the malonylurea ring. It is, therefore, interesting to try to correlate some of the observed paramagnetic resonance patterns with the occurrence of specific groups in the side chains of the molecules. A quintet of average spacing 12 oersteds was obtained from molecules which contained an isopropyl group, nostal, ipral, and alurate. Radiation was assumed to remove a single CH_3 leaving a set of four nearly equivalent H atoms. A quintet with the same spacing was also observed from molecules which had a methyl butyl group, sigmodal, nembutal, and seconal. Breakage by radiation of the bond between carbon 1 and 2 results in the same free radical as in the above case and would therefore explain the similarities in the results. Barbital and medomin which possessed an ethyl group gave a triplet of average spacing 11 oersteds. This triplet was taken to originate from the two equivalent H atoms obtained with the removal of a CH_3 by radiation. It is also pertinent to recall that a triplet of triplets of total spread 140 oersteds and average spacings 10 and 40 oersteds was recorded only from all the derivatives studied which included a phenyl group such as luminal, rutonal, alphenal, and mebaral. One of the tentative explanations given, the removal of the H atom in the para position and the coupling by pair for the remaining four H atoms, will eventually have to be checked by further experimental work. The remaining derivatives yielded signals which were either too complex or not interesting from the correlation point of view. This group included neonal, amytal, and dial which showed evidence of the presence of the free electron close to one of the N atoms in the malonylurea ring.

The effect of radiation on the barbituric acid derivative molecules seem to be centered on either one of the side chains in position 5. The only exceptions

are neonal, amytal, and dial which show as a most important process the removal of a single H atom from position 1 or 3 on the barbituric acid ring. A reduction in the length of either one of the side chains in position 5 might result in a decrease in the duration of the biological action of these irradiated barbiturates. However, it is realized that the electron paramagnetic resonance method, combined with the boric acid glass method of preparation, freezes initial processes only. Many secondary processes are of importance to understand a radiation damage mechanism. Experiments to elucidate the role of secondary reactions were designed for nembutal. The results will be published at a later date.

ACKNOWLEDGMENTS

The author is indebted to the Defence Research Board for the loan of most of the original microwave equipment used in this research. The electrical shop of the Canadian Army Signal Corps Research and Development Establishment designed and built the two Zeeman modulation coils and machined and silver-plated the H_{012} rectangular cavity resonator. The Commercial Product Division of the Atomic Energy of Canada Ltd. made available whatever radiation facilities were required for this work. Thanks are also due to Dr. H. Wesemeyer of the Geological Survey of Canada, who made many pertinent comments on the contents of this report and reviewed the manuscript before its submission for publication.

REFERENCES

CHATTEN, L. G. and LEVI, L. 1957. Appl. Spectroscopy, **11**, 177.
COLE, T., HARDING, J. T., PELLAM, J. R., and YOST, D. M. 1957. J. Chem. Phys. **27**, 593.
COLE, T. and MCCONNELL, H. M. 1958. J. Chem. Phys. **29**, 451.
CONGER, A. D. and RANDOLPH, M. L. 1959. Radiation Research, **11**, 54.
FONER, S. N., JEN, C. K., COCHRAN, E. L., and BOWERS, V. A. 1958. J. Chem. Phys. **28**, 351.
GORDY, W., ARD, W. B., and SHIELDS, H. 1955*a*. Proc. Natl. Acad. Sci. **41**, 983.
——— 1955*b*. Proc. Natl. Acad. Sci. **41**, 996.
GORDY, W. and MIYAGAWA, I. 1960. Radiation Research, **12**, 211.
GORDY, W., SMITH, W. V., and TRAMBARULO, R. F. 1953. Microwave spectroscopy, 1st ed. (John Wiley & Sons, Inc., New York), p. 236.
HOLLANDER, J. M., PERLMAN, I., and SEABORG, G. T. 1953. Revs. Modern Phys. **25**, 469,
INGRAM, D. J. E. 1955. Spectroscopy at radio and microwave frequencies (Butterworths Scientific Publications).
LAPPERT, M. F. 1956. Chem. Rev. **56**, 959.
LEVI, L. 1957. Bull. Narcotics, **11**, 30.
LEVI, L. and HUBLEY, C. E. 1956. Anal. Chem. **28**, 1591.
LEWIS, G. N., LIPKIN, D., and MAGEL, T. T. 1941. J. Am. Chem. Soc. **63**, 3005.
MAYNERT, E. W. and VAN DYKE, H. B. 1949. J. Pharmacol. Exptl. Therap. **96**, 217.
NEWMAN, M. S. 1956. Steric effects in organic chemistry (John Wiley & Sons, Inc., New York).
O'MEARA, J. P. and SHAW, T. M. 1957. Food Technol. **11**, 132.
PATT, H. M. 1953. Physiol. Revs. **33**, 35.
REID, C. 1958. Quart. Revs. **12**, 205.
SCHMIDT, H. 1896. Ann. Physik. **58**, 103.
SMALLER, B. and MATHESON, M. S. 1958. J. Chem. Phys. **28**, 1169.
SHOOLERY, J. N. and WEAVER, H. E. 1955. Ann. Rev. Phys. Chem. **6**, 433.
WHIFFEN, D. H. 1958. Quart. Revs. **12**, 250.

THE HALL EFFECT AND RESISTIVITY OF TELLURIUM[1]

R. W. McKay and W. E. Gravelle[2]

ABSTRACT

The Hall effect and resistivity of seven crystalline samples of highly purified tellurium were investigated over the temperature range −190° C to +350° C. The samples were grown from zone-refined tellurium with an adaptation of the method of Tammann. The effective impurity concentrations were in the range 5×10^{-6} to 5×10^{-5} atomic per cent. The measurements were made with an a-c. method of high sensitivity.

X-Ray investigations indicated that the purest sample was a single crystal, but that the others were polycrystalline. However, differences in the observed properties as a result of crystal structure were not large.

At high temperatures pure tellurium exhibits an anomalous behavior in its Hall effect, and three proposed explanations of this anomaly were investigated in view of the data of this research. At much lower temperatures, it was concluded that tellurium behaved as a simple semiconductor with unique conduction and valence bands with a non-degenerate carrier distribution.

INTRODUCTION

During the past twenty years the properties of semiconductors have been studied by many investigators. Most of this effort has been concentrated on those materials for which practical applications have been found, especially germanium, silicon and, more recently, various intermetallic compounds. The element tellurium, on the other hand, has received very little attention although several anomalies in its behavior are of interest.

All samples of tellurium which have been studied so far have been found to be *p*-type at low temperatures regardless of the nature of the impurity content. As is the case with many materials which are *p*-type at low temperatures, the Hall effect of tellurium changes sign as the temperature is raised. The temperature at which this reversal occurs is higher for samples with greater impurity content and no reversal occurs if enough impurities are present. For samples of sufficient purity to exhibit this reversal, a second reversal of the sign of the Hall effect occurs at a higher temperature. This high temperature reversal is a unique property of tellurium. Several theories have been suggested to explain this anomalous behavior. The experimental evidence found in the literature is insufficient to determine which, if any, of these theories is correct.

The purpose of the present investigation is to provide more accurate experimental results on a range of samples, including some with the highest degree of purity, in order to throw more light on the theories of the anomalous Hall effect reversal. There is disagreement also among the results of various observers regarding the value of the intrinsic activation energy, the variation

[1]Manuscript received November 10, 1960.
Contribution from the Department of Physics, University of Toronto, Toronto, Ont.
[2]National Research Council Student 1955–1958. This paper is based on the work submitted in March 1959 for the Ph.D. degree in the University of Toronto. Present address: Defence Research Telecommunications Establishment, Defence Research Board, Ottawa.

of carrier mobility with temperature, and several other properties of tellurium. A further purpose of this work is an improvement in the accuracy of measurement of these properties.

Crystalline samples of high purity have been produced using the method of zone refining which has not previously been used for tellurium. Measurements of Hall effect and resistivity have been made by an a-c. method of high sensitivity. This method is free from errors due to magneto- thermoelectric effects which are difficult to eliminate from d-c. measurements. Although the results obtained improve the accuracy with which the properties of tellurium are known, it has not been found possible to confirm without ambiguity any of the theories of the anomalous Hall effect reversal.

PREVIOUS WORK

The atoms of tellurium crystals are arranged in spiral chains in a hexagonal close-packed structure. The work of Scanlon and Lark-Horovitz (1947) and of Bridgman (1938) indicates that tellurium exists in only one crystalline form over the range of temperatures and pressures normally available.

The electrical properties of tellurium have been studied using evaporated films, single crystals, and polycrystalline samples. Bottom (1949) studied the anisotropy in the resistivity of tellurium and found the resistivity to be 1.9 times greater perpendicular to the c-axis (chain-axis) than parallel to it. He found no dependence of the Hall effect on orientation.

All samples of tellurium so far studied have been p-type at low temperatures. Fukuroi *et al.* (1952) found that small additions of antimony increased the acceptor activity and Moss (1952) showed that tellurium with more than 0.3% antimony shows semimetallic properties. Kronmuller *et al.* (1956) studied the effects of other impurities and found none which produced n-type behavior. This is not surprising when the position of tellurium in the periodic table is considered.

Nussbaum (1953, 1954) investigated alloys of tellurium and selenium. The electrical properties of the alloys are similar to those of pure tellurium since the two elements and their alloys are isomorphous.

Johnson (1948) stated that both the electron and hole mobilities vary as $T^{-3/2}$. However, later work by Nussbaum (1953) contradicted Johnson's results and showed a proportionality of hole mobility to $T^{-0.675}$. Calculations based on Bottom's data agree approximately with this. These results are compared with values obtained in this work in a later section.

Tellurium, in common with most semiconductors which are p-type at low temperatures, shows a reversal in sign of Hall coefficient as the temperature is increased. At still higher temperatures a second reversal occurs in tellurium which was first observed by Wold (1916). Various attempts to explain this anomalous reversal have been made by Fukuroi and Tanuma (1952), Callen (1954), Epstein *et al.* (1957), and Fritzsche (1952). Caldwell and Fan (1959), using the results of absorption experiments in conjunction with the calculations of Reitz (1957), give support to the theory of Epstein. These theories are discussed in detail in the section on high temperature data.

The energy gap between the valence and conduction bands has been calculated by several observers from their experimental results. Values determined from the intrinsic resistivity data are in the range 0.32 to 0.34 ev (Bottom 1952; Nussbaum 1953; Kronmuller *et al.* 1956). Fukuroi (1949) and Tanuma (1954) derived the energy gap using other data and found a value of 0.33 ev. Earlier workers had found higher values from 0.36 ev to 0.38 ev (Scanlon and Lark-Horovitz 1947; Johnson 1948). Measurements of the energy gap have also been made by photoelectric and optical absorption methods by Moss (1952) and Loferski (1952, 1954). Their values are, in general, still higher and range from 0.35 ev to 0.41 ev.

EXPERIMENTAL PROCEDURE

The Hall effect and resistivity of crystalline tellurium were measured by an a-c. method in which an alternating current in the specimen and a constant magnetic field produced the Hall voltage. Several sources of error which depend on thermal gradients in the specimen can superimpose spurious e.m.f.'s on the Hall voltage. These are eliminated by a-c. methods of measuring the Hall effect.

The samples were cylindrical in form with probes for the electrical measurements welded in place as shown in Fig. 1. The Hall coefficient R_H and resistivity of such specimens can be calculated from the following formulae:

$$R_H = (\pi d/4B)(V_H/I), \tag{1}$$

$$\rho = (\pi d^2/4l)R. \tag{2}$$

In these equations, d, B, V_H, and I are the diameter of the rod, the magnetic induction, the Hall voltage, and the specimen current respectively; l is the distance between the resistance probes and R is the resistance between them. The derivation of these equations assumes that the current density is uniform at all points in the sample between the resistance probes and that the Hall probes are on a diameter normal to the magnetic field.

The voltages V_H and V_R, where V_R is the voltage between the resistance probes, were measured with a differential amplifier, and R was measured with an a-c. Kelvin bridge circuit. The current I was found with the relation $I = V_R/R$.

The temperature of the specimen was controlled with a cryostat at low temperatures and with a furnace at high temperatures. The cryostat and furnace were designed to fit between the pole pieces of an electromagnet. The temperatures were measured with a thermocouple and potentiometer.

The tellurium* before purification had a purity of about 99.99%. It was then purified by the method of zone refining. Crystalline samples were prepared by a method based on that of Tammann (Buckley 1951). The mold for crystal growth was a pyrex tube with a closed capillary at one end. This was inserted with the open end downward into a long vertical pyrex tube containing some tellurium. A tubular furnace surrounded the system.

*The tellurium used was provided through the courtesy of the International Nickel Co.

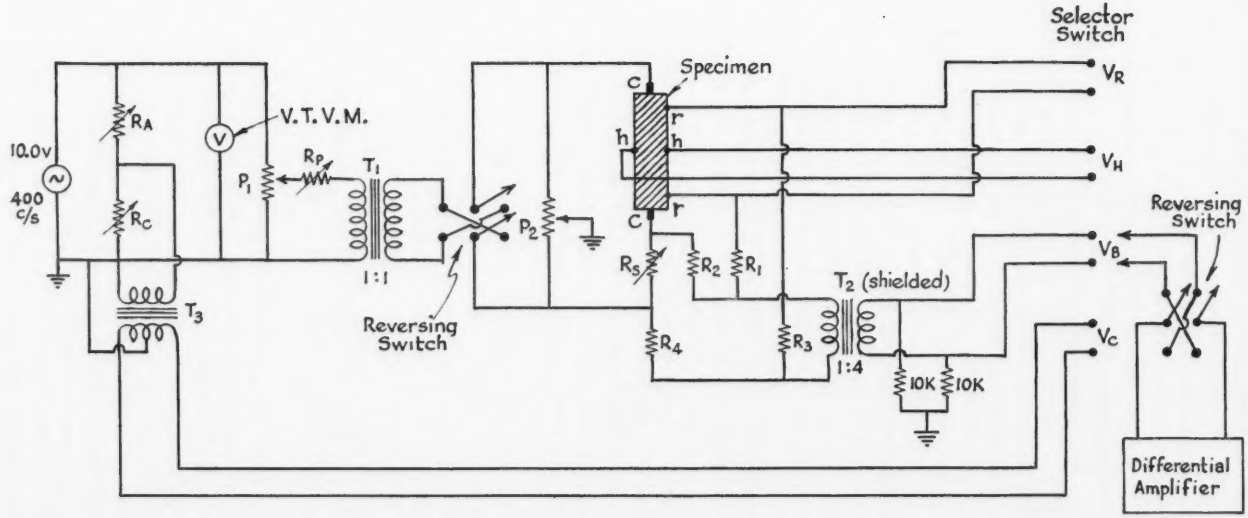

FIG. 1. Simplified diagram of the measuring circuit. V_R is the voltage between resistance probes r, r. V_H is the voltage across the Hall probes h, h. V_B is output from Kelvin bridge and V_C is a calibrating voltage.

The system was evacuated and the tellurium was outgassed at about 350° C for 2 hours. The furnace temperature was then increased to melt the tellurium and an inert gas was admitted into the system to force the melt into the mold. The system was sealed and about 15 minutes was allowed for the re-establishment of thermal equilibrium. The temperature of the furnace was then slowly reduced to form a sample.

To ensure that the cooling advanced along the mold, the furnace was constructed to give a large temperature gradient along its length. For this reason, the spacing in the heater winding decreased and the amount of insulation increased with distance from the top of the furnace. The furnace had a thermal gradient of about 5° C/cm over a length of about 10 cm with the temperature increasing toward the bottom. The top of the capillary was set near the top of this range and the temperature at this point was set at slightly above the melting point before the inert gas was admitted.

The furnace was slowly cooled by reducing the heater current slightly at frequent intervals. The large thermal mass of the furnace prevented rapid changes in the temperature for small changes in the current. In this way it was possible to keep the rate of cooling below about 2° C/min. Thus the velocity of crystal growth could be kept below about 0.4 cm/min.

After the sample was removed from the furnace, it was immersed in hydrofluoric acid to remove the surrounding glass.

A jig was devised to permit the accurate placement and the support of the Hall and resistance probes. It consists of a length of teflon rod with an axial hole to accommodate the specimen and radial holes (all in the same plane) to accommodate the probes. One side of the teflon cylinder was planed to make it flat and to provide better thermal contact with the copper plate supporting it in the specimen chamber.

The teflon jig containing the specimen was strapped to a copper strip, Fig. 2. The Hall and resistance probes consisting of short lengths of 20-mil platinum wire with copper leads attached by spot welding were mounted on the jig and welded to the specimen by condenser discharge. Some trouble was experienced at high temperatures due to swelling of the teflon, resulting in breaking the welded contacts.

The copper strip to which the specimen was attached was joined to a long monel tube. This tube passes through a short glass tube centered at the top of the removable joint on the specimen chamber (Fig. 2). A short length of monel below the copper strip and teflon disks on the monel tube ensure that the specimen is centered in the chamber. The monel with low thermal conductivity conducts little heat out of or into the chamber. The copper plate, however, helps to give a uniform temperature in the specimen.

The thermocouple leads were continuous from the junction on the back of the copper support to external terminals. The specimen leads and the copper thermocouple lead were insulated with spun glass which was not impaired by the highest temperatures reached (about 350° C).

All leads passed through a small side tube in the removable joint (Fig. 2). Rubber tubing containing stopcock grease was placed over this side tube and clamped to form a vacuum seal. Vacuum wax sealed the monel tube.

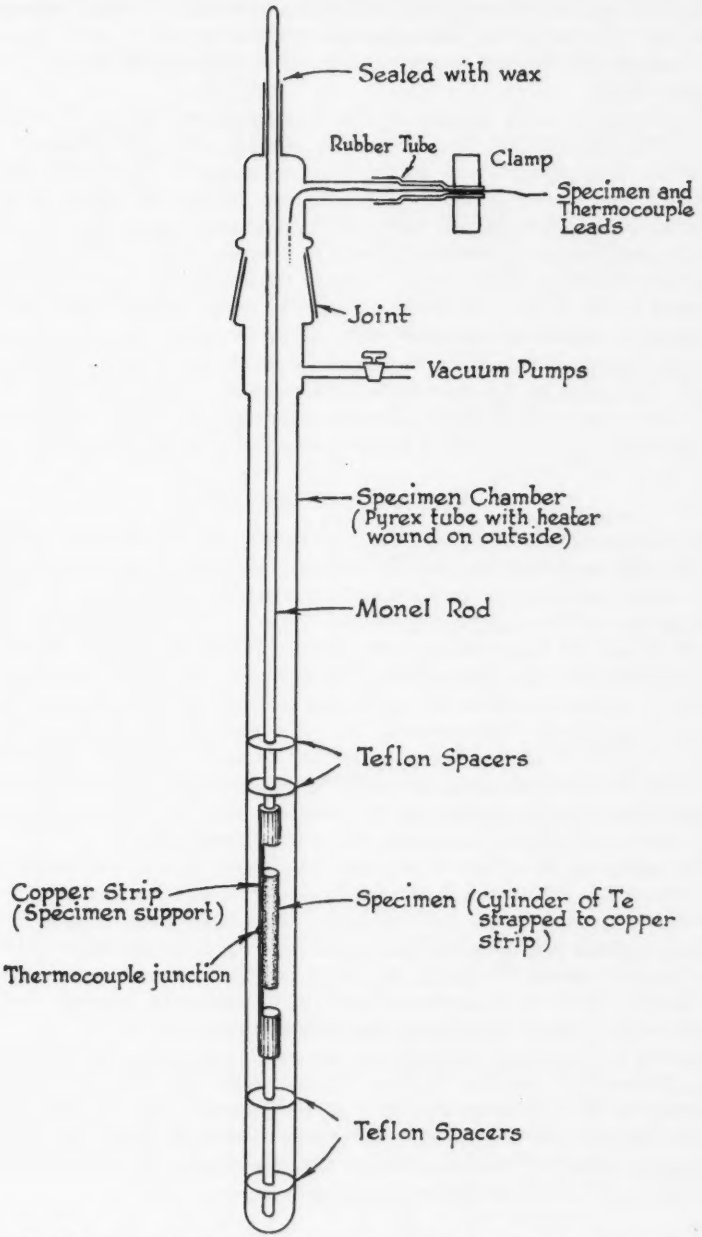

FIG. 2. The specimen holder. This holder is inserted in the cryostat or furnace with the specimen coming between the poles of the magnet.

The Hall probes were centered in the magnetic field by visual alignment of the top of the monel rod. The specimen was then rotated to give maximum Hall voltage and thereby ensure that the Hall probes were normal to the magnetic field.

The simplified circuit diagram in Fig. 1 indicates the method of measurement. The sensitivity of the differential amplifier was approximately 0.04 microvolt. This permitted an accuracy in measuring the Hall coefficient of $\pm(0.26/I)$ cm³/coulomb where I is the current through the sample in milliamperes. At temperatures near the lower reversal temperature, the resistivity is large and I must be less than 10 ma to prevent ohmic heating. At high temperatures where the resistivity is small larger currents were used. Thus the small values of the Hall coefficient near the lower reversal point could be measured to ± 0.03 cm³/coulomb while near the upper reversal point the accuracy was somewhat better. For larger values of R_H the accuracy is limited by the calibration of the attenuator in the amplifier to slightly better than 1%. The accuracy of resistivity measurements being made by a null method was between $\pm 0.1\%$ for higher values and $\pm 0.3\%$ for lower values.

EXPERIMENTAL RESULTS

Measurements were made over the temperature range $-190°$ C to $+350°$ C. The samples were numbered serially but complete sets of data were obtained over this temperature range for only four samples 7, 8, 9, and 10. X-Ray investigations with a Laue back-reflection camera were made on five samples: 5, 7, 8, 9, and 10. Laue photographs taken at intervals along the lengths of the samples show that only sample 9 is a single crystal. The c-axis of this sample is inclined at about 60° to the rod axis and is nearly normal to the diameter joining the Hall contacts. The other samples are polycrystals with various degrees of preferred orientation and various grain sizes. Qualitative estimates show that the grain sizes and degrees of orientation are largest for sample 10 and smaller for samples 7, 8, and 5 in that order. Samples 8 and 5 have very small grains and almost no preferred orientation.

The experimental values of the Hall coefficient R_H and the resistivity ρ were plotted in the usual form: $\log R_H$ vs. $10^3/T$ and $\log \rho$ vs. $10^3/T$. The curves are given in Figs. 3–7 inclusive. The calculations required in the analysis of these data were made with the values of R_H and ρ taken from the experimental curves. Rewelding the electrical contacts produced changes in the results which were small compared with differences between samples. Therefore only the average values for each sample are given.

Some of the values determined from the results are summarized in Table I. The approximate effective impurity content was determined by methods discussed in the following section. The temperatures T_1, T_2, and T_m are respectively the low temperature reversal of Hall coefficient, the high temperature reversal, and the temperature corresponding to the maximum in the absolute value of Hall coefficient occurring between T_1 and T_2.

TABLE I

Characteristic temperatures

Sample	Effective impurity concentration ($cm^{-3} \times 10^{-15}$)	T_1, °K	T_2, °K	T_m, °K
3	7.4	253		
4	16	274		
5		270	498	
7	13	269	513	290
8	9.0	258	513	288
9	1.4	213.5	513	238
10	3.7	235	513	267

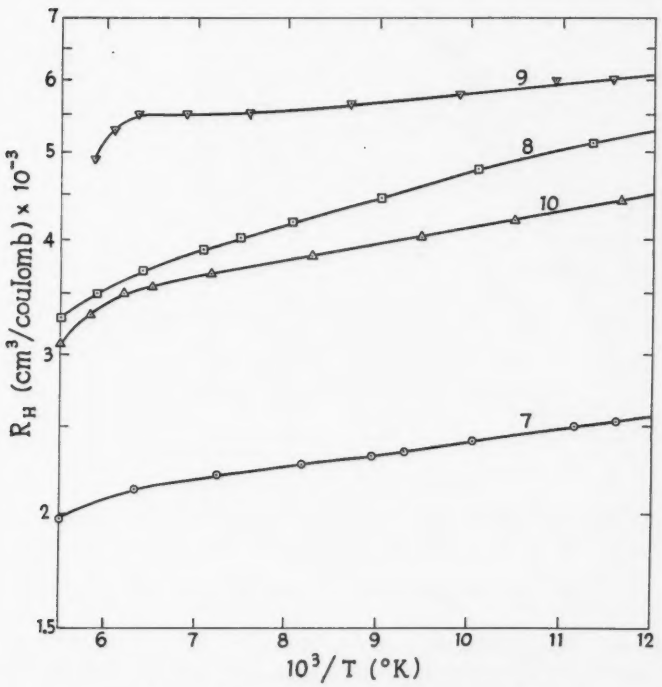

FIG. 3. Low temperature measurements of R_H.

DENSITIES AND ACTIVATION ENERGIES OF ACCEPTOR LEVELS

If the acceptors approach saturation at temperatures below that at which intrinsic conduction becomes appreciable, R_H approaches a constant value from which the number of acceptors N can be found by the equation

$$N = 3\pi/(8eR_H). \tag{3}$$

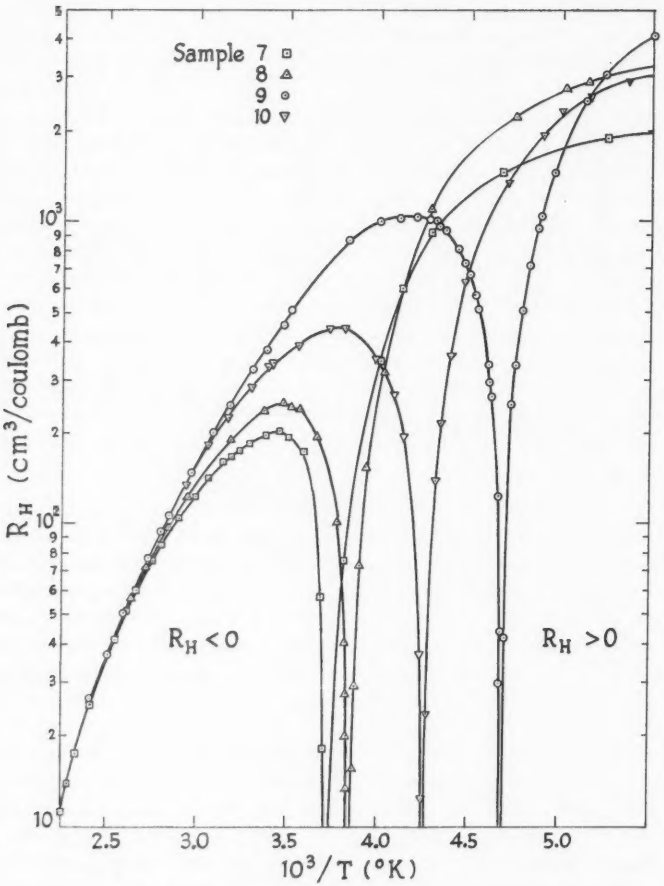

FIG. 4. Intermediate temperature measurements of R_H.

For sample 9, R_H levels off at 5400 cm³/coulomb giving $N = 1.4 \times 10^{15}$ acceptors per cm³. All the other samples have more impurities and the acceptors do not reach saturation before intrinsic activation begins. For these samples only rough estimates of the number of acceptor centers are possible by this method.

A method suggested by Hutson (1957) but not previously used for analysis of data on tellurium can be applied to samples which do not reach saturation. If E_F, E_v, and E_a are the energies of the Fermi level, of the top of the valence band, and of the acceptor levels respectively and m_2 the effective mass of holes then the number of holes is approximately given by

$$n_2 = 2(2\pi m_2 kT/h^2)^{3/2} \exp(E_v - E_F)/kT \tag{4}$$

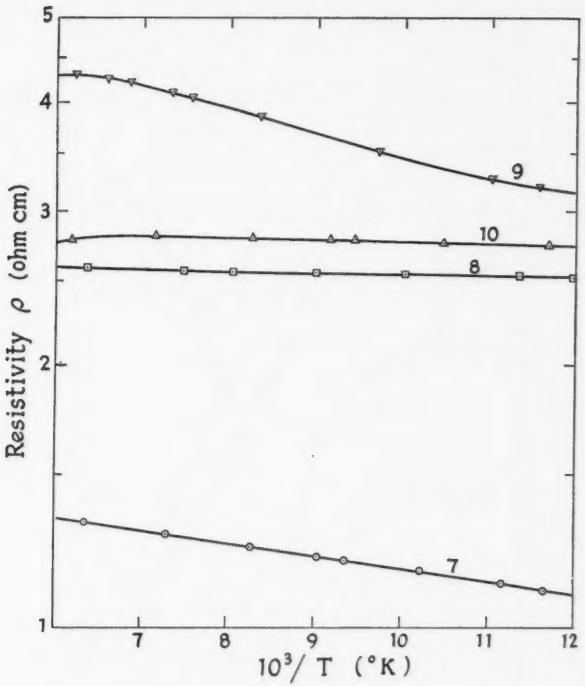

FIG. 5. High temperature measurements of R_H.

and the number of ionized acceptors by

$$n_a = N(1+\tfrac{1}{2}\exp(E_a-E_F)/kT)^{-1}. \tag{5}$$

In the extrinsic region where the number of electrons in the conduction band is negligible $n_a = n_2$. From these equations a function y_1 can be defined.

$$y_1 = \frac{n_a^2}{(N-n_a)2(2\pi mkT/h^2)^{3/2}} = 2\left(\frac{m_2}{m}\right)^{3/2}\exp\left(-(E_a-E_v)/kT\right). \tag{6}$$

The value of n_a can be found from the measured Hall coefficient using $n_a = 3\pi/(8eR_H)$ and the function y_1 can be calculated for a number of trial values of N, the density of acceptor levels. For the correct choice of N one would expect $\log y_1$ to be nearly a linear function of $1/T$ since the ratio of the effective hole mass to the electron mass does not vary strongly with temperature.

A set of such curves for sample 9 was plotted for various values of N. The closest approach to linearity was for $N = 1.37\times10^{15}$. The method is very sensitive to small changes in the choice of N.

None of the curves referred to in the previous paragraph remain linear at the low temperature end. A possible explanation of this behavior is that

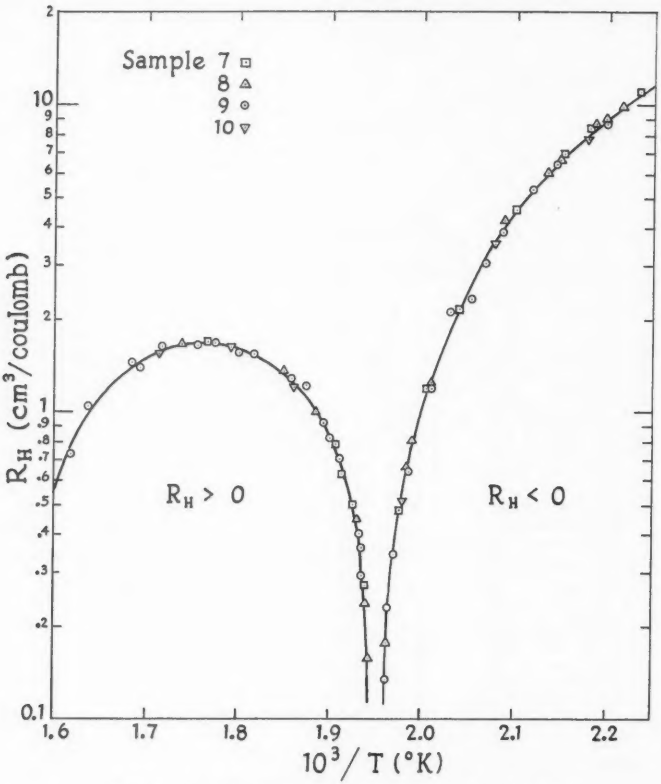

FIG. 6. Low temperature measurements of resistivity.

the acceptors may not all be of one kind or have the same activation energy. Equation (6) can readily be generalized to cover the case of more than one activation energy. However, since the approximation in equation (4) is valid only for spherical symmetry (scalar effective hole mass, m_2) and does not apply exactly to tellurium, results obtained by assuming more than one activation energy will not be quoted.

For an estimate of the acceptor density of the remaining samples, a third method was used.

The relation for the Hall coefficient assuming an isotropic, two-band model is

$$R_H = \frac{3\pi}{8e} \frac{n_2 - n_1 b^2}{(n_2 + n_1 b)^2} \tag{7}$$

where n_1 is the density of free electrons in the conduction band and b is the ratio electron mobility/hole mobility (u_1/u_2). The condition that R_H vanishes is then:

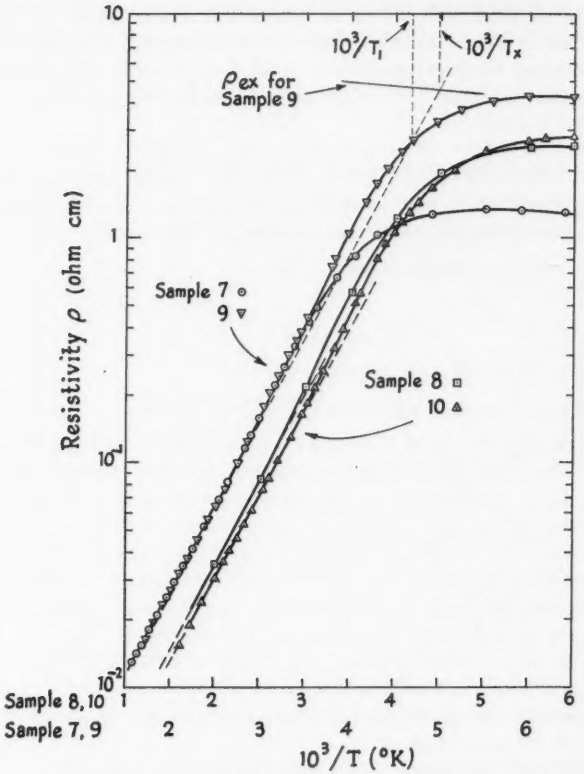

FIG. 7. High temperature measurements of resistivity.

(8) $$n_2 = n_1 b^2, \qquad T = T_1.$$

Also at any temperature,

(9) $$n_2 = n_1 + n_a,$$

and

(10) $$n_1 n_2 = n_i^2,$$

where

(11) $$n_i \equiv A T^{3/2} \exp(-E_g(0)/2kT)$$

and A depends only on the effective carrier masses and is considered to be constant.

Eliminating n_1, n_2, and n_i from equations (8), (9), (10), and (11)

(12) $$n_a(T_1) T_1^{-3/2} = \frac{A(b^2-1)}{b} \exp(-E_g(0)/2kT_1).$$

Thus a graph of log $(n_a(T_1)T_1^{-3/2})$ vs. $1/T_1$ should be linear, and by inserting the known value of $n_a(T_1)$ for sample 9 and the known energy gap, the values of $n_a(T_1)$ for the other samples were found from their reversal temperatures. These values are listed in Table I where the assumption is made that $n_a(T_1) = N$, the total acceptor density.

RESISTIVITY AT HIGH TEMPERATURES

From Fig. 7 it can be seen that in the high temperature or intrinsic region the resistivity ρ can be expressed by an equation of the form

$$\log \rho = \log \rho_\infty + (B/T).$$

However,

$$1/\rho = en_i u_2(b+1). \tag{13}$$

Substituting for n_i from (11) we obtain

$$\log \rho = \text{const} - \log(u_2(b+1)T^{3/2}) + (E_g(0)/2kT).$$

For many semiconductors $u_2 \propto T^{-3/2}$ and b is constant, and under these conditions the value of $E_g(0)$ can be determined from the constant B. The values of $E_g(0)$ determined in this way for samples 7, 8, 9, and 10 are 0.310, 0.312, 0.294, and 0.294 ev respectively, giving a mean of 0.30 ev. Previous observers have given values from 0.32 to 0.34 derived from resistivity curves. The discrepancy is possibly due to the fact, not previously reported, that there is a change in slope of the resistivity curves for all samples below 380° K and our values are taken from the straight segment above 380° K rather than from the mean slope over the intrinsic range. However, as will be shown, b is not constant for tellurium, nor does $u_2 \propto T^{-3/2}$ so that there is no theoretical reason for $u_2(b+1)T^{3/2}$ to be constant so that any determination of $E_g(0)$ by the above method must be of doubtful validity.

The values of ρ_∞ for samples 7, 8, 9, and 10 were 7.1, 9.0, 8.93, and 10.3 $\times 10^{-4}$ ohm cm. It is thought that this variation in ρ_∞ is due to different crystal orientation in the various samples and is within the range of 1.9 to 1 given by Bottom (1949) for conductivity perpendicular and parallel to the c-axis.

The high temperature Hall coefficient, on the other hand, does not appear to depend on crystal orientation, being approximately the same for all samples. This again is in agreement with the work of Bottom.

VARIATION OF MOBILITIES WITH TEMPERATURES

A direct calculation from the experimental results is possible only for the hole mobility in the low temperature range where there are no electrons in the conduction band and the carriers are holes resulting from the ionization of acceptor impurities. In this temperature range

$$R_H = 3\pi/8en_a \tag{14}$$

and

$$\rho = (en_a u_2)^{-1} \tag{15}$$

where n_a is the number of ionized acceptors and u_2 is the hole mobility. From these equations one can obtain the hole mobility u_2 by eliminating n_a to give

$$u_2 = \frac{8}{3\pi}\frac{R_H}{\rho}. \tag{16}$$

The values of log u_2 for sample 9 found in this way are plotted against log$(10^3/T)$ in Fig. 8, from log$(10^3/T) = 0.75$ to 1.05. If an attempt is made to fit an equation having the form $u_2 = AT^{-\alpha}$ to this curve the exponent α varies from 0.8 for the lower temperature segment of the curve to 0.5 for the upper

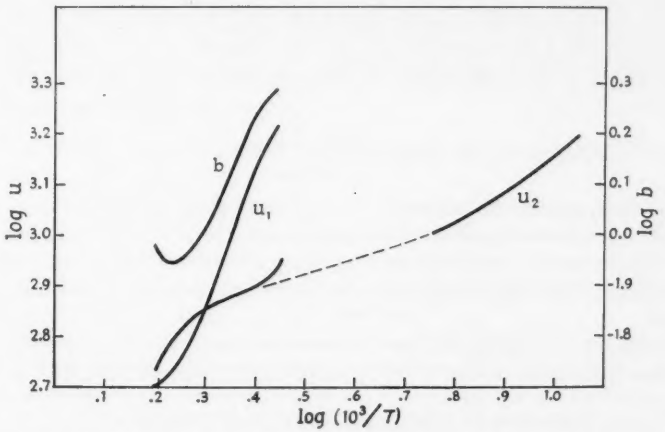

FIG. 8. Variation of electron and hole mobility with temperature.

temperature segment. These results do not agree with the theoretical variation of mobility with temperature for either lattice scattering ($T^{-3/2}$) or scattering by ionized impurities ($T^{3/2}$). They are, however, in agreement with the expermental results of Nussbaum (1953).

According to Debye and Conwell (1954) the theoretical $T^{-3/2}$ dependence of mobility for the lattice scattering mechanism was derived by Bardeen and Shockley on the assumption that the conduction band edge is located at the center of the Brillouin zone and that the dependence on temperature is considerably altered if this is not so.

The estimation of u_2 at high temperatures is less direct since it is necessary to adjust the value of one constant to obtain a fit between the curves for high and low temperatures.

At sufficiently high temperatures the impurity density is negligible compared with the density of intrinsic carriers. That is, $n_a \ll n_1$ or n_2, and $n_1 = n_2 = n_i$. Under these conditions

$$R_H = -(3\pi/8en_i)(b-1)/(b+1) \tag{17}$$

$$1/\rho = en_iu_2(b+1). \tag{18}$$

Eliminating n_i from (17) and (18) gives

$$b-1 = -8R_H/3\pi u_2\rho. \tag{19}$$

It has been previously shown from the linearity of the resistivity graphs that $u_2(b+1)T^{3/2} = C$. Eliminating b from these equations gives

$$u_2 = \frac{4R_H}{3\pi}+\frac{CT^{-3/2}}{2}. \tag{20}$$

In Fig. 8 between $\log(10^3/T) = 0.2$ and $\log(10^3/T) = 0.45$ values of u_2 calculated from this equation are shown for a value of C chosen to make the curve as nearly as possible continuous with the low temperature segment.

The values of b corresponding to the estimates of u_2 were then calculated from (19) for the intrinsic range. In the intermediate temperature range the formula

$$b = \frac{1-8R_H/3\pi u_2\rho}{1-en_a u_2\rho} \tag{21}$$

may be used, taking the value of $n_a = 1.4\times10^{15}$ given for sample 9 in Table I. This formula is obtained from equations (7) and (9), together with $1/\rho = eu_2(n_2+bn_1)$, assuming that $n_a \ll n_1$, i.e. that intrinsic carriers still predominate. The correcting term $en_a u_2\rho$ is less than 20% for any value plotted.

The electron mobility can now be obtained from the definition of b, i.e. $u_1 = bu_2$. Estimates of the electron mobility are also plotted in Fig. 8.

THEORIES OF THE HALL EFFECT REVERSAL AT T_2

Three theories have been proposed for the anomalous reversal of sign of R_H at high temperatures. A discussion of these theories follows.

(a) The Defect-Acceptor Theory

In this theory proposed by Fritzsche (1952) and discussed by Tanuma (1954) the reversion to p-type behavior at high temperatures is supposed to result from additional holes produced by thermal-lattice defects acting as electron traps. The authors of this theory assume that the density N_D of thermal-lattice defects is given by

$$N_L = N_L a \exp(-E/2kT) \tag{22}$$

where N_L is the density of lattice sites, a depends on the ratio, N_D/N_L and is close to unity, and E is the defect-activation energy. Equation (22) applies if defects of the Schottky type predominate. The authors also assume that all defect-acceptors are activated so that $n_a = N_D$ at high temperatures.

To produce a predominance of holes at high temperatures, E must exceed E_g so that, as the temperature rises, N_D begins to be appreciable somewhat below the higher reversal temperature T_2. With further rise in temperature, N_D quickly dominates the activity and causes R_H to be positive above T_2.

Thus, at high temperatures somewhat above T_2, N_D should be the dominant

source of carriers and the graph of $\log \rho$ vs. T^{-1} should show a slope proportional to E. Thus the curve of $\log \rho$ vs. T^{-1} at high temperatures should exhibit a slope which increases the rising temperature from the value corresponding to E_g to the value corresponding to E ($> E_g$). Since such a change in slope was not observed, we consider this theory to be untenable. This does not imply that defects do not occur but merely that they are not sufficiently numerous at T_2 to account for the reversal of sign of Hall effect at this temperature.

(b) The Dual Valence Band Theory (Epstein *et al.* 1957)

According to this theory, a lower valence band of high mobility accommodates more holes as the temperature rises so that the average hole mobility increases relative to the electron mobility. R_H then becomes positive when the mobility ratio $b = u_1/u_2$ becomes less than unity (cf. equation (17) for the high temperature Hall coefficient).

(c) The Dual Conduction Band Theory (Fukuroi and Tanuma 1952; Nussbaum 1953; and Callen 1954)

This resembles theory (*b*) in that the high temperature reversal of R_H is due to a decrease in b with rising temperature. The proposed mechanism is, however, a second conduction band of low mobility lying somewhat above the edge (bottom) of the main conduction band. The higher band accommodates more electrons as the temperature rises.

In either theory (*b*) or (*c*) the mobility ratio b varies with temperature in such a way that $(b-1)$ becomes zero at the reversal temperature, in agreement with the curves shown in Fig. 8. The curves for u_1 and u_2 in Fig. 8 suggest that the electron mobility u_1 varies with temperature nearly in the normal way whereas the hole mobility u_2 does not. This would seem to indicate that the dual valence band theory (*b*) is a more likely explanation of the anomaly than the dual conduction band theory (*c*).

The work of Caldwell and Fan (1959) also supports this view. Their measurements of infrared absorption indicate the existence of holes in a lower valence band and also that these holes have a lower effective mass and higher mobility.

REFERENCES

BOTTOM, V. E. 1948. Phys. Rev. **74**, 1218.
——— 1949. Phys. Rev. **75**, 1310.
——— 1952. Science, **115**, 570.
BRIDGMAN, P. W. 1925. Proc. Am. Acad. Arts. Sci. **60**, 305.
——— 1938. Proc. Am. Acad. Arts Sci. **72**, 157.
——— 1940. Proc. Am. Acad. Arts Sci. **74**, 21.
BUCKLEY, H. E. 1951. Crystal growth (John Wiley & Sons, Inc.).
CALDWELL, R. S. and FAN, H. Y. 1959. Phys. Rev. **114**, 664.
CALLEN, H. B. 1954. J. Chem. Phys. **22**, 518.
DEBYE, P. P. and CONWELL, E. M. 1954. Phys. Rev. **93**, 693.
EPSTEIN, A. S., FRITZSCHE, H., and LARK-HOROVITZ, K. 1957. Phys. Rev. **107**, 412.
FRITZCHE, H. 1952. Science, **115**, 571.
FUKUROI, T. 1951. Sci. Repts. Research Insts. Tohoku Univ. A, **3**, 175.
FUKUROI, T. and TANUMA, S. 1952. Sci. Repts. Research Insts. Tohoku Univ. A, **4**, 353.
FUKUROI, T., TANUMA, S., and MUTO, Y. 1954. Sci. Repts. Research Insts. Tohoku Univ. A, **6**, 18.

FUKUROI, T., TANUMA, S., and TOBISAWA, S. 1949. Sci. Repts. Research Insts. Tohoku Univ. A, **1**, 373.
——— 1950. Sci. Repts. Research Insts. Tohoku Univ. A, **2**, 233, 238.
——— 1952. Sci. Repts. Research Insts. Tohoku Univ. A, **4**, 283.
HUTSON, A. R. 1957. Phys. Rev. **108**, 222.
JOHNSON, V. A. 1948. Phys. Rev. **74**, 1255.
KRONMULLER, VON H., JAUMANN, J., and SEILER, K. 1956. Z. Naturforsch. **11a**, 243.
LOFERSKI, J. J. 1952. Phys. Rev. **87**, 905.
——— 1954. Phys. Rev. **93**, 707.
LOFERSKI, J. J. and MILLER, P. H. 1951. Phys. Rev. **83**, 876.
MOSS, T. S. 1952. Photoconductivity in the elements (Butterworth Publication).
NEURINGER, L. J. 1959. Phys. Rev. **113**, 1485.
NUSSBAUM, A. 1953. Tech. Rept. No. 1, Contract AF-33-(6-16)-78, Univ. of Penna.
——— 1954. Phys. Rev. **94**, 337.
REITZ, J. R. 1957. Phys. Rev. **105**, 1240.
SCANLON, W. and LARK-HOROVITZ, K. 1947. Phys. Rev. **72**, 530.
SHOCKLEY, W. 1950. Electrons and holes in semiconductors (D. Van Nostrand Co.).
TANUMA, S. 1954. Sci. Repts. Research Insts. Tohoku Univ. A, **6**, 159.
WOLD, P. I. 1916. Phys. Rev. **7**, 169.

A POWER SERIES EXPANSION OF THE MASTER EQUATION[1]

N. G. VAN KAMPEN

ABSTRACT

In order to solve the master equation by a systematic approximation method, an expansion in powers of some parameter is needed. The appropriate parameter is the reciprocal size of the system, defined as the ratio of intensive and extensive variables. The lowest approximation yields the phenomenological law for the approach to equilibrium. The next approximation determines the mean square of the fluctuations about the phenomenological behavior. In equilibrium this approximation has the form of a linear Fokker–Planck equation. The higher approximations describe the effect of the non-linearity on the fluctuations, in particular on their spectral density. The method is applied to three examples: density fluctuations, Alkemade's diode, and Rayleigh's piston. The relation to the expansion recently given by Siegel is also discussed.

1. THE PROBLEM

Let a be a fluctuating physical quantity, $P(a,t)$ its probability distribution at time t. If a possesses Markov character, $P(a,t)$ obeys the equation

$$\frac{\partial P(a,t)}{\partial t} = \int \{W(a|a')P(a',t) - W(a'|a)P(a,t)\}\, da', \tag{1}$$

where $W(a|a')$ is the transition probability per unit time from a' to a. Equation (1) is the differential form of the Chapman–Kolmogorov equation and is often called the "master equation". The right-hand side can be formally expanded in a series,

$$\frac{\partial P(a,t)}{\partial t} = \sum_{n=1}^{\infty} \frac{1}{n!}\left(-\frac{\partial}{\partial a}\right)^n \alpha_n(a)P(a,t), \tag{2}$$

where α_n is the nth moment of the transition probability, or "derivate moment",

$$\alpha_n(a) = \int (a'-a)^n W(a'|a)\, da'.$$

The expansion (2) was given by Kramers (1940) and Moyal (1949). The Fokker–Planck equation (Fokker 1913, 1914; Planck 1917; Wang and Uhlenbeck 1945) is obtained from it by cutting off after $n = 2$,

$$\frac{\partial P(a,t)}{\partial t} = -\frac{\partial}{\partial a}\alpha_1(a)P(a,t) + \frac{1}{2}\frac{\partial^2}{\partial a^2}\alpha_2(a)P(a,t). \tag{3}$$

Clearly, this cutting off is not a systematic approximation procedure, because (2) is not a series expansion in powers of some small parameter.* Our purpose is to provide a systematic approximation method for (2).† For a special case

[1]Manuscript received November 28, 1960.
Contribution from the Institute for Theoretical Physics, Rijksuniversiteit te Utrecht, Nederland.

*For instance, one might just as well agree to rearrange the terms in (2) according to successive derivatives of P and omit all terms with higher derivatives than the second. Or one might, like Lax (1960), expand in "orders of non-linearity".

†The step from (1) to (2) is not entirely harmless. It can be shown for the example in Section 6 that certain terms are lost. These terms are not analytic in our expansion parameter and cannot, therefore, be treated by a power series expansion. Fortunately they are also extremely small.

(viz., the current fluctuations in a diode, see Section 6) such an expansion has been given previously (van Kampen 1959); we now treat the general case.

Note.—The name Fokker–Planck equation is sometimes confined to a more restricted kind of equation, to wit

$$\frac{\partial P(a,t)}{\partial t} = c_1 \frac{\partial}{\partial a} aP + c_2 \frac{\partial^2 P}{\partial a^2}, \tag{4}$$

with constants c_1 and c_2. We shall call this equation—first studied by Rayleigh (1891)—the *linear* Fokker–Planck equation.

2. POWER SERIES EXPANSION OF (2)

Rewrite the transition probability $W(a|a')$ as a function of the length of the jump, $\Delta a = a - a'$, and its starting point a',

$$W(a|a') = W(a';\Delta a). \tag{5}$$

So far the variable a has not been specified; it may be an extensive or an intensive quantity. We now stipulate that a is extensive. The corresponding intensive quantity X is related to it by

$$a = \Omega X,$$

where Ω is a measure for the size of the system. The essential point is that *the size of the jump, Δa, is properly expressed in terms of the extensive quantity, whereas the dependence on a' in (5) is properly expressed in terms of the intensive quantity X.* More precisely, if we write

$$W(a';\Delta a) = \Phi(X';\Delta a) = \Phi\left(\frac{a'}{\Omega};\Delta a\right),$$

the function Φ no longer involves Ω implicitly, in contrast with $W(a';\Delta a)$.* That this is so can be seen from the examples in Sections 4, 6, 7.

Since the dependence on Ω has now been made explicit, it is possible to expand in reciprocal powers of Ω. The moments α_n, when expressed as functions of X,

$$\int (\Delta a)^n \, \Phi(X;\Delta a) \, d\Delta a = \alpha_n(X),$$

no longer contain Ω.

Next one has to estimate how the successive derivatives of $P(a,t)$ depend on Ω. For this it is necessary to anticipate the kind of solution one is interested in. If one studies equilibrium alone, the interesting values of a are of order $\Omega^{\frac{1}{2}}$. It is then convenient to introduce a "*normalized*" *variable* $x = \Omega^{-\frac{1}{2}}a = \Omega^{\frac{1}{2}}X$. However, equation (2) can also be used to describe states that differ macroscopically from equilibrium. In such states a will have a mean value of order Ω, and a spread around this mean of order $\Omega^{\frac{1}{2}}$. Accordingly we put

$$a = \Omega\phi(t) + \Omega^{\frac{1}{2}}x.$$

ϕ is the function of time to be determined presently, x is the new variable.

*This requirement may be weakened: it is sufficient that Φ can be expanded in a power series of Ω^{-1}. Compare the example of Section 7.

After transforming from the variable a to the variable x, (2) becomes

$$\frac{\partial P(x,t)}{\partial t} - \Omega^{\frac{1}{2}}\phi'(t)\frac{\partial P(x,t)}{\partial x} = \sum_{n=1}^{\infty}\frac{\Omega^{-\frac{1}{2}n}}{n!}\left(-\frac{\partial}{\partial x}\right)^n \alpha_n\{\phi(t)+\Omega^{-\frac{1}{2}}x\}P(x,t).$$

The leading term on the right is

$$-\Omega^{-\frac{1}{2}}\alpha_1\{\phi(t)\}\frac{\partial P(x,t)}{\partial x}.$$

This can be made to cancel the second term on the left by subjecting $\phi(t)$ to the condition

$$\phi'(t) = \frac{1}{\Omega}\alpha_1\{\phi(t)\}. \tag{6}$$

This is just the macroscopic, phenomenological law. The remaining equation is

$$\frac{\partial P(x,t)}{\partial t} = -\Omega^{-\frac{1}{2}}\frac{\partial}{\partial x}\left[\alpha_1\{\phi(t)+\Omega^{-\frac{1}{2}}x\} - \alpha_1\{\phi(t)\}\right]P + \sum_{n=2}^{\infty}\frac{\Omega^{-\frac{1}{2}n}}{n!}\left(-\frac{\partial}{\partial x}\right)^n \alpha_n\{\phi(t)+\Omega^{-\frac{1}{2}}x\}\,P. \tag{7}$$

It is convenient to put $t/\Omega = \tau$, so that the new time scale increases with Ω, in agreement with the increase of the relaxation time. Then, expanding the right-hand side of (7) in powers of $\Omega^{-\frac{1}{2}}$, and rearranging terms

$$\frac{\partial P(x,\tau)}{\partial \tau} = \sum_{m=2}^{\infty}\frac{\Omega^{-\frac{1}{2}(m-2)}}{m!}\sum_{n=1}^{m}\binom{m}{n}\alpha_n^{(m-n)}\{\phi(\tau)\}\left(-\frac{\partial}{\partial x}\right)^n x^{m-n}P. \tag{8}$$

In this equation all factors Ω are shown explicitly, so that the relevance of the several terms is indicated by their degree in $\Omega^{-\frac{1}{2}}$. The positive powers of Ω have been removed by means of (6).

For many purposes it is useful to find the successive *moments* rather than the distribution function itself. The general formula (8) gives

$$\frac{d}{d\tau}\langle x^k\rangle = \sum_{m=2}^{\infty}\frac{\Omega^{-\frac{1}{2}(m-2)}}{m!}\sum_{n=1}^{m,k}\binom{m}{n}\alpha_n^{(m-n)}\{\phi(\tau)\}\frac{k!}{(k-n)!}\langle x^{m+k-2n}\rangle, \tag{9}$$

the upper limit of n being either m or k, whichever is smaller.

It is noteworthy that for many special cases exact results can be extracted from (9). For instance, if $\alpha_1(X)$ is a linear function,

$$\frac{d}{d\tau}\langle x\rangle = \alpha_1'.\langle x\rangle.$$

This can be solved to give $\langle x\rangle_\tau = \text{const.}\ \phi(\tau)$. It will usually be convenient to choose $\phi(0)$ equal to $\langle a\rangle_0$, so that $\langle x\rangle_0 = 0$; our equation then shows that $\langle a\rangle_\tau = \phi(\tau)$ for all later τ.* Similarly, if $\alpha_2(X)$ happens to be linear, one finds a rigorous equation for $\langle x^2\rangle$. If all $\alpha_n(X)$ are linear, it is possible to find successive equations for all $\langle x^k\rangle$; such a case is the example in Section 4.

*More directly, from either (1) or (2) one has rigorously $(d/dt)\langle a\rangle = \langle\alpha_1(a)\rangle$; if α_1 is linear, this is equal to $\alpha_1(\langle a\rangle)$, which proves that $\langle a\rangle$ obeys the macroscopic equation.

3. THE ZEROTH ORDER APPROXIMATION

Neglecting all terms that vanish for $\Omega \to \infty$,

$$\frac{\partial P}{\partial \tau} = -\alpha_1'\{\phi(\tau)\}\frac{\partial}{\partial x}xP+\frac{1}{2}\alpha_2\{\phi(\tau)\}\frac{\partial^2 P}{\partial x^2}. \tag{10}$$

This would be a linear Fokker–Planck equation of the type (4) if the coefficients were not time dependent. Nevertheless the initial-value problem can be solved.

Suppose the initial distribution at $\tau = 0$ is

$$P(x,0) = \delta(x-x_0). \tag{11}$$

We define

$$s(\tau) = \log\frac{\alpha_1\{\phi(0)\}}{\alpha_1\{\phi(\tau)\}}, \tag{12}$$

so that $s(0) = 0$, and $ds/d\tau = -\alpha_1'\{\phi(\tau)\}$. Then (10) reduces to

$$\frac{\partial P}{\partial s} = \frac{\partial}{\partial x}xP-\frac{\alpha_2\{\phi(\tau)\}}{2\alpha_1'\{\phi(\tau)\}}\frac{\partial^2 P}{\partial x^2}.$$

Putting $x = ye^{-s}$ and $P(x,s) = e^{s}Q(y,s)$,

$$\frac{\partial Q}{\partial s} = -\frac{\alpha_2\{\phi(\tau)\}}{2\alpha_1'\{\phi(\tau)\}}e^{2s}\frac{\partial^2 Q}{\partial y^2}.$$

The solution of this equation is given by Chandrasekhar (1943)

$$Q(s) = [4\pi\gamma(s)]^{-\frac{1}{2}}\exp\left[-\frac{(y-x_0)^2}{4\gamma(s)}\right],$$

where

$$\gamma(s) = -\int_0^s\frac{\alpha_2\{\phi(\tau)\}}{2\alpha_1'\{\phi(\tau)\}}e^{2s}ds = \frac{1}{2}\int_0^\tau\alpha_2\{\phi(\tau)\}e^{2s(\tau)}d\tau.$$

Thus we finally find

$$P(x,\tau) = [2\pi\sigma^2]^{-\frac{1}{2}}\exp\left[-\frac{(x-x_0e^{-s})^2}{2\sigma^2}\right],$$

where

$$\sigma^2(\tau) = e^{-2s(\tau)}\int_0^\tau\alpha_2\{\phi(\tau)\}e^{2s(\tau)}d\tau. \tag{13}$$

In order to find the probability distribution of a with given initial distribution

$$P(a,0) = \delta(a-a_0) = \delta(a-\Omega X_0),$$

one first has to solve

$$d\phi/d\tau = \alpha_1(\phi), \qquad \phi(0) = X_0.$$

This can always be done by a quadrature,

$$\tau = \int_{x_0}^{\phi} \frac{d\phi}{\alpha_1(\phi)}.$$

One then has to determine $s(\tau)$ and $\sigma^2(\tau)$ from (12) and (13). The final result is

$$P(a,\tau) = [2\pi\Omega\sigma^2]^{-\frac{1}{2}} \exp\left[-\frac{\{a-\Omega\phi(\tau)\}^2}{2\Omega\sigma^2}\right]. \tag{14}$$

This is a Gaussian peak, whose width is of the order of the equilibrium fluctuations, and whose center moves according to the phenomenological law.* Higher approximations will destroy the Gaussian shape.

4. FIRST EXAMPLE: DENSITY FLUCTUATIONS

A box of volume Ω communicates through a small hole with an infinitely large volume, filled with a dilute gas with density ρ (Fig. 1). The number N of particles in Ω obeys the master equation (in suitable time units)

$$\frac{\partial P(N)}{\partial t} = \frac{N+1}{\Omega} P(N+1) - \frac{N}{\Omega} P(N) + \rho\{P(N-1) - P(N)\}. \tag{15}$$

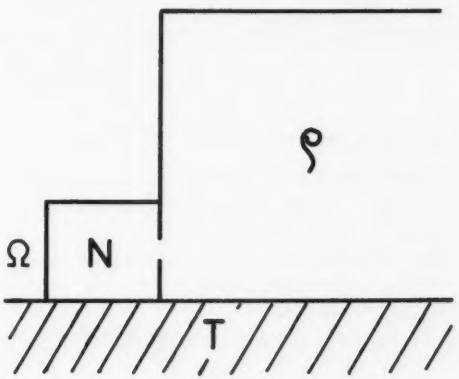

FIG. 1.

N is the extensive variable, the density $X = N/\Omega$ the intensive one. The transition probability is

$$W(N;\Delta N) = \frac{N}{\Omega}\delta_{\Delta N,-1} + \rho\,\delta_{\Delta N,+1} = \Phi(X;\Delta N).$$

The moments $\alpha_n(X)$ are given by

$$\alpha_n(X) = (-1)^n X + \rho.$$

*This result has been employed previously in evaluating the entropy of non-equilibrium states (van Kampen 1959).

The macroscopic equation (6) is

$$\frac{dX}{dt} = \frac{\rho - X}{\Omega},$$

with the solution

$$X = \phi(\tau) = X_0\, e^{-\tau} + \rho(1 - e^{-\tau}),$$

where X_0 is the density at $\tau = 0$. The equilibrium value is $X^{eq} \equiv \phi(\infty) = \rho$, as was to be expected. One finds furthermore

$$s(\tau) = \tau,$$

$$\sigma^2(\tau) = (1 - e^{-\tau})\,(\rho + X_0 e^{-\tau}).$$

Hence (14) takes the form

$$(16)\quad P(N,\tau) = [2\pi(1-e^{-\tau})(\Omega\rho + N_0 e^{-\tau})]^{-\frac{1}{2}} \exp\left[-\frac{\{N - N_0 e^{-\tau} - \Omega\rho(1-e^{-\tau})\}^2}{2(1-e^{-\tau})(\Omega\rho + N_0 e^{-\tau})} \right].$$

This example is sufficiently simple to check the result (16) in several ways. First one finds rigorously from either (1) or (2)

$$(d/dt)\langle N \rangle = \langle \alpha_1(N) \rangle = -\langle N \rangle/\Omega + \rho.$$

$$(d/dt)\langle N^2 \rangle = 2\langle N\alpha_1(N) \rangle + \langle \alpha_2(N) \rangle$$

$$= -2\,\frac{\langle N^2 \rangle}{\rho} + \left(2\rho + \frac{1}{\Omega}\right)\langle N \rangle + \rho.$$

These equations can be solved to give

$$\langle N \rangle_\tau = N_0 e^{-\tau} + \Omega\rho\,(1 - e^{-\tau}).$$

$$\langle N^2 \rangle_\tau - \langle N \rangle_\tau^2 = (N_0 e^{-\tau} + \Omega\rho)(1 - e^{-\tau}).$$

This agrees exactly with the mean and variance of the Gaussian (16). The higher terms in $P(N,\tau)$, therefore, while destroying its Gaussian shape, do not affect the first two moments.

As a second check one may compare the equilibrium value of (16)

$$(17)\qquad P(N,\infty) = [2\pi\Omega\rho]^{-\frac{1}{2}} \exp\left[-\frac{(N - \Omega\rho)^2}{2\Omega\rho} \right],$$

with the correct expression

$$P^{eq}(N) = \frac{(\Omega\rho)^N}{N!}\, e^{-\Omega\rho}.$$

For this purpose we expand $\log P^{eq}(N)$ near its maximum, which is at $N_m = \Omega\rho - \frac{1}{2} + O(\Omega^{-1})$.

$$\log P^{eq}(N) = \log P^{eq}(N_m) - \frac{1}{2}\,\frac{(N - N_m)^2}{\Omega\rho + O(\Omega^{-1})} + \frac{1}{3!}\,\frac{(N - N_m)^3}{(\Omega\rho)^2} + \ldots.$$

This agrees with (17) when terms of order $\Omega^{-\frac{1}{2}}$ are neglected.

As a final check it is possible to solve (15) exactly with the aid of the characteristic function, defined by

$$F(\xi,t) = \langle e^{\xi N}\rangle_t = \sum_{N=0}^{\infty} e^{\xi N} P(N,t).$$

The solution is

$$\log F(\xi,t) = \Omega\rho(1-e^{-\tau})(e^{\xi}-1)+N_0\log(1-e^{-\tau}+e^{\xi-\tau}).$$

Let this be expanded to second order in ξ

$$\log F(\xi,t) = [\Omega\rho(1-e^{-\tau})+N_0e^{-\tau}]\xi+\tfrac{1}{2}[\Omega\rho(1-e^{-\tau})+N_0e^{-\tau}(1-e^{-\tau})]\xi^2.$$

This approximate expression is just the characteristic function of the Gaussian distribution (16).

5. EQUILIBRIUM FLUCTUATIONS

In order to describe the fluctuations in equilibrium one has to substitute for $\phi(\tau)$ in the general equation (8) its equilibrium value $\phi(\infty)$, so that the quantities $\alpha_n^{(m-n)}$ become constants.* The zeroth order equation (10) then reduces to

$$\frac{\partial P(x,\tau)}{\partial\tau} = -\alpha_1'\frac{\partial}{\partial x}xP+\frac{1}{2}\alpha_2\frac{\partial^2 P}{\partial x^2}. \tag{18}$$

This is the linear Fokker–Planck equation (4). The solution with initial distribution (11) is well known,

$$P(x,\tau) = \left[\frac{\pi\alpha_2}{-\alpha_1'}(1-e^{\alpha_1'\tau})\right]^{-\frac{1}{2}}\exp\left[-\frac{(x-x_0e^{\alpha_1'\tau})^2}{(-\alpha_2/\alpha_1')(1-e^{2\alpha_1'\tau})}\right]. \tag{19}$$

(Of course, for all realistic cases $\alpha_1'<0$, $\alpha_2>0$.) The difference between this solution and (14) consists in the fact that the present one is only valid for initial distributions which are confined to a range of order 1 in the x-scale, i.e. of order $\Omega^{\frac{1}{2}}$ in the a-scale, around the equilibrium value.

The next approximation adds to the right-hand side of (18)

$$\frac{1}{3!}\Omega^{-\frac{1}{2}}\left\{-3\alpha_1''\frac{\partial}{\partial x}x^2P+3\alpha_2'\frac{\partial^2}{\partial x^2}xP-\alpha_3\frac{\partial^3 P}{\partial x^3}\right\}. \tag{20}$$

(Note that the resulting equation can also be obtained directly from (2) by breaking off $\alpha_1(a)$ after the second order of a, $\alpha_2(a)$ after the first order, $\alpha_3(a)$ after the zeroth order, and omitting all higher terms.) The first order equation can be solved to the order $\Omega^{-\frac{1}{2}}$ by treating the additional term (20) as a perturbation. That is, one substitutes the zeroth order solution (19) in (20), and solves the resulting inhomogeneous equation for P.

Alternatively one can find the successive moments, using (9), which for the equilibrium region simplifies to

$$\frac{d}{d\tau}\langle x^k\rangle = \sum_{m=2}^{\infty}\Omega^{-\frac{1}{2}(m-2)}\sum_{n=1}^{m,k}\binom{k}{n}\frac{\alpha_n^{(m-n)}}{(m-n)!}\langle x^{m+k-2n}\rangle. \tag{21}$$

*We write α_n for the nth moment of Δa, taken at the equilibrium. $\alpha_n^{(k)}$ denotes the kth derivative of $\alpha_n(X)$ *with respect to* X, also at the equilibrium value of X.

Explicitly,

$$(22a) \qquad (d/d\tau)\,\langle x\rangle = \alpha_1'\langle x\rangle + \tfrac{1}{2}\Omega^{-\frac{1}{2}}\alpha_1''\langle x^2\rangle + \tfrac{1}{6}\Omega^{-1}\alpha_1'''\langle x^3\rangle + O(\Omega^{-3/2}),$$

$$(22b) \qquad (d/d\tau)\,\langle x^2\rangle = 2\alpha_1'\langle x^2\rangle + \alpha_2 + \Omega^{-\frac{1}{2}}\alpha_1''\langle x^3\rangle + \Omega^{-\frac{1}{2}}\alpha_2'\langle x\rangle + O(\Omega^{-1}),$$

$$(22c) \qquad (d/d\tau)\,\langle x^3\rangle = 3\alpha_1'\langle x^3\rangle + 3\alpha_2\langle x\rangle + O(\Omega^{-\frac{1}{2}}).$$

Now let the initial distribution be given by (11), so that

$$\langle x\rangle_0 = x_0, \qquad \langle x^2\rangle_0 = x_0^2, \qquad \langle x^3\rangle_0 = x_0^3.$$

It is then possible to solve the set of equations (22) in successive orders and to find from it $\langle x\rangle$ as a function of τ to order Ω^{-1}. For convenience we choose such units that $\alpha_1 = -1$, $\alpha_2 = 2$. Then one has to zeroth order

$$\begin{aligned}
\langle x\rangle_\tau &= x_0 e^{-\tau},\\
\langle x^2\rangle_\tau &= x_0^2 e^{-2\tau} + 1 - e^{-2\tau},\\
\langle x^3\rangle_\tau &= x_0^3 e^{-3\tau} - 3x_0 e^{-3\tau} + 3x_0 e^{-\tau}.
\end{aligned}$$

Subsequently one finds to order $\Omega^{-\frac{1}{2}}$

$$\langle x^2\rangle_\tau = x_0^2\, e^{-2\tau} + 1 - e^{-2\tau} + \Omega^{-\frac{1}{2}}(1-e^{-\tau})\{(a_2' + 3\alpha_1''')x_0 e^{-\tau} + \alpha_1''(x_0^3 - 3x_0)e^{-2\tau}\}.$$

Finally to order Ω^{-1},

$$\begin{aligned}
(23) \qquad \langle x\rangle_\tau = {} & x_0 e^{-\tau} + \tfrac{1}{2}\Omega^{-\frac{1}{2}}\alpha_1''\{1 - 2e^{-\tau} + e^{-2\tau} + x_0^2(e^{-\tau} - e^{-2\tau})\}\\
& + \tfrac{1}{2}\Omega^{-1}\{\alpha_1''^2(x_0^3 - 3x_0)(\tfrac{1}{2}e^{-\tau} - e^{-2\tau} + \tfrac{1}{2}e^{-3\tau})\\
& \quad - (3\alpha_1''^2 + \alpha_1''\alpha_2')x_0(e^{-\tau} - e^{-2\tau})\}\\
& + \tfrac{1}{2}\Omega^{-1}(3\alpha_1''^2 + \alpha_1''\,\alpha_2' + \alpha_1''')x_0\tau e^{-\tau}\\
& + \tfrac{1}{12}\,\Omega^{-1}\alpha_1'''(x_0^3 - 3x_0)(e^{-\tau} - e^{-3\tau}).
\end{aligned}$$

As an example of the moment method we compute the *spectral density* of the fluctuations to order Ω^{-1}. The autocorrelation function is obtained from (23) by multiplying with x_0 and averaging over the equilibrium distribution $P^{\text{eq}}(x_0)$. For this one needs the equilibrium moments, which can be found to any desired order from (21) by putting the left side equal to zero

$$\begin{aligned}
\langle x\rangle^{\text{eq}} &= \tfrac{1}{2}\Omega^{-\frac{1}{2}}\alpha_1'' + O(\Omega^{-3/2}),\\
\langle x^2\rangle^{\text{eq}} &= 1 + \tfrac{1}{2}\,\Omega^{-1}\{\tfrac{5}{2}\,\alpha_1''^2 + \tfrac{3}{2}\,\alpha_1''\,\alpha_2' + \tfrac{1}{3}\,\alpha_1''\alpha_3 + \alpha_1''' + \tfrac{1}{2}\,\alpha_2''\} + O(\Omega^{-2}),\\
\langle x^3\rangle^{\text{eq}} &= \Omega^{-\frac{1}{2}}\{\tfrac{5}{2}\,\alpha_1'' + \alpha_2' + \tfrac{1}{3}\,\alpha_3\} + O(\Omega^{-3/2}),\\
\langle x^4\rangle^{\text{eq}} &= 3 + O(\Omega^{-1}).
\end{aligned}$$

With the aid of these values one finds for the autocorrelation function

$$\begin{aligned}
\langle x(0)x(\tau)\rangle \equiv \langle x_0\langle x\rangle_\tau\rangle^{\text{eq}} = {} & e^{-\tau}\\
& + \tfrac{1}{2}\,\Omega^{-1}[\tfrac{1}{2}\,\alpha_1''^2 + \{\alpha_1''^2 + \tfrac{3}{2}\,\alpha_1''\,\alpha_2' + \tfrac{2}{3}\,\alpha_1''\,\alpha_3 + \alpha_1''' + \tfrac{1}{2}\,\alpha_2''\}\,e^{-\tau}\\
& \quad + \{\alpha_1''^2 - \tfrac{1}{3}\,\alpha_1''\,\alpha_3 e\}^{-2\tau}\\
& \quad + \{3\alpha_1''^2 + \alpha_1''\,\alpha_2' + \alpha_1'''\}\tau e^{-\tau}].
\end{aligned}$$

The last term may be combined with the term $e^{-\tau}$ to give $e^{-\lambda\tau}$ with

$$\lambda = 1-\tfrac{1}{2}\Omega^{-1}(3\alpha_1''^2+\alpha_1''\,\alpha_2'+\alpha_1''').$$

The constant term $\frac{1}{4}\Omega^{-1}\alpha_1''^2$ exhibits the fact that $\langle x\rangle^{\text{eq}}$ does not vanish, so that

$$\lim_{\tau\to\infty}\langle x(0)x(\tau)\rangle = (\langle x\rangle^{\text{eq}})^2 = (\tfrac{1}{2}\Omega^{-\frac{1}{2}}\alpha_1'')^2.$$

Hence (24) may also be written

$$\langle\{x(0)-\langle x\rangle^{\text{eq}}\}\{x(\tau)-\langle x\rangle^{\text{eq}}\}\rangle =$$
$$[1+\tfrac{1}{2}\Omega^{-1}\{\alpha_1''^2+\tfrac{3}{2}\alpha_1''\,\alpha_2'+\tfrac{2}{3}\alpha_1''\,\alpha_3+\alpha_1'''+\tfrac{1}{2}\alpha_2'\}]\,e^{-\lambda\tau}+\{\alpha_1''^2-\tfrac{1}{3}\alpha_1''\,\alpha_3\}e^{-2\tau}.$$

From this follows the fluctuation spectrum

$$(25)\quad S_x(\omega) = \frac{2}{\pi}\left[\frac{1+\tfrac{1}{2}\Omega^{-1}\{-2\alpha_1''^2+\tfrac{1}{2}\alpha_1''\,\alpha_2'+\tfrac{2}{3}\alpha_1''\,\alpha_3+\tfrac{1}{2}\alpha_2''\}}{\lambda^2+\omega^2}\right.$$
$$\left.+\frac{\Omega^{-1}\{\alpha_1''^2-\tfrac{1}{3}\alpha_1''\,\alpha_3\}}{4+\omega^2}\right].$$

Bernard and Callen (1960) arrived at the conclusion that the fluctuation spectrum is entirely independent of the non-linear terms. According to (25), this is only correct for $\Omega\to\infty$. (In fact it can be seen from our examples that both coefficients $\{\ \}$ in (25) do not happen to vanish.)

6. SECOND EXAMPLE: ALKEMADE'S DIODE

(Alkemade 1958; van Kampen 1960)

Consider the circuit of Fig. 2. The whole system is kept at constant temperature T. The two electrodes have different work functions, and electrode 1 is supposed to operate under saturation conditions. The number of electrons N on the left condenser plate obeys the master equation (in suitable time units)

$$(26)\quad \frac{\partial P(N)}{\partial t} = P(N+1)-P(N)+\zeta\{e^{-\epsilon(N-1)}P(N-1)-e^{-\epsilon N}P(N)\}.$$

Here $\epsilon = e^2/kTC$, and ζ is a constant depending on both work functions. The expansion parameter Ω is the capacity C of the condenser, or rather

$$\Omega = kTC/e^2 = \epsilon^{-1}.$$

For the extensive parameter we take $a = N$, so that $X = \epsilon N$. The Kramers–Moyal equation in terms of a is

$$\frac{\partial P(N,t)}{\partial t} = \sum_{n=1}^{\infty}\frac{1}{n!}\left(-\frac{\partial}{\partial N}\right)^n\{(-1)^n+\zeta e^{-X}\}P(N,t).$$

The macroscopic equation is

$$(27)\quad \frac{dX}{d\tau} = -1+\zeta e^{-X}.$$

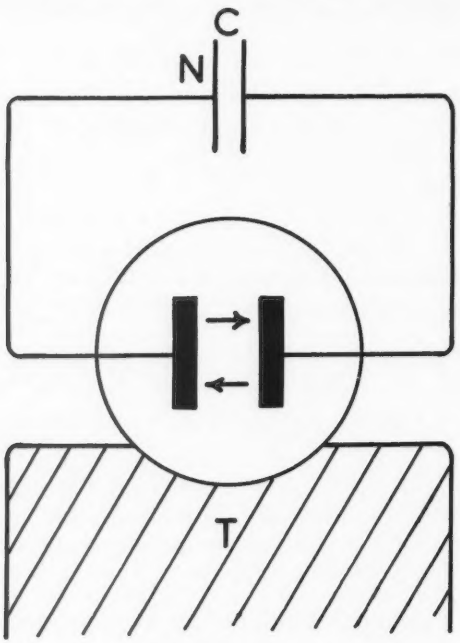

FIG. 2.

Equilibrium obtains for $X = \log \zeta$, which determines the contact potential X_c. Writing (27) in the form

$$\frac{dN}{dt} = e^{-(X-X_c)} - 1,$$

one recognizes the usual I–V characteristic of the diode.

The solution of (27) is

$$X(\tau) - X_c = \log(1+e^{\tau_0-\tau}), \tag{28}$$

where τ_0 is an integration constant given by

$$e^{\tau_0} = e^{X(0)-X_c} - 1.$$

One subsequently finds

$$s(\tau) = \log \frac{e^{\tau}+e^{\tau_0}}{1+e^{\tau_0}}$$

and

$$\sigma^2(\tau) = 1+\frac{e^{\tau+\tau_0}+\tau e^{2\tau_0}-e^{2\tau_0}-3e^{\tau_0}-1}{(e^{\tau}+e^{\tau_0})^2}. \tag{29}$$

This is in agreement with the result obtained previously (van Kampen 1960). The distribution $P(N,t)$ is the Gaussian (14) with $\phi(\tau)$ taken from (28) and $\sigma^2(\tau)$ from (29). The equilibrium distribution is, to this order,

$$P^{eq}(N) = \frac{1}{\sqrt{2\pi\Omega}} \exp\left[-\frac{(N-\Omega X_e)^2}{2\Omega}\right]. \tag{30}$$

The spectral density of the equilibrium fluctuations is obtained from (25) by substituting

$$\alpha_1'' = \alpha_1''(X_e) = 1,$$

$$\alpha_2 = -1, \qquad \alpha_2'' = 1,$$

$$\alpha_3 = 0.$$

The result is again identical with the one obtained previously.

According to (30) the average number of electrons in equilibrium is $\langle N\rangle^{eq} = \Omega X_e$. According to (23), however, there is a higher order correction $\Omega^{\frac{1}{2}}\langle x\rangle^{eq} = \frac{1}{2}\alpha_1'' = \frac{1}{2}$. [Incidentally, this corrected value happens to be the exact one, because the exact equilibrium distribution is

$$P^{eq}(N) = [2\pi\Omega]^{-\frac{1}{2}} \exp\left[-\frac{(N-\Omega X_e-\frac{1}{2})^2}{2\Omega}\right], \tag{31}$$

as can easily be found from (26).] It means that the equilibrium distribution as found from the zeroth order equation, viz. (30), differs from the exact one through higher order terms. In this case these higher order terms do not destroy the Gaussian shape, but merely cause a shift. Accordingly the value for the contact potential, $X_e = \log \zeta$, is not the exact one. Using the explicit value for ζ, one finds for the exact contact potential

$$X_e + \tfrac{1}{2}\,\Omega = (W_1 - W_2)/kT,$$

where W_1 and W_2 are the work functions of both electrodes. The fact that the equilibrium value of the potential in lowest order, X_e, does not exactly correspond with the expected value, $W_1 - W_2$, has given rise to some discussion (MacDonald 1957; Alkemade 1958; Marek 1959).

7. THIRD EXAMPLE: RAYLEIGH'S PISTON

(Rayleigh 1891; Zernike 1929)

In one dimension a heavy particle with mass M is subjected to collisions with light gas molecules with mass m and velocity distribution $f(v)$ (Fig. 3). A collision of a molecule with velocity v changes the velocity V of the heavy particle into

$$V' = V + \frac{2m}{M+m}(v - V) = V + \Delta V.$$

One thus obtains a master equation for the velocity distribution $P(V,t)$, with transition probability

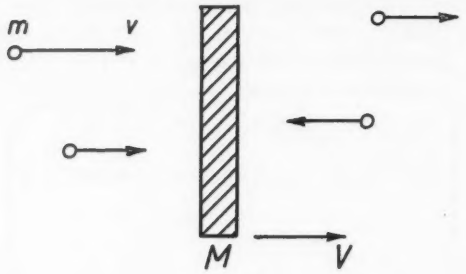

FIG. 3.

$$W(V'|V) = \nu\left(\frac{M+m}{2m}\right)^2 |V'-V| f\left(\frac{M+m}{2m}V' - \frac{M-m}{2m}V\right), \tag{32}$$

where ν is the number of molecules per unit length.

Although the concept of intensive and extensive variables is somewhat alien to this system, a similar distinction can be made. Indeed, the individual jumps in V are due to collisions with the gas molecules, and are therefore appropriately measured in terms of the momentum MV. On the other hand, the probability distribution of these jumps depends on the velocity V itself. Thus one is led to the following identification

$$a = \frac{M}{m}V, \qquad X = V, \qquad \Omega = \frac{M}{m}. \tag{33}$$

The transition probability (32) then takes the form

$$W(a;\Delta a) = \tfrac{1}{4}\nu(1+\Omega^{-1})^2|\Delta a| f\{X+\tfrac{1}{2}(1+\Omega^{-1})\Delta a\}.$$

This expression is not entirely independent of Ω. However, it can be expanded in powers of Ω^{-1}, so that the previous treatment can still be applied with minor modifications. This leads to the usual expansion in m/M.

A more elegant application of the previous treatment, however, is possible if one puts

$$a = \frac{M+m}{m}V, \qquad X = V, \qquad \Omega = \frac{M+m}{m}. \tag{34}$$

The transition probability now takes the form

$$W(a;\Delta a) = \tfrac{1}{4}\nu\,|\Delta a\,| f(X+\tfrac{1}{2}\Delta a) = \Phi(X;\Delta a),$$

entirely independent of Ω. Hence the results of the previous sections can now be literally applied.

The macroscopic equation, which describes the approach of $\langle V\rangle$ to its equilibrium value $\langle V\rangle^{\text{eq}} = 0$, is rather unmanageable. We therefore only study the equilibrium fluctuations. The zeroth approximation is the linear Fokker–Planck equation (18) with

$$\alpha_1' = \frac{1}{4}\nu \int_{-\infty}^{+\infty} (\Delta a)|\Delta a| f'(\tfrac{1}{2}\Delta a)\, d\Delta a,$$

$$\alpha_2 = \frac{1}{4}\nu \int_{-\infty}^{+\infty} (\Delta a)^2|\Delta a| f(\tfrac{1}{2}\Delta a)\, d\Delta a.$$

If f is the Maxwell distribution,

$$\alpha_1' = -\frac{m}{2kT} \qquad \alpha_2 = 4\nu\left(\frac{2kT}{m}\right)^{\frac{1}{2}}.$$

After transforming back to the usual variables $V = \Omega^{-\frac{1}{2}}x$, $t = \Omega\tau$ the Fokker-Planck equation becomes

$$\frac{\partial P(V,t)}{\partial t} = \nu \frac{4m}{M+m}\left(\frac{2kT}{\pi m}\right)^{\frac{1}{2}} \frac{\partial}{\partial V}\left\{VP + \frac{kT}{M+m}\frac{\partial^2 P}{\partial V^2}\right\}. \tag{35}$$

This is the well-known Rayleigh equation, but for the appearance of $M+m$ in place of M. The reason is that we have expanded in powers of $m/(m+M)$ rather than in m/M. The lowest order of the expansion in m/M can, of course, easily be obtained from (35) by simply replacing $M+m$ with M.

The next term in the expansion is (20), but all coefficients vanish because of symmetry.* The term of order Ω^{-1} can also be found; if one puts $m/kT = 1$, and $m/M = \mu$, the result is, when written as an expansion in μ,

$$\frac{\partial P(V,t)}{\partial t} = \frac{\nu}{\sqrt{2\pi}}\left[\frac{8\mu}{1+\mu}\left\{\frac{\partial}{\partial V}V + \mu\frac{\partial^2}{\partial V^2}\right\}P \right. \tag{36}$$

$$\left. +8\mu\left\{-\mu^2\frac{\partial^2}{\partial V^2} + \frac{1}{6}\frac{\partial}{\partial V}V^3 + \frac{3}{2}\mu\frac{\partial^2}{\partial V^2}V^2 + \frac{8}{3}\mu^2\frac{\partial^3}{\partial V^3}V + \frac{4}{3}\mu^2\frac{\partial^4}{\partial V^4}\right\}P\right].$$

The terms on the second line are of order μ relative to those on the first line. They agree with the result of Siegel (1960).

An advantage of expanding in μ rather than Ω^{-1} is that the equilibrium distribution, when expressed in the normalized co-ordinate $\mu^{\frac{1}{2}}V$ is independent of μ. Hence it must satisfy each term of the expansion separately. This can be verified from (36). The equilibrium distribution, when expressed in $\Omega^{\frac{1}{2}}V$, contains higher terms in Ω^{-1} and hence does not satisfy the separate terms of the expansion in Ω^{-1} (see next section). That is the reason why it is not an exact solution of (35).

8. RELATIONS FOLLOWING FROM THE KNOWN EQUILIBRIUM DISTRIBUTION

So far the equilibrium distribution has been found as a special solution of the master equation. It often happens, however, that it is known a priori. Then this known solution can be used, by substituting it in the general equation, to find relations between the α's. For instance, it follows from (18) that to lowest order the equilibrium distribution is given by

*Recently MacDonald (private communication) has suggested an asymmetric modification of the Rayleigh piston model, for which these coefficients do not vanish.

$$P^{eq}(x) = [-\pi\alpha_2/\alpha_1']^{-\frac{1}{2}} \exp\left[-\frac{x^2}{-\alpha_2/\alpha_1'}\right]. \tag{37}$$

The variance $(-\alpha_2/2\alpha_1')$ of this Gaussian is usually known from equilibrium statistical mechanics. Hence one obtains a relation between α_2 and α_1', which corresponds to the usual Einstein relation for Brownian movement.

Additional relations can only be obtained if higher order terms of the equilibrium distribution are also known. In some cases one knows that (37) is exact to all orders. Thus, taking again $\alpha_1' = -1$, $\alpha_2 = 2$,

$$\begin{aligned} \langle x^k \rangle &= 0, && \text{(odd } k\text{)} \\ \langle x^k \rangle &= (k-1)!!. && \text{(even } k\text{)} \end{aligned} \tag{38}$$

On substituting in (21) the separate powers of Ω yield

$$\sum_{n=1}^{m,k} \frac{(m+k-2n-1)!!}{n!(k-n)!(m-n)!} \alpha_n^{(m-n)} = 0,$$

where $m = 2, 3, \ldots$; $k = 1, 2, \ldots$; $m+k$ even; n running from 1 up to m or k, whichever is smaller. It is easily seen that for $m = 2$ these equations are identically satisfied. For $m = 3$ they lead to

$$\alpha_1'' = 0, \qquad 3\alpha_2' + \alpha_3 = 0. \tag{39}$$

For $m = 4$,

$$2\alpha_1''' + \alpha_2'' = 0, \qquad 4\alpha_2'' + 4\alpha_3' + \alpha_4 = 0. \tag{40}$$

More generally one finds that all even derivatives of α_1 vanish (at equilibrium) whereas for odd m,

$$2\alpha_1^{(m)} + \alpha_2^{(m-1)} = 0.$$

The Rayleigh piston furnishes an example of an equilibrium distribution that is known to all orders of Ω, but is not independent of Ω. Indeed

$$P^{eq} \propto \exp\left[-\frac{MV^2}{2kT}\right] \propto \exp\left[-\frac{m}{2kT}(1-\Omega^{-1})x^2\right].$$

Putting $m/kT = 1$ one has instead of (38),

$$\langle x^k \rangle = (k-1)!!(1-\Omega^{-1})^{-\frac{1}{2}k}.$$

Substituting in (21) and separating the various powers of Ω, one finds in the same way as before that (39) is still valid, but (40) must be replaced with

$$2\alpha_1''' + \alpha_2'' + 4\alpha_1' = 0,$$

$$4\alpha_2'' + 4\alpha_3' + \alpha_4 + 4\alpha_2 = 0.$$

These relations can be verified by explicit computations.

MacDonald (1957) has emphasized that (37) need not be correct to all orders. In fact, in our example of Section 4 it is certainly only correct in zeroth order. Yet it may be asserted that the equilibrium distribution must be Gaussian under the following conditions.

(i) The energy of the total system is quadratic in the fluctuating quantity a; and

(ii) the transition probability $W(a|a')$ contains some physical parameter (other than Ω) as a factor, which permits to scale down its magnitude without affecting its functional dependence on a and a'.

The first condition ensures that, according to equilibrium statistical mechanics, the probability distribution is

$$P^{\text{eq}}(x) \propto e^{-E/kT} \propto e^{-cx^2}. \tag{41}$$

For instance, this condition rules out the case of density fluctuations. The second condition is necessary because (41) is only exact for infinitely small interaction. The scaling parameter permits to go to the limit of infinitely small interaction, so that (41) becomes exact. It may then be concluded that (41) must also be exact for all other values of the scaling parameter, because P^{eq} does not depend on the magnitude of $W(a|a')$, but only on its functional dependence of a and a'.

Both conditions are fulfilled in the case of Rayleigh's piston, if the variable a is defined according to (33) rather than (34), the scaling parameter being ν. Hence the Gaussian distribution is valid for all values of M/m—which of course is well known. In the case of the diode, the electrical energy of the circuit is proportional to the square of $X-(W_1-W_2)/kT$, so that equilibrium statistical mechanics indeed leads to (31). The exchange of electrical energy with thermal energy of the heat bath can be scaled down by decreasing the area of the electrodes. (This area should occur as a factor in the right-hand side of (26), although for convenience it was not written explicitly but absorbed in the time unit.) This explains why (31) has to be exact.

9. COMPARISON WITH SIEGEL'S EXPANSION

Recently Siegel (1960) has given an ingenious transformation of the Kramers–Moyal expansion (2), namely

$$\frac{\partial P}{\partial t} = e^{-\frac{1}{2}x^2} \sum_{m=1}^{\infty} \sum_{l=1}^{m} A_{lm} \left(\frac{1}{2}x - \frac{\partial}{\partial x}\right)^{m-l+1} \left(\frac{1}{2}x + \frac{\partial}{\partial x}\right)^{l} e^{\frac{1}{2}x^2} P. \tag{42}$$

The expansion only applies to the neighborhood of equilibrium (our Section 5). The units are chosen such that $-\alpha_2/2\alpha_1' = 1$, and it is assumed that the equilibrium distribution is rigorously $\propto e^{-\frac{1}{2}x^2}$. The coefficients A_{lm} are related to our moments $\alpha_n(X)$ by

$$A_{lm} = \frac{1}{\sqrt{2\pi}} \frac{1}{l!} \sum_{k=l}^{m} \frac{\Omega^{-\frac{1}{2}(m-k+1)}}{(k-l)!(m-k+1)!} \int_{-\infty}^{+\infty} H_k(x) \alpha_{m-k+1}(\Omega^{-\frac{1}{2}}x) e^{-\frac{1}{2}x^2} dx, \tag{43}$$

where $H_k(x)$ denotes a Hermite polynomial,

$$H_k(x) = e^{\frac{1}{2}x^2} \left(-\frac{d}{dx}\right)^k e^{-\frac{1}{2}x^2}. \tag{44}$$

Siegel suggests that in (43) the successive values of m should constitute successive orders of approximation, and he shows for the case of the Rayleigh

piston that, indeed, A_{lm} is of order $\Omega^{-\frac{1}{2}m}$ (Ω being given by (33)). As we have obtained a power series expansion for *all* cases, it is now possible to check Siegel's suggestion generally. From (43) follows with the aid of (44),

$$A_{lm} = \frac{1}{\sqrt{2\pi}} \frac{1}{l!} \sum_{k=l}^{m} \frac{\Omega^{-\frac{1}{2}(m+1)}}{(k-l)!(m-k+1)!} \sum_{\nu=0}^{\infty} \frac{\Omega^{-\frac{1}{2}}}{\nu!} \alpha_{m-k+1}^{(k+\nu)}(0) \int_{-\infty}^{\infty} x^{\nu} e^{-\frac{1}{2}x^2}\, dx.$$

This shows that A_{lm} is of order $\Omega^{-\frac{1}{2}(m+1)}$, so that the successive terms of Siegel's expansion are indeed of increasing order of smallness.*†

Siegel's aim is rather to give a systematic expansion, which achieves two other purposes:

(i) in each approximation (i.e., if (42) is broken off at an arbitrary value m_0 of m) the correct equilibrium distribution $e^{-\frac{1}{2}x^2}$ should be an exact solution;

(ii) each approximation should be "semidefinite", meaning that all solutions should tend to $e^{-\frac{1}{2}x^2}$ for $t \to \infty$.

The first purpose seems to me a laudable one, albeit mainly for reasons of elegance. Admittedly, it is an awkward feature of the systematic expansion that it leads to the denominator $M+m$ rather than M in (35), although it is not incorrect. For practical purposes, however, such as the computation of the fluctuation spectrum, a systematic power series expansion is more convenient.

Siegel achieves the second purpose by a mathematical construction, which may be roughly described as follows. After cutting off the expansion of the master equation at m_0, suitably chosen higher order terms are added such as to make the resulting equation "semidefinite". This construction could also be applied to our expansion (8). However, I do not feel that one ought to impose the requirement (ii) of being "semidefinite" on the successive approximations. It is true that, for each m_0 for which the cutoff series is not "semidefinite", there exist solutions that do not tend to the equilibrium distribution $e^{-\frac{1}{2}x^2}$. Such a behavior, however, only shows that the approximation used is not good enough for these solutions.‡ By adding higher order terms to make the equation "semidefinite" one does not improve the approximation. One only replaces the incorrect solutions by other solutions, which do tend to $e^{-\frac{1}{2}x^2}$, but are otherwise equally incorrect.

REFERENCES

ALKEMADE, C. T. J. 1958. Physica, **24**, 1029.
BERNARD, W. and CALLEN, H. B. 1960. Phys. Rev. **118**, 1466.
CHANDRASEKHAR, S. 1943. Revs. Modern Phys. **15**, 1.
FOKKER, A. D. 1913. Thesis, Leiden.
——— 1914. Ann. Physik, **43**, 810.

*The reason we find $A_{lm} \sim \Omega^{-\frac{1}{2}(m+1)}$, as compared to Siegel's $A_{lm} \sim \Omega^{-\frac{1}{2}m}$, is that he writes an additional factor $\Omega^{\frac{1}{2}}$ in the transition probability, which simply amounts to using a different time scale.

†For example, as mentioned in Section 7, it can be verified that our next approximation (36) coincides with the next approximation given by Siegel, apart from terms of order $(m/M)^2$.

‡Generally speaking, that occurs when the initial distribution is a very rapidly varying function, such that the terms involving higher derivatives are not small. It follows that a solution with initial condition (11) must not be regarded as a physically possible one, but only as a means to represent solutions that are sufficiently smooth for the approximation to be valid.

VAN KAMPEN, N. G. 1959. Physica, **25**, 1294.
——— 1960. Physica, **26**, 585.
KRAMERS, H. A. 1940. Physica, **7**, 284 (Collected Scientific Papers (Amsterdam **1956**), p. 754).
LAX, M. 1960. Revs. Modern Phys. **32**, 25.
MACDONALD, D. K. C. 1957. Phys. Rev. **108**, 541.
MAREK, A. 1959. Physica, **25**, 1358.
MOYAL, J. E. 1949. J. Roy. Statist. Soc. (B) **11**, 150.
PLANCK, M. 1917. Sitzungsber. Preuss. Akad. Wissens. p. 324 (Physikalische Abhandlungen und Vorträge II (Braunschweig 1958) p. 435).
Lord RAYLEIGH. 1891. Phil. Mag. **32**, 424 (Scientific Papers (Cambridge 1902) **3**, 473).
SIEGEL, A. 1960. J. Math. Phys. **1**, 378.
——— Proceedings of the 2nd International Symposium on Rarified Gas Dynamics, Berkeley 1960. To be published.
WANG, M. C. and UHLENBECK, G. E. 1945. Revs. Modern Phys. **17**, 323.
ZERNIKE, F. 1929. Handbuch der Physik **3**, 419.

THE FINITE BEAM SPACE-CHARGE LIMITED DIODE AS A NOISE TRANSDUCER[1]

R. A. McFarlane[2]

ABSTRACT

A method is presented for calculating the noise properties of a cylindrical electron beam from a space-charge limited diode electron gun. The multivelocity character of the beam is considered and correction is made for finite beam diameter. The ratio of anode noise current to full shot noise is found to depend on $\omega^{1/2}/V_{0a}$ where ω is the frequency and V_{0a} the anode voltage.

INTRODUCTION

Haus (1955) has demonstrated that four independent parameters are required to completely specify the noise properties of an electron beam from a thermionic cathode. He shows that under small signal, single velocity assumptions, the electron beam can be represented as a lossless passive transducer, where output noise quantities are linear functions of input quantities. There are found two noise invariants, S and Π, which remain unchanged under such a conservative transformation. The non-conservative nature of a multivelocity electron beam was indicated by Siegman *et al.* (1957), who made detailed calculations of the four noise parameters, Ψ, Φ, Π, and Λ, as a function of the Fry-Langmuir distance variable ξ, in the region of a space-charge limited diode immediately beyond the potential minimum.

The beam noise properties at or beyond the electron gun anode are more directly accessible to experiment than are those near the potential minimum. The present work describes a method for calculating the anode noise parameters in terms of input quantities at a plane slightly beyond the potential minimum. This is essentially a determination of the transducer matrix elements T_{ij}, where the formal representation is

$$(1) \qquad \begin{bmatrix} \Psi_a \\ \Phi_a \\ \Pi_a \\ \Lambda_a \end{bmatrix} = [T_{ij}] \begin{bmatrix} \Psi_{in} \\ \Phi_{in} \\ \Pi_{in} \\ \Lambda_{in} \end{bmatrix}.$$

Input values of Ψ, Φ, Π, and Λ used in the numerical calculations were those found by Siegman. Included in the analysis is a point-by-point correction for the finite beam diameter (Kornelsen 1957). This is facilitated by the use of an analog computer to solve a modified form of the electronic equation (Hutter 1952, 1953). A particular electron gun is examined at three frequencies and over a range of anode voltages.

[1]Manuscript received August 30, 1960.
Contribution from the Eaton Electronics Research Laboratory, McGill University, Montreal, Que.
[2]Now at the Research Laboratory of Electronics, Massachusetts Institute of Technology, Cambridge, Massachusetts.

The results of the computation for Ψ show a dependence on frequency and gun anode voltage not previously reported. A companion paper presents the results of measurements made by this author and other workers and compares them with the present calculations.

THEORY

To include the effect of finite beam diameter on the plasma frequency in a cylindrical beam, Parzen (1952) proposed that the d-c. current density J_0 be replaced in the electronic equation (Hutter 1952, 1953) by an effective value J_{0e}, given by

$$J_{0e} = p^2 J_0 \tag{2}$$

where p is the usual plasma frequency reduction factor. Under the assumption of zero total current, the electronic equation becomes

$$\frac{\partial^2 Y}{\partial \tau^2} - \frac{1}{u_0}\left[\frac{\partial^2 u_0}{\partial \tau^2} - p^2 \frac{eJ_0}{m\epsilon_0}\right] Y = 0 \tag{3}$$

where the a-c. signal current modulation is

$$J_\omega = \frac{Y}{u_0} e^{-j\omega\tau} \tag{4}$$

and the a-c. velocity modulation is

$$v_\omega = \frac{-1}{j\omega J_0}\left\{\frac{\partial Y}{\partial \tau} - \frac{Y}{u_0}\frac{\partial u_0}{\partial \tau}\right\} e^{-j\omega\tau} . \tag{5}$$

Kornelsen (1957) has assumed the region in the gun between the potential minimum and the anode to be a Llewellyn gap with zero initial acceleration. The d-c. velocity is then given by

$$u_0 = \frac{1}{2}\frac{eJ_0}{m\epsilon_0}\tau^2 + u_{0m} \tag{6}$$

where τ is the transit time from the potential minimum and u_{0m} is an initial velocity used to characterize the multivelocity beam. Equation (3) becomes

$$\frac{\partial^2 Y}{\partial \tau^2} - K\frac{(1-p^2)}{u_0} Y = 0 \tag{7}$$

where

$$K = eJ_0/m\epsilon_0 \tag{8}$$

and this is the final form to be solved on the computer.

The plasma frequency reduction factor is taken to be that of the first radial mode in a cylindrical beam with a surrounding conducting cylinder at infinity. In applying this form of correction to an accelerated beam, it is assumed that the effective current density at any point in the gun can be characterized by the reduction factor for a drifting beam of the same radius

and d-c. velocity. Higher order modes and mode coupling are neglected. The result here obtained is more accurate than the W.K.B. solution by Rowe (1952) and the more restricted method of Kosmahl (1959).

The development of the modified electronic equation (7) involves small signal, single velocity assumptions which are unquestionably violated in the region of the potential minimum. It might also be remarked that neither the modified electronic equation nor the Llewellyn–Peterson equations (Pierce 1950) admit to the existence or development of real kinetic power when the input plane is selected at the potential minimum, although the conservation of S is maintained. To overcome these difficulties, the present method of solution restricts the application of the electronic equation to a region in the gun over which the assumptions made in its derivation can be reasonably presumed valid. The statistical calculations of Siegman *et al.* provide a criterion for determining an appropriate input plane and make it possible to specify the initial noise quantities to be used.

At an input plane where the beam has developed real kinetic power, there exists correlation between the current and kinetic voltage fluctuations. As shown by Bloom (1955) and Beam (1955) the noise properties at such a cross section can be represented by three independent noise inputs. If $\overline{V_1^2}$ and $\overline{J_1^2}$ are the total mean square fluctuations per unit bandwidth per unit beam area for the input kinetic noise voltage and current, the three inputs are specified by

$$\overline{V_{\mathrm{I}}^2} = (1-k_1^2)\overline{V_1^2} \qquad \overline{J_{\mathrm{I}}^2} = 0 \tag{9a}$$

$$\overline{V_{\mathrm{II}}^2} = 0 \qquad \overline{J_{\mathrm{II}}^2} = (1-k_2^2)\overline{J_1^2} \tag{9b}$$

$$\overline{V_{\mathrm{III}}^2} = k_1^2\overline{V_1^2} \qquad \overline{J_{\mathrm{III}}^2} = k_2^2\overline{J_1^2} \tag{9c}$$

with

$$\frac{J_{\mathrm{III}}}{V_{\mathrm{III}}} = \frac{k_2}{k_1}e^{j\theta}\left[\frac{\overline{J_1^2}}{\overline{V_1^2}}\right]^{1/2}. \tag{9d}$$

The correlation coefficients are such that

$$0 \leqslant k_1 \leqslant 1,$$

$$0 \leqslant k_2 \leqslant 1.$$

For convenience in discussion, the following definitions are made, using quantities calculated by Siegman. Their relation to Haus' noise parameters is indicated.

$$\delta^2 = \frac{\overline{J_1^2}}{2eJ_0} = 4\pi\Psi \tag{10a}$$

$$\mu^2 = \frac{2eJ_0}{4k^2T_e^2}\overline{V_1^2} = \frac{2eJ_0}{4k^2T_e^2}4\pi\Phi \tag{10b}$$

$$\Pi' = \mathrm{Re}\,\frac{\overline{V_1J_1^*}}{2kT_e} = \frac{4\pi\Pi}{2kT_e} \tag{10c}$$

$$\Lambda' = \mathrm{Im}\,\overline{\frac{V_1 J_1^*}{2kT_c}} = \frac{4\pi\Lambda}{2kT_c} \tag{10d}$$

$$S' = [\mu^2\delta^2 - \Lambda'^2]^{1/2} = \frac{4\pi S}{2kT_c} \tag{10e}$$

Values for these quantities are published as a function of the distance parameter ξ.

From (9) and (10) it is apparent that

$$\Pi' = \mu\delta k_1 k_2 \cos\theta \tag{11a}$$

$$\Lambda' = -\mu\delta k_1 k_2 \sin\theta. \tag{11b}$$

An input plane ξ having been specified, the values of θ and the product k_1k_2 are determined. As will be demonstrated, a proper selection of k_2 leads to the conservation of real kinetic power and with k_2 specified there results an unambiguous determination of all input quantities.

THE ANALOG COMPUTER SOLUTION

Kornelsen (1957) has discussed in detail the use of an analog computer to solve the finite beam electronic equation. Only a short summary of the method will be presented here. A schematic diagram of the computer is shown in Fig. 1. The procedure used by Kornelsen is briefly as follows.

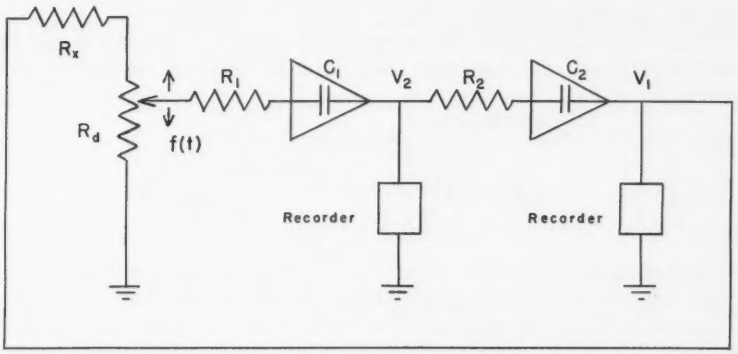

FIG. 1. Analog computer schematic. Two operational amplifiers are used as integrators. V_1 corresponds to the quantity Y of equation (7) and V_2 to its time derivative. The circuit constants are determined by equating coefficients of the parallel equations.

(1) The computer is set up to solve an equation corresponding exactly in form to equation (7).

(2) Two time normalizations are made. If T is the independent variable, t, real time on the computer, and τ, gun transit time, normalization is such that at a point representing the gun anode

$$T = \alpha t_a = \rho\tau_a = 1$$

and this serves to define α and ρ.

(3) The quantity $(1-p^2)/u_0$, for a given beam radius and frequency, is determined as a function of time using equation (6), and an assumed initial velocity u_{0m}. The function $f(t)$ indicated in Fig. 1 is the term $(1-p^2)/u_0$ normalized to its maximum value and this is set on the computer by a loaded tapped potentiometer.

(4) The necessary circuit constants are determined by equating coefficients of the parallel equations.

(5) Kornelsen then introduces the initial values of the noise current and velocity by setting appropriate values for V_{11} and V_{21}: the voltages representing the initial values of the function Y and its time derivative. The computer output voltages V_{1a} and V_{2a} can then be used to evaluate the anode noise current and velocity.

Considerable simplification is possible in step (5) and the results can be conveniently summarized by evaluating what are equivalent to the transducer matrix elements of equation (1) (McFarlane 1959). This follows from the observation that, for a given gun voltage and frequency, the computer output voltages are linearly related to the input voltages.

$$V_{1a} = a_0 V_{11} - a_1 V_{21} \tag{12a}$$

$$V_{2a} = -b_0 V_{11} + b_1 V_{21} \tag{12b}$$

The coefficients a_0, a_1, b_0, and b_1 are positive and their determination constitutes the complete solution.

Noting that R_2C_2 is one of the computer integrator time constants and that η and ξ are the usual Fry-Langmuir normalized potential and distance variables respectively, define

$$c_0 = 2\alpha R_2 C_2 a_0 - b_0, \tag{13a}$$

$$c_1 = 2\alpha R_2 C_2 a_1 - b_1, \tag{13b}$$

$$g = \frac{\alpha R_2 C_2 \omega}{\rho} \cdot \frac{kT_e}{2eV_{01}}, \tag{13c}$$

$$\lambda = K\tau_s \frac{\alpha}{\rho} \frac{R_2 C_2}{u_{01}}, \tag{13d}$$

V_{0a} = gun anode voltage,

$V_{01} = \dfrac{kT_e}{e}\eta(\xi)$ where $\eta(\xi)$ specifies the input plane,

$u_{01}^2 = 2\dfrac{e}{m}V_{01}$,

τ_s = transit time from the potential minimum to the plane ξ, as determined from equation (6) and an assumed value for u_{0m}.

After some lengthy algebra, summarized in the Appendix, it is found that the noise quantities at the electron gun anode are

$$(14a)\quad \delta_a^2 = \frac{V_{0l}}{V_{0a}}\{g^2a_1^2\mu^2+a_0^2k_2^2\delta^2+(a_1\lambda+a_0)^2\delta^2+2ga_0a_1\Pi'-2ga_1(a_1\lambda+a_0)\Lambda'\}$$

$$(14b)\quad \mu_a^2 = \frac{1}{g^2}\cdot\frac{V_{0a}}{V_{0l}}\{g^2c_1^2\mu^2+c_0^2k_2^2\delta^2+(c_1\lambda+c_0)^2\delta^2+2gc_0c_1\Pi'-2gc_1(c_1\lambda+c_0)\Lambda'\}$$

$$(14c)\quad \Pi_a' = (a_1c_0-a_0c_1)\left\{\Pi'+\Lambda'-\frac{\lambda}{g}k_2^2\delta^2\right\}$$

$$(14d)\quad \Lambda_a' = \frac{1}{g}\{g^2a_1c_1\mu^2+a_0c_0k_2^2\delta^2+(a_1\lambda+a_0)(c_1\lambda+c_0)\delta^2+g(a_1c_0+a_0c_1)\Pi' -g[a_1(c_1\lambda+c_0)+c_1(a_1\lambda+a_0)]\Lambda'\}$$

$$(14e)\quad S_a'^2 = (a_1c_0-a_0c_1)^2\left\{(1+k_2^2)\mu^2\delta^2-(\Pi'-\Lambda')^2+\frac{\lambda^2}{g^2}k_2^2\delta^4-\frac{2\lambda}{g}\delta^2(\Pi'+k_2^2\Lambda')\right\}.$$

These have been obtained by combining the noise outputs of each of the three independent inputs of equation (9). In the computation k_2 is chosen to conserve Π' in equation (14*c*). The quantity δ^2 represents the ratio of the total mean square current fluctuations to full shot noise. A companion paper (McFarlane 1961) discusses experimental measurements of this quantity at the anode of a space-charge limited diode electron gun.

CALCULATIONS

The specific diode studied was the one on which the indicated measurements were made. It had the following properties:

Type	Pierce-parallel flow
Cathode–anode spacing	0.156 in.
Effective beam diameter	0.023 in.
Perveance	3.86×10^{-6} amp/v$^{3/2}$
Cathode temperature	1160° K

The evaluation of the anode noise quantities required the specification of the plane at which the calculation was to start, the four fluctuation terms (10*a*, *b*, *c*, *d*) at this plane, and the transit time from the potential minimum to the input plane. For the present work an input plane at $\xi = 5$ was convenient for computer operation. The potential at this plane is 0.359 volt above the minimum of potential in the gun and at this plane S and Π have attained their final values.

The input noise quantities depend upon the frequency parameter $a = \omega/2\omega_{pm}$, where ω_{pm} is the plasma frequency at the potential minimum defined by

$$(15)\qquad \omega_{pm} = \left[\frac{\pi}{\epsilon_0^2}\frac{e^2}{m}\frac{1}{2kT_c}\right]^{1/4} J_0^{1/2}$$

Table I shows the frequency parameter for the cases studied.

TABLE I

Frequency (Mc/s)	Gun voltage	Frequency parameter a
1,400	100	0.845
	200	0.502
	300	0.371
	500	0.253
4,250	100	2.53
	300	1.11
	500	0.756
	1,000	0.450
9,520	300	2.49
	1,000	1.01

To obtain the noise input terms for frequency parameters other than those calculated by Siegman, the input plane was fixed at $\xi = 5$ and values of δ^2, μ^2, Π', and Λ' were found by interpolation. Siegman shows that the use of a value of u_{0m}^2 defined by

$$u_{0m}^2 = \frac{2}{\pi}\frac{kT_c}{m}, \tag{16}$$

for the evaluation of δ^2 using the Llewellyn–Peterson equations, gives good agreement at $a = 0$ and $a = 0.25$ but predicts values for δ^2 greater than those found from the statistical computations for frequency parameters of $a = 0.5$ and 1.0. The present calculations were based on a value of u_{0m}^2 equal to twice that given by equation (16). It is believed that a more accurate determination of δ_a^2 was obtained at larger values of the frequency parameter.

In the present work, the value of k_2 was obtained by requiring invariance of Π'. For all the cases studied, k_2 was less than its maximum allowable value of unity. For frequency parameters greater than 0.5, k_1 was also less than unity. As a decreased from 0.5 to 0.25, however, a value of $k_1 = 1.035$ was indicated. The discrepancy was not considered serious for the present work but was interpreted as indicating that the validity of the method of calculation might be open to question for values of the frequency parameter less than 0.25. The difficulty can apparently be removed for the lower frequencies by advancing the input plane toward the anode. This possibly implies the necessity of a minimum transit angle between the potential minimum and the plane at which the computation is started.

The results of the calculation are summarized in Table II. Both input and anode quantities are given. The theoretical dependence of the smoothing below shot noise of the anode noise current fluctuations can be seen by examining the quantity of $\delta_a^2 V_{0a}/\omega^{1/2}$, the calculated values for which are shown in Table III.

CONCLUSIONS

By restricting the solution of the electronic equation to the conservative region of a space-charge limited diode, the noise transducer properties of a finite electron beam have been determined. The general form of the equations

TABLE II

Summary of theoretical input and anode noise quantities

Frequency (Mc/s)	Gun voltage	δ^2		μ^2		Π'		Δ'		S'	
		Input	Anode	Input	Anode	Input	Anode	Input	Anode	Input	Anode
1,400	100	0.412	0.104	1.59	151	0.220	0.220	0.428	3.89	0.686	0.718
	200	0.265	5.15×10^{-3}	2.91	364	0.275	0.275	0.585	4.28	0.655	0.690
	300	0.204	3.34×10^{-3}	4.30	—	0.297	—	0.701	—	0.622	—
	500	0.166	2.00×10^{-3}	8.55	857	0.315	0.315	1.00	4.08	0.648	0.717
4,250	100	0.800	0.159	0.65	84.0	0.135	0.135	0.282	3.58	0.663	0.751
	300	0.502	5.77×10^{-3}	1.24	461.	0.182	0.182	0.374	5.10	0.695	0.771
	500	0.377	3.43×10^{-3}	1.81	858.	0.233	0.233	0.460	5.38	0.685	0.714
	1,000	0.242	1.55×10^{-3}	3.33	1660.	0.283	0.283	0.624	5.02	0.645	0.710
9,520	300	0.800	8.81×10^{-3}	0.65	314.	0.135	0.135	0.282	5.20	0.663	0.784
	1,000	0.466	2.63×10^{-3}	1.35	1944.	0.198	0.198	0.394	7.11	0.688	0.701

TABLE III

Frequency (Mc/s)	Gun voltage	$\delta_a^2 V_{0a}/\omega^{1/2}$
1,400	100	1.105×10^{-4}
	200	1.099×10^{-4}
	300	1.067×10^{-4}
	500	1.065×10^{-4}
4,250	100	0.975×10^{-4}
	300	1.059×10^{-4}
	500	1.051×10^{-4}
	1,000	0.946×10^{-4}
9,520	300	1.080×10^{-4}
	1,000	1.075×10^{-4}

shows a similarity to what might be expected for a lossy non-reciprocal transducer (Haus 1955). This is due to the presence of an unspecified correlation coefficient k_2. By requiring that the transformation conserve real kinetic power, it is found that the parameter S, also conserved in a lossless transformation, remains within 10 per cent of its initial value. The dependence of δ_a^2 on anode voltage and frequency is at variance with earlier theories. The present calculations indicate that, for the particular gun at least, δ_a^2 is proportional to the square root of the frequency and inversely proportional to the gun voltage. Theories not including the correction for finite beam diameter and starting at the potential minimum show δ_a^2 proportional to ω^2/V_{0a}^2. The difference in these two types of variation is sufficient that experiment should be able to distinguish between them. A companion paper (McFarlane 1961) undertakes this investigation.

ACKNOWLEDGMENTS

The present research was part of a program for the study of the physics of electron beams, which is sponsored at the Eaton Electronics Research Laboratory by the Defence Research Board. The author would like to thank Professor G. A. Woonton, the program director, Dr. E. V. Kornelsen, Dr. B. A. McIntosh, and Dr. R. F. C. Vessot for many stimulating discussions.

REFERENCES

BEAM, W. R. 1955. RCA Rev. **16**, 458.
BLOOM, S. 1955. RCA Rev. **16**, 179.
HAUS, H. A. 1955. J. Appl. Phys. **26**, 560.
HUTTER, R. G. E. 1952. Sylvania Technologist, **V**, 94.
——— 1953. Sylvania Technologist, **VI**, 6.
KORNELSEN, E. V. 1957. Ph.D. Thesis, McGill University, Montreal.
KOSMAHL, H. G. 1959. IRE Trans. **ED-6**, 235.
MCFARLANE, R. A. 1959. Ph.D. Thesis, McGill University, Montreal.
——— 1961. Can. J. Phys. **39**. This issue.
PARZEN, P. 1952. J. Appl. Phys. **23**, 215.
PIERCE, J. R. 1950. Traveling-wave tubes (D. Van Nostrand Company, Inc., New York).
ROWE, H. E. 1952. Technical Report 239, Research Laboratory of Electronics, M.I.T., Oct. 24.
SIEGMAN, A. E., WATKINS, D. A., and HSIEH, H. S. 1957. J. Appl. Phys. **28**, 1138.

APPENDIX

The Calculation of Anode Noise Quantities

The general case is examined where the three independent noise inputs of equation (9) are specified at any plane, and the solution is carried out to determine the noise values at the anode. A conversion from velocity modulation to kinetic voltage has been made, where the kinetic voltage is

$$V_\omega = -\frac{mu_0 w_\omega}{e}. \tag{A.1}$$

The problem is solved formally by using the square roots of quantities representing quadratic content. As it is quadratic content that is determined at the gun anode, the results are physically meaningful. Unit bandwidth is assumed. The algebra is very long (McFarlane 1959) and only the results will be presented.

(1) Kinetic Voltage Input Only

It is found that the anode quantities are

$$J_{\omega aI} = -jg^* J_0 \mu (1-k_1^2)^{1/2} \frac{kT_c}{(V_{0a}V_{01})^{1/2}} \frac{1}{(2eJ_0)^{1/2}} \frac{V_{1a}}{V_{21}} \tag{A.2}$$

$$V_{\omega aI} = \mu (1-k_1^2)^{1/2} \left(\frac{V_{0a}}{V_{01}}\right)^{1/2} \frac{2kT_c}{(2eJ_0)^{1/2}} \left[\frac{V_{2a}}{V_{21}} + d\frac{V_{1a}}{V_{21}}\right] \tag{A.3}$$

where

$$g^* = \frac{\alpha R_2 C_2 \omega}{\rho},$$

$$d = 2\alpha R_2 C_2.$$

The computer input condition is $V_{11} = 0$.

(2) Current Input Only

It is found that the anode quantities are

$$J_{\omega aII} = (1-k_2^2)^{1/2} \delta (2eJ_0)^{1/2} \left(\frac{V_{01}}{V_{0a}}\right)^{1/2} \frac{V_{1a}}{V_{11}} \tag{A.4}$$

$$V_{\omega aII} = \frac{-u_{0a}u_{01}}{j\eta J_0 g^*} \delta (2eJ_0)^{1/2} (1-k_2^2)^{1/2} \left[\frac{V_{2a}}{V_{11}} + d\frac{V_{1a}}{V_{11}}\right]. \tag{A.5}$$

The computer input condition is $(V_{21}/V_{11}) = -\lambda$.

(3) Correlated Input

The computer input for the correlated noise input is

$$\frac{V_{21}}{V_{11}} = -jg\frac{k_1}{k_2}\frac{\mu}{\delta} e^{-j\theta} - \lambda.$$

The calculation of anode noise requires the determination of real and imaginary components.

$$(A.6)\quad J_{\omega aIII} = k_2\delta(2eJ_0)^{1/2}\left(\frac{V_{0I}}{V_{0a}}\right)^{1/2}\left[\frac{V_{1aR}}{V_{1IR}}+j\frac{V_{1aI}}{V_{1II}}\right]$$

$$(A.7)\quad V_{\omega aIII} = \frac{-u_{0a}u_{0I}}{j\eta J_0 g^*}k_2\delta(2eJ_0)^{1/2}\left\{\left[\frac{V_{2aR}}{V_{1IR}}+d\frac{V_{1aR}}{V_{1IR}}\right]+j\left[\frac{V_{2aI}}{V_{1II}}+a\frac{V_{1aI}}{V_{1II}}\right]\right\}$$

where R and I refer to the use of the real and imaginary parts of V_{2I}/V_{1I}.

Using the appropriate computer input terms for each of the three independent noise inputs, evaluating the required computer outputs by equations (12*a*), (12*b*), and noting the relations of equations (11*a*) and (11*b*) and the definitions (10*a*, *b*, *c*, *d*, *e*), equations (14*a*, *b*, *c*, *d*, *e*) follow.

MICROWAVE NOISE IN ACCELERATED ELECTRON STREAMS[1]

R. A. McFarlane[2]

ABSTRACT

Measurements have been made of the noise current fluctuations on the electron beam from a space-charge limited diode electron gun, at 1,400 Mc/s, 4,250 Mc/s, and 9,520 Mc/s. Theories which do not consider the finite beam diameter and the multivelocity nature of the stream in the region of the potential minimum are in poor agreement with experiment. The measurements here reported and those of other workers are compared with the results of theoretical calculations in which these two effects are considered. Significant improvement in agreement with experiment is realized.

INTRODUCTION

Since the early measurements by Cutler and Quate (1950) of the noise current fluctuations on a beam of electrons from a space-charge limited diode gun, workers have been interested in the noise figure of longitudinal beam amplifiers, using such guns. Haus (1955) showed that two parameters, S and Π, are significant in determining the minimum noise figure of these devices. Subsequent investigations have centered on the measurement of these two quantities and the construction of guns with increasingly complicated geometry and axial potential profiles, with a view to decreasing the noise figure of the devices. Most of the work has been done in the region of 3000 Mc/s. Although four independent parameters are required to specify the noise properties of an electron beam (Haus 1955), experimental study of these as a function of frequency and gun voltage has received limited attention (Kornelsen 1957; Vessot 1957). Where agreement has been obtained between experiment and the more elementary theory, it appears to have been the consequence of the proper selection of frequency and gun operating conditions.

The present work reports measurements on a space-charge limited diode gun of the anode noise current fluctuations at 1,400, 4,250, and 9,520 Mc/s, over a range of gun voltages from 100 to 1,000 volts. By relating these fluctuations to full shot noise, what has been obtained is essentially a measure of Haus' parameter Ψ, i.e. the self-power density spectrum of the noise current modulation. The smoothing below full shot noise calculated from theories which do not take into account finite beam diameter and the multivelocity nature of the electron beam in the region immediately beyond the potential minimum are in poor agreement with the experimental measurements. Consideration of these effects has been given in a companion paper and the agreement between theory and experiment is significantly improved.

[1]Manuscript received August 30, 1960.
Contribution from the Eaton Electronics Research Laboratory, McGill University, Montreal, Que.
[2]Now at the Research Laboratory of Electronics, Massachusetts Institute of Technology, Cambridge, Massachusetts.

THE EXPERIMENTAL VACUUM TUBES

The electron gun used for the reported measurements was a parallel flow Pierce type designed to produce a cylindrical beam of electrons. It employed an oxide cathode in front of which was a beam-forming electrode of the required Pierce shape. A 0.031-in. aperture in the beam-forming electrode determined the diameter of the electron beam leaving the cathode. The cathode–anode spacing was 0.156 in. which included a 0.004-in. retraction of the cathode behind the beam-forming electrode to provide thermal isolation. To simplify construction, the anode was approximated by a plane. The tubes used at 1,400 Mc/s and 4,250 Mc/s had an anode aperture of 0.062 in. and interception of beam current by the anode was small. To improve coupling of the electron beam to the 9,520 Mc/s cavity, the anode aperture was reduced to 0.031 in. and this resulted in an increase in interception for the two highest frequency tubes.

The resonant cavities used to couple the noise power resulting from beam current fluctuations to the microwave receiver were located just beyond the electron gun anode. The tubes for measurements at 1,400 Mc/s and 4,250 Mc/s employed a disk seal structure to which external cavities were attached. At 9,520 Mc/s, the small cavity size required that it be placed entirely within the vacuum envelope. A coaxial line coupled the noise power to the receiver.

The tube properties are summarized in Table I. It is observed that for

TABLE I

Electrical and mechanical properties of the tubes studied

Tube number	D-1	D-2	I-1	I-2
Cavity type Anode and cavity aperture (in.)	External .062	External .062	Internal .031	Internal .031
Frequency (Mc/s)	4,030 1,395	4,250 1,455	9,520	9,520
Average perveance amp/$v^{3/2}$	2.46×10^{-8}	3.82×10^{-8}	3.90×10^{-8}	2.43×10^{-8}
Interception	3.8%–1.5% 200–500 v	0.2%–0.02% 200–500 v	2.8%	7%

each type, the tube with the higher perveance value had the lower interception. This is interpreted to mean that the cathodes of tubes D-1 and I-2 were positioned further behind the beam-forming electrode than for optimum operation. All tubes employed long cylindrical electron collectors biased at 45 volts above the anode potential in order to reduce the effect of secondary electrons. Sealed to each tube was an ionization gauge to provide a continuous indication of pressure within the vacuum envelope. During operation, pressures of 5×10^{-9} mm of Hg were typical.

MEASURING APPARATUS

The receiving system was based on the radiometer technique of Dicke (1946). A block diagram of the apparatus is shown in Fig. 1. The electron gun was gated by a 35 c.p.s. square wave and the beam noise coupled to a conventional microwave receiver. Following detection by a bolometer, the receiver output was synchronously detected with the modulating wave form

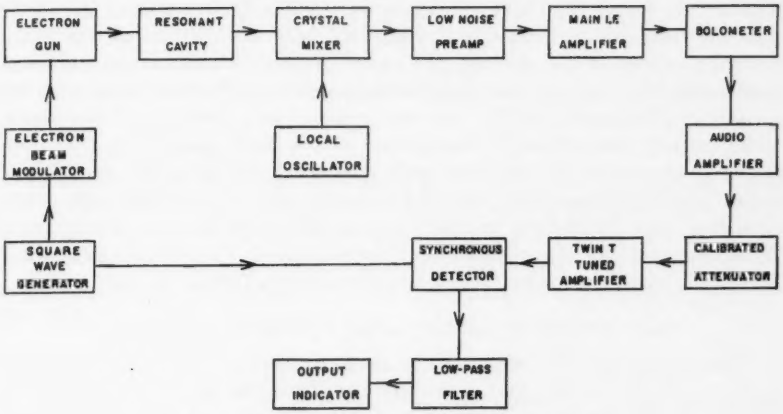

FIG. 1. Block diagram of noise measuring system.

as reference. In operation, the receiving apparatus was linear to 0.1 db over a greater than 30-db range of input signals. The noise on electron beams of less than 1 μa was readily detected.

MEASUREMENT OF ANODE NOISE CURRENT FLUCTUATIONS

The experiment consisted of raising the cathode temperature and observing the magnitude of the noise power coupled to a resonant cavity at the gun anode, as the beam current increased to its space-charge limited value. The form of the variation of noise with d-c. beam current is shown in Fig. 2. Two

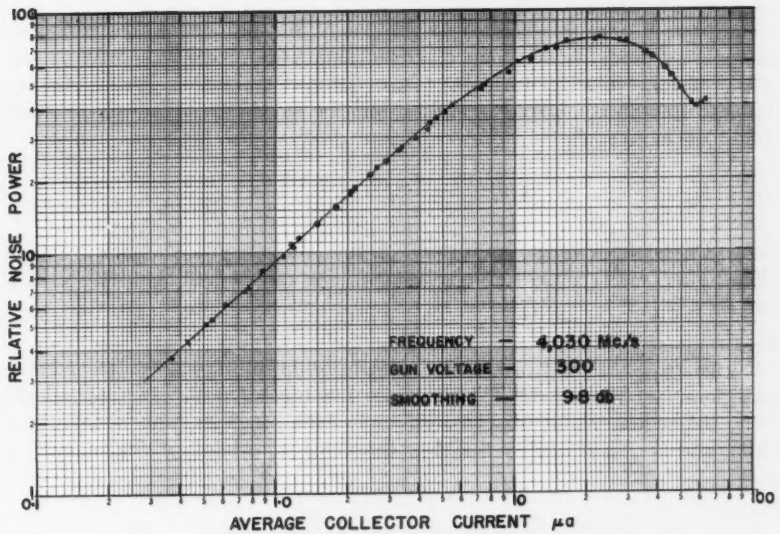

FIG. 2. Electron beam noise at the gun anode as a function of current.

distinct regions of the curve are apparent. At low beam currents the diode gun was temperature-limited and the initial noise fluctuations on the beam were unmodified at the electron gun anode. As the cathode temperature was raised, the beam current increased to its space-charge limited value, and the greater charge density within the gun resulted in a decrease of the anode noise current fluctuations. Extrapolation of the linear portion of the curve serves to determine the full shot noise content of the beam for any current value. The noise smoothing is defined from the ratio of measured noise power at space-charge limitation, to that value of shot noise indicated by the shot noise asymptote for the space-charge limited current. This form of normalization obviates the necessity of absolute noise power measurements.

CALCULATION OF ANODE NOISE CURRENT SMOOTHING

Three methods have been used to compute the smoothing of the anode noise current below full shot noise. For the latter two, values of the current density J_0 and the beam diameter were required. In a space-charge limited planar diode, the current density is given by:

$$J_0 = 2.33\times10^{-6}\frac{V_{0a}^{3/2}}{d^2} \tag{1}$$

where d is the anode–cathode spacing and V_{0a} is the gun voltage. An effective beam diameter was found by comparing the observed perveance with the theoretical current density. The mean perveance of tubes D-2 and I-1 was 3.86×10^{-8} amp/v$^{3/2}$ and this was considered representative of a properly operating gun. This indicates that the effective beam diameter was 2.3×10^{-2} in. which is 73% of the aperture in the beam forming electrode.

(a) The Llewellyn–Peterson Equations

The computation was started at the potential minimum. Full shot noise, uncorrelated Rack velocity fluctuations, and a d-c. velocity equal to the r.m.s. thermal velocity were the assumed input conditions. Using the coefficients quoted by Pierce (1950), it can be shown that the anode noise smoothing is given by

$$\delta_a^2 = \frac{V_{01}}{V_{0a}}+\frac{9}{8}\frac{\omega^2 d^2}{V_{0a}^2}(4-\pi)\frac{kT_c}{m} \tag{2}$$

where V_{01} is the voltage equivalent of the r.m.s. thermal velocity and is given by kT_c/e. T_c is the cathode temperature assumed to be 1160° K. The first term in (2) is negligible at high frequencies, since $V_{01} = 0.1$ volt.

(b) Computer Solution I

Kornelsen (1957), in developing the finite beam solution, specified as input conditions just those indicated above for the Llewellyn–Peterson equations. Using the general result for δ_a^2 determined in the previous paper (McFarlane 1961), and noting $\Pi = \Lambda = \lambda = 0$ at the potential minimum, the smoothing is:

$$\delta_a^2 = \frac{V_{01}}{V_{0a}} [g^2 a_1^2 (4-\pi) + a_0^2].$$

In determining a_0 and a_1, the computer is started at a point corresponding to zero transit time.

(c) Computer Solution II

This calculation has been discussed in detail in the companion paper (McFarlane 1961). The computation was started at a plane in front of the potential minimum using as input quantities the noise parameters found by Siegman *et al.* (1957). The correlation coefficient k_2 was determined by requiring the conservation of real kinetic power. Its actual value only slightly affects δ_a^2.

COMPARISON OF THEORETICAL AND EXPERIMENTAL RESULTS

The experimental values of noise smoothing observed at the gun anode are compared with the results of the three theoretical determinations in Figs. 3, 4, and 5. The 1,400 Mc/s measurements on tubes D-1 and D-2 agreed to well within experimental error and they have been shown as one measurement. At 4,250 Mc/s only slight differences between the tubes were observed, while at 9,250 Mc/s two distinct sets of measurements appeared.

The predictions of the Llewellyn–Peterson equations and the first computer solution are strong functions of frequency and, as would be anticipated,

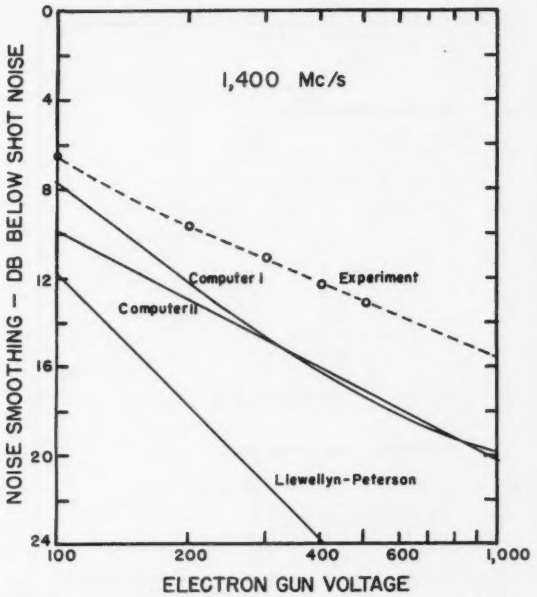

FIG. 3. Smoothing as a function of gun voltage at 1,400 Mc/s.

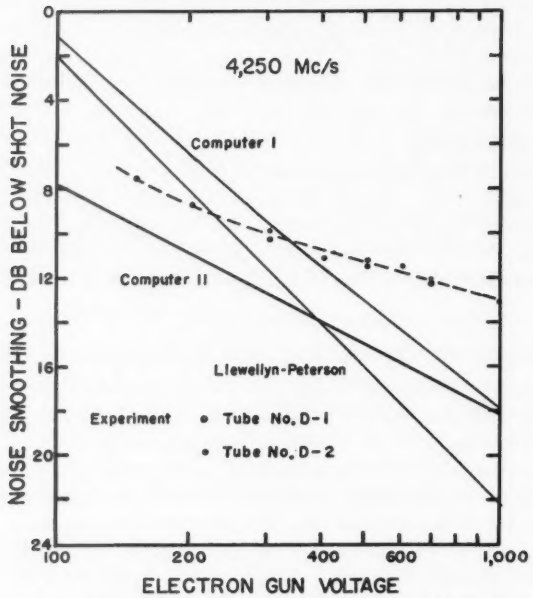

FIG. 4. Smoothing as a function of gun voltage at 4,250 Mc/s.

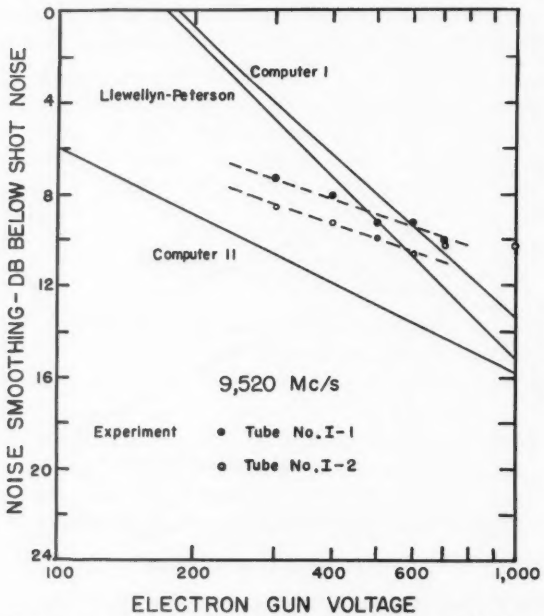

FIG. 5. Smoothing as a function of gun voltage at 9,520 Mc/s.

TABLE II

Observed values of $\delta_a^2 V_{0a}/\omega^{1/2}$

	Tube D-1 $\delta_a^2 V_{0a}/\omega^{1/2}$		Tube D-2 $\delta_a^2 V_{0a}/\omega^{1/2}$		Tube I-1 $\delta_a^2 V_{0a}/\omega^{1/2}$	Tube I-2 $\delta_a^2 V_{0a}/\omega^{1/2}$
Gun anode voltage	1,395 Mc/s	4,050 Mc/s	1,455 Mc/s	4,250 Mc/s	9,520 Mc/s	9,520 Mc/s
100	2.41×10^{-4}	—	2.26×10^{-4}	—	—	—
150	—	—	—	1.65×10^{-4}	—	—
200	2.29×10^{-4}	—	2.28×10^{-4}	1.70×10^{-4}	—	—
300	2.54×10^{-4}	2.03×10^{-4}	2.48×10^{-4}	1.76×10^{-4}	2.28×10^{-4}	1.73×10^{-4}
400	—	—	2.49×10^{-4}	1.90×10^{-4}	2.62×10^{-4}	2.01×10^{-4}
500	2.73×10^{-4}	2.36×10^{-4}	2.58×10^{-4}	2.21×10^{-4}	2.52×10^{-4}	2.14×10^{-4}
600	—	2.74×10^{-4}	—	—	2.94×10^{-4}	2.14×10^{-4}
700	—	2.76×10^{-4}	—	2.60×10^{-4}	2.86×10^{-4}	2.80×10^{-4}
1,000	—	3.14×10^{-4}	—	—	—	3.90×10^{-4}

the agreement between them improves as the frequency is increased. Both indicate a more rapid change of smoothing with gun voltage than is observed experimentally.

The second computer solution predicts a variation of smoothing with gun voltage in better agreement with that observed. At all frequencies the theoretical smoothing is consistently greater than that observed, the discrepancy being somewhat larger at high gun voltages.

To examine the experimental measurements for the theoretical dependence on $\omega^{1/2}/V_{0a}$ determined in the companion paper, the observed smoothing values have been used to calculate $\delta_a^2 V_{0a}/\omega^{1/2}$ and the results are presented in Table II. Considering that the measurements extend over a frequency range of 6.8:1, the data do not show any serious deviation from the $\omega^{1/2}$ variation predicted. The increase of $\delta_a^2 V_{0a}/\omega^{1/2}$ as the gun voltage was raised is attributed to the progressively higher cathode temperature required to space-charge limit the gun. As the cathode temperature was increased, the quadratic velocity input was increased, resulting in a higher value of the anode current fluctuations. Zacharias and Smullin (1959) have examined the effect of cathode resistance on the noise parameters of the emitted beam and find that it results in an increase in the quadratic velocity content and in the presence of negative real kinetic power. While it is not exactly clear how these effects modify the input conditions assumed by Siegman, the net result is a further increase in anode noise.

The observed noise current fluctuations are 3–4 db higher than those predicted by theory. The difference cannot be attributed to interception noise. McIntosh (1958, 1959) showed that aperture interception results in increased beam noise only when a relatively large fraction of the beam is intercepted. In view of the agreement between the zero and high magnetic field smoothing data of McIntosh, it is also concluded that the excess noise does not result from the lens effect of the anode aperture (Knechtli 1958).

The experimental results of Vessot (1957) and McIntosh (1958, 1959), using a higher perveance electron gun of similar design, have been analyzed to discover if a similar behavior of the noise was present. The data is presented in Table III.

The first three columns are from Vessot's measurements and the final

TABLE III

Values of $\delta_a^2 V_{0a}/\omega^{1/2}$ measured by Vessot and McIntosh

Gun anode voltage	$\delta_a^2 V_{0a}/\omega^{1/2}$			
	230 Mc/s	1,010 Mc/s	3,055 Mc/s	3,050 Mc/s
100	2.34×10^{-4}	1.70×10^{-4}	1.55×10^{-4}	—
200	1.74×10^{-4}	1.41×10^{-4}	2.09×10^{-4}	—
300	1.85×10^{-4}	1.40×10^{-4}	2.07×10^{-4}	1.72×10^{-4}
400	1.67×10^{-4}	1.42×10^{-4}	1.91×10^{-4}	—
500	1.77×10^{-4}	1.38×10^{-4}	—	1.94×10^{-4}
600	1.69×10^{-4}	1.17×10^{-4}	2.07×10^{-4}	—
700	—	—	1.97×10^{-4}	1.92×10^{-4}
900	2.04×10^{-4}	1.38×10^{-4}	2.39×10^{-4}	—

column is based on McIntosh's oxide cathode data. The author has made no theoretical calculation of $\delta_a^2 V_{0a}/\omega^{1/2}$ for this gun. The dependence of the noise current smoothing on frequency and gun voltage is in reasonable agreement with the form predicted for the present electron gun.

CONCLUSIONS

The accurate description of the transport of fluctuation quantities of current and velocity between the potential minimum and anode of a space-charge limited diode electron gun requires that account be taken of the non-conservative nature of the electron stream immediately beyond the potential minimum and of the effect of finite beam diameter in the high velocity region. Using the results of density function calculations to specify the beam noise properties at a plane in the gun beyond the potential minimum, it is possible to determine the anode noise parameters by means of a computer solution of the finite beam electronic equation.

The theory indicates a dependence of the anode noise current smoothing on the one-half power of the frequency and the inverse first power of the gun voltage. The expected dependence was found in the measurements here reported and in those of other workers.

ACKNOWLEDGMENTS

The author wishes to thank Professor G. A. Woonton for his guidance and encouragement throughout the course of the work.

The present research was part of a program for the study of the physics of electron beams, which is sponsored at the Eaton Electronics Research Laboratory by the Defence Research Board. The author gratefully acknowledges personal financial assistance from the National Research Council received in the form of three studentships during the period of the research.

REFERENCES

CUTLER, C. C. and QUATE, C. F. 1950. Phys. Rev. **80**, 875.
DICKE, R. H. 1946. Rev. Sci. Instr. **17**, 268.
HAUS, H. A. 1955. J. Appl. Phys. **26**, 560.
KNECHTLI, R. C. 1958. IRE Trans. **ED-5**, No. 2, 84.
KORNELSEN, E. V. 1957. Ph.D. Thesis, McGill University, Montreal.
McFARLANE, R. A. 1959. Ph.D. Thesis, McGill University, Montreal.
——— 1961. Can. J. Phys. **39**. This issue.
McINTOSH, B. A. 1958. Ph.D. Thesis, McGill University, Montreal.
——— 1959. Can. J. Phys. **37**, 285.
PIERCE, J. R. 1950. Travelling-wave tubes (D. Van Nostrand Company, Inc., New York).
RACK, A. J. 1938. Bell System Tech. J. **17**, 592.
SIEGMAN, A. E., WATKINS, D. A., and HSIEH, H. S. 1957. J. Appl. Phys. **28**, 1138.
VESSOT, R. F. C. 1957. Ph.D. Thesis, McGill University, Montreal.
ZACHARIAS, A. and SMULLIN, L. D. 1959. Technical Report 358, Research Laboratory of Electronics, M.I.T., Nov. 12.

Zn:Tl PHASE DIAGRAM AT VERY LOW THALLIUM CONCENTRATIONS[1]

E. H. McLaren[2] and F. Weinberg[3]

ABSTRACT

The Zn:Tl liquidus has been accurately determined from pure Zn (419.505° C) to the monotectic transition temperature (416.926° C at 0.42 at.% Tl) using precision resistance thermometry. The upper solidus was determined approximately from measurements of the distribution coefficient (~0.01) and the solid solubility limit (~0.004 at.% Tl) of thallium in zinc. A value 1.53±0.1 kcal/mole for the latent heat of fusion of pure zinc was calculated from the freezing point depressions.

INTRODUCTION

An investigation has been made of the Zn:Tl phase diagram from pure zinc to the monotectic composition as part of a study of solute segregation in ingots of very dilute zinc alloys.

Heycock and Neville (1897), using resistance thermometry, determined the monotectic reaction temperature of the Zn:Tl system as 416.5° C and the monotectic composition as 0.45 at.% Tl. They also determined two points on the hypomonotectic liquidus at 0.126 and 0.393 at.% Tl. In the present investigation, the liquidus and monotectic points were accurately determined by resistance thermometry for a series of Zn:Tl alloys in the concentration range 0.0002 to 0.88 at.% Tl. In addition, the upper solidus was determined approximately from measurements of the distribution coefficient and the solid solubility limit of thallium in zinc. A value of 1.53±0.1 kcal/mole for the latent heat of fusion of pure zinc was calculated from the freezing point depressions and was critically compared with Kubaschewski's (1950) selected value of 1.74±0.03 kcal/mole.

EXPERIMENTAL

Alloy Preparation

The alloys (1030-g samples) were prepared by melting weighed amounts of 99.999+% zinc* and 99.99% thallium under dry nitrogen atmospheres in high purity graphite crucibles. The samples were held at 650° C for 7 days to complete solution. Certain of the very dilute alloys contained Tl^{204} (β^-, 0.77 Mev; half life, 3 years) as a tracer in order to locate the thallium for segregation studies and to measure thallium concentrations for distribution coefficient determinations.

[1]Manuscript received December 15, 1960.
Contribution from the Division of Applied Physics, National Research Council, Ottawa, Canada, and the Division of Physical Metallurgy, Mines Branch, Department of Mines and Technical Surveys, Ottawa, Canada.
Issued as N.R.C. No. 6231.

[2]Applied Physics Division, National Research Council, Ottawa, Canada.
[3]Physical Metallurgy Division, Mines Branch, Department of Mines and Technical Surveys, Ottawa, Canada.

*Both New Jersey Super Pure and Chemically Pure grades of zinc were used as solvent (see McLaren 1958).

Liquidus

(a) Method

The apparatus and techniques used for high precision thermal analyses of several high purity metals by platinum resistance thermometry have been fully described by McLaren (1957, 1958, 1959). The alloys, contained in graphite crucibles, were solidified under dry nitrogen atmospheres in a well-lagged metal block furnace. The platinum resistance thermometer was inserted into pyrex thermometer wells that were axially positioned in the cylindrical melts. Freezing techniques have been developed to eliminate or greatly reduce the uncertainties caused by supercooling in liquidus point determinations of very dilute alloys.

During a normal freeze, the alloy freezes radially from the outside to the center of the crucible at a rate controlled by the over-all furnace cooling rate. A very dilute zinc alloy supercools as much as 0.04° C before solidification begins, then the temperature of the alloy slowly rises toward the equilibrium liquidus temperature. This slow recalescence effectively masks the primary arrest on the cooling curve and contributes to an uncertainty in the liquidus point determination. To overcome this difficulty, freezing is induced by removing the thermometer from the well when the alloy becomes supercooled, allowing it to cool, and then replacing it in the well. This operation results in the rapid nucleation and growth of a thin mantle of solid metal on the thermometer well which releases sufficient latent heat to raise the melt immediately to its equilibrium liquidus temperature. Thereafter, solidification proceeds normally from the crucible walls.

The first solid to freeze, immediately after overcoming the supercooling by this induced freezing technique, has the solute concentration that is closest to the equilibrium concentration in the solid at the liquidus point of the alloy. Therefore, the solute concentration gradient in this first solid primarily determines the accuracy that is attainable in the temperature measurement of the liquidus point. The most important factors in setting up this concentration gradient are the over-all solute concentration in the alloy, solute segregation coefficient, rate of freezing, and the slope of the liquidus for the alloy system.

Figure 1 illustrates how 6 p.p.m. thallium (containing some Tl^{204} as a tracer) in zinc segregates during a slow induced freeze. This figure includes macrophotographs and autoradiographs of horizontal and vertical sections cut from the ingot. The autoradiographs show that segregation on freezing for this solute in zinc is so great that most of the Tl^{204} appears swept into a thin cylinder between the mantle and the main freezing interface.

Since the solute concentration gradient in the first frozen solid of this alloy is very small, the melt temperature on a slow induced freeze remains nearly constant for a large fraction of the total freezing time:* this enables precise temperature measurements to be readily made. The highest precision is attained for very dilute alloys because these ingots solidify primarily by a

*Typical cooling curves on very dilute zinc alloys are shown by McLaren (1957, 1958).

large grained outer shell advancing with a smooth interface into the remaining liquid: this closely approximates the freezing of a single crystal with a plane interface advancing into a homogeneous liquid.

For less dilute alloys and the same freezing rates the over-all grain size in the solidified ingots decreases and a zone of equiaxed grains that nucleate in the unfrozen liquid appears. As a result, significant amounts of solute become trapped in intergranular regions and the relation between melt temperatures and liquidus temperatures becomes less well defined.

Table I gives the reproducibilities in the temperature measurements that

TABLE I

Precision of temperature measurement

Conc. thallium (wt. %)	Reproducibility of liquidus temp. (°C)
0.0001	0.0002
0.001	0.0002
0.01	0.0005
0.1	0.002
1.0	0.02
1.3 (monotectic)	<0.01

were found on repeated liquidus point determinations on the dilute Zn:Tl alloys. The experiments were carried out with interface growth rates between 0.2 and 0.5 cm/hr.

(b) Results

In this investigation, a liquidus point determination was made first on the zinc solvent; then the thallium alloy was prepared and its liquidus point determined. Temperatures were related to the liquidus point 419.505° C (Int. 1948) of a sample (S.4) of New Jersey Super Pure Zinc having an alloy melting range of about 0.001° C (see McLaren 1958, 1959): Table II summarizes the freezing points that were measured.

TABLE II

Liquidus (T_L) and monotectic (T_{mono}) temperatures of Zn:Tl alloys related to the liquidus point T_L (Zn) of a sample (S.4) of high purity zinc at 419.505° C (Int. 1948)

Thallium content		$T_L(Zn)-T_L(Zn:Tl)$ liquidus (°C)	$T_L(Zn)-T_{mono}$ monotectic (°C)	Liquidus slope (°C/at. %)
wt. %	at. %			
0 (S.4)	0 (S.4)	0.0	—	—
0.00075	0.00023	0.0012	—	−5.22
0.0059	0.0018	0.0130	—	−7.22
0.0071	0.0022	0.0139	2.6	−6.32
0.0567	0.0177	0.109	2.6	−6.16
0.283	0.0885	0.571	2.6	−6.45
1.01	0.316	1.92	2.58	−6.08
1.36	0.425	2.56	2.58	−6.02
1.38	0.431	2.56	2.58	−5.94
1.71	0.535		2.58	
2.06	0.644		2.58	
2.82	0.882		2.58	
			Mean slope	−6.18° C/at.% Tl
			Mean deviation	±0.37° C/at.% Tl

PLATE I

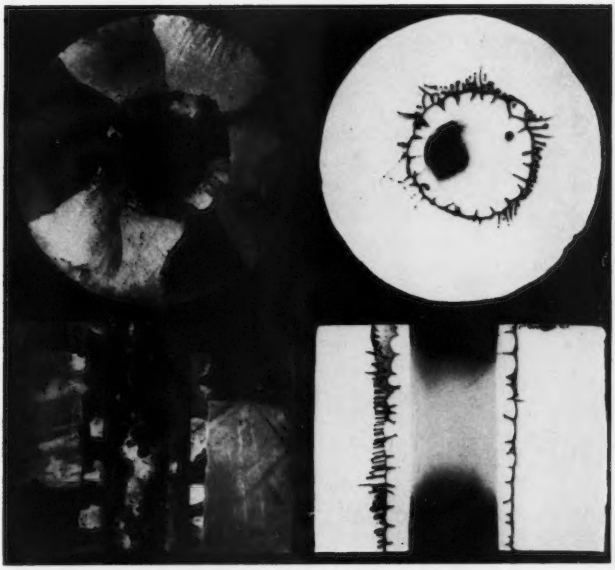

FIG. 1. Macrophotographs and autoradiographs (tracer Tl^{204}) of horizontal and vertical sections cut from an ingot of 6 p.p.m. Zn:Tl alloy following induced freezing (ingot diameter 35 mm).

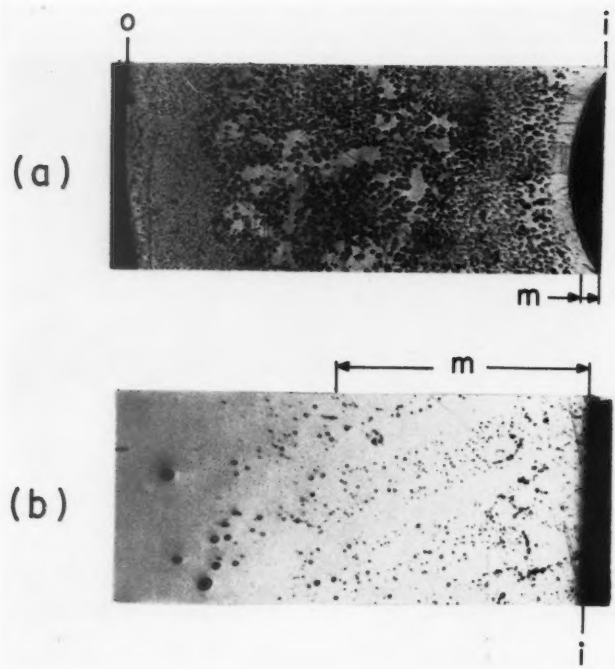

FIG. 2. (*a*) Micrograph of a polished and etched horizontal section cut from a monotectic Zn:Tl alloy showing the cross section from crucible wall, *o*, to thermometer well, *i* (radial length ~12 mm).

(*b*) Micrograph showing a fine spheroidal dispersion of thallium-rich phase in the fast-frozen induced mantle, *m*.

Solidus

To locate the solidus, measurements were made of the distribution coefficient, k, of thallium in zinc, defined as the ratio C_s/C_0, where C_s is the concentration in the solid that separates at the liquidus temperature of the alloy, and C_0 is the concentration of the initial liquid alloy. Two methods were tried.

First, the ratio of the relative concentration of Tl^{204} in first-frozen solid to the initial homogenized concentration was determined following a controlled solidification of rods of Zn:Tl alloy as described by Yue and Clark (1960). Turnings for beta counting were machined from the rods and pressed into standard samples for 2π and 4π counting.

Secondly, the ratio C_s/C_0 was determined for alloys that were solidified in the regular cylindrical ingots following induced freezing. Turnings were machined from the outside radius of the ingots to obtain samples of the first-frozen material, C_s, following recovery from supercool. In this case, samples (15 g) of the homogenized liquid, C_0, were extracted and water-quenched in pyrex ladles prior to the ingot solidification; cuttings made across a full section were used for standard counting samples.

The C_s samples used in both methods were obtained from material solidified at rates of 0.2–0.5 cm/hr.

For alloys of initial concentrations in the range 6 to 100 p.p.m., the measured k values ranged from 0.006 to 0.02, with an average value of about 0.01. A correlation between measured k value and alloy concentration was not found. Large variations (up to 30%) were found in the counting rates of selected samples of C_0 and C_s material from the same alloy. The presence of microsegregations of thallium in these samples was shown by autoradiographs on sample turnings. Smaller variations (10%) in counting rate were found among samples of C_0 material cut from the fast-frozen samples removed from the regular cylindrical ingots before solidification. We attribute the uncertainties in our determinations of the distribution coefficient of thallium in zinc to these microsegregations, beta counting being particularly sensitive to self-absorption variations in non-homogeneous samples.

Thermal analyses on the hypomonotectic Zn:Tl alloys showed that the solid solubility limit of thallium in zinc must lie between 0.0071 and 0.057 wt.% Tl. Prominent monotectic arrests (5% of total time) were found on melting and freezing (total time 3 hours) a 0.057 wt.% Tl alloy. In contrast, monotectic arrests were imperceptible on thermal curves of 0.0071 wt.% Tl alloy at these rates of fusion and were barely detectable when cooling and heating rates were further reduced (total time 17 hours). The monotectic arrests revealed in the latter case were undoubtedly due to non-equilibrium divorced monotectic. The solid solubility limit being in this concentration range implies that the distribution coefficient of thallium in zinc at the monotectic temperature is in the range 0.005 to 0.04. This is in general agreement with the results of the concentration measurements made at greater dilution.

In consideration of the above measurements, we have arbitrarily selected 0.01 as a representative value of the distribution coefficient of thallium in zinc.

Monotectic

The monotectic composition, 0.42 at.% Tl, was calculated using the values determined for the mean slope of the liquidus and for the depression of the monotectic temperature below the freezing point of pure zinc. This monotectic reaction temperature was determined as 416.926±0.003° C, with a pressure coefficient of +0.0043° C for 1 atmosphere over the melt. This pressure coefficient is identical with that previously found for pure zinc (see McLaren 1957).

Figure 2*a* shows a micrograph of a sectioned monotectic alloy following induced freezing. The thallium-rich phase is dispersed in a spheroidal state in the zinc-rich matrix. Figure 2*b* shows a micrograph of the region near the thermometer well: the thallium-rich phase appears in finer dispersion in the fast-frozen induced mantle than in the slowly frozen main portion of the ingot.

Phase Diagram

Figure 3 shows the phase diagram for dilute Zn:Tl as determined by this investigation. The liquidus was constructed using the freezing points given in Table II and the solidus was approximately located using a distribution

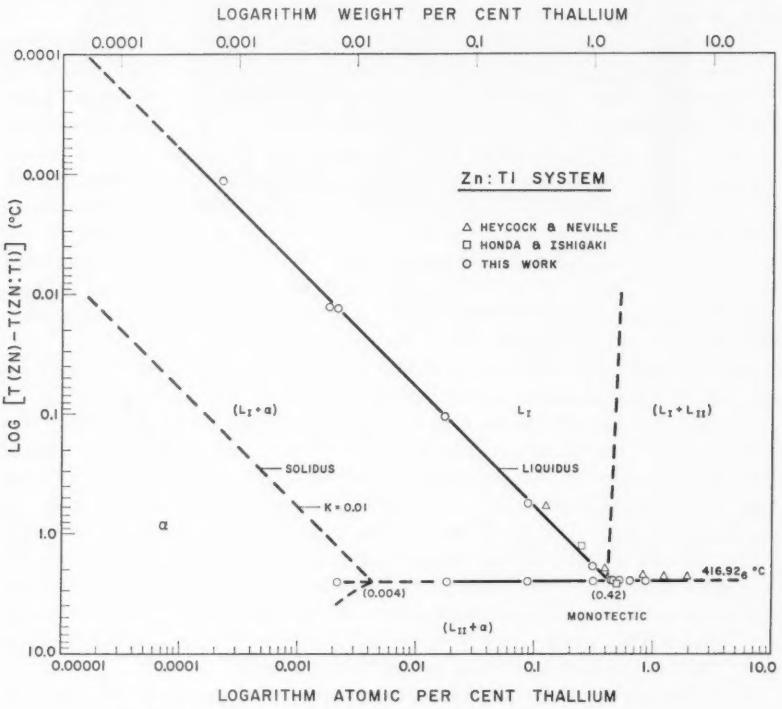

FIG. 3. Zn:Tl phase diagram at very low thallium concentrations.

coefficient of 0.01 for thallium in zinc. Freezing points determined on the Zn:Tl system by Heycock and Neville (1897) and Honda and Ishigaki (1925) are included on the diagram of Fig. 3.

DISCUSSION

The liquidus, within experimental error, appears to vary linearly with thallium concentration from pure zinc to the monotectic composition. The major uncertainty in locating the liquidus arises in assigning composition values for the series of alloys. The amount of thallium lost by evaporation and incomplete solution during the alloy preparation is not known. However, since the liquidus points of the alloys have a high reproducibility after preparation (Table I) and generally lie very close to a smooth curve drawn between the freezing temperature of pure zinc and the monotectic temperature, it is probable that the concentration uncertainty in the liquidus as drawn in Fig. 3 is inside $\pm 5\%$ over most of the range investigated. It is doubtful that whole ingot chemical analyses could be made with higher precision, especially for the extremely dilute alloys.

Latent Heat of Fusion of Pure Zinc

Values for ΔH, the latent heat of fusion of pure zinc, can be obtained from standard thermodynamic relations.

In 1939, Hayes and Chipman derived a form of Van't Hoff's law relating ΔH to the freezing point depressions of very dilute metal solutions:

$$\Delta H = R\, T_f^2 (1-k)/m_L \tag{1}$$

where T_f is the freezing point of the pure metal, k is the solute distribution coefficient, m_L is the slope of the liquidus, and R is the gas constant. For our experimental results this relation gives a value of

$$\Delta H = 1.53 \pm 0.1 \text{ kcal/mole},$$

the uncertainty arising mainly from uncertainties in solute concentrations.

An alternative expression containing ΔH, and involving the pure metal only, is that in which Lumsden (1952) relates ΔH to the freezing point, its pressure coefficient, and the decrease in molar volume on solidification:

$$\Delta H = T_f\, \Delta V (dp/dT_f). \tag{2}$$

McLaren (1957) determined the pressure coefficient of the freezing temperature of pure zinc as $+0.0043 \pm 0.0001°$ C for 1 atmosphere. The value of ΔV commonly quoted (0.27 cc/mole (2.8% shrinkage)) is that of Pelzel and Sauerwald (1941), while Saeger and Ash (1932) obtained 0.36 cc/mole (3.8% shrinkage). These lead to values of 1.1 kcal/mole and 1.4 kcal/mole respectively. Because of the uncertainty in the value of ΔV, equation (2) is substantially less precise than equation (1) as a means of obtaining ΔH, but it can be combined with the result of equation (1) to give a value of ΔV of 0.39 cc/mole in moderately close agreement with Saeger and Ash's result.

Previous determinations of the latent heat of fusion of pure zinc have been summarized by Kubaschewski (1950, 1958) in a review paper on the latent

heats of fusion of metals; he selected a value 1.74 ± 0.03 kcal/mole for ΔH for pure zinc. This value appears to be based partly on his own calorimetry, for which he quotes a precision of about 6%, and rather strongly on heats of fusion calculated by Lumsden (1948) from Heycock and Neville's (1897) freezing point depressions (solutes Sn, Bi, Tl, Pb, Sb, Mg), and by Honda and Ishigaki (1925) from their own freezing point investigations (solutes Cd, Tl, Ag, Al).

Both groups used alloys of synthetic composition and the purity of the zinc solvent is not specified. It is certain that melt temperatures could not attain equilibrium liquidus temperatures during recalescence in Heycock and Neville's experimental arrangement which utilized massive resistance thermometers and small (250 g) ingots. Also, because of the immersion effects* found by Heycock and Neville (1895) in an earlier investigation on the freezing point of zinc, it can be clearly deduced that the 250-g ingots used in their alloy investigations would provide insufficient immersion† to overcome serious stem losses. Honda and Ishigaki's thermal analyses were made on only two alloys in each solute system: they used thermocouple thermometry and cooling rates that we estimate to be 10–100 times greater than those used in this investigation. They report a liquidus point depression of 2.70° C from pure zinc for a Zn:Tl alloy of 0.50 at.% thallium: this depression is 0.12° C greater than the depression of the monotectic reaction temperature found in this investigation.

Because of these considerations, the better than 2% precision attached to Kubaschewski's selected value of ΔH is not justified and the former value‡ of 1.6 kcal/mole for the heat of fusion of zinc selected from an earlier literature survey by Kelley (1936) should not have been discounted in Kubaschewski's review. It is surprising that these large uncertainties§ are still present in the accurate evaluation of a simple thermochemical constant.

The results of this investigation on dilute Zn:Tl alloys support the lower value of ΔH as selected by Kelley (1936) and the higher value of the volume shrinkage on solidification as determined by Saeger and Ash (1932). Additional work is contemplated on the establishment of the binary phase diagrams at extreme dilution for other solutes in zinc; this will provide additional information for the determination of the latent heat of fusion of pure zinc.

ACKNOWLEDGMENTS

The authors are grateful to Mr. E. G. Murdock for his valuable assistance in the experimental work, and to the X-ray and Nuclear Radiations Section, N.R.C., for the use of 4π counting equipment.

*Freezing temperature decreased 0.78° C on reducing ingot size from 700 g to 400 g (diameter 42 mm).

†This difficulty has been overcome in our investigations by the use of large ingots and modern Meyers thermometers (see McLaren 1959).

‡This value for ΔH was also selected by Rossini *et al.* (1952) in their compilation of thermodynamic properties.

§Some of the uncertainty found in the determination of these thermodynamic properties may be the result of, as yet, unaccounted effects of orientation, lattice defects, and porosity in the solid phase.

REFERENCES

HAYES, A. and CHIPMAN, J. 1939. Trans. Am. Inst. Mining Met. Engrs. **135**, 85.
HEYCOCK, C. T. and NEVILLE, F. H. 1897. J. Chem. Soc. Trans. **71**, 383.
——— 1895. J. Chem. Soc. Trans. **67**, 185.
HONDA, K. and ISHIGAKI, T. 1925. Sci. Repts. Tôhoku Imp. Univ. (1) **14**, 219.
KELLEY, K. K. 1936. U.S. Bur. Mines Bull. No. 393.
KUBASCHEWSKI, O. 1950. Z. Elektrochem. **54**, 281.
KUBASCHEWSKI, O. and EVANS, E. LL. 1958. Metallurgical thermochemistry (Pergamon Press), p. 308.
LUMSDEN, J. 1948. Discussions Faraday Soc. No. **4**, 60.
——— 1952. Thermodynamics of alloys (Inst. of Metals, London), p. 102.
McLAREN, E. H. 1957. Can. J. Phys. **35**, 1086.
——— 1958. Can. J. Phys. **36**, 585.
——— 1959. Can. J. Phys. **37**, 422.
PELZEL, E. and SAUERWALD, F. 1941. Z. Metallk. **33**, 229.
ROSSINI, F. D., WAGMAN, D. D., EVANS, W. H., LEVINE, S., and JAFFE, I. 1952. Selected values of chemical thermodynamic properties, National Bureau of Standards (Washington), Circular No. 500, p. 667.
SAEGER, C. M. and ASH, E. J. 1932. J. Research Natl. Bur. Standards, **8**, 37.
YUE, A. S. and CLARK, J. B. 1960. Trans. Am. Inst. Mining Met. Engrs. **218**, 55.

EFFECTS OF EQUATORIAL SPREAD-*F* IRREGULARITIES ON C. W. TRANSMISSIONS[1]

M. S. V. Gopal Rao and B. Ramachandra Rao

ABSTRACT

A study is made into the effects of spread-*F* conditions on continuous wave (c. w.) transmissions between Colombo and Waltair over a distance of about 1300 kilometers. It is shown that under suitable conditions increased fading rate of the received c. w. signals is a sufficient indication of spread *F* and gives a genuine index of its intensity. Pulse and c. w. methods are used simultaneously to study the time variations of spread-*F* intensity at separated points. The results indicate that the horizontal extent of spread-*F* occurrence in the N.–S. direction is greater than 650 km.

The probability distributions of signal amplitudes in the c. w. fading records were closer to Rayleigh type under normal conditions than during spread-*F* conditions. It is suggested that the c. w. flutter fading is caused by the presence of spread-*F* irregularities in the appropriate zone of reflection in the *F*-region of the ionosphere.

1. INTRODUCTION

The strong positive correlation reported between the radio star scintillations and spread *F* (Ryle and Hewish 1950; Little and Maxwell 1951) suggested the occurrence of the required irregularities in extensive patches of considerable horizontal extent even up to 920 km (Briggs 1958). It has been shown that the fluctuations sometimes observed in the intensity of the radio waves received from the direction of some star constellations, are due to their passage through the ionospheric irregularities. Effects similar to this should also be observable in the case of c. w. transmissions through the *F*-region if spread-*F* irregularities are prevailing in the relevant zone of reflection. The present paper is concerned with the study of some of these effects. With this end in view c. w. signals from the regular broadcasting station Colombo have been picked up and the signal fading observed is studied in relation to the simultaneously observed overhead spread-*F* conditions at Waltair (geographic latitude 17°41′ N.; geomagnetic 7.4° N.).

2. SCHEME OF OBSERVATIONS AND METHOD OF ANALYSIS

Continuous wave signals on 11.717 Mc/sec from Colombo (Ceylon) situated at about 1300 km roughly to the south of Waltair, the receiving site, were recorded using conventional equipment consisting of a communications type SX-42 receiver, d-c. amplifier, and an Esterline-Angus pen recorder. About 100 of these fading records, each of 5 to 10 minutes' duration, were taken during the months of January and February, 1959, at different times of the night between 1800 hours and 2300 hours Indian Standard Time (I.S.T.), an interval during which the transmissions are available. Simultaneously with each of these recordings, spread-*F* conditions are observed at Waltair using

[1]Manuscript received November 2, 1960.
Contribution from the Ionospheric Research Laboratories, Andhra University, Waltair, India.

the conventional vertical incidence ionospheric pulse sounding equipment. Each time the group height range (in km) over which the 1*F* echo spreads has been recorded by visual observation so as to express the intensity of local spread-*F* conditions in terms of the indices 0–10 in accordance with the scheme defined by Gopala Rao *et al.* (1960). In all these 100 occasions, pulse soundings were made only on a frequency of 6.4 Mc/sec, which is found to be nearly the equivalent vertical incidence frequency corresponding to the first hop *F* reflection in the present c. w. transmissions. Exact evaluation of this frequency will not be necessary or important since the equatorial spread-*F* characteristics would not differ much with the operating frequency. Examination of the $f_0 F_2$ and maximum usable frequency (m.u.f.) (3000 km) data of Trichinopoly, and Trivandrum stations (All India Radio (A.I.R.)), which are in the vicinity of the second and third hop reflection points in the *F*-region, indicated that the frequency of 11.717 Mc/sec was generally greater than the optimum working frequencies (o.w.f.) for the 2*F* and 3*F* propagation modes between Colombo and Waltair. Thus the 1*F* mode is expected to be mostly predominant in these transmissions and gives information about the ionospheric *F*-region conditions at a location 650 km south of Waltair (near Madras).

Fading rate in cycles per minute in each of the c. w. records is defined here as the number of maxima occurring per minute. In order to keep consistency only fluctuations greater than 10% of the average amplitude of fading were considered.

3. RESULTS OF PRELIMINARY ANALYSIS

A striking feature in most of the c. w. records is a consistent increase in the fading rate whenever spread *F* occurred at Waltair. This consistency itself suggested the occurrence of spread-*F* conditions at 650 km south of Waltair and also where the c. w. transmissions from Colombo encounter the *F*-region before reaching Waltair. Despite the simplicity of equipment, it is well known that the c. w. method has a serious limitation in that the waves received by different group paths are not resolved. Observations of spread-*F* echoes by the c. w. method can therefore be neither simple nor reliable as is the case with the pulsed radio echo method. The present series of simultaneous observations have positively indicated that, under the present experimental conditions, the enhanced c. w. fading rate is a genuine representation of spread-*F* conditions. Typical fading records taken on January 18, 1959 at 2300 hours I.S.T. when there was no spread *F* at Waltair and the one taken on January 21, 1959 at 2030 hours I.S.T. when spread-*F* index on 6.4 Mc/sec at Waltair is 9 are shown in Figs. 1*a* and *b* respectively.

All the fading rates in the c. w. records connected with 0 spread-*F* index at Waltair are separately averaged and the rest are grouped into 5 ranges with 1–2, 3–4, etc., spread-*F* indices. The average c. w. fading rates connected with each of these groups are shown in Table I. The average c. w. fading rate was only 10.7 cycles/minute under 0 or no spread-*F* condition at Waltair. Three- to four-fold increase in the average fading rate is observed

TABLE I

Results of preliminary analysis

Spread-*F* index group	c. w. fading rate in cycles/minute
0	10.7
1–2	30.1
3–4	33.8
5–6	42.6
7–8	34.8
9–10	40.8

whenever spread *F* of any degree occurred at Waltair although no systematic increase could be observed in the c. w. fading rate with increasing degree of spread *F* recorded at Waltair. In these circumstances c. w. fading rate cannot be used as a measure of the degree of spread *F*, although in general there is a positive indication that the enhanced fading rate is caused by spread-*F* irregularities. This discrepancy is explained in the following section by considering the possible time differences in the occurrence of a certain intensity of spread *F* at the overhead point at Waltair and at 650 km south of Waltair.

4. TIME SHIFTS IN THE TEMPORAL VARIATIONS OF SPREAD *F* AT SEPARATED POINTS

In a second series of observations during the months of January and February, 1960, continuous c. w. recordings together with overhead pulse observations were made at closer time intervals between 1900 hours and 2300 hours I.S.T. Further, in this series vertical incidence spread-*F* observations were made on a group of 10 spot frequencies which included 6.6 Mc/sec as one of the spots to cover the frequency range over which spread-*F* echoes are observable. The variations, with time, of the fading rate of c. w. signals from Colombo and of the spread-*F* index at Waltair averaged on all the spot frequencies as well as the index on 6.6 Mc/sec alone as obtained on some of the nights are illustrated in Figs. 2 and 3. These figures readily show reasonable similarity in the variations together with an observable time shift as expected. It is also clear that the time variations of the average spread-*F* index and that on 6.6 Mc/sec alone are very much similar indicating the uniformity of spread-*F* index time variations at different frequencies. The lack of systematic increase found in the values of Table I can now be attributed to the grouping of the simultaneously observed parameters. On the other hand if we shift either of the curves in such a way that the nearest similarities in the maxima and minima coincide, considerable correspondence is evident in the variations. By plotting the observations of the c. w. fading rates around the maxima and minima against the values on the corresponding portions of the maxima and minima in the spread-*F* index variation curves ignoring the time shift, the scatter plot shown in Fig. 4 is obtained. It will be seen from this figure that a fairly good linear dependence exists between the c. w. fading rate and the average spread-*F* index. The existence of a systematic variation in the c. w. fading rates with the changes in the degree of spread *F* is thus revealed.

PLATE I

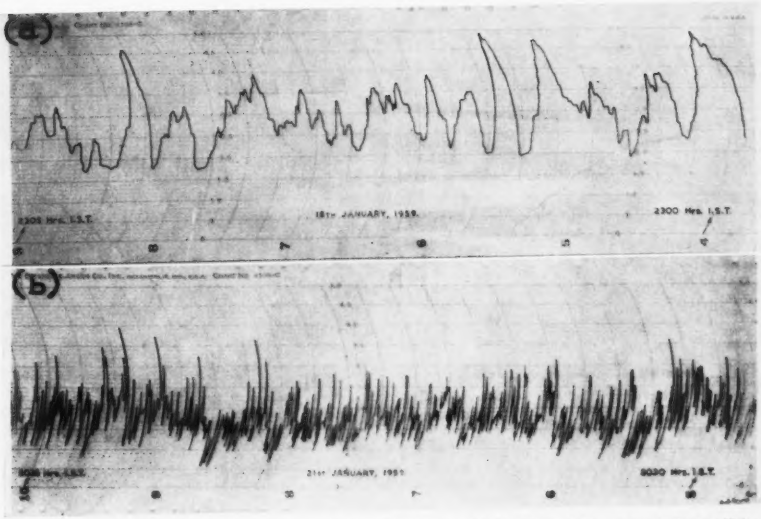

FIG. 1. Typical c. w. fading records as (*a*) unaffected and (*b*) affected by spread-*F* conditions.

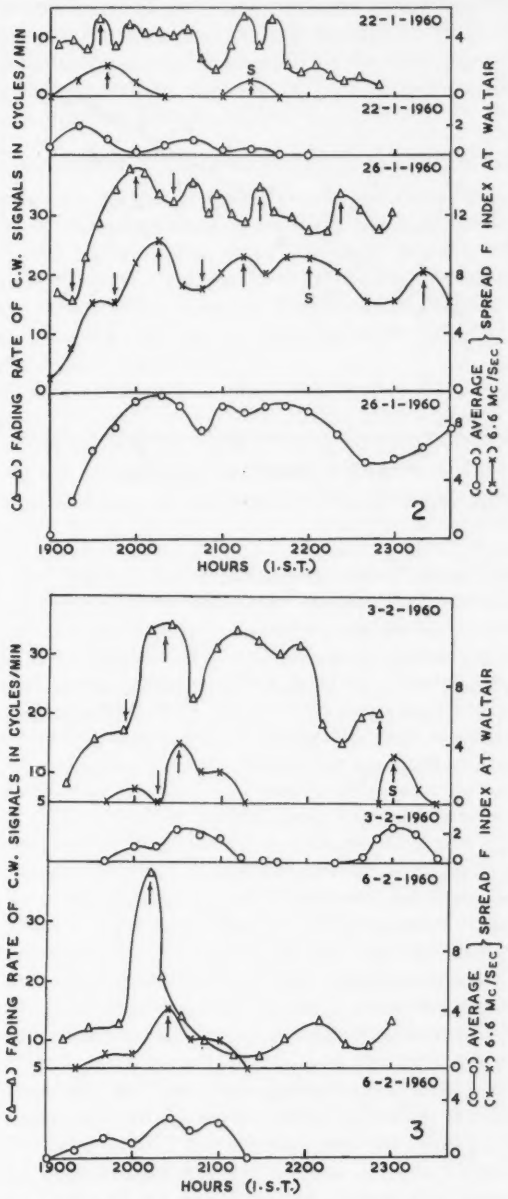

FIGS. 2–3. Time variations of fading rate of c. w. signals from Colombo and spread-*F* index at Waltair.

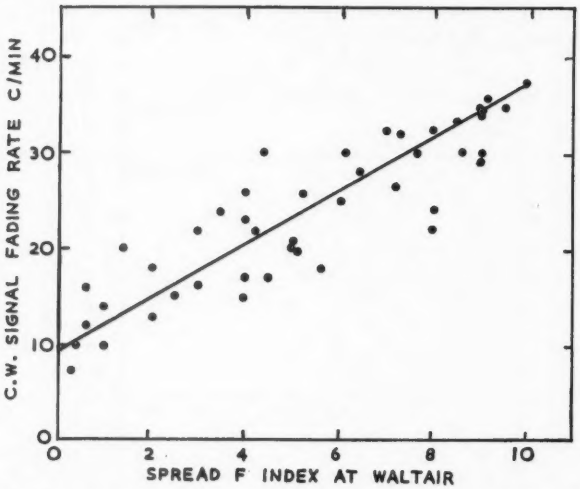

FIG. 4. Fading rate of c. w. signals from Colombo versus spread-*F* index at Waltair (time shifts ignored).

Examination of some of the similarities, shown in Figs. 2 and 3 by arrows and several other similar variation curves, indicated an earlier occurrence of certain maximum or minimum, in the c. w. fading rates with respect to those of spread-*F* index variations at Waltair. The distance of 650 km and the observed time shifts may be utilized to obtain a quantity with the dimensions of velocity. Considering the average time shift corresponding to the first major peaks, which is about 20 minutes, a velocity of 540 m/sec is obtained. This represents only the apparent velocity in the N.–S. direction. However, it does not seem to be reasonable to associate this with any movement or drift because there is some evidence (unpublished) to believe that the timing and magnitude of the first peak spread-*F* index is closely related with local factors such as height changes in the evening hours. The first peak spread-*F* index at each place seems to occur earlier or later according as the rate of increase of $h'F$ in the early evening hours after sunset is large or small. As this rate is generally largest near the magnetic equator and smaller successively at points farther from the equator, the peak spread-*F* index occurs generally earlier on c. w. records when compared to observations at overhead point. Hence the observed time shifts are not interpreted as due to any genuine drift of irregularities.

In this connection it is interesting and useful to consider the results of F_2-region horizontal drifts at Waltair reported by Ramachandra Rao and Bhagiratha Rao (1959). At about 2000 hours I.S.T. the drift is reported to be mainly towards the north with an average magnitude of 80 m/sec. If we assume that this drift pattern is unaffected by spread-*F* conditions and spread-*F* irregularities generated at one location are carried by these drifts,

it will take at least 2 hours 15 minutes for a travel of 650 km. The secondary maxima in the spread-*F* variation at Waltair denoted by 'S' in Figs. 2 and 3, occurring (approximately) around 2 hours after the first major maximum in the c. w. fading rate variations might have been caused by the northward component of the general *F*-region drifts.

5. COMPARISON WITH C. W. FLUTTER PHENOMENON

Sometimes along with the rapid fading under spread-*F* conditions a quivering noise superposed on the programme is heard in the loud-speaker giving an impression that still higher fading rates might be present than could be recorded by the instrument. It is likely that the amplitudes of such fast-fading components are smaller than could be recorded or considered in the present analysis in which the fluctuations less than 10% of the average amplitude of fading were neglected.

These experimental conditions remind one of the 'flutter phenomenon' reported by Subba Rao and Somayajulu (1949). They reported a peculiarly rapid fading of c. w. signals from Madras and Colombo transmissions received at Waltair during the nights in the months of February to June, 1948. This period corresponds roughly to the same part of the sunspot cycle as the current investigation period. They reported that the quasi-flutter frequency was low (20–30 cycles/minute) before sunset and increased to 120–140 cycles/minute during night hours. No mention was made by them about any amplitude restrictions in the evaluation of the fading rates. However, from the fading records published by them it is clear that this fast-fading flutter component is much smaller in amplitude than the average amplitude of fading. The background of the present investigation suggests that this flutter phenomenon might have been caused by spread-*F* conditions prevailing in the appropriate zone of reflection. It may be noted that recently Wright (1959) also reported several similarities between the flutter on the c. w. transmissions and spread-*F* phenomenon.

6. AMPLITUDE DISTRIBUTION ANALYSIS OF FADING RECORDS

The fading patterns of the c. w. records in this investigation have been generally random except on few occasions when some kind of quasi-periodic fading occurred. From observation of a large number of these records, it is found that the depth of fading is somewhat reduced when transmissions are suspected to be affected by spread-*F* conditions as against normal conditions. In order to study this and other features, the probability distributions of the signal amplitudes were studied for some of the records. The deflection of the pen recorder pointer varied linearly with the input signal voltage at the receiver. The amplitude of the signal in terms of the chart divisions was determined at a series of equally spaced time intervals of 0.625 second. The probability distribution of the amplitudes was obtained. This was compared with the Rayleigh type distribution given by

$$P(R) = \frac{R}{\psi} \exp(-R^2/2\psi)$$

where 'R' is any amplitude in the observed range, and $\psi = R_m^2$, R_m being the most probable amplitude. Substituting the experimental value for R_m, the theoretical values of $P(R)$ were calculated for various values of 'R' and were multiplied by a suitable constant so as to obtain a best fit. On comparison it was found that distributions were nearer to the Rayleigh type during normal conditions than when there was spread F associated with rapid fading in the c. w. records. Some of the typical distribution curves are shown in Fig. 5.

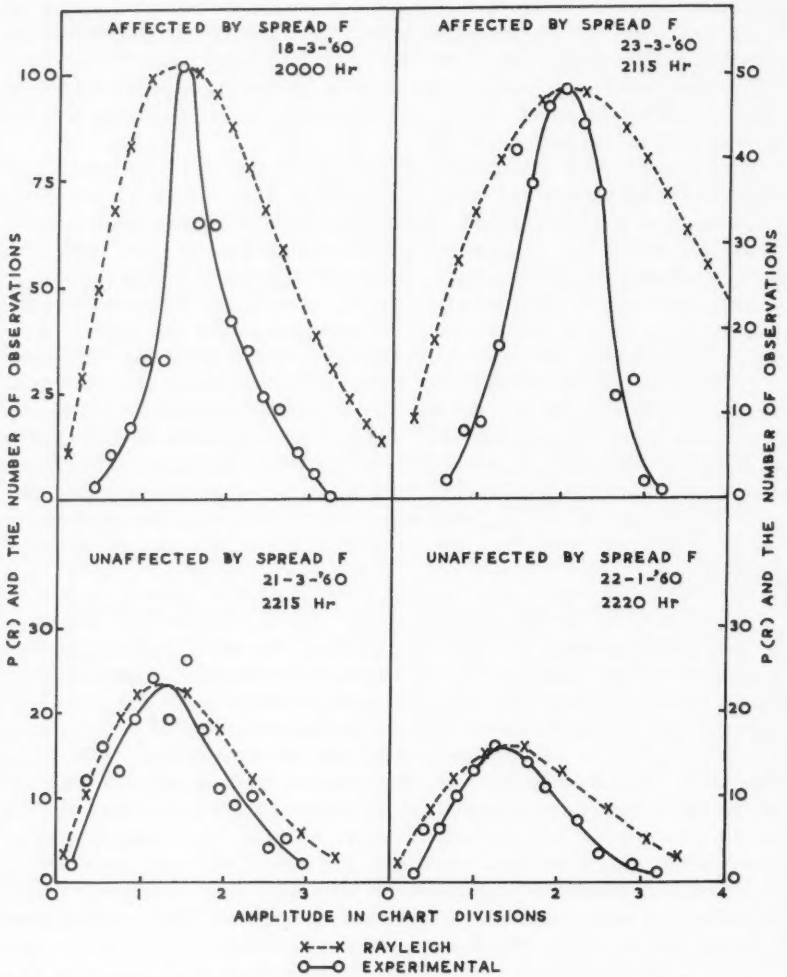

FIG. 5. Typical amplitude distributions of c. w. fading of transmissions from Colombo on 11.717 Mc/sec, as received at Waltair.

McNicol (1949) has shown that Rayleigh distribution is only a special case which occurs when the downcoming waves consist only of a large number of scattered waves of approximately the same group path but with phase paths differing from one another by random fractions of a wavelength. According to his findings the deviation from the Rayleigh type observed in this investigation indicates the presence of a steady component in addition to the randomly fading component. This leads to the fact that under most severe conditions of spread *F* the depth of fading is reduced or the proportion of the steady component of the signal increases. This is consistent with the smaller amplitude of the flutter fading referred to earlier and supports the view that flutter phenomenon is caused by spread-*F* irregularities. It is of interest to note that a similar situation namely the reduction in the depth of fading under fast-fading conditions has recently been reported by Koch *et al.* (1960) in connection with c. w. transmissions through auroral regions. This leads to some similarity between spread-*F* and auroral conditions regarding the nature of the irregularities.

Spread-*F* irregularities are therefore observable and can be studied even with simple c. w. equipment under suitable conditions when periodic fading due to other causes does not interfere to vitiate the observations. Results of the present investigation suggest that patches of spread-*F* irregularities extend horizontally in a scale greater than 650 km in the N.–S. direction at this location.

ACKNOWLEDGMENT

We are indebted to the Council of Scientific and Industrial Research of India for financial support of these investigations.

REFERENCES

Briggs, B. H. 1958. J. Atmospheric and Terrest. Phys. **12**, 34.
Gopala Rao, M. S. V., Ramachandra Rao, B., and Ramachandra Rao Pant, P. 1960. J. Atmospheric and Terrest. Phys. **17**, 345.
Koch, J. W., Beery, W. M., and Petrie, H. E. 1960. Natl. Bur. Standards, Rept. No. 6701, 8.
Little C. G. and Maxwell, A. 1951. Phil. Mag. **42**, 267.
McNicol, R. W. E. 1949. Proc. Inst. Elec. Engrs. Part III, **96**, 517.
Ramachandra Rao, B. and Bhagiratha Rao, E. 1959. J. Atmospheric and Terrest. Phys. **14**, 94.
Ryle, M. and Hewish, A. 1950. Monthly Notices Roy. Astron. Soc. **110**, 381.
Subba Rao, N. S. and Somayajulu, Y. V. 1949. Nature (London), **163**, 442.
Wright, R. W. H. 1959. J. Geophys. Research, **64**, 2203.

NOTES

GAMMA DOSE IN A HOLE IN A UNIFORMLY CONTAMINATED PLANE: CONTRIBUTION BY GROUND PENETRATION*

C. E. CLIFFORD

In assessing the protection against γ-radiation provided by a hole in a contaminated field it is necessary to consider the contribution to the total dose produced by γ-radiation that penetrates the ground from contamination around the hole. As the diameter of the hole decreases this component becomes comparable to the component due to radiation backscattered from the sky or skyshine. Usually the effect of "lip" penetration is ignored since it can be eliminated simply by removing the contamination within a few feet of the edge of the hole. However, when this contamination is not easily removed—for example, in the case of a foxhole if it was buried when the foxhole was dug—the ground penetration component could be a significant fraction of the total dose. This ground penetration component could also be important in the case of a corner basement shelter particularly if contamination was washed off the roof and piled up against the outer basement wall.

In recent work at the Defence Research Chemical Laboratories (Clifford 1960) measurements were made of the dose distributions in a particular hole by ground penetration of γ's from uniform contamination of the surrounding plane. Some of the more important results of these measurements are given and compared with calculations from the work on γ-scattering carried out at the National Bureau of Standards by Spencer.

The cylindrical hole studied was 2 meters in diameter and 2 meters deep. The wall, floor, and lip of the hole were made of a sand and cement concrete. Cs^{137} was chosen as the contaminant since the γ-ray energy (0.66 Mev) is close to the average energy of the γ-rays emitted by fission "fallout" a few hours after detonation of a weapon. All dose measurements were made by combining the results of single source determinations to give the values that would have been obtained with uniform contamination. During an exposure the source was placed in a slight depression in the concrete "ground", so that its effective center was at "ground" level, and covered with a lead shield to eliminate any skyshine dose to the detectors in the hole.

The depth variations of dose due to ground penetration both along the axis of the hole and along a line halfway between the axis and the wall of the hole are shown in Fig. 1 for a uniform ground contamination of 1 mc Cs^{137}/meter^2. The distributions down the center and halfway to the wall are quite similar. The dashed curve gives the calculated dose along the central axis and was obtained from the work of Spencer. At lower depths agreement is good while at shallow depths the experimental values are lower than those calculated.

*Issued as DRCL Report No. 310A.

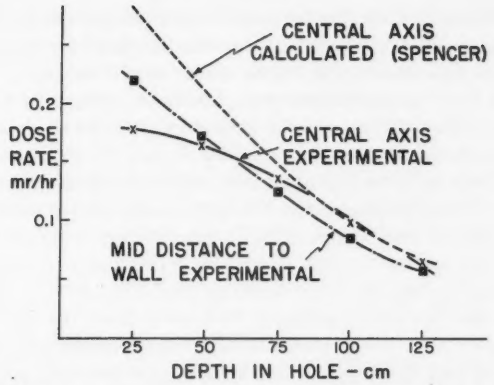

FIG. 1. Dose rate due to ground penetration of γ-radiation into a hole in a concrete plane uniformly contaminated with 1 mc Cs^{137}/meter^2. Diameter of hole is 2 meters.

Figure 2 shows the dependence of the ground penetration dose on the area of contamination for two depths on the central axis. Over 90% of the dose is due to contamination within 1 foot of the edge of the hole and it was found that contamination in the region beyond 60 centimeters contributed less than 1/10th of 1% of the dose received from the first 60 centimeters. For comparison, a contamination of 1 mc Cs^{137}/meter^2 over an area of 400 meters radius gives a dose of 12.1 mr/hr and over an area of 200 meters radius 11.5 mr/hr at a height of 1 meter above the surface. In the latter case skyshine doses in a 2-meter diameter hole 2 meters deep are 0.74, 0.46, and 0.22 mr/hr at depths of 0.25, 0.50, and 1 meter (Clifford *et al.* 1959). At a depth of 1 meter the total dose (skyshine plus ground penetration) is therefore approximately 3% of the dose at 1 meter above the surface and of this roughly one-third is due to ground penetration which can be eliminated by clearing away the contamination within 2 feet of the edge of the hole. For the case of a smaller

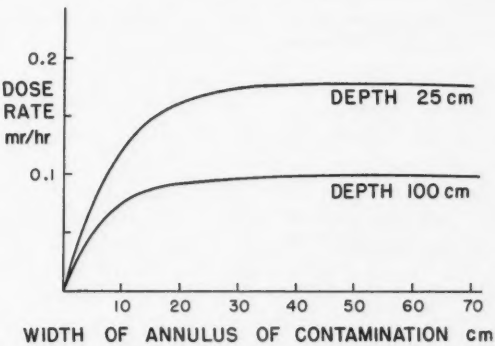

FIG. 2. Dependence of dose rate due to ground penetration on extent of contamination. Dose rate measured on axis of a 2-meter diameter hole in a plane contaminated with 1 mc Cs^{137}/meter^2.

diameter hole, elimination of the lip penetration component would give an even greater improvement in shielding since the skyshine component is more dependent than the lip penetration on the diameter of the hole.

The individual dose measurements that had been integrated to study the effect of uniform contamination were analyzed in order to study the effect of lip penetration in detail and to see whether or not an elementary method could be used for dose calculations in this and other shielding problems involving lip geometry. Since infinite media data are available for many materials and energies (Goldstein 1954; Fano 1959) it was felt that it would be useful to relate the observed values in this particular experiment to corresponding known infinite media data. For the limiting case of a detector close to the lip and below ground level with a source well away from the lip, it appeared reasonable to expect that the detector would receive approximately one-half of the scatter dose that it would receive at the corresponding lip penetration distance in an infinite concrete medium. Its dose build-up factor would then be $(B_\infty/2+\frac{1}{2})$ where B_∞ is the dose build-up factor for an infinite medium. In Fig. 3 summary curves of the observed dose build-up factors are expressed

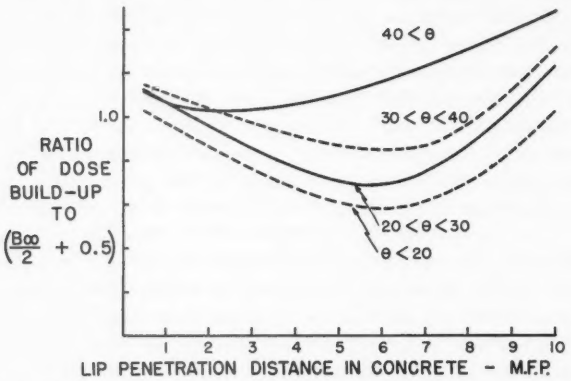

FIG. 3. Ratio of dose build-up to $(B_\infty/2+0.5)$ vs. lip penetration distance, for lip penetration of a concrete hole using Cs^{137} sources.

as fractions of $(B_\infty/2+\frac{1}{2})$ and are plotted against the concrete lip penetration distances in mean free paths (m.f.p.). The data, total 230 points from all detector locations in the foxhole, were arbitrarily divided into four approximately equal groups depending on the direction angle θ of the source to detector direction below the horizon. The lower curve summarizes the readings with $\theta < 20°$, the others with θ between 20° and 30°, 30° and 40°, and $\theta > 40°$. For each group the average deviation of a point from the curve was $4\frac{1}{2}\%$. From these curves it would appear that the dose due to ground penetration for a shielding case involving lip geometry of a circular hole could be approximated by taking $(B_\infty/2+\frac{1}{2})$ for distances less than 10 m.f.p. At shallow depths this elementary approach would be increasingly in error but no more than a factor of 2.

To study lip geometry build-up factors in further detail, laboratory measurements were made of the dose transmitted between points on intersecting sides of a 1-meter cube of homogeneous absorber, lucite+36% sucrose solution, using similar techniques as in the hole experiments.

Source and detector positions were chosen so that the dose at fixed lip penetration distances of 2, 4, 6, or 8 m.f.p. could be measured as a function of θ, the angle of penetration from the source plane. The observed dose build-up factors were expressed as fractions of one-half the infinite medium build-up factor $(B_\infty/2+\frac{1}{2})$ and are shown in Fig. 4 as a function of θ. The ratios are

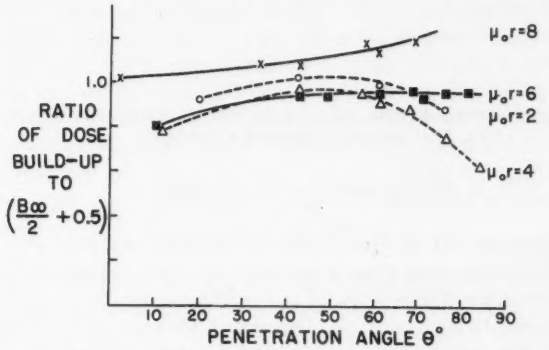

FIG. 4. Ratio of dose build-up to $(B_\infty/2+0.5)$ vs. penetration angle θ, for lip penetration of a rectangular lucite tank using Cs^{137} sources.

grouped around a value of 1. At large values of θ, i.e. source close to the lip and detector away from the lip, the ratios decreased for the 2 and 4 m.f.p. cases. At these shorter lip penetration distances a considerable amount of the scattered radiation that reached the detector was generated in material close to the source. As θ increases the amount of this material becomes less and it is not unreasonable that the build-up should decrease. At greater lip penetration distances, radiation scattered in material close to the source is less likely to reach the detector because of the greater absorption of lower energy radiation and a decrease in build-up with increasing θ is less likely.

The ground penetration dose in a hole in a uniformly contaminated plane can be obtained by an integration over a distribution of point sources. For the foxhole studied, the average deviation, from the observed values on the central axis, of the ground penetration dose calculated using $(B_\infty/2+\frac{1}{2})$ was about 4% at depths of 50, 75, 100, and 125 centimeters. At the most shallow depth measured, 25 centimeters, the deviation was 14%. The use of $(B_\infty/2+\frac{1}{2})$ in calculating the dose produced by an individual point source probably would be in error at lip penetration distances greater than 8 m.f.p. for a rectangular lip of lucite or 10 m.f.p. for a circular hole in concrete. However, as discussed above, in the case of foxhole shielding the contribution from radiation that has penetrated more than 8 m.f.p. would contribute only a small error.

CLIFFORD, C. E. 1960. Defence Research Chemical Laboratories, DRCL Report 310.
CLIFFORD, C. E., CARRUTHERS, J. A., and CUNNINGHAM, J. R. 1959. Defence Research Chemical Laboratories, DRCL Report 296.
FANO, U., SPENCER, L. V., and BERGER, M. J. 1959. Penetration and diffusion of X-rays, Handbuch der Physik, Vol. XXXVIII/2.
GOLDSTEIN, H. and WILKINS, E. J. 1954. Calculations of the penetration of gamma rays, NYO-3075, June 1954.
SPENCER, L. V. Structure shielding against fallout radiation from nuclear weapons, OCDM. To be published.

RECEIVED DECEMBER 7, 1960.
DEFENCE RESEARCH CHEMICAL LABORATORIES,
DEPARTMENT OF NATIONAL DEFENCE,
OTTAWA, CANADA.

DIMENSIONS DES GRAINS AU COURS DE LA PRÉCIPITATION DES ÉMULSIONS IONOGRAPHIQUES

I. BATTHYANY* ET P. DEMERS

Avec la collaboration de M. Jean Côté de l'Institut de Microbiologie de l'Université de Montréal, nous avons examiné avec un microscope électronique RCA-EMU-2C des échantillons d'émulsion No 22 précipités à diverses vitesses d'agitation (Demers 1958; Fournaux, Demers et Demers 1960). L'agitation la plus lente choisie permet à peine d'éviter la stagnation des nappes de diverses densités; la plus rapide évite à peine la formation de bulles d'air. Pendant ces essais la vitesse d'écoulement des réactifs A et B dans la méthode du double jet appliquée, est restée comprise entre les limites choisies.

On a obtenu pour les vitesses $v = 1$, 2 et 4 tours par seconde (t.p.s.), la distribution des diamètres granulaires d lus sur les négatifs photographiques au grandissement X 17 143. La distribution s'accorde sensiblement dans les trois cas avec une formule de Gauss, avec $d = 0.17\ \mu$, $0.12\ \mu$ et $0.10\ \mu$, $\sigma = 0.037\ \mu$, $0.033\ \mu$, $0.18\ \mu$. Ces trois valeurs de d s'accordent avec une droite dans une représentation log d, $1/v$, selon la formule:

$$d = 0.088\ e^{-0.654/v};$$

de la sorte une vitesse v infinie assure le diamètre le plus petit possible, $0.088\ \mu$ ou 880 Å.

On a aussi tracé la distribution en volume F, le volume moyen est comme suit: $1.2\times10^{-6}\ \mu^3$, $1.7\times10^{-6}\ \mu^3$ et $5\times10^{-6}\ \mu^3$ environ.

Nous avons ensuite prélevé des échantillons à des époques successives au cours de la précipitation d'un lot d'émulsions. Cette série de mesures sert à comprendre le mécanisme de la formation et de la croissance des cristaux. Au début les cristaux sont petits et rares, à la fin ils sont plus gros et plus nombreux. Le volume moyen des grains $\bar{F}$ augmente à mesure que le volume des

*Adresse actuelle: en stage au laboratoire du Professeur Max Morand, Sorbonne, Paris.

solutions versées V augmente. Si le nombre des grains n reste fixe, $\bar{F}$ est proportionnel à V, sinon, il est proportionnel à V/n, et si on suppose que n varie avec V selon une loi en puissance constante:

$$\bar{F} = a' V^{b'}$$

et pour le diamètre:

$$\bar{d} = a V^{b}.$$

Si le nombre n reste fixe, $b = \frac{1}{3}$, sinon $b > \frac{1}{3}$.

Effectivement, entre $V = 17$ tours et $V = 327$ tours, le diamètre augmente selon une puissance b comprise entre $\frac{1}{3}$ et $\frac{1}{2}$. Cela signifie qu'après 17 tours versés, le nombre des grains s'accroît peu, le bromure d'argent précipité à partir de ce moment sert surtout à accroître la dimension des grains déjà présents, et il se forme peu de nouveaux germes.

Des dénombrements exacts de grains sur des portions aliquotes des échantillons permettraient de mieux comprendre le mécanisme en question. Les dénombrements sur les grains très fins, de diamètre voisin de 0.04 μ, sont difficiles; ceux que nous avons pu faire s'accordent, à leurs erreurs expérimentales près, avec les mesures de diamètre.

Nous remercions le Conseil National des Recherches, l'Office des Recherches Scientifiques (Ministère de l'Industrie et du Commerce, Québec) et le Ministère de la Jeunesse (Québec), pour leur aide financière.

DEMERS, P. 1958. Ionographie, les émulsions nucléaires, principes et applications (Les Presses Universitaires de Montréal, Montréal, Qué.).
FOURNAUX, J., DEMERS, J. et DEMERS, P. 1960. Can. J. Phys. **38**, 1482.

REÇU LE 7 NOVEMBRE, 1960.
DÉPARTEMENT DE PHYSIQUE,
UNIVERSITÉ DE MONTRÉAL,
MONTRÉAL, QUÉ.

OBSERVATIONS OF UNUSUAL LOW-FREQUENCY PROPAGATION MADE ON 12 NOVEMBER, 1960

J. S. BELROSE AND D. B. ROSS

INTRODUCTION

The intense solar eruptions of 10, 12, and 15 November, 1960, produced marked effects on the propagation of radio waves. Some of these were recorded in a series of experiments which have been undertaken by the Radio Physics Laboratory for the purpose of studying the lower ionosphere at high latitudes by means of propagation of long waves, in particular the effects of polar cap disturbance (PCD) events. High-frequency absorption measuring equipment

indicates that the pronounced polar cap absorption (PCA), occurring during such events, is usually restricted to geomagnetic latitudes greater than 60°, and is only observed south of about 60° geomagnetic latitude after the commencement of the geomagnetic storm, i.e. the distortion of the earth's field can result in an equatorial extension of the PCA. The class 3+ flare which began at 1325 on 12 November was accompanied by a major sudden ionospheric disturbance (SID). A few minutes later, at 1352, a marked increase of cosmic-ray intensity was observed, which was accompanied by a marked disturbance in the *D* region. Since the PCD began coincident with the SC of a great geomagnetic storm, which began at 1348 on 12 November, presumably due to the class 3 flare at 1009 on 10 November, the observed effects of the PCD at geomagnetic latitudes of 60° and below was of unprecedented magnitude. It is the purpose of this note to give an outline of the effects observed on 12 November, 1960, and a tentative interpretation of them. The detailed deductions depend on much accumulated information from our studies of such events, but we do not intend to discuss this evidence here, since it will be published separately in the near future.

THE OBSERVED EFFECTS

The field strength of 77.15-kc and 82.05-kc transmissions from the U.S.A.F. transmitters at Thule and Goose Bay are being monitored at Churchill, and the field strength of 70.384-kc transmissions from the Decca Navigator transmitter located at Comfort Cove is recorded at Ottawa. In addition frequency stable 80-kc transmissions from a transmitter operated by the Radio Physics Laboratory at Ottawa are recorded at Churchill. In this experiment both phase and amplitude variations are recorded, the phase variations are measured with reference to a very stable oscillator located at the receiving site. The various transmission paths are shown in Fig. 1.

Records of the field strength of the various l.f. transmissions made on 12–13 November are shown in Fig. 2, together with similar records made on 8–9 November for comparison. The sudden beginning of the PCD on 12 November is strikingly shown in the record for transmissions from Comfort Cove to Ottawa. The onset of the PCD effect followed the large SID, which began at 1323, and reached a maximum at 1332. The SID effect is clearly one of great magnitude, since the l.f. field strength increased to a value greater than the usual quasi-peak nighttime value (SID effects result in general in an increase in the field strength for these transmissions). The enhanced signal began to decrease after 1332, in the usual way, until 1410, when a new and continuing source of electron production became apparent. In the absence of a PCD, the excess flare-produced ionization would have decayed, resulting in a return of the l.f. field strength to normal as sketched by the broken curve. The solar flare proton stream apparently produced an ionized layer at the base of the ionosphere whose gradient was sufficiently sharp to support the enhanced propagation of l.f. radio waves. The SID was not seen on the northern records because it occurred too near sunrise. The enhanced field strengths in the early phases of the PCD are evident in all recordings.

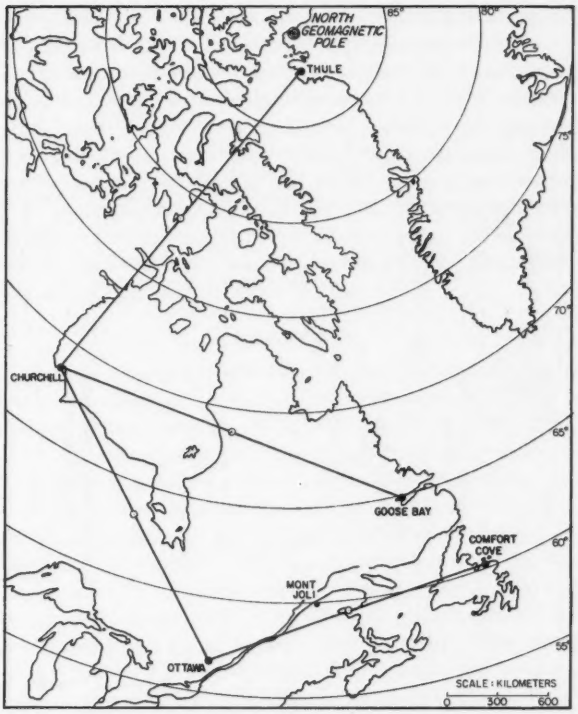

FIG. 1. Map showing the various l.f. propagation paths.

The second observable feature began at 1900 on 12 November and showed as a marked decrease in all l.f. field strengths. No diurnal variation was observed at sunset and sunrise on 12 and 13 November for the Comfort Cove – Ottawa transmission, and no diurnal variations at all are evident for high latitude transmissions for a period of days.

The deduced phase variations for 80-kc transmissions between Ottawa and Churchill for 12–13 November are also shown in Fig. 2, together with a similar record made on 10–11 November for comparison. The usual quiet day variation shows a decreased phase lag by day (lower reflection heights), an increased phase lag at night, and slow phase fading at night. The SID at 1325 is scarcely discernible, since it occurred too soon after sunrise to produce a marked effect. The small change detected is also confused by a small decrease which began somewhat earlier, at 1318. The SID effect although very small is quite different from normal since the phase lag continued to decrease from 1330 until 1354, at which time a more rapid decrease began. By 1515 the phase lag was about 0.5 cycle less than normal. There was little or no diurnal variation of the phase for a period of days. The PCD effect of 12 November was still in progress when a second PCD began at 0300 on 15 November.

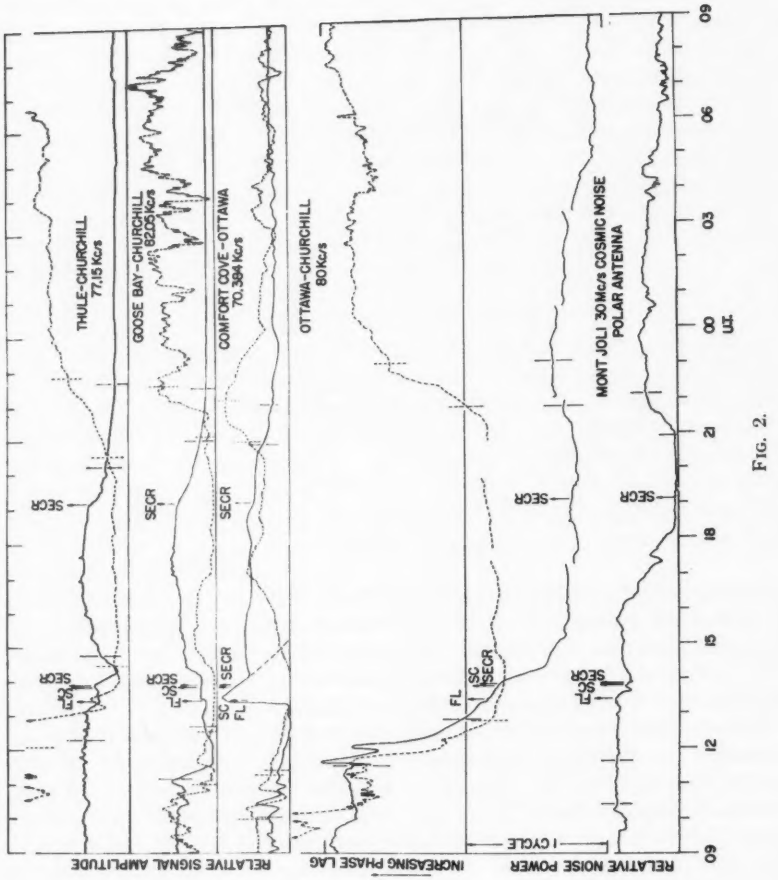
RELATIVE SIGNAL AMPLITUDE
INCREASING PHASE LAG
RELATIVE NOISE POWER
THULE-CHURCHILL
77.15 Kc/s
GOOSE BAY-CHURCHILL
82.05Kc/s
COMFORT COVE-OTTAWA
70.394 Kc/s
OTTAWA-CHURCHILL
80Kc/s
MONT JOLI 30Mc/s COSMIC NOISE
POLAR ANTENNA
SECR
SC
FL
1 CYCLE
09
06
03
00
21
18
15
12
09
UT

FIG. 2.

It is not possible from our recordings of relative phase lag to deduce an apparent height of reflection. The change of phase from night-to-day of 1.2–1.8 cycles is consistent with the interpretation that the predominant mode of propagation is that of a once reflected sky wave. For such a model the change of phase from night-to-day corresponds to a change in apparent reflection height of about 11–16 km, and the decreased reflection height during the most intense period of the disturbance, on 12–13 November, corresponds to a depression in the reflection height of 4–6 km. It is thought that these l.f. waves are reflected from heights below 70 km during the day, perhaps from heights near 65 km, and hence during the peak of the disturbance reflection probably occurred from heights near 60 km.

DISCUSSION

The beginning of observable effects in l.f. propagation at 1354 and 1900 on 12 November and 0300 on 15 November coincide closely with pronounced enhancements of ground neutron monitor count rates recorded at Ottawa and Churchill. Low-frequency propagation is apparently very sensitive to ionization density and gradient changes at the base of the ionosphere. Weak events evident in the nighttime propagation of the northern circuits on 10–11 and 11–12 November are interpreted as being a PCD event following the class 3 flare at 1009 on 10 November. This flare originated from the same sunspot group as those on 12 and 15 November. Measurements made at Churchill (Montalbetti and McEwen 1961) of hydrogen emission from the night sky indicate the presence of considerably more hydrogen than normal on the nights of 10–11 and 11–12 of November. The remarkable feature of a lack of any diurnal variation during the PCD suggests production of electron densities (and electron density gradients) near 60 km, which are adequate to reflect l.f. waves day or night independent of ionospheric processes, such as attachment of free electrons to form negative ions during the night. The lower edge of the ionization produced must be determined mainly by the characteristics of the bombarding particles, such as the steepness of the energy spectrum.

This lack of a diurnal variation has already been pointed out by Ortner *et al.* (1960), who recorded high latitude v.l.f. transmissions during previous events. These workers in addition concluded that the pertinent reflecting strata was located at heights of 15–20 km, but this is not consistent with our observations.

When the PCD event is weak, i.e. a weak proton event affecting propagation at high latitudes, or a strong event affecting propagation near the low

FIG. 2. Collocation of l.f. propagation recordings together with recordings of 30 Mc/s cosmic radio noise made at Mont Joli on a polar-directed antenna. This latter record is included for comparison of starting times of the PCA with the beginning of the effects observed on our Comfort Cove – Ottawa transmission. The solid curves show the variations observed on 12–13 November, and the broken curves show variations observed on a normal day for comparison (which for the signal amplitude records is the 8–9 November, and for the phase record the 10–11 November). The short vertical lines represent the times when the sun's zenith angle is 102° and 90° 50′ (ground sunrise and sunset) at the mid-point of the path. The vertical arrows with captions SC, SECR, and FL represent the times of the beginning of the SC geomagnetic storm, the beginning of sudden enhancements of cosmic rays observed at Ottawa and Churchill, and the beginning of the visible solar flare.

latitude extent of the disturbance, the diurnal variation of field strength of l.f. transmissions is opposite to that normally observed, i.e. the daytime field strengths are greater than normal, and the nighttime field strengths are less than normal. The transition from night-to-day occurs quite suddenly during twilight conditions at the path mid-point. A marked feature of the disturbance pattern is the absence of fading, indicating quasi equilibrium of the ionization produced at the base of the ionosphere. When the proton event is strong the diurnal variation disappears entirely, and the observed field strength is about that of a normal day. This accounts for the apparent differences between the observed behavior of 16-kc propagation from Rugby as received at Upsala (during the 23 February 1956 event (Belrose *et al.* 1956)), and as received at Kiruna (during the May and June 1959 events (Ortner *et al.* 1960)). As the disturbance weakens, it is the nighttime propagation which is predominantly affected, i.e. the excess ionization due to the slowly dying disturbance lies between those heights where the waves are normally reflected during the day and during the night (between 65–85 km). This conclusion is substantiated by our measurement of phase.

BELROSE, J. S., DEVENPORT, M. H., and WEEKES, K. 1956. J. Atmospheric and Terrest. Phys. **8**, 281.
MONTALBETTI, R. and MCEWEN, D. J. 1961. Can. J. Phys. **39**. This issue.
ORTNER, J., EGELAND, A., and HULTQVIST, B. 1960. IRE Trans. **AP-8**, 621.

RECEIVED FEBRUARY 3, 1961.
DEFENCE RESEARCH TELECOMMUNICATIONS ESTABLISHMENT,
DEFENCE RESEARCH BOARD,
OTTAWA, CANADA.

THE IONOSPHERIC DISTURBANCE OF NOVEMBER 12 AND 16, 1960

W. S. CAMPBELL AND P. L. HUBERT

The purpose of this note is to summarize the absorption effects recorded at ionospheric sounding stations in Canada during the disturbed period between November 12 and 16, 1960. The locations of the stations and the characteristics of the ionosondes are tabulated in Table I. Ottawa, St. John's, and Winnipeg are considered to be middle latitude stations; Churchill is located in the auroral zone, and Resolute Bay is situated in the polar cap region. The routine sounding program consists of frequency sweeps through the h.f. spectrum at 15-minute intervals.

TABLE I

Station	Latitude	Longitude	Geomagnetic latitude	Peak pulse power (kw)
Resolute Bay	74.7° N.	94.9° W.	83.2°	1
Churchill	58.8° N.	94.2° W.	68.0°	10
Winnipeg	49.9° N.	97.4° W.	59.8°	1
St. John's	47.6° N.	52.7° W.	58.0°	1
Ottawa	45.4° N.	75.9° W.	57.0°	10

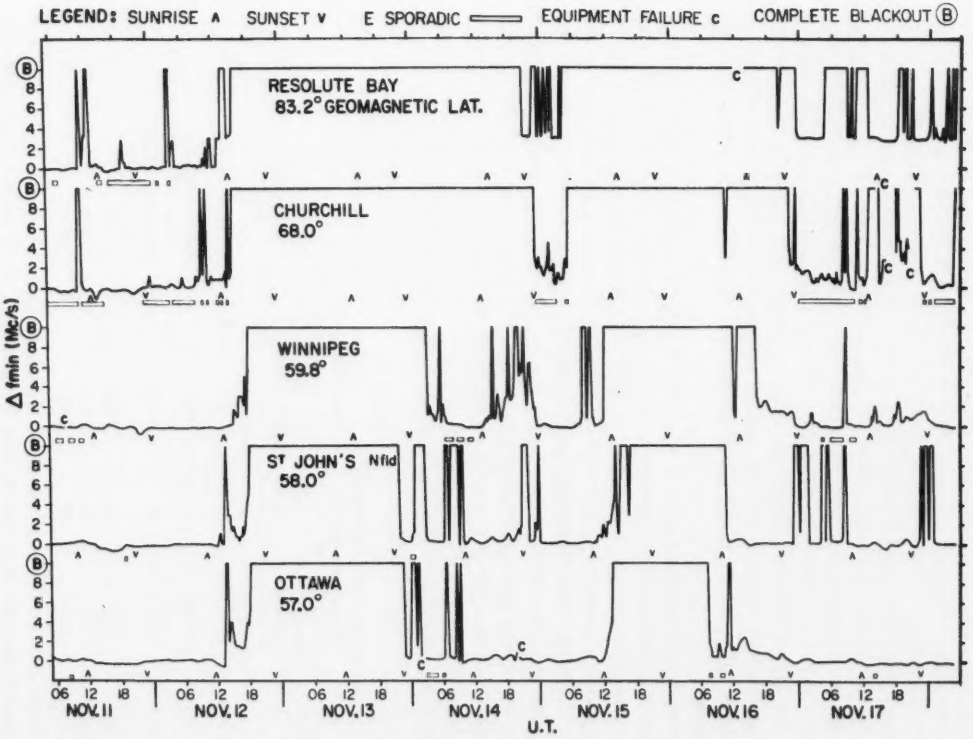

FIG. 1. $\Delta f_{\min}$ for the period November 11 to 17, 1960.

The best parameter for the qualitative measurement of absorption that can be obtained from ionograms is the lowest radio wave frequency at which an echo is recorded ($f_{\min}$). The $f_{\min}$ increases with increasing absorption. When the $f_{\min}$ exceeds the highest radio wave frequency, which the ionosphere can reflect at that time, no echoes will be observed, a condition generally known as "black-out". However, $f_{\min}$ is only a qualitative measure of absorption since it is relative to the over-all sensitivity of the sounding system.

A good indication of the presence of abnormal absorption can be obtained by comparing the observed value of $f_{\min}$ with the value of $f_{\min}$ normally observed on other days at the same time. The parameter $\Delta f_{\min}$ will be used to indicate the difference between the observed $f_{\min}$ and its monthly median value for the same time. In Fig. 1, $\Delta f_{\min}$ is shown as a function of universal time for all five stations, for the period November 11–17. Times of sunrise and sunset at a height of 50 km and times of occurrence of sporadic E are also shown.

It may be noticed from Fig. 1 that the durations of black-out at the polar and auroral zone stations (Resolute and Churchill) are quite similar. The two black-outs are separated by a period of partial recovery lasting for a few hours, on the nights of November 14 and 15. The other three medium latitude stations all show similar characteristics but the period of partial recovery begins one day earlier on the night of November 13–14. The recovery period is characterized by strong absorption and sporadic E which are typical of the auroral ionosphere. The durations of the main black-outs at Winnipeg were somewhat longer than at Ottawa and St. John's.

The main features of the black-outs are summarized in Table II.

TABLE II

Station	Black-out starting Nov. 12		Black-out starting Nov. 15		Conditions prior to the black-outs	First normal day after the black-out
	Approx. time of start black-out (U.T.)	Duration in hours	Approx. time of start black-out (U.T.)	Duration in hours		
Resolute Bay	1530	53	0430	43	Occasional high $f_{\min}$ and black-out	25/11/60
Churchill	1515	56	0530	41	Occasional high $f_{\min}$ and black-out	19/11/60
Winnipeg	1800	33	1200	24	Quiet	18/11/60
St. John's	1800	28	1545	18	Quiet	18/11/60
Ottawa	1815	28	1330	18	Quiet	17/11/60

Acknowledgment is given to the Department of Transport for operation of the ionospheric sounding stations.

Received February 3, 1961.
Defence Research Telecommunications Establishment,
Defence Research Board,
Ottawa, Canada.

HYDROGEN EMISSIONS DURING THE PERIOD NOVEMBER 9–16, 1960

R. MONTALBETTI* AND D. J. MCEWEN†

At Churchill, Manitoba (geomagnetic latitude 68° N.) a photometer is operated on a continuous basis to monitor the H_β emissions from the night sky. It consists simply of a narrow band interference filter oscillated to scan a wavelength interval of about 200 Å in some 45 seconds and a photomultiplier tube as detector. The photometer is programmed to view five positions in sequence in 40° steps, starting at 10° above the northern horizon. A complete survey along the meridional line is made in 5 minutes.

In Fig. 1, the intensity of the H_β emissions, grouped into intensity intervals as given in the legend for the figure, is plotted as a function of universal time and for each of the five directions. Figure 1 also shows the maximum variation in the Z component of the magnetic field at Churchill for each hourly interval. An index of 1 is used for a change of 50γ, 2 for a change of between 50γ and 100γ, and so on up to 8. Any variation greater than 400γ is indexed as 9.

The strongest hydrogen emissions were observed on the night of November 12/13 when the intensity reached some 600 R. According to Chamberlain's (1954) analysis this corresponds to a flux of the order of 10^8 protons/cm^2 sec. Within the time resolution of each meridional survey no systematic motion is evident. Strong bursts of H_β emissions appeared over the entire meridional line at about the same time. These bursts follow strong radio-wave absorption peaks as measured by the Churchill riometer aimed towards the zenith. In Table I the times of strong auroral-type absorption peaks and the times of strong emissions are given.

TABLE I

Time of peak absorption, U.T.	Time of peak H_β emissions, U.T.	Max. value of H_β intensity, R	Max. value of absorption, db
0700 Nov. 13	0740	270	>12
	0800	350	
1015	1030	650	>12
1145	1210	330	10
0045 Nov. 14	(overcast sky)		7
0115			5
0530	0555	65	5
0615	0625	75	4

Whether there were strong emissions between 0600 hours and 0618 hours November 13 cannot be determined as aurora occurred of such intensity as to saturate the photometer. The time delay between the radio-wave absorption and the light emissions is the order of half an hour. During the night of

*Defence Research Telecommunications Establishment, Ottawa, Ont.
†Defence Research Northern Laboratory, Churchill, Man.

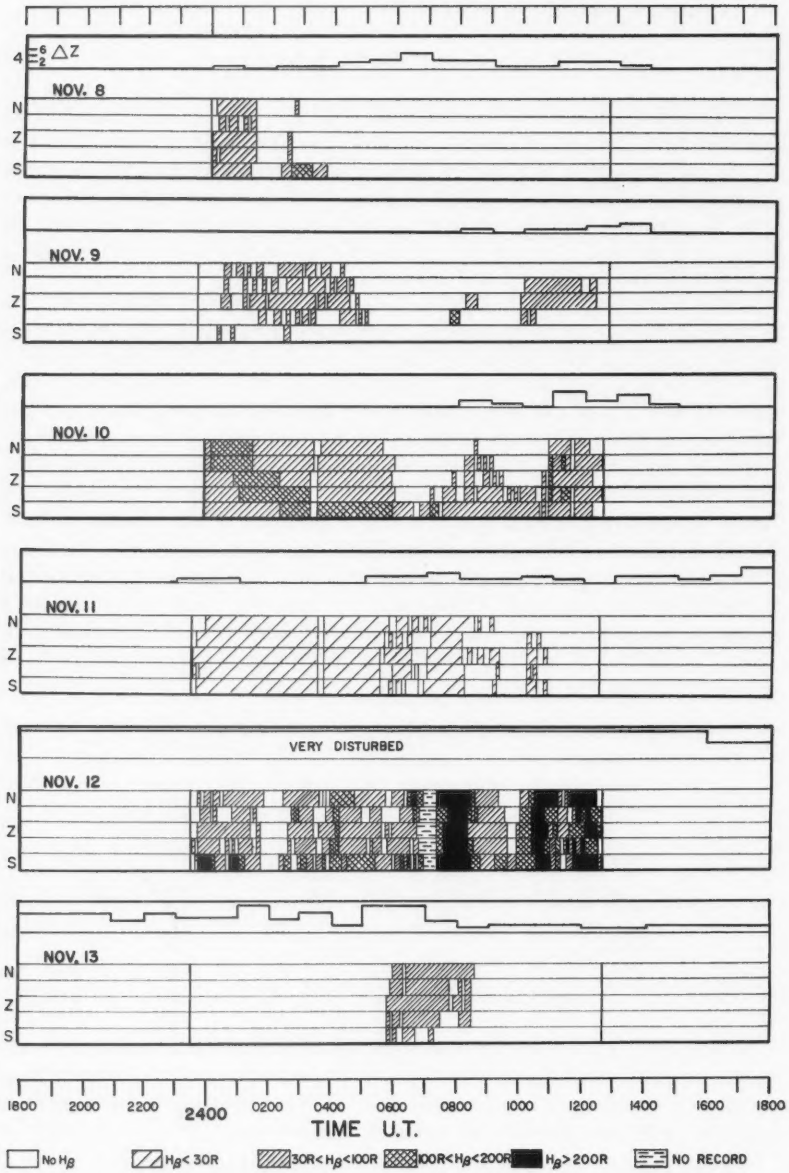

FIG. 1. Intensity of H_β emissions and magnetic disturbances at Churchill, Manitoba, for the period November 9 to 16, 1960.

November 12/13 strong rayed auroral forms and, more important, strong type *A* aurorae were observed. Observations at Churchill indicate that strong hydrogen emissions occur during type *A* auroral displays.

For the two nights prior to the strong disturbance, hydrogen emissions were observed practically all night although they were not as intense. On November 10/11 the peak in the emissions appeared to move from the northern to the southern horizon while on November 11/12 rather weak intensities were measured covering the entire sky for many hours. It would be expected that if the proton fluxes causing H_β emissions are responsible, in part, for the radio absorption phenomena, then absorption should have been observed on November 10/11. This does not appear to be the case, though Belrose has reported evidence for enhanced low-level ionization at this time.

On the basis of absorption and magnetic observations, there were apparently two large events, namely one during November 12/13 and one during November 15/16. Large proton fluxes and unusual aurorae were observed with the first event. It is unfortunate that the nights of November 14/15 and November 15/16 were completely overcast. Thus it is unknown whether large proton fluxes were associated with the second event. Observations from other stations as to whether type *A* aurorae occurred would be valuable.

The 600 R measured on November 12/13 must be taken as unusual. The peak intensities observed with the photometer in operation since December 10, 1959, have been approximately 150 R. On February 10/11, 1958, when a similar geomagnetic storm occurred, H_β intensities reached values of 850 R (1959) as measured with a scanning spectrometer.

BELROSE, J. S. and ROSS, D. B. 1961. Can. J. Phys. **39**. This issue.
CHAMBERLAIN, J. W. 1954. Astrophys. J. **120**, 360.
MONTALBETTI, R. 1959. J. Atmospheric and Terrest. Phys. **14**, 200.

RECEIVED FEBRUARY 3, 1961.
DEFENCE RESEARCH TELECOMMUNICATIONS ESTABLISHMENT,
DEFENCE RESEARCH BOARD,
OTTAWA, CANADA,
AND
DEFENCE RESEARCH NORTHERN LABORATORY,
CHURCHILL, MANITOBA.

GEOMAGNETIC VARIATIONS BETWEEN NOVEMBER 12 AND NOVEMBER 16, 1960

E. R. NIBLETT

Exceptionally large geomagnetic disturbances have been reported from observatories in many different parts of the world during this interval. At Canadian observatories the disturbances between the hours of 06 U.T. and 12 U.T. on November 13 were comparable with the largest that have been recorded in this country.

Figure 1 shows mean hourly values of horizontal force, H, at Victoria, Agincourt, and Meanook observatories during the five Greenwich days. At Baker Lake and Resolute the mean hourly values of the principal horizontal component (X for Baker Lake and Y for Resolute) have been plotted, since H is not recorded in these locations. The lowest plot in Fig. 1 shows the hourly range of H at Meanook observatory. The times of two sudden storm commencements, 13:48 on November 12 and 13:04 on November 15, are indicated by arrows. The locations of the five observatories are given in Table I.

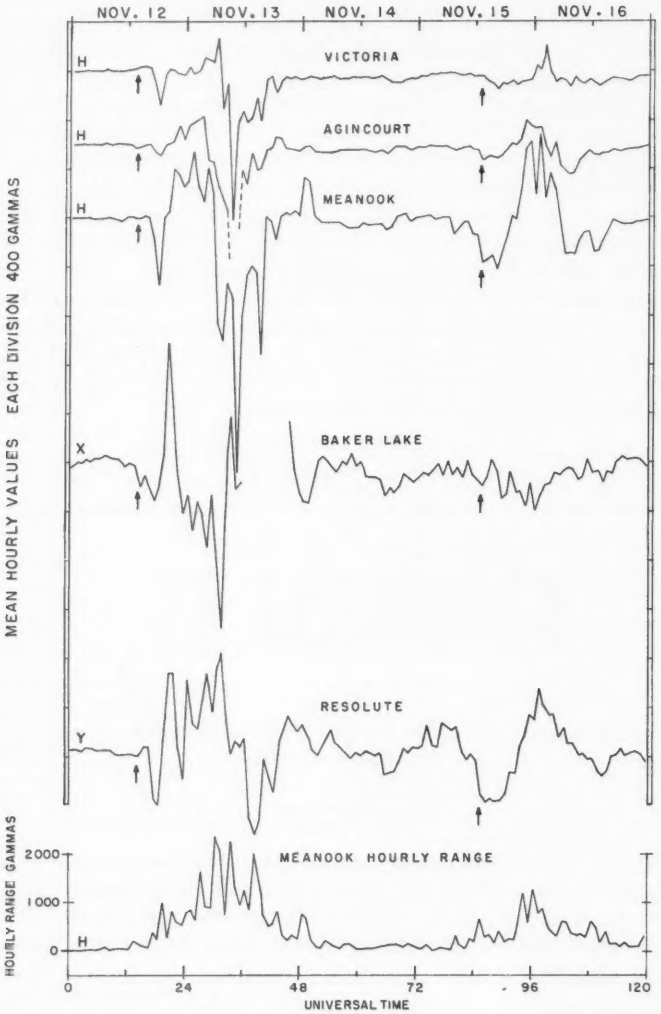

FIG. 1. Horizontal force variations at Canadian magnetic observatories.

TABLE I

Observatory	Geographic		Geomagnetic	
	Latitude	Longitude	Latitude	Longitude
Victoria	48.5° N.	123.4° W.	54.3° N.	292.7° E.
Agincourt	43.8 N.	79.3 W.	55.2 N.	346.9 E.
Meanook	54.6 N.	113.3 W.	61.9 N.	300.7 E.
Baker Lake	64.3 N.	96.0 W.	73.9 N.	314.8 E.
Resolute	74.7 N.	94.9 W.	83.1 N.	287.7 E.

The stations south of the auroral zone, Victoria, Agincourt, and Meanook, show a similar pattern of disturbance throughout the five days. Two magnetic storms are evident, separated by more than a day of relatively little activity. Significant features of the first storm are a decrease in H from about 16:30 to 19:30 on November 12, an enhancement from then till 06 on the 13th, and an extremely large depression between 06 and 18 on the same day. Reasonably quiet conditions were not restored till approximately 02:30 on the 14th. The very large rapid fluctuations typical of magnetic storms near the auroral zones developed 4 to 5 hours after the SSC at 13:48 and persisted till about 21:00 on the 13th.

In the second and less intense storm the horizontal force went through a moderate depression immediately after the SSC, a strong enhancement which reached its peak at about 00 hours on the 16th, and a final moderate depression. Moderate rapid fluctuations set in after the SSC and large storm fluctuations occurred between 21:00 on the 15th and 09:00 on the 16th.

All the variations described above were larger at Meanook than at Victoria or Agincourt. This suggests that the succession of events was controlled at these locations by auroral zone currents, not an equatorial ring current. Classical storm-time patterns which are often obvious in magnetograms from low and middle latitudes are seldom evident in Canada during an individual storm. On the other hand the horizontal force at the three observatories shows a tendency to be depressed during the local a.m. hours and enhanced during the p.m. hours. This is consistent with the usual behavior of disturbance daily variation near the auroral zone.

The two observatories north of the auroral zone show intense but less regular disturbance patterns. The SSC on the 15th is almost obscured by large background noise at both stations. Baker Lake shows scarcely any contrast between the second storm and the irregular fluctuations preceding it. Systematic trends during the a.m. and p.m. hours are not obvious there. At Resolute both storms are characterized by enhanced H during the p.m. hours and depressed H during the a.m. hours.

Some data on the two sudden storm commencements and on K indices are given in Table II. A third SSC is reported by the IUGG Association of Geomagnetism and Aeronomy to have occurred at 10:21 on November 13. Conditions at the Canadian observatories were much too disturbed at this time for an identification to be possible.

TABLE II

Observatory	Greenwich date	SSC's Time	SSC's Amplitude D X	SSC's Amplitude H Y	SSC's Amplitude Z Z	Activity ΣK_p	Activity ΣK	Activity K_{max}	Activity Periods of K_{max}
Victoria	Nov. 12	13:48	− 7′	48	25	33	35	8	7
	13					67	64	9	3, 4, 5, 6
	14					37	32	6	1
	15	13:04	− 8′	17	11	42	40	7	8
	16					45	44	8	1, 2
Agincourt	Nov. 12	13:48	− 9′	56	18	33	27	7	8
	13					67	67	9	1, 2, 3, 4, 5, 7
	14					37	37	8	1
	15	13:04	− 3′	13	6	42	38	7	8
	16					45	43	8	1, 2
Meanook	Nov. 12	13:49	−17′	106	−108	33	31	8	7
	13					67	65	9	2, 3, 4, 5, 6
	14					37	37	7	1
	15	13:05	−14′	−62	−27	42	44	8	8
	16					45	48	8	1
Baker Lake	Nov. 12	13:49	−82	−46	−120	33	32	9	7
	13					67	57	9	3, 4, 5
	14					37	34	5	1, 2, 3, 7
	15	13:05	?	?	?	42	42	7	8
	16					45	37	6	1
Resolute	Nov. 12	13:46	−85	−47	−35				
	15	13:02	?	?	?				

NOTE: Small differences in the times recorded for SSC's at different observatories are probably due to clock errors on the magnetograms. The K indices for Resolute are not available. ΣK_p is the daily sum of the eight planetary K indices. ΣK is the daily sum of the eight indices at the specified observatory. "Periods of K_{max}" refers the to three hourly intervals during which the K index was a maximum.

RECEIVED FEBRUARY 3, 1961.
DOMINION OBSERVATORY,
DEPARTMENT OF MINES AND TECHNICAL SURVEYS,
OTTAWA, CANADA.

OBSERVATIONS OF AURORAL IONIZATION DURING THE PERIOD NOVEMBER 11–16, 1960

H. V. SERSON AND B. C. BLEVIS

The present note describes observations of auroral ionization made by the Defence Research Telecommunications Establishment during the period from November 11 to November 16, 1960, inclusive. Measurements both of auroral luminosity and of the amplitude of echoes obtained on radar systems operating at ultra high frequencies were made. These measurements were supplemented by observations of the magnetic disturbance. The data are displayed graphically in the accompanying diagrams.

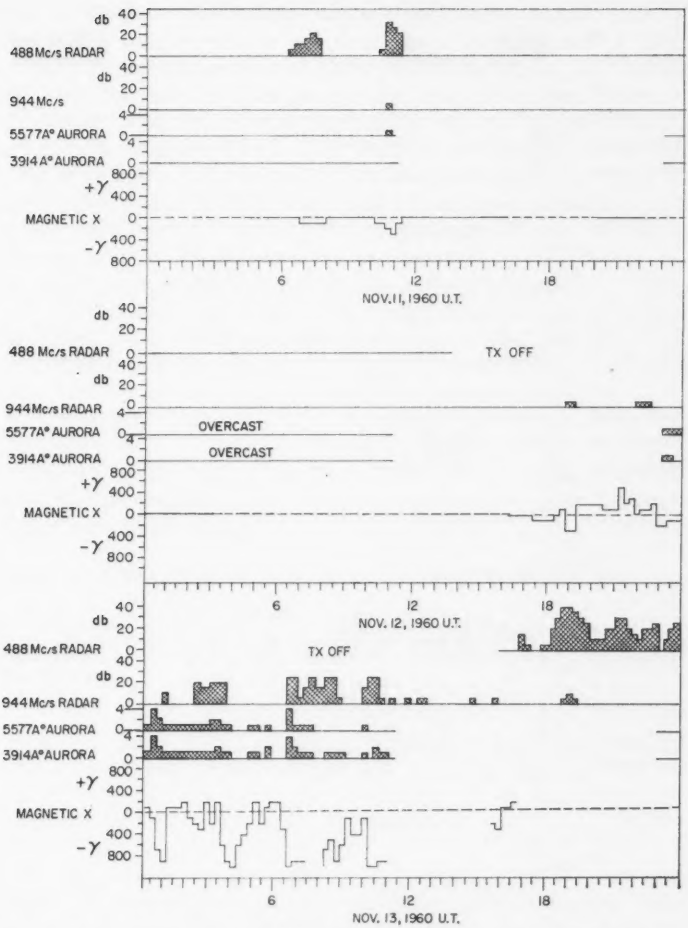

FIG. 1. Radar, photometric, and magnetic observations, November 11 to 13, 1960.

The auroral radar observations were made on two similar systems operating at 488 Mc/s and 944 Mc/s, each having a peak power of 5 kw, pulse length of 500 μsec, and beam width of 2.5°. The transmitting and receiving sites are situated just west of Ottawa. The antennas illuminate an area at the 100-km height level centered roughly over Moosonee, Ontario (geomagnetic latitude 62.2° N.). It is from this region that echoes are obtained.

The histograms give values of the peak amplitude of echoes for intervals of 1/100th of a day. Echo amplitude is plotted in 5-db steps above noise levels of −126 dbm and −123 dbm for the 488 Mc/s system and 944 Mc/s system

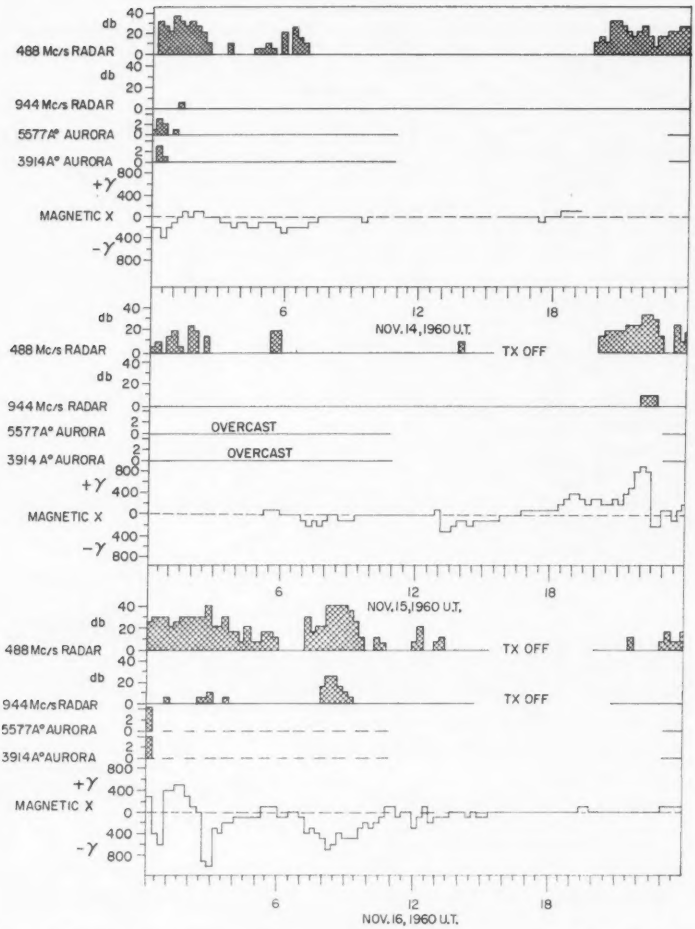

FIG. 2. Radar, photometric, and magnetic observations, November 14 to 16, 1960.

respectively. Comparison of the relative amplitude of echoes on the two frequencies during periods when both systems were operating simultaneously suggests that the 488 Mc/s system would probably have been saturated a large part of the time from late on November 12 until noon on November 13.

A two-channel recording photometer is located at the receiving site having a beam width, bearing, and elevation similar to that of the radar receiving system. This photometer is arranged to look alternately through a 5577 Å and a 3914 Å filter. The results are plotted below the radar observations in the diagrams. The ordinate scale gives the peak value of the intensity for

periods of 1/100th of a day increasing in decade steps. A scale value of unity corresponds to an intensity of less than about 1 kilorayleigh; a scale value of 4 indicates intensities greater than 100 kilorayleighs. The photometric records are interrupted by daylight and the presence of cloud cover.

It is noticed that the relative intensity at the two wavelengths does not always remain constant. This is made evident by inspection of the results at the two wavelengths for the period just before noon on November 13. It is significant that during the particular times when the intensity of the 3914 Å band exceeded that of the 5577 Å line, Montalbetti and McEwen (1961) report unusually strong H_β emissions at Churchill.

The peak value of the change in the magnetic X-component at Moosonee, Ontario, as measured on a three-component flux gate magnetometer, is also given in the figures. Portions of this record are missing because of failure of the recording meter. Deviations from quiet day values of greater than 1000 gammas were frequently obtained during the period in question.

The period from November 11 to November 16, 1960, showed unusually high auroral activity particularly during the nights of November 12/13 and November 15/16. Although there is no direct correlation between the radar and photometric observations of aurora, strong features appear in both records associated with large changes in the magnetic field.

MONTALBETTI, R. and MCEWEN, D. J. 1961. Can. J. Phys. **39**. This issue.

RECEIVED FEBRUARY 3, 1961.
DEFENCE RESEARCH TELECOMMUNICATIONS ESTABLISHMENT,
DEFENCE RESEARCH BOARD,
OTTAWA, CANADA.

AURORAL RADAR OBSERVATIONS AT 48 MC/S DURING THE PERIOD OF THE 12 NOVEMBER, 1960, SOLAR EVENT*

A. G. MCNAMARA

Simultaneous records from three auroral radars of similar characteristics have been analyzed for the period 11 November to 16 November, 1960. The radars are located at Churchill, Saskatoon, and Ottawa, for which the geomagnetic latitudes are 68° N., 60.5° N., and 57° N. The radars operate near 48.5 Mc/s with a 300-μsec pulse of 1-kilowatt peak power. The data plotted are the occurrences of echoes in half-hourly intervals, starting on the hour and half-hour. The solid bars on Fig. 1 indicate auroral echoes obtained at Churchill, Saskatoon, and Ottawa. The histograms are the half-hourly meteor echo counts on the Ottawa auroral radar. For reference to other solar and geophysical events, the times of the two major sudden commencements (SC) of magnetic storms on 12 November and 15 November are indicated by the arrows.

*Issued as N.R.C. No. 6226.

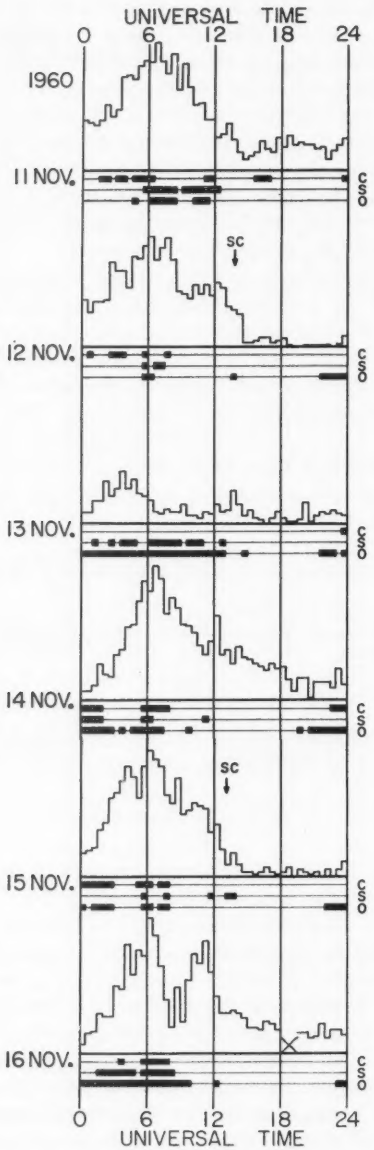

FIG. 1. Echo occurrences on 48 Mc/s auroral radars. The solid bars are the occurrences of auroral echoes at Churchill (C), Saskatoon (S), and Ottawa (O). The histograms are the meteor echo rates on the Ottawa auroral radar. SC indicates the time of a sudden commencement.

The primary event was a solar flare at 13:25 U.T., on 12 November, followed by a cosmic-ray increase, and followed in turn at 13:50 U.T. by a sudden commencement. Within minutes of the SC, echoes were observed for a 7-minute period at Ottawa. Strong signal absorption, indicated by an abrupt drop in the meteor rate on the Ottawa auroral radar, began in the period 14:30 U.T. The meteor count reached a minimum from 19:00 to 20:00 U.T. when no meteors were detected. Thereafter there was a slow return of meteor echoes, the mean rate during the following 24 hours (13 November) being about one-third of normal. At the other two radars, the meteor rates were also reduced to a fraction of the normal rate for a period of approximately 24 hours. Since the meteoric reflections occur at heights around 90 km, the meteor effect is interpreted as caused by a widespread low-level absorption, a polar cap absorption (PCA) event.

In the 24 hours following the 12 November sudden commencement, the behavior of the auroral echo occurrence at the three stations is noteworthy. Echoes started at Ottawa at 21:30 U.T., 12 November, and were nearly continuous for 15 hours. The height of reflection of auroral echoes is 100–110 km. Activity on the Saskatoon radar during the same time was present but weaker and more intermittent, while at Churchill there were no echoes observed in the entire 24-hour period. This geographical pattern of occurrence could be attributed to a real variation in the ionization distribution. However, when considered in the light of observations showing large values of radio-frequency absorption, and reports of intense visual and magnetic activity at high latitudes, it appears more likely that intense echoes at 48.5 Mc/s would have been present at all stations if not for strong absorption at low heights.

On 15 November, another sequence of solar flare, cosmic-ray increase, and sudden commencement occurred. The SC at 13:05 U.T. was followed in 20 minutes by echoes, this time only on the Saskatoon radar. During the 10 hours following the SC, the meteor rates fell to low values, but recovered rapidly to normal at Ottawa with the coming of darkness. A feature peculiar to the 15 November sequence is the short period of nighttime absorption centered around 08:00 to 09:00 U.T. 16 November.

The combined results of three widely separated v.h.f. auroral radars show interesting patterns of activity. Short bursts of echoes are sometimes associated in time with sudden commencements. These echoes are not intense which may account for the fact that only the more favorably situated radars detect them. The evidence cited for this large PCA event suggests that at such times the strong low-level absorption significantly alters the detection capabilities of a v.h.f. auroral radar, and may distort the apparent geographical distribution of the reflecting ionization.

Received February 3, 1961.
Division of Radio and Electrical Engineering,
National Research Council,
Ottawa, Canada.

PROPAGATION OF METEOR BURST SIGNALS DURING THE POLAR DISTURBANCE OF NOVEMBER 12–16, 1960

L. A. MAYNARD

In a meteor burst communications system, short signal impulses are observed at a receiving terminal each time a suitable ionized trail is established in the lower ionosphere. Most signal bursts arise from meteors originating in the vicinity of 80 to 100 km.

If *D*-region absorption is present over a large area near the center of the transmission path, then meteor burst signals will be absorbed, provided the absorption takes place below the meteoric region.

Since meteoric signals are random in amplitude and occurrence, the effect of absorption on the signals must be considered statistically. This may be done by measuring the time that the signal level remains above a certain gate level or decision level. This time, expressed as a fraction of the sampled period, is called duty cycle. The dependence of duty cycle on decision level has been fairly well established. As a first approximation, it is found that for a 10-db change in decision level at the receiver, the duty cycle changes by approximately 10 to 1. It can be shown that a 10-db change in decision level is essentially equivalent to a 10-db change in transmitter power or to a 10-db change in transmission loss due to absorption. A rough estimate of changes in transmission loss due to absorption can be made by observing deviations from the normal diurnal variation in signal duty cycle. This note will describe the behavior of a meteor burst propagation link during the large disturbance of November 12–16, 1960.

Figure 1 shows the 30 Mc/s absorption at mid-path on a meteor burst communications circuit between Goose Bay, Labrador, and Ottawa, Ontario, as measured by a 30 Mc/s riometer. Times shown in these figures are U.T.

Figure 2 shows a plot of 104.1 Mc/s meteoric signal duty cycle over this path. The shaded region on this graph represents the normal limits of the variation in duty cycle due to the diurnal variation in meteoric activity and to the random nature of the meteoric signal. Signal duty cycle is seen to drop below its normal range for three intervals during the four days plotted. These periods of signal black-out coincide fairly well with peaks in absorption as measured by the riometer at mid-path on the link. These three periods are the only times in a test period of over 14 months that 104.1 Mc/s meteor burst signals have been significantly affected by absorption. Gaps in duty cycle plot in this figure and Fig. 3 are due mainly to cluttering of the meteoric signals by auroral-type signals.

The 41.3 Mc/s signal duty cycle shown in Fig. 3, is affected to a greater extent by the absorption. Significant changes in duty cycle occur as early as 1400 U.T. on November 12, about $\frac{3}{4}$ hour after the solar flare at 1325 U.T.

During the period from 18:00 to 20:30, November 12, the 104.1 Mc/s duty cycle deviated by a factor greater than 1000 to 1 from normal, causing a signal black-out.

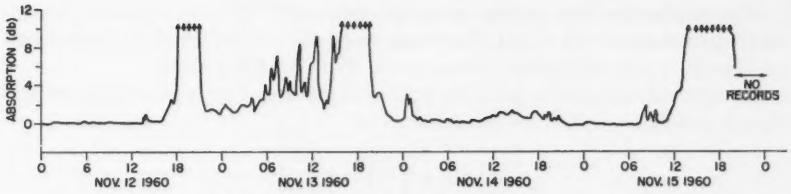

FIG. 1. Mid-path absorption at 30 Mc/s.

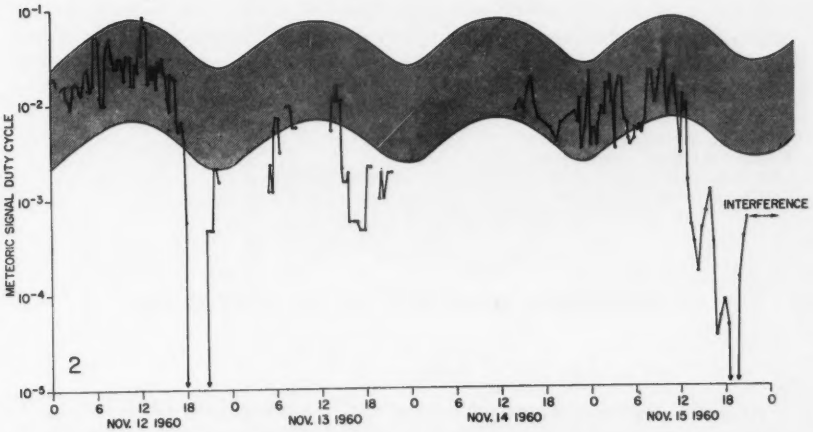

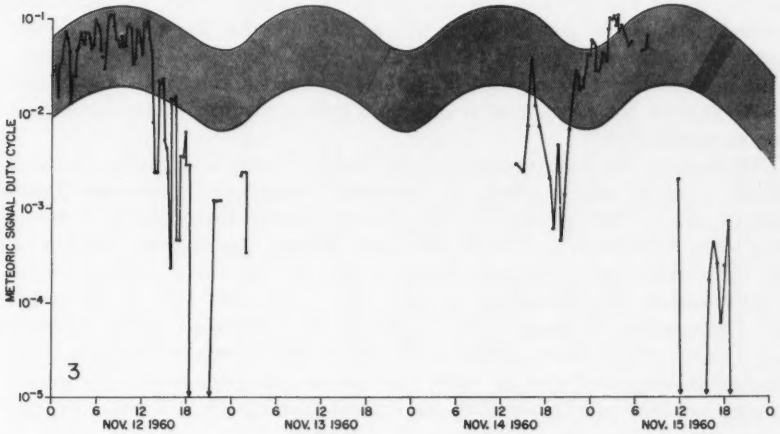

FIG. 2. 104.1 Mc/s duty cycle.
FIG. 3. 41.3 Mc/s duty cycle.

This sudden decrease in duty cycle coincides with the abrupt rise in absorption at 1800 shown in Fig. 1. This change in duty cycle could be interpreted as oblique signal absorption in excess of 30 db at 104.1 Mc/s.

An approximate relationship between oblique signal absorption and vertical signal absorption might be assumed to be

$$A_0 = 2A_v \left(\frac{f_v}{f_0}\right)^2 \sec \phi \text{ db},$$

where A_v is vertical absorption in db at mid-path at frequency f_v, f_0 is the oblique frequency used over the transmission path, and ϕ is the angle of incidence at the layer.

If one interprets the observed signal effects in terms of the absorption one might expect to observe on the mid-path riometer, it appears that the signal effects are adequate to assume the absorption was located mainly below the meteoric region of 80 to 100 km.

Received February 3, 1961.
Communications Laboratory,
Defence Research Telecommunications Establishment,
Defence Research Board,
Shirley Bay, Ottawa, Ontario.

IONOSPHERIC ABSORPTION ON NOVEMBER 12, 1960

E. L. Vogan and T. R. Hartz

An active region appeared on the sun early in November, 1960. During its passage across the disk it gave rise to a number of large and outstanding flares, which in turn produced a series of noteworthy terrestrial disturbances. Flares in this region emitted relativistic particles on at least three occasions and caused a number of large geomagnetic and ionospheric storms. In Table I are listed the principal flares and the sudden commencement geomagnetic storms that, on the basis of the optical and radio importance of the flares, are thought to result from them. In at least one case, some ambiguity exists concerning the causative flare.

Throughout the disturbed period, the Radio Physics Laboratory operated 30 Mc/s cosmic noise receivers, or riometers as they have been called (Little and Leinbach 1959), at Resolute Bay, Coral Harbour, Churchill, Cape Jones, Val d'Or, and Ottawa. At Churchill and Ottawa, additional riometers on 60 Mc/s were also in operation. Figure 1 shows a recording made on one of the Ottawa 30 Mc/s riometers during the period 1200–1800 U.T. on November 12. The significant features in this record are the rapid solar noise bursts starting at 1328 and 1344, the sudden ionospheric disturbance beginning at 1326 and continuing until at least 1430, the intense and spiky solar noise during the period 1420 to at least 1800, the intense (greater than 14 db) polar cap

TABLE I

Date	Time (U.T.)	Importance	Solar co-ordinates	Frequencies of major noise bursts at meter wavelengths (Mc/s)	Starting time of noise bursts (U.T.)	Associated SC geomagnetic storm	Flare–storm time delay (hours)	Associated PCA
Nov. 10	1009–1307	3	28 N. 28 E.	200 55	1020 1035	12 d 13 h 48 m	52	Nil
Nov. 12	1325–1922	3+	26 N. 5 W.	200 55 50 30	1327 1327 1327 1328	13 d 10 h 21 m	21	Nov. 12–15
Nov. 14	0246–0520	2	29 N. 19 W.	200	0315	15 d 13 h 04 m?	34	Nil
Nov. 15	0207–0427	3	26 N. 35 W.	200 100	0220 0224	15 d 13 h 04 m?	11	Nov. 15–19
Nov. 20	2019–2023	1	25 N. 90 W.	108	2033	21 d 06 h 32 m?	10	Nov. 21–23

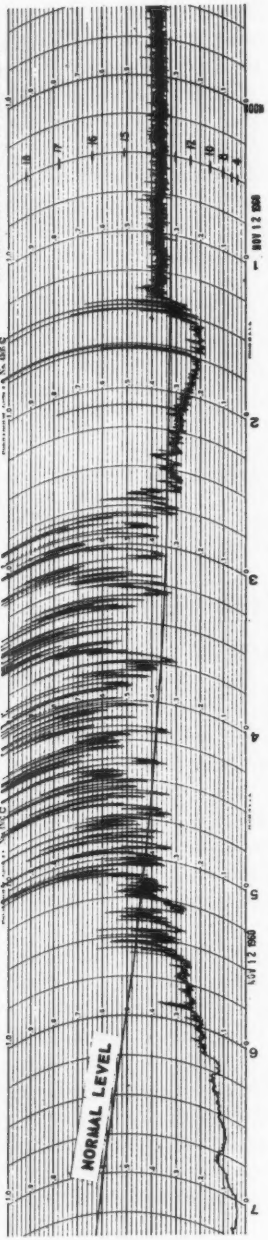

FIG. 1. 30 Mc/s riometer record illustrating some of the important features on November 12, 1960.

type absorption evident after 1800, but for which evidences can be seen in this figure as early at 1540. (It should be noted that the receiving antenna was not directed at the sun so that absolute levels of solar noise are not available from the riometer record; nevertheless the character of the solar noise in the interval can be seen in Fig. 1.)

Polar cap absorption (PCA), though usually confined to geomagnetic latitudes greater than about 60°, has been known to occur at lower latitudes after some large perturbation of the earth's magnetic field. On November 12, the sudden commencement magnetic storm began very soon after a PCA producing flare, so that this type of absorption was observable that day on all the riometers. Moreover, since the magnetic field was disturbed for a number of days, polar cap absorption was observable at all stations at least until November 18, and at some stations until November 22. A more detailed description of these events will be published in a forthcoming paper; the present contribution discusses some of the distinctive features in the data.

Some features of the early stages of the PCA on November 12 are portrayed as a latitude–time profile in Fig. 2. The respective curves give the times of the

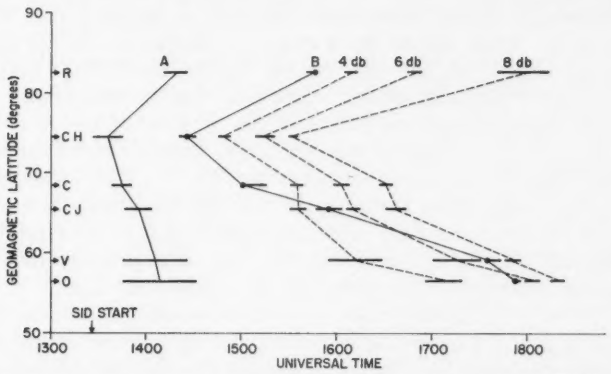

FIG. 2. Latitude–time profile showing start of polar cap absorption at 30 Mc/s for November 12, 1960.

following features: the start of the PCA, curve A; a noticeably sharp change in the rate of increase of absorption, curve B; and the attainment of the 4-, 6-, and 8-db absorption levels. In each case the horizontal bars indicate the uncertainty in the timing of that point, while the dots in curve B give the most probable time as determined by a close inspection of all available data at the respective stations. At the start of the flare, the ionosphere was illuminated by the sun at all stations except Resolute: the apparent delay in the start of the PCA there should not be taken as evidence for a delay in the arrival of the solar protons. Furthermore, in the Coral Harbour records the SID, if it occurred, cannot be distinguished from the start of the PCA. Since the ground

level cosmic-ray increase did not start before 1345 U.T. (Rose, unpublished data), it seems reasonable to assume that the PCA also did not start earlier than this, even though increased absorption is evident on the records as early as 1326 U.T. At the southern stations the late start for the PCA must be taken as somewhat uncertain because of the presence of solar noise on all the recordings. In an attempt to ascertain the importance of the solar noise in the various parts of the riometer records, the solar emissions were evaluated from independent recordings at 50 Mc/s made with a lobe-switched interferometer. While these data cannot be used to remove the uncertainty in the time of the start of the polar cap absorption, they do permit a better appraisal to be made of the location in time of the higher absorption contours in the respective riometer records. Furthermore, such prominent features as the sharp change in the rate of increase of absorption, curve B, remain unaffected by the solar noise. On this basis the shape of the absorption contours shown in Fig. 2 must be considered real, leading to the conclusion that the build-up of absorption at the southern stations proceeds more slowly than at the more northerly stations.

At approximately 1900 U.T. on November 12, the ground level cosmic-ray monitors observed a second pronounced increase in counting rate (Rose, unpublished data). While the 30 Mc/s riometers showed no change at this time—they were already beyond their dynamic range—the 60 Mc/s riometers at Ottawa and Churchill both showed a sharp increase in absorption.

Yet another absorption feature is observable in some of the records on November 12. Coincident with the magnetic storm sudden commencement at 1348, the Cape Jones record and, to a lesser extent, the Churchill record showed the short duration absorption feature that has been identified elsewhere as X ray induced and a feature of the sudden commencement in the auroral zone (Brown *et al.* 1961). Similarly, on November 15 at approximately 1304 U.T. the same feature is evident in the Churchill and Cape Jones records.

The start of the PCA on November 15 occurred before local sunrise in the ionosphere at each of the observing stations: the steep increase in absorption took place as the ionosphere became illuminated by the sun. The actual starting time of the weak nighttime PCA is somewhat uncertain because of auroral absorption during the early morning hours, but there is evidence from the various stations for a starting time at 0720 U.T. with an uncertainty of ± 30 minutes. It is not possible to identify any systematic variation of starting time with latitude for this event.

The PCA on November 21 did not exceed 3 db whereas the two earlier events showed absorption greater than 14 db.

The authors are indebted to the various people who assisted with the operation of the riometers and with the data analysis. They have also made use of unpublished data from the Fraunhofer Institute, Freiburg, Germany, the High Altitude Observatory, Boulder, Colorado, and the National Bureau of Standards, Boulder, Colorado.

BROWN, R. R., HARTZ, T. R., LANDMARK, B., LEINBACH, H., and ORTNER, J. 1961. J. Geophys. Research. In press.
LITTLE, C. G. and LEINBACH, H. 1959. Proc. I.R.E. 47, 315.
ROSE, D. C. Unpublished data.

RECEIVED FEBRUARY 3, 1961.
RADIO PHYSICS LABORATORY,
DEFENCE RESEARCH TELECOMMUNICATIONS ESTABLISHMENT,
OTTAWA, CANADA.

THE SOLAR NOISE BURST OF NOVEMBER 12, 1960*

A. E. COVINGTON, G. A. HARVEY, AND L. R. MCNARRY

The intense burst of solar radio noise which accompanied the now well-known flare of November 12, 1960, has been observed at the discrete frequencies of 2800 Mc/s and 48 Mc/s at the Radio Observatory of the Radio and Electrical Engineering Division of the National Research Council. These observations will be presented and the essential information noted. Figure 1 shows a reconstruction of the high-frequency burst while Fig. 2 shows a portion of the low-frequency record.

2800 Mc/s event.—When the solar patrol observations were begun at $12^h\ 40^m$ U.T., the solar flux was found to be increasing slightly, and by $13^h\ 20^m$ U.T. an increase of 11 units of flux had been recorded in excess of the daily level of 147 flux units (where 1 unit of flux is equal to 10^{-22} watts per square meter per cycle per second). At this time, $13^h\ 20^m$, the increase became more rapid and showed a noticeable departure from the residual receiver noise; by $13^h\ 23^m$ the flux had reached 50 flux units, by $13^h\ 24\frac{1}{2}^m$ the flux had reached 100 units, and by $13^h\ 27^m$ a level of 3000 units. The intense part of the burst shows a number of oscillations, with a peak value of flux of 5500 units at $13^h\ 45^m$. The burst declined rapidly from this peak value to a level of 300 units at $14^h\ 06^m$. This was followed by an enhanced post burst increase and the occurrence of a number of superimposed relatively smaller bursts. At $19^h\ 00^m$ the quiet sun level was reached and no further activity was recorded during the remaining two hours of observations.

48 Mc/s event.—A portion of the 48 Mc/s film record is shown in Fig. 2 (note that the times recorded on the film are E.S.T. and are 1 minute fast). This record has the output of the 2800 Mc/s radiometer simultaneously recorded as a single curve which moves upwards for increasing signal strength. The sloping curve across the upper track represents a portion of the 2800 Mc/s record as the burst level increases from 85 flux units to 160 flux units. In Fig. 1 these levels are shown as broken lines. The time, $13^h\ 24^m\ 27^s$ at which the 85-flux level is reached has been taken as the high-frequency burst commencement. The 48 Mc/s burst started abruptly at $13^h\ 27^m\ 36^s$ and in relation to the somewhat arbitrarily chosen starting time for the higher frequency burst,

*Issued as N.R.C. No. 6234.

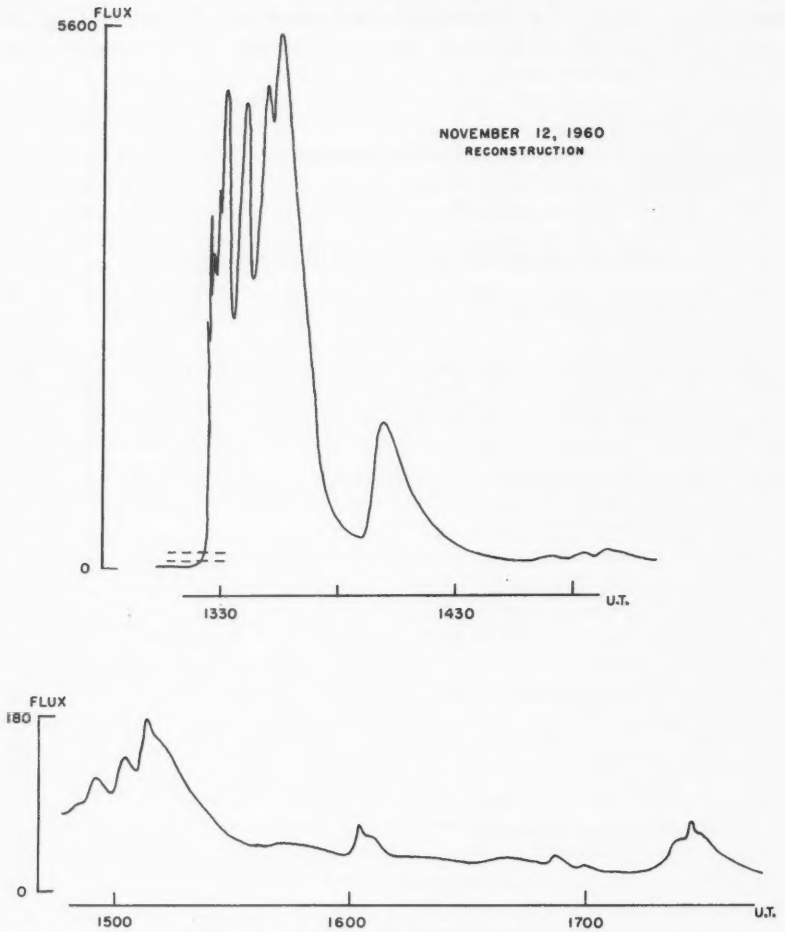

FIG. 1. Reconstruction of 2800 Mc/s solar burst.

a delay time of 189 seconds is obtained. The 48 Mc/s storm continued until $19^h\ 09^m$.

The two faint bands of noise at approximately $13^h\ 23^m\ 56^s$ and $13^h\ 24^m\ 12^s$ are probably due to other weaker type III bursts associated with the solar eruption. The other broad, faint bands of noise at $13^h\ 26^m$ are due to interference. Other burst activity occurred before the principal event, from $12^h\ 30^m$ to $12^h\ 32^m$ and from $12^h\ 55^m$ to $13^h\ 00^m$ and at $13^h\ 09^m$.

RECEIVED FEBRUARY 3, 1961.
DIVISION OF RADIO AND ELECTRICAL ENGINEERING,
NATIONAL RESEARCH COUNCIL,
OTTAWA, CANADA.

PLATE I

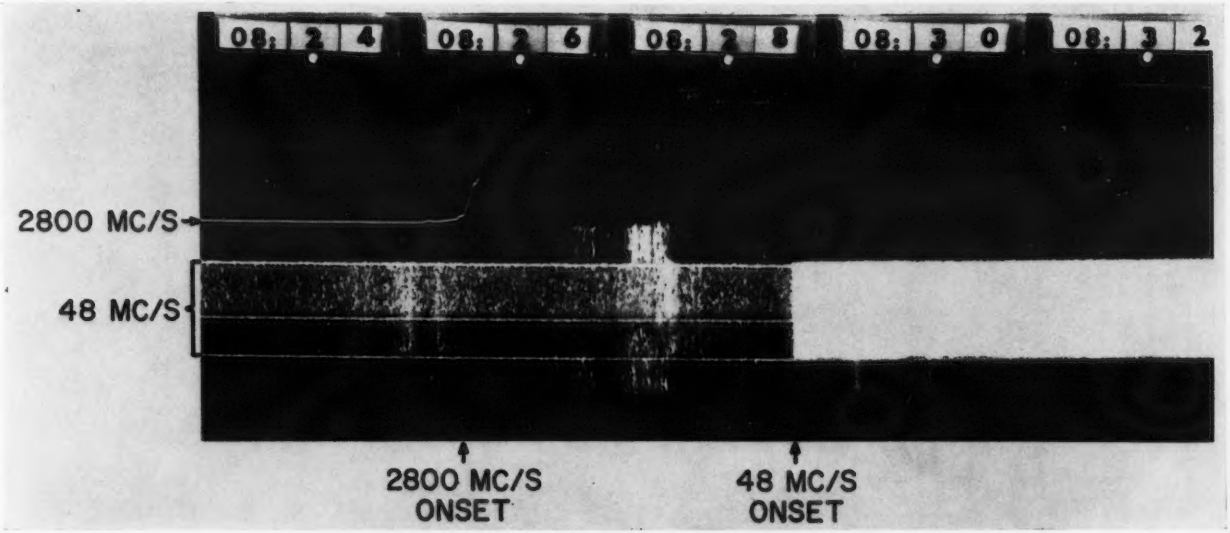

FIG. 2. Film record of combined 48 Mc/s and 2800 Mc/s solar noise bursts.

LETTERS TO THE EDITOR

Under this heading brief reports of important discoveries in physics may be published. These reports should not exceed 600 words and, for any issue, should be submitted not later than six weeks previous to the first day of the month of issue. No proof will be sent to the authors.

Frequency Measurement of Standard Frequency Transmissions[1, 2]

Measurements are made at Ottawa, Canada, using N.R.C. caesium-beam frequency resonator as reference standard (with an assumed frequency of 9 192 631 770 c.p.s.). Frequency deviations from nominal are quoted in parts per 10^{10}. A negative sign indicates that the frequency is below nominal.

Date, January 1961	MSF, 60 kc/s	GBR, 16 kc/s		WWVB, 60 kc/s
		8½-hour average*	24-hour average†	
1	N.M.	−133	−136	N.M.
2	−129	−134	−133	N.M.
3	−148	−138	−139	−155
4	−141	−140	−140	−154
5	−143	−134	−139	N.M.
6	−147	−136	N.M.	−155
7	−137	−138	−140	N.M.
8	N.M.	−139	−141	N.M.
9	−150	−138	−140	−149
10	−157	−141	−144	−154
11	−146	−140	−142	−152
12	−154	−141	−141	−146
13	−153	−145	−148	−154
14	−148	−145	−147	N.M.
15	−146	−146	−144	N.M.
16	N.M.	−146	−147	−154
17	N.M.	−145	−147	−159
18	−158	−146	−148	−155
19	−122	−146	−147	−142
20	N.M.	−144	−147	−149
21	−157	N.M.	N.M.	N.M.
22	−152	N.M.	N.M.	N.M.
23	−167	N.M.	N.M.	−156
24	−155	−147	−150	−155
25	−155	−150	−149	−155
26	−153	−144	−149	−152
27	−151	−142	−147	−151
28	−149	−149	−150	N.M.
29	−152	−149	−152	N.M.
30	−158	−153	−153	−155
31	−162	−153	−153	−154
Average	−150	−143	−145	−153
Midmonthly mean of WWV	−150			

NOTE: N.M. no measurement.
*Time of observations: 22.45 to 07.15 hours U.T.
†Time of observations: 15 to 15 hours U.T.

RECEIVED FEBRUARY 13, 1961.
DIVISION OF APPLIED PHYSICS,
NATIONAL RESEARCH COUNCIL,
OTTAWA, CANADA.

S. N. KALRA

[1]Issued as N.R.C. No. 6220.

[2]Cf. Kalra, S. N. 1959. Can. J. Phys. **37**, 1328.

ANNOUNCEMENTS

The New Unit of Atomic Mass*

At the 10th General Assembly of the International Union of Pure and Applied Physics, held in Ottawa in September, 1960, the following resolution was adopted unanimously:

> "The 10th General Assembly of the I.U.P.A.P. recommends the adoption of the exact number 12 as the relative nuclidic mass of the carbon isotope of mass number 12. This action will effect a unification of the physical scale of relative nuclidic masses and the chemical scale of atomic weight."

This resolution was recommended by the Study Committee (of I.U.P.A.P.) on Nuclidic Masses (President, J. Mattauch), the Commission (of I.U.P.A.P.) on Symbols, Units, and Nomenclature, and the International Union of Pure and Applied Chemistry.

The new unit of mass is to be designated by the symbol u: thus, $^{12}C = 12$ u. Readers are urged to be "u", rather than "non-u".

At the instruction of the General Assembly of I.U.P.A.P., the Commission on Nuclidic Masses has arranged, as a public service, to distribute reprints of a new mass table (Everling, König, Mattauch, and Wapstra, Nuclear Phys. **18**, 529 (1960)) in which nuclidic masses are expressed in terms of both the new unit and the old unit of atomic mass. These reprints may be obtained from the undersigned at 50 cents per copy or 10 copies for $4.00.

RECEIVED MARCH 2, 1961.
MCMASTER UNIVERSITY,
HAMILTON, ONTARIO.

H. E. DUCKWORTH
SECRETARY
COMMISSION ON NUCLIDIC MASSES

*This work was supported in part by the U.S. Air Force through the Air Force Office of Scientific Research of the Air Research and Development Command, and by the National Research Council of Canada.

The New Standard for the Metre[1]

An event took place on 14 October, 1960, at the 11th International Conference on Weights and Measures which is of great interest to every scientist concerned with the measurement of length. On that date the physical prototype for the International Metre, a platinum iridium bar bearing two fine lines, which, since 1889, has preserved the world's basic unit of length, was relegated to the position of an honored scientific museum piece by the adoption of the following resolution to base henceforth the International Metre on a wavelength of light:

> "1. Le Mètre est la longueur égale à 1 650 763, 73 longueurs d'onde dans le vide de la radiation correspondant à la transition entre les niveaux $2p_{10}$ et $5d_5$ de l'atome de krypton 86.
>
> 2. La Définition du Mètre en vigueur depuis 1889, fondée sur le Prototype International en platine iridié, est abrogée.
>
> 3. Le Prototype International de Mètre sanctionné par la Première Conférence Générale des Poids et Mesures de 1889 sera conservé au Bureau International des Poids et Mesures dans les mêmes conditions que celles qui ont été fixées en 1889."

This new definition of the metre was drawn intentionally in broad general terms so that it would not be complicated by practical instructions for its realization which will be changed from time to time to take account of new spectroscopic, interferometric, electronic, and other techniques that will permit a better realization of the ideal definition. The International Committee of Weights and Measures was invited by a second resolution of the 11th Conference to issue such instructions from time to time and at its October meeting issued its first, which were as follows:

> "Conformément au paragraphe 1 de la Résolution 2 adoptée par la Onzième Conférence Générale des Poids et Mesures (octobre 1960), le Comité International des Poids et Mesures recommande que la radiation du krypton 86 adoptée comme étalon fondamental de longueur soit réalisée au moyen d'une lampe à décharge à cathode chaude contenant du krypton 86 d'une pureté non inférieure à 99 pour cent, en quantité suffisante pour assurer la présence de krypton solide à la température de 64° K, cette lampe étant munie d'un capillaire ayant les caractéristiques suivantes: diamètre intérieur 2 à 4 millimètres, épaisseur des parois 1 millimètre environ.
>
> "On estime que la longueur d'onde de la radiation émise par la colonne positive est égale, à 1 cent-millionième (10^{-8}) près, à la longueur d'onde correspondant à la transition entre les niveaux non perturbés, lorsque les conditions suivantes sont satisfaites:

[1]Issued as N.R.C. No. 6239.

1. le capillaire est observé en bout de façon que les rayons lumineux utilisés cheminent du côté cathodique vers le côté anodique;
2. la partie inférieure de la lampe, y compris le capillaire, est immergée dans un bain réfrigérant maintenu à la température du point triple de l'azote, à 1 degré près;
3. la densité du courant dans le capillaire est $0,3 \pm 0,1$ ampère par centimètre carré."

Physicists will probably be interested in the way in which the transition from the prototype standard to the wavelength standard was effected. In 1927 the 7th International Conference of Weights and Measures authorized a relationship between the wavelength of the cadmium red line and the International Metre which made the wavelength in normal air $6438.4696 \times 10^{-10}$ metres. On this value all spectroscopic wavelengths have since been based as well as all interferometric determinations of length for science and industry. The value chosen was the average of a number of experiments conducted up to 1927 to relate this wavelength to the International Metre. It should be pointed out that this action risked the possibility that, at some later date when the metre was defined officially on a wavelength basis, there might arise the necessity of accepting either a discontinuity in the length of the metre or a revision of all spectroscopic tables and interferometric determinations of length. The 1927 relationship between the metre and the cadmium line was defined for normal air instead of vacuum. This introduced a measure of uncertainty in succeeding years as to the constitution of normal air. When the consultive committee for the definition of the metre met in 1953 to consider the procedure to be used in the transition from the physical standard of the metre to a wavelength standard it recognized the necessity that the new definition be in terms of a vacuum wavelength. It therefore decided that the 1927 wavelength in air for the red line should be reduced to vacuum by means of the formula—often called the Edlén formula—for the dispersion of normal air adopted at Rome in 1952 by the Mixed Commission for Spectroscopy. Having thus established the vacuum wavelength for the red line of cadmium as $6440.2490_7 \times 10^{-10}$ it was possible to relate to it the vacuum wavelength of any other spectral line deemed a potential candidate for use as the new base for the metre. The spectral lines of three elements in particular were intensely studied for their general suitability and in particular for their sensitivity to changes of wavelength and line symmetry as a result of perturbations imposed on the atoms by such factors as pressure, temperature, electric current, etc. The elements were isotopes of cadmium, mercury, and krypton. Finally, krypton 86 was chosen as the most suitable. Details of the research work on which this decision was based and the discussion of them can be found in the Procès Verbaux of the International Committee and of the Consultive Committee for the Definition of the Metre for the years 1953 to 1960 as well as elsewhere in the scientific literature. The International Committee accepted the recommendation of the Consultive Committee and presented the resolution cited above to the 11th General Conference.

The International Committee and the General Conference could be reassured that no duality of the metre had been introduced by the action of 1927 in defining the cadmium red line in terms of the international prototype metre by some recent Canadian work reported to the Conference at the time of its meeting. Dr. K. M. Baird of the Division of Applied Physics, National Research Council, made observations on four 1-metre bars compared directly, recently, and at different times, with the international prototype at Sèvres and produced evidence to show that the new definition of the International Metre preserved the continuity of this unit to $2:10^7$, which is of the order of accuracy and precision with which the International Metre has been reproduced since 1889.

It is perhaps worth noting some facts about the International Conference on Weights and Measures which is unfortunately not too familiar to the average physicist. The Conference is probably the oldest international scientific organization in the world. It has operated since 1875 under the authority of a treaty called the Convention du Mètre and it is generally responsible for the whole field of fundamental physical standards of measurement and the orderly development of our international measurement system. The Conference itself meets at least once in six years. An International Committee of Weights and Measures, elected by the Conference, consisting of 18 members chosen for their individual qualifications in the field of fundamental measurement, is responsible for the actual carrying out of the work under the authority of the Conference and for the direction of the laboratories of the International Bureau of Weights and Measures at Sèvres, France. To aid the International Committee to come to decisions on technical matters there are a number of consultive committees consisting of distinguished experts representing the major national physical laboratories and others appointed for their individual distinction in the field concerned. Each is under the chairmanship of a member of the International Committee. These advisory committees are at present six in number and cover the following fields: electricity, photometry, thermometry, the definition of the second (of time), the definition of the metre, standards of measure for ionizing radiation.

An earlier decision taken by the 10th Conference in 1954 was of great importance and might also be noted. This was a resolution which authorized the International System of Units (abbreviation S.I.), which give the basic dimensions and the corresponding units for our scientific measurement system. These are:

length, metre; mass, kilogramme; time, second; electric current, ampère; temperature, thermodynamic degree; brightness, candela.

This system is an evolution of the original metric system consisting only of length, metre; mass, kilogramme. In addition to being the basis of all scientific measurement it is also in the metric countries, now constituting a substantial world majority, the basis of all legal measurement.

RECEIVED MARCH 2, 1961.
DIVISION OF APPLIED PHYSICS,
NATIONAL RESEARCH COUNCIL,
OTTAWA, CANADA.

L. E. HOWLETT
VICE-PRÉSIDENT
COMITÉ INTERNATIONAL DES POIDS ET MESURES

NOTES TO CONTRIBUTORS

Canadian Journal of Physics

MANUSCRIPTS

General.—Manuscripts, in English or French, should be typewritten, double spaced, on paper 8½×11 in. **The original and one copy are to be submitted.** Tables and captions for the figures should be placed at the end of the manuscript. Every sheet of the manuscript should be numbered. Style, arrangement, spelling, and abbreviations should conform to the usage of recent numbers of this journal. Greek letters or unusual signs should be written plainly or explained by marginal notes. Characters to be set in boldface type should be indicated by a wavy line below each character. Superscripts and subscripts must be legible and carefully placed. Manuscripts and illustrations should be carefully checked before they are submitted. Authors will be charged for unnecessary deviations from the usual format and for changes made in the proof that are considered excessive or unnecessary.

Abstract.—An abstract of not more than about 200 words, indicating the scope of the work and the principal findings, is required, except in Notes.

References.—References should be listed **alphabetically by authors' names,** unnumbered, and typed after the text. The form of the citations should be that used in current issues of this journal; in references to papers in periodicals, titles should not be given and only initial page numbers are required. The names of periodicals should be abbreviated in the form given in the most recent *List of Periodicals Abstracted by Chemical Abstracts*. All citations should be checked with the original articles and each one referred to in the text by the authors' names and the year.

Tables.—Tables should be numbered in roman numerals and each table referred to in the text. Titles should always be given but should be brief; column headings should be brief and descriptive matter in the tables confined to a minimum. Vertical rules should not be used. Numerous small tables should be avoided.

ILLUSTRATIONS

General.—All figures (including each figure of the plates) should be numbered consecutively from 1 up, in arabic numerals, and each figure referred to in the text. The author's name, title of the paper, and figure number should be written in the lower left corner of the sheets on which the illustrations appear. Captions should not be written on the illustrations.

Line drawings.—Drawings should be carefully made with India ink on white drawing paper, blue tracing linen, or co-ordinate paper ruled in blue only; any co-ordinate lines that are to appear in the reproduction should be ruled in black ink. Paper ruled in green, yellow, or red should not be used. All lines must be of sufficient thickness to reproduce well. Decimal points, periods, and stippled dots must be solid black circles large enough to be reduced if necessary. Letters and numerals should be neatly made, preferably with a stencil (**do NOT use typewriting**) and be of such size that the smallest lettering will be not less than 1 mm high when the figure is reduced to a suitable size. Many drawings are made too large; originals should not be more than 2 or 3 times the size of the desired reproduction. Whenever possible two or more drawings should be grouped to reduce the number of cuts required. In such groups of drawings, or in large drawings, full use of the space available should be made; the ratio of height to width should conform to that of a journal page (4¾×7½ in.), but allowance must be made for the captions. **The original drawings and one set of clear copies (e.g. small photographs) are to be submitted.**

Photographs.—Prints should be made on glossy paper, with strong contrasts. They should be trimmed so that essential features only are shown and mounted carefully, with rubber cement, on white cardboard, with no space between those arranged in groups. In mounting, full use of the space available should be made. **Photographs are to be submitted in duplicate;** if they are to be reproduced in groups one set should be mounted, the duplicate set unmounted.

REPRINTS

A total of 100 reprints of each paper, without covers, are supplied free. Additional reprints, with or without covers, may be purchased at the time of publication.

Charges for reprints are based on the number of printed pages, which may be calculated approximately by multiplying by 0.6 the number of manuscript pages (double-spaced typewritten sheets, 8½×11 in.) and including the space occupied by illustrations. Prices and instructions for ordering reprints are sent out with the galley proof.

Contents

Printed in Canada *by* University of Toronto Press